Dual Fluorescence of a Few Organic Molecules: Intramolecular Charge Transfer and Intramolecular Proton Transfer

A dissertation
as partial fulfilment for the degree of
Doctor of Philosophy in Chemistry

by

Santosh Kumar Behera

Roll No. 11612207

Department of Chemistry
Indian Institute of Technology Guwahati
Guwahati 781039
Assam, India

April 2016

Statement

The work contained in this thesis entitled **"Dual Fluorescence of a Few Organic Molecules: Intramolecular Charge Transfer and Intramolecular Proton Transfer"** is the outcome of the research work carried out by me under the supervision of Prof. G. Krishnamoorthy, Department of Chemistry, Indian Institute of Technology Guwahati, India.

In keeping with the general practice of reporting scientific observations, due acknowledgements have been made whenever work described here has been based on the findings of other investigators. This work has not been submitted elsewhere for the award of any degree.

Santosh Kumar Behera

Santosh Kumar Behera

Department of Chemistry,
Indian Institute of Technology Guwahati,
Guwahati – 781 039, India
13th April, 2016

Dr. G. Krishnamoorthy
Head, Central Instruments Facility
& Professor of Chemistry

INDIAN INSTITUTE OF TECHNOLOGY GUWAHATI
Guwahati 781 039, Assam, India
Tel: +91 – 0361 – 258 2315 (W), 258 4315 (H)
Fax: +91 – 0361 – 2582349
E-mail: gkrishna@iitg.ernet.in, gkrishna_2000@yahoo.com

Certificate

It is certified that the work contained in thesis entitled "**Dual Fluorescence of a Few Organic Molecules: Intramolecular Charge Transfer and Intramolecular Proton Transfer**" by Santosh Kumar Behera is an authentic record of the results obtained from the research work carried out under my supervision in the Department of Chemistry, Indian Institute of Technology Guwahati, India.

Guwahati
12 April 2016

G. Krishnamoorthy

Dedicated
to
My Grandfather
Late. Khatia Behera

Acknowledgements

I have incurred many debts of gratitude to my supervisor Prof. G. Krishnamoothy who has been an honest supervisor. He introduced me to the field of fluorescence spectroscopy and taught me how to solve research problems. His constant encouragement and support was with me throughout the PhD tenure and that made easy for me to complete my thesis work. I highly appreciate the guidance that he has provided. I find myself privileged to have worked under his guidance. I take this opportunity to thank his family for being with us.

I would like to thank my doctoral committee members Prof. T. Punniyamurthy (Chairman), Prof. P. K. Giri and Dr. A. S. Achalkumar who constantly encouraged me with their valuable suggestions and constructive criticism.

I take this opportunity to thank IIT Guwahati and CSIR for providing me Fellowship for my PhD programme. I thank Department of Chemistry for providing instrumental and computational facilities and CIF for instrumental facilities. I will always remain thankful to scientific staff of CIF and department of chemistry.

I take this opportunity to thank Prof. S. S. Ghosh, Prof. M. Ray, Dr. L. M. Kundu, Dr. M. Qureshi and Prof. G. Das for teaching me during the period of course work. I remain thankful to Dr. M. Qureshi for allowing me to use his microwave oven for the synthesis. I thank our collaborator Dr. M. Sathiyendiran, University of Hyderabad and Dr. Biman B. Mandal, IIT Guwahati. I thank my friend Harikrishna for helping me in the theroretical calculations. I really thank my former and present labmates, Dr. Francis A.S. Chipem, Dr. Anusuya Mishra, Dr. N. Dash, Dr. Soumya Chatrarjee, Ashim, Saugata, Minati, Himadree, Ila for their endless help and co-operation. A big thank to Dr. Francis A.S. Chipem for assisting me to learn different instrumental techniques. I would like to thank my senior Himanshu Sekhar Jena for his advice and support throughout the journey of PhD period. I would like to thank all my PhD batchmates for making a friendly environment. My best thank goes to Harikrishna, Manoj and Saugata for being always with me during my good and bad times. Besides, I would like to thank all my juniors, friends and seniors of chemistry and other departments of IIT Guwahati, who are attached with me and have made my stay in the campus colourful.

I remain grateful to my teachers from other universities/colleges namely R. N. Mallik, Dr. P. K. Satapathy, S. Pruty, P. Basnatia, B. K. Swain, S. K. Sahoo, S. P. Dash, P. Mahapatra, Dr. P. K. Satapathy, Prof. U. N. Dash, Prof. P. K. Mahanty, Prof. S. Jena, Prof. G. C. Pradhan, Prof. S. P. Rout and A. Behara for their blessings, help and unconditional support. I take this opportunity to thank some of my teachers' wife namely Bijayini Dash, Pranati Prusty and Rasmi Devi. Especially I would like to thank B. D. Gouda, B. Gouda, Milon and Lella, who are always with me during my good and bad times and are always happy with my progress and success.

I would like to thank my younger brother Susanta Kumar Behera. He is the strong bridge between me and my research. My parents have been the source of inspiration throughout my life. Today I am here because of their sacrifices, blessings, love and affection. I am so grateful to my grandfather Late. Khatia Behera.

Grateful to Goddess Maa Kali, Dhadasahi for being with me.

Sincerely,

Santosh Kumar Behera

~Synopsis~

Molecules upon electronic excitation undergoes electron redistribution which often enhances the charge donating ability of the donor and accepting capacity of the acceptor, similarly acidity of the acid group and basicity of the basic group. This will lead to intramolecular charge transfer (ICT) state in system in which donor and acceptor are connected by a spacer and proton transfer in system which contains the acidic and basic groups.

Grabowski *et al.* proposed that the donor is nearly perpendicular to the other part of the molecule in the highly polar ICT state known as twisted ICT (TICT) state. The TICT mechanism states that the emission occurs from the locally excited state as well as the TICT state.

Excited state intramolecular proton transfer (ESIPT) is a photoinduced proton transfer process which also leads to dual emission. ESIPT is basically a photo tautomerisation in which a proton transfers from acidic group to basic group via intramolecular hydrogen bond. This phototautomer generally produces a large Stokes shifted fluorescence.

No doubt, ESIPT and ICT processes are individually gained attention. Simultaneously, some structural modifications of ESIPT/ICT dyes lead to an interesting photoinduced process called proton coupled charge transfer. The coupling between these two (ICT and ESIPT) processes primarily depends on molecular structure of the fluorophores.

In this thesis TICT and ESIPT of some organic molecules were investigated. The thesis was spitted into eight chapters and a summary of the chapters are presented below:

Chapter 1: Introduction

This chapter gives a brief description to TICT, ESIPT and proton coupled charge transfer process with literature survey. The chapter ends with a brief note on motivation for the present thesis work.

Chapter 2: Material, Methods and Instrumentations

The second chapter provides the details about the source of the chemicals and the solvents used in the present work and the procedures followed for the syntheses of fluorophores. This chapter also elaborates preparation of the samples and the methods used for the analyses as well as for the calculations. In addition, the details of some of the important instruments used are also concisely discussed.

Chapter 3: Relay Proton Transfer Triggered Twisted Intramolecular Charge Transfer in 2-(4'-*N*,*N*-Dimethylaminophenyl)imidazo[4, 5-c]pyridine

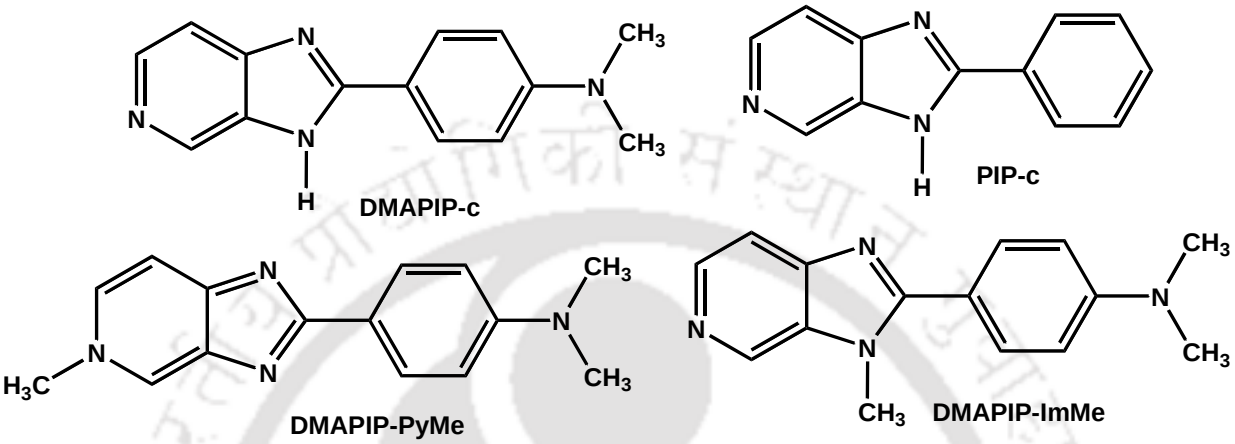

Chart 1: Structure of DMAPIP-c and related molecules.

Chapter 3 covers the investigations of mechanism for the dual emission of 2-(4'-*N*, *N*-dimethylaminophenyl)imidazo[4,5-c]pyridine (DMAPIP-c) in protic solvents (**Chart 1**). Theoretical calculations were carried out to corroborate the experimental findings. Unlike DMAPIP-c, the methyl derivatives do not emit dual fluorescence in protic solvents. The deprotonation studies suggest that the enhancement in TICT emission of anionic form of DMAPIP-c is limited to protic environment. The spectral characteristics of DMAPIP-c were also studied in methanol-acetonitrile binary solvent mixture. The relative intensity of the TICT emission (with respect to that of normal emission) rises with methanol amount in the acetonitrile–methanol binary solvent mixture. The studies also show that a 1:3 hydrogen bond complex is formed between DMAPIP-c and protic solvent and it is responsible for the TICT emission (**Scheme 1**). Based on the results a relay proton transfer tiggered TICT emission is proposed (**Scheme 2**). The emission energies obained by TDDFT calculations were also very close to experimental values.

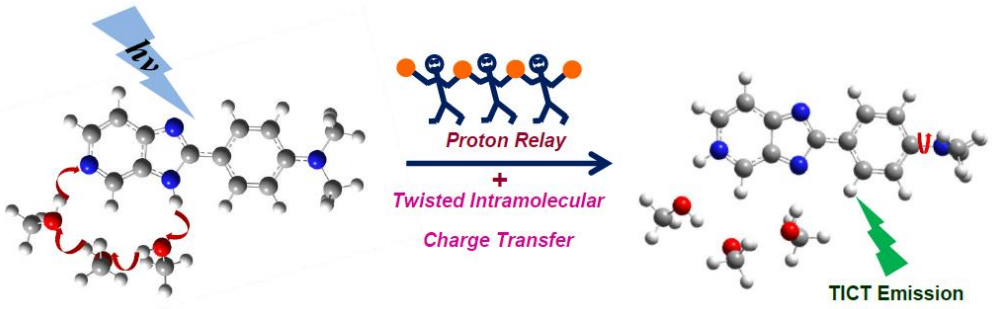

Scheme 1: Three methanol molecules are involved in the proton relay process.

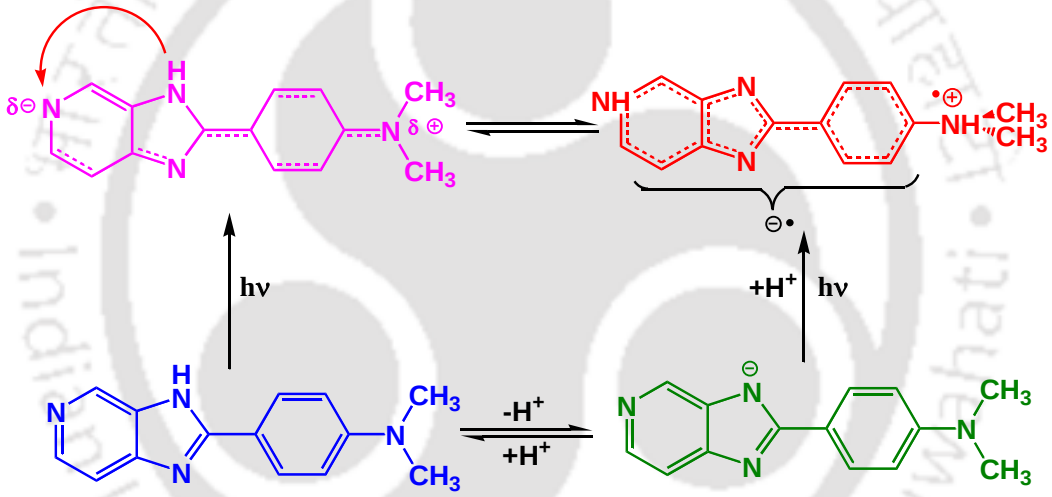

Scheme 2: The path for the formation of the TICT state.

Chapter 4: Intramolecular Proton Transfer Triggered Twisted Intramolecular Charge Transfer in Cucurbit-7-uril: Role of Internal Water.

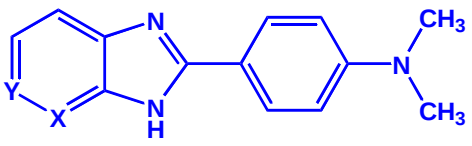

DMAPIP-b, X = N, Y = CH

DMAPIP-c, X = CH, Y = N

Chart 2: Structure of DMAPIP-b and DMAPIP-c.

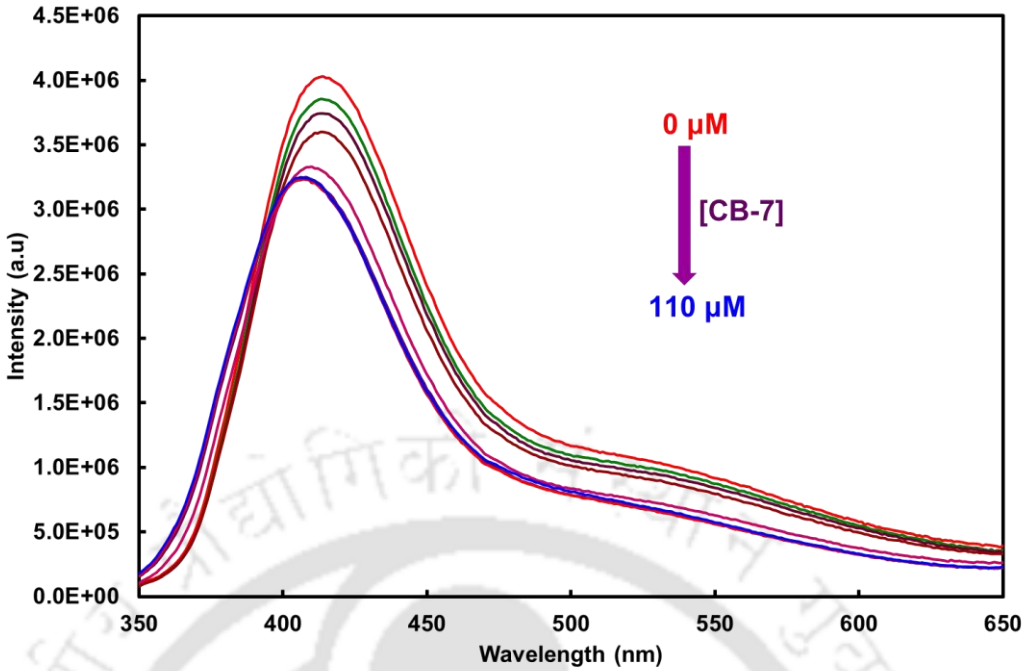

Figure 1: Fluorescence spectra neutral DMAPIP-c with varying concentration of CB-7. (λ_{exc} = 335 nm)

This chapter reports the spectral properties of the 2-(4'-*N*,*N*-dimethylaminophenyl)imidazo[4,5-b]pyridine (DMAPIP-b) and DMAPIP-c (**Chart 2**) in CB-7 cavity. The chapter divided into two sections. In first section, the interaction of neutral DMAPIP-b and DMAPIP-c with CB-7 is discussed. The fluorophores form 1:1 inclusion complex with CB-7 in aqueous solution. The binding constants obtained for the inclusion complex of these guests with CB-7 is higher than those of with cyclodextrin complex of these guests. The electronic spectral changes and the NMR studies reveal that the guests enter the CB-7 cavity through imidazopyridine moiety. **Figure 1** depicts the fluorescence spectra of DMAPIP-c in different concentration of CB-7. The presence of TICT emissions of guests in CB-7 advocates that the internal water molecules are present along with the guest in the complexes. Further, it is clear that those water molecules are involved in the intermolecular proton transfer (double or relay) process inside CB-7. The relative enhancement of TICT emissions of guest molecules in CB-7 depend on the position of nitrogen.

Second section focuses on the effect of CB-7 on the cationic equilibrium of the guests. Additionally, the cationic behaviour of DMAPIP-b is reinvestigated in neat water with fluorescence emission and excitation spectra. The pK_a of these guests in CB-7 are higher in comparison to those in water and cyclodextrin. **Chart 3** depicts the different possible

monocations of DMAPIPs. All the three MCs of DMAPIP-b are present in water at S_0 and S_1 states. Like in water, all the three MCs of DMAPIP-b are also present in CB-7 in both states. But the cationic equilibrium is shifted from more polar MC1 towards less polar MC2 and MC3 in CB-7. In the S_0 state, where DMAPIP-c exists as MC1 and MC3 in water, it is present in all the monocationic form in CB-7. However, in S_1 state it exists as MC2 and MC3 in both water and CB-7. Like in water, MC2 is also formed from MC1 in the excited state by biprotonic tautomerization in CB-7.

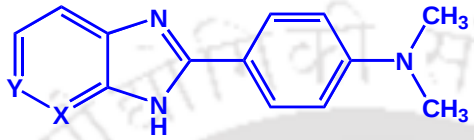

DMAPIP-b, X = N, Y = CH

DMAPIP-c, X = CH, Y = N

Protonation site	Monocation (MC)
N,*N*-Dimethylamino group	MC1
Imidazole nitrogen	MC2
Pyridyl nitrogen	MC3

Chart 3: Monocations of DMAPIP-b and DMAPIP-c.

Chapter 5: Excited State Intramolecular Proton Transfer in 4-(3-(*1H*-benzo[d]imidazol-2-yl)-5-tert-butyl-4-hydroxybenzyl)-2-(*1H*-benzo[d]imidazol-2-yl)-6-tert-butylphenol: Effect of Solvent and pH

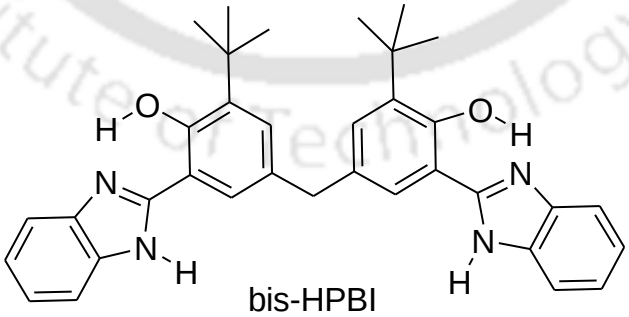

bis-HPBI

Chart 4: Structure of bis-HPBI.

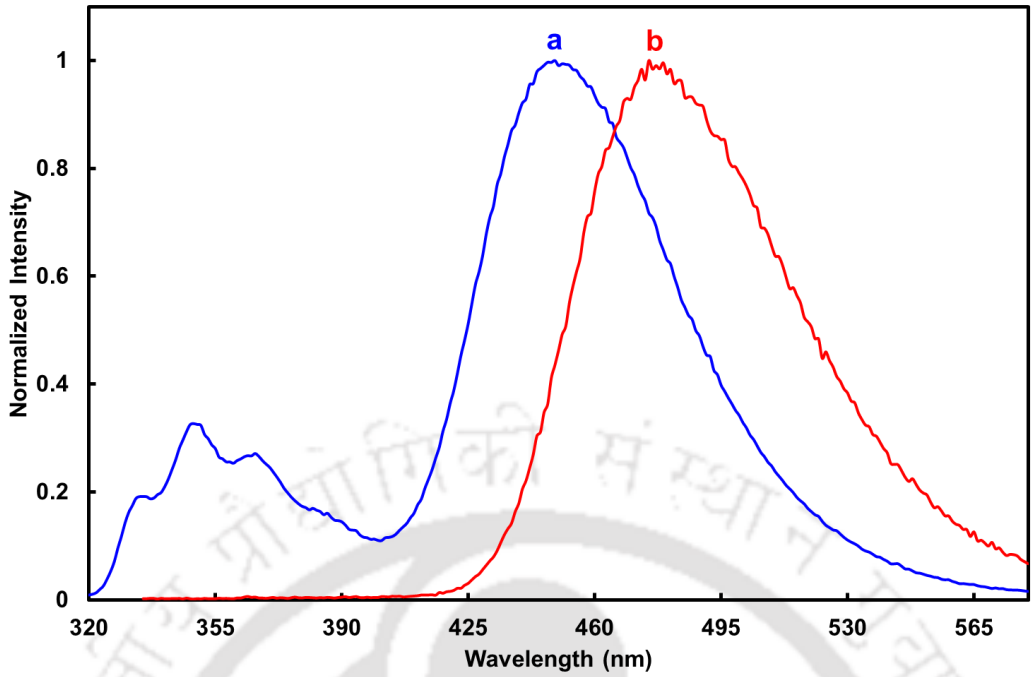

Figure 2. Fluorescence spectra of (a) HPBI and (b) bis-HPBI in methanol.

The fifth chapter describes the ESIPT of a new derivative of 2-(2'-hydroxyphenyl)benzimidazole (HPBI), which contains two alkyl substituted HPBI (bis-HPBI), **Chart 4.** The chapter divided into two sections. In first section, the photophysical properties of bis-HPBI is investigated in various organic solvents and also compared with that of HPBI. Unlike HPBI, bis-HPBI emits exclusively intense tautomer emission in all the solvents including protic solvents with a very faint or no normal emission (**Figure 2**). This may be due to effect of bulky *t*-butyl substituents ortho to –OH group that may obstacles for the formation of *trans*-enol in bis-HPBI. Though bis-HPBI contains two HPBI moities theoretical and experimental studies ruled out a double proton transfer and only one HPBI moieties participated in the process and second one behaves as substituents.

In the second section, the prototropic behaviour of bis-HPBI is invetsiagted in aqueous media and compared with that of HPBI. bis-HPBI is having strong tautomer emission also in neutral aqueous solution like organic solvents. Enhancement of tautomer band intensity upon deprotonation of single –OH also supports the single proton transfer hypothesis in bis-HPBI. On the other hand, the tautomer emission decreases in acidic solution with initial addition of acid due to quenching by hydrogen bonding. At higher concentration when the imdazole nitrogen is protonated the tautomer emission is partially recovered due to dissociation and

reorganization of cation. In strongly acidic solution the dissociation of –OH group from cation is prevented and emission observed only from cation of bis-HPBI.

Chapter 6: Aggregation Induced Enhanced Emission of 4-(3-(benzo[d]thiazol-2-yl)-5-tert-butyl-4-hydroxybenzyl)-2-(benzo[d]thiazol-2-yl)-6-tert-butylphenol

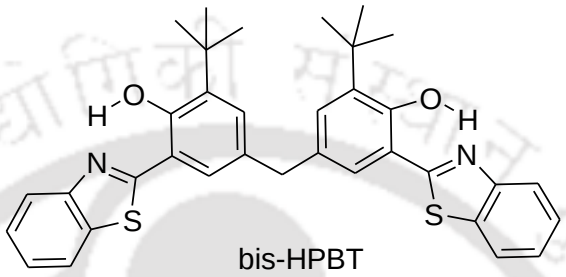

bis-HPBT

Chart 5: Structure of bis-HPBT

This chapter elaborates the investigations of the aggregation-induced emission enhancement of the 4-(3-(benzo[d]thiazol-2-yl)-5-tert-butyl-4-hydroxybenzyl)-2-(benzo[d] thiazol-2-yl)-6-tert-butyl phenol (bis-HPBT, **Chart 5**). The fluorophore is insoluble in water and well soluble in THF. The absorption and fluorescence spectral studies reveal that at higher water fractions (f_w) the molecule aggregates to form fibres. At f_w= 70 %, it is observed that bis-HPBT exhibits maximum aggregation induced enhance emission AIEE (**Figure 3**). The red shifted absorption spectra and the increase in fluorescence intensity indicates that bis-HPBT exhibits J-aggregation. The DFT calculations also suggests that the bis-HPBT is non-planar as it is substituted by bulky *tert*-butyl groups and therefore, full face to face stacking is not possible in aggregated state. Another remarkable characteristic of bis-HPBT is almost exclusively highly Stokes shifted tautomer emission is observed from aggregates. AIEE is due to restricted intramolecular rotation of Carbon-Carbon bond connecting the hydroxyphenyl ring and benzthiazole ring. The aggregated structure is very sensitive to ions and the aggregation is ruptured upon interaction with ions. The aggregate emission is also observed inside the HeLa cell.

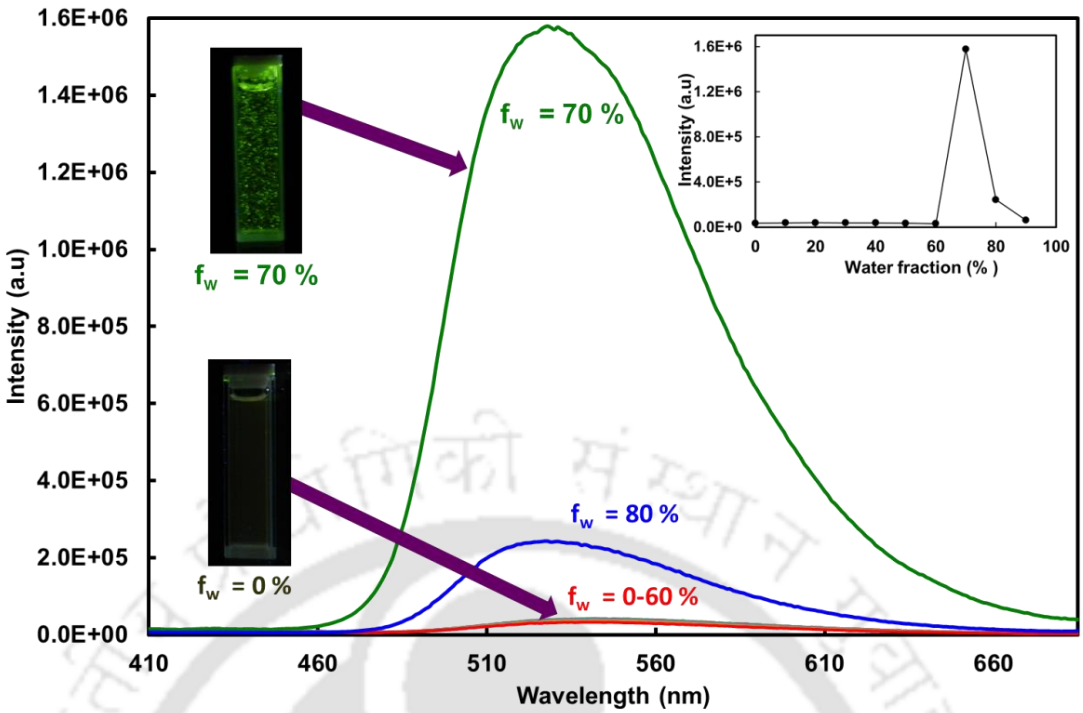

Figure 3: Fluorescence emission spectra of bis-HPBT in different water/THF mixtures, λ_{exc} = 365 nm. Inset shows the variation of fluorescence intensity with increase in water fraction.

Chapter 7: Intramolecular Proton Transfer versus Intramolecular Charge Transfer in 2-(4'-amino-2'-hydroxyphenyl)-*1H*-imidazo-[4,5-c]pyridine: Effect of Solvent and pH

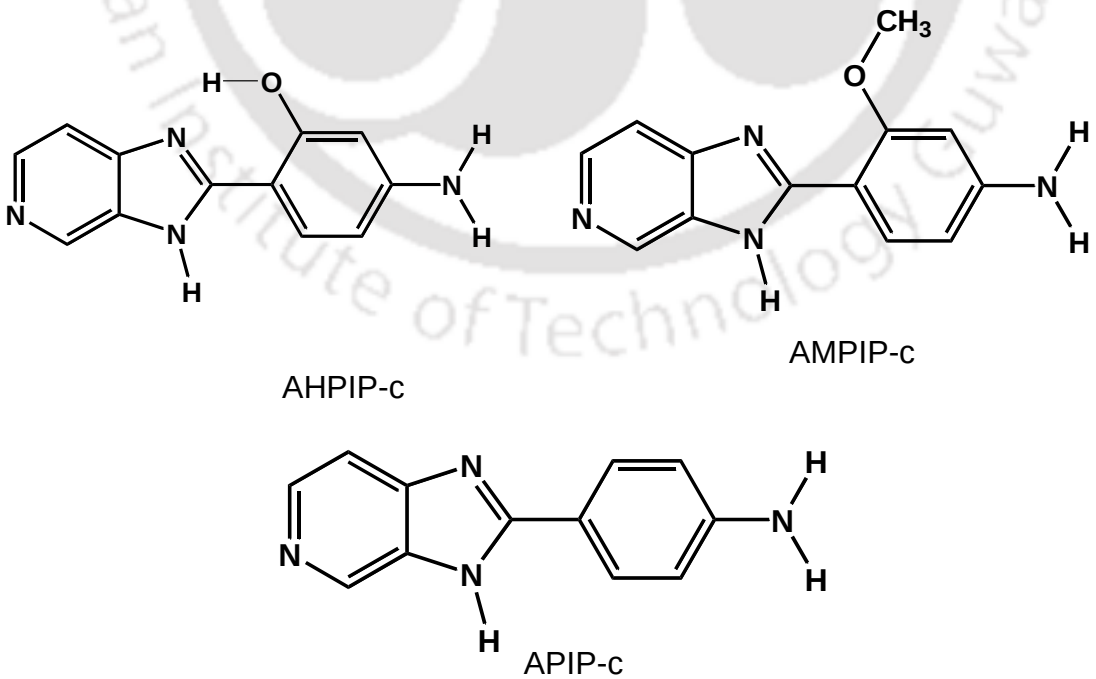

Chart 6: Structure of AHPIP-c and related molecules.

Chapter 7 contains the spectral behaviour of a new molecule, 2-(4'-amino-2'-hydroxyphenyl)-*1H*-imidazo-[4,5-c]pyridine (AHPIP-c). The main objectives of the studies are to ascertain the roles of intermolecular hydrogen bond, intramolecular hydrogen bond and proton transfer in the ICT process and to find whether intramolecular hydrogen bond or proton transfer is competent enough to promote ICT. AHPIP-c exhibits normal and tautomer emissions in aprotic as well as in protic solvents due to ESIPT. To comprehend the competition between the ICT and ESIPT processes, the photophysical properties of methoxy derivative, 2-(4'-amino-2'-methoxyphenyl)-*1H*-imidazo-[4,5-c]pyridine (AMPIP-c), 2-(4'-aminophenyl)-*1H*-imidazo-[4,5-c]pyridine (APIP-c) and PIP-c (**Chart 6**) were also investigated. APIP-c displays twisted ICT (TICT) emission only in protic solvents, on the other hand, when –OH group of AHPIP-c is replaced by $–OCH_3$ group, AMPIP-c emits weak TICT emission in methanol.

Chapter 8: Summary and Scope for the Future Work

The thesis ends with a summary of the presnt work and scope for the future work.

Contents

List of abbreviations

ADC	Analogue to Digital Converter
AR	Analytical Grade
AIE	Aggregation Induced Emission
AIEE	Aggregation Induced Emission Enhancement
AHPIP-c	2-(4'-amino-2'-hydroxyphenyl)-*1H*-imidazo-[4,5-c]pyridine
AMPIP-c	2-(4'-amino-2'-methoxyphenyl)-*1H*-imidazo-[4,5-c]pyridine
CB	Cucurbit-n-uril
CD	Cyclodextrin
CIS	Configuration Interaction Singles
DFT	Density Functional Theory
DHIA	*N*,*N*′-di[3-Hydroxy-4-(2′-benzothiazole)phenyl]isophthalic amide
DHBIA	*N*,*N*′-di[3-Hydroxy-4-(2′-benzothiazole)phenyl]5-tert-butyl-isophthalicamide
DMAP	4-(Dimethylamino)pyridine
DMAPIP-b	2-(4′-*N*,*N*-Dimethylaminophenyl)imidazo[4,5-b]pyridine
DMAPIP–c	2-(4′-*N*,*N*-Dimethylaminophenyl)imidazo[4,5-c]pyridine
DMF	*N*,*N*-Dimethylformamide
DMABN	4-Dimethylaminobenzonitrile
DMSO	Dimethylsulfoxide
DSC	Differential Scanning Calorimetry
ESIPT	Excited State Intramolecular Proton Transfer
ESPT	Excited State Proton Transfer
HOMO	Highest Occupied Molecular Orbital

HPBI	2-(2'-Hydroxyphenyl)benzimidazole
bis-HPBI	4-(3-(1H-benzo[d]imidazol-2-yl)-5-tert-butyl-4-hydroxybenzyl)- 2-(*1H*-benzo[d]imidazol-2-yl)-6-tert-butylphenol
HPBO	2-(2'-Hydroxyphenyl)benzoxazole
bis-HPBO	4-(3-(benzo[d]oxazol-2-yl)-5-tert-butyl-4-hydroxybenzyl)-2-(benzo[d]oxazo-2-yl)-6-tert-butylphenol
HPBT	2-(2'-Hydroxyphenyl)benzothiazole
bis-HPBT	4-(3-(benzo[d]thiazol-2-yl)-5-tert-butyl-4-hydroxybenzyl)-2-(benzo[d]thiazol-2-yl)-6-tert-butylphenol
HPIP-b	2-(2'-Hydroxyphenyl)-3*H*-imidazo[4,5-*b*]pyridine
HRMS	High Resolution Mass Spectrometry
ICT	Intramolecular Charge Transfer
ImMe	1-Methyl-2-(4′-(*N*,*N*-dimetylaminophenyl)imidazo[4,5-b]pyridine
IEF-PCM	Integral Equation Formalism-Polarizable Continuum Model
IPT	Intramolecular Proton Transfer
LUMO	Lowest Unoccupied Molecular Orbital
MC	Monocation
MCP	Micro-Channel Plate
MO	Molecular Orbital
NMR	Nuclear Magnetic Resonance
OLED	Organic Light Emitting Diode
PMT	Photomultiplier Tube
PIP-c	2-(2'-Hydroxyphenyl)-*1H*-imidazo [4,5-*c*]pyridine

PT	Proton Transfer
Py-Me	*N*,*N*-Dimethyl-4-(4-methyl-*4H*-imidazo[4,5-b]pyridin-2-yl) Benzenamine
RIR	Restricted Intramolecular Rotation
TAC	Time-to-Amplitude Converter
TCSPC	Time Correlated Single Photon Counting
TDDFT	Time Dependent Density Functional Theory
TGA	Thermal Gravimetry Analysis
TICT	Twisted intramolecular charge transfer
THF	Tetrahydrofuran
TLC	Thin Layer Chromatography
UV	Ultraviolet
UV-Vis	Ultraviolet-Visible

List of Figures

Figure 7.7. Fluorescence spectra of AMPIP-c in (1) cyclohexane, (2) ethylacetate, (3) dioxane, (4) acetonitrile, (5) 1-propanol, and (6) methanol, λ_{exc} =310nm.

Figure7.8. The instrument response function (a) and the fluorescence decays of AMPIP-c in methanol (b) along with fitted curve and residue plot, λ_{em} = 385 nm.

Figure 7.9. Lippert-Mataga plot using normal emission of APIP-c (●), AMPIP-c (■), and AHPIP-c (▲).

Figure 7.10.Fluorescence spectra of PIP-c in different solvents: (1) ether, (2) butanol, (3) 1-propanol, (4) ethanol, (5) methanol, λ_{exc} = 290 nm.

List of Tables

Table 7.3. Absorption Band Maxima (λ_{max}^{ab}, nm) and Fluorescence Band Maxima (λ_{max}^{fl}, nm) of AHPIP-c in Different Solvents.

Table 7.4. Fluorescence Lifetime of Shorter Wavelength Emission (τ_S , ns) and Longer Wavelength Emission (τ_L , ns) of AHPIP-c in Different Solvents Along With The Corresponding Chi Square (χ^2).

Table 7.5. Absorption Band Maxima (λ_{max}^{ab}, nm) and Fluorescence Band Maxima (λ_{max}^{fl}, nm) of AMPIP-c in Different Solvents.

Table 7.6. Fluorescence Lifetime of AMPIP-c in Different Solvents Along With the Corresponding Chi Square (χ^2), λ_{em} = 385 nm (Values in the Parentheses are the Relative Amplitudes).

Table 7.7. DFT Optimized Parameters for AHPIP-c, AMPIP-c and APIP-c.

Table 7.8. Absorption Band Maxima (λ_{max}^{ab}, nm) and Fluorescence Band Maxima (λ_{max}^{fl}, nm) of PIP-c.

List of Charts

List of Schemes

Chapter 1

Introduction

1.0. Introduction

1.1. Dual Fluorescence

The intramolecular charge transfer (ICT) and intramolecular proton transfer (IPT) are some of the excited state processes that leads to dual fluorescence.

1.2.0. Intramolecular Charge Transfer

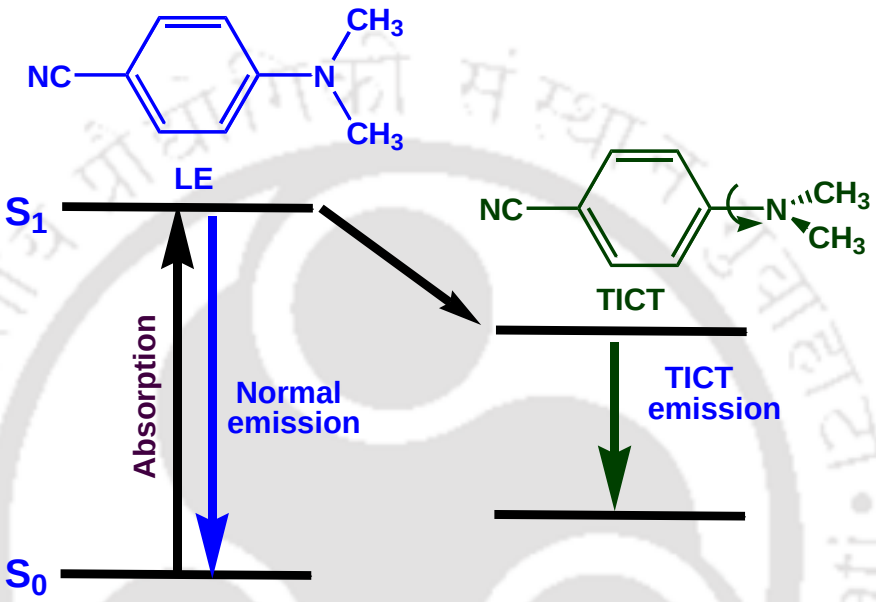

Scheme 1.1. Dual emission due to TICT process.

Absorption of photon by organic molecules having electron donor and acceptor connected by a spacer or a single bond, triggers the charge transfer from the donor to the acceptor in the electronic excited state of the molecule. As a result, the dipole moment of the molecule is enhanced and it relaxes to a highly polar and more stable state known as the ICT state. This photoinduced process causes dual fluorescence, the emissions take place from both the locally excited state and the ICT state.[1-7] Of the different mechanisms proposed to understand the formation of the ICT state, twisted ICT (TICT) is the most accepted one.[6-12]

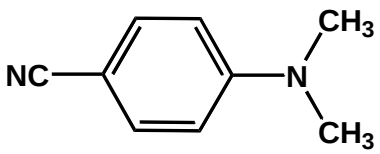

Chart 1.1. Structure of 4-Dimethylaminobenzonitrile.

4-Dimethylaminobenzonitrile (DMABN, **Chart 1.1**) is an archetypal donor-acceptor system emitting dual fluorescence in polar solvents because of TICT.[1] According to the TICT model, the charge transfer from donor to acceptor moiety in the excited state is accompanied by the rotational relaxation of the donor moiety from the planar to a perpendicular (twisted) conformation called TICT state (**Scheme 1.1**). As photoinduced ICT plays an important in photochemical and photobiological processes including photosynthesis, vision and mutation of nucleic acid (DNA) base pairs, the interest on ICT has multiplied.[13-16]

1.2.1. Factors Affecting the ICT Emission

It is well established that the polarity and the viscosity of the medium control the formation and stabilization of the ICT state in many ICT emitting fluorophores. The effects of polarity, viscosity and hydrogen bonding on ICT emission are briefly discussed below:

1.2.2. Polarity and Viscosity

Due to the polar nature of the ICT state, the rate of formation and stabilization of the ICT state increases with enhancing the polarity of the environment. 5-(4-dimethylamino-phenyl)-penta-2,4-dienoic acid methyl/ethyl esters exhibit single emission in nonpolar solvent and dual emission in polar solvents (**Chart 1.2**).[17,18] Recently, Righini *et al.*found that the formation of ICT state of *all*-trans-β-Apo-8′-carotenal depends on the polarity and polarizabilty of the solvents. They also found that in polar solvents intensity of the ICT band increases.[19] But in general, the increase in polarity does not affect the ICT emission monotonically.[1,2, 20-23] As the ICT state is stabilized in polar solvents, the nonradiative decay from the ICT state to the low lying states also affected by the polarity of the media. *E.g.*, the dipole moment of TICT state of DMABN (**Scheme 1.1**) is more than that in triplet state due to appreciable charge transfer character of the TICT state.[1,2] As a consequence, with rise in polarity the energy gap between the TICT state and the triplet state decreases. According to energy gap law of nonradiative transition, the rate of ISC increases with decrease in energy gap between the triplet and singlet state.[24,25] Hence, the triplet yield of DMABN increases and TICT emission decreases, as the polarity of the medium increases.[26] Large solvatochromic shift of the emission band and very high dipole moment value indicate that the ICT process is strongly dependent on the polarity of the medium.

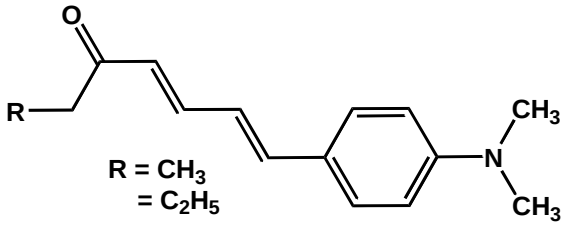

Chart 1.2. 5-(4-dimethylamino-phenyl)-penta-2,4-dienoic acid methyl/ethyl esters.

It is obvious that the twisting motion primarily depends on the viscosity of the medium. As TICT generated by twisting of the donor group, the medium viscosity also affects the formation of the TICT state. Upon increasing the viscosity of the medium the barrier of twisting increases and thus the formation of TICT state is less favoured. TICT process of molecules having small donor group is almost independent of viscosity.[27,28] But, at very high viscosity the TICT process may be affected as friction plays an important role.[29-31] On contrary, when the rotating group is bulky, even with moderate viscosity the rate TICT process decreases.[32]

Apart from these factors, hydrogen bonding plays a vital role in the formation and stabilization of ICT state.[33] The role of hydrogen boding in the ICT process is briefly explained in the following sections.

1.2.3. Hydrogen Bonding with Electron Donor

Cazeau-Dubroca *et al*. reported the effect of hydrogen bonding of the solvent on the donor group.[34-37] They suggested that hydrogen bonding of the solvent with charge donor produces a twisted conformer in the ground state and such ground state twisted conformer upon excitation emit ICT fluorescence. The Cazeau-Dubroca hypothesis was severely challenged by Al-Hassan and Azumi. They observed the of longer wavelength emission in non-hydrogen bonding polymer matrices also.[38] Cazeau-Dubroca*et al*. claimed that the presence of water traces introduced in the non-hydrogen bonding polymer matrices is the cause for the dual fluorescence of DMABN.[39] Although Kijimato *et al.*'s study supports the Cazeau-Dubroca's hypothesis[40] due to the absence of any clear evidence to substantiate the mechanism. Therefore, the Cazeau-Dubroca's hypothesis was easily rejected. In addition, few groups established that the ground state hydrogen bonding at the donor does not promote ICT rather it retards the formation of the ICT state in DMABN.[41,42] Zachariasse *et al.* reported that the ground state twist of the amino group is not essential for the ICT emission of DMABN derivatives, 3,5-dimethyl-4-(dimethylamino)benzonitrile (**Chart 1.3**).[43]

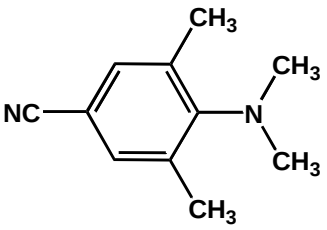

Chart 1.3. Structure of 3,5-dimethyl-4-(dimethylamino)benzonitrile.

Dreuw *et al.* investigated the role of water in the ICT emission of 4-(dimethylamino)methylbenzoate. Based on the theoretical calculations, they predicted that in the gas phase it is the dimethylamino nitrogen hydrogen bonded complex but not the carboxylate hydrogen bonded molecule that is responsible for the ICT emission.[44]

Aminocoumarins are also the interesting class of molecules having different type of hydrogen bonding between the amino group and the solvents. It was proposed that in ground state, the electron donating amino group acts as a hydrogen bond donor (**Chart 1.4**).[45,46] Conversely, such hydrogen bonds favour the formation of the ICT state. Recently, Krystkowiak *et al.* reported the deactivation of 6-aminocoumarin via ICT in the excited state through hydrogen bonding with various solvents having hydrogen bond accepting capacity.[47] On the basis of *ab initio* study, they also showed that structure with five interacting water molecules in the surrounding to amino group of 6-aminocoumarin is the most stable structure.[48]

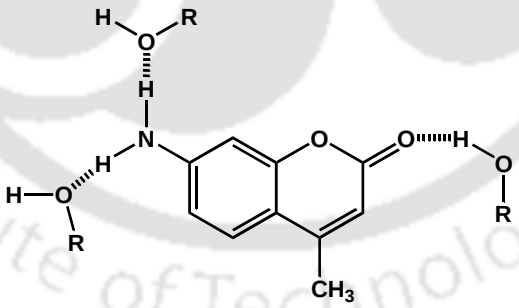

Chart 1.4. Structure of aminocoumarin with hydrogen bonding with protic solvent.

1.2.4. Hydrogen Bonding With Electron Acceptor

Several studies reveal that hydrogen bonding with the electron acceptor accelerates the flow of charge from the donor to the acceptor, thereby favours the ICT process. Ma *et al.* reported the formation of a hydrogen bond between methanol and cyano group in the ICT state of DMABN**.** Their report suggested that the charge separation in the ICT state favours the hydrogen bond formation between cyan group of DMABN and methanol.[49] Zhao *et al.* based

on their results, proposed that the hydrogen bond between the cyano group and methanol is strengthened in the TICT state, which can facilitate the deactivation process of the excited DMABN in methanol via internal conversion.[50]

Cazeau-Dubroca *et al.* based on their hypothesis suggested that the hydrogen bonding of ethanol with dimethylamino group is responsible for the formation of the ICT state of 4-(dimethylamino)pyridine(DMAP, **Chart 1.5**).[36] However, Araki *et al.* showed that the pre-twisted conformer is not responsible for the ICT emission of 4-(dimethylamino)pyridine.[51] Later on the studies of Herbich *et al.* and Demeter *et al.* revealed that the hydrogen bonding of the protic solvent with pyridine nitrogen of 4-(dimethylamino)pyridine is responsible for the ICT emission in hexane.[52-54]

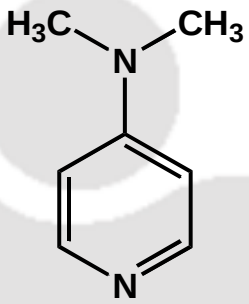

Chart 1.5. Structure of 4-(dimethylamino)pyridine.

Herbich *et al.* also investigated the photophysics of 4-dialkylaminopyrimidines (**Chart 1.6**) class of donor-acceptor systems similar to DMAP.[41,42,52] They observed only single emission from the ICT state for *ortho*-substituted analogue of 4-dialkylaminopyrimidine (**Chart 1.6b**). But 4-dialkylaminopyrimidine emits both normal emission and the ICT emission in polar aprotic solvents. The weak ICT emission of 4-dialkylaminopyrimidine is well developed in presence of protic solvents or Zn^{2+} ions (**Chart 1.6c**). Further monoexponetial decay of the ICT emission indicates that only single hydrogen bonded complex is responsible for the ICT emission. This was assigned to the hydrogen bond formed through pyrimidine nitrogen para to amino group.

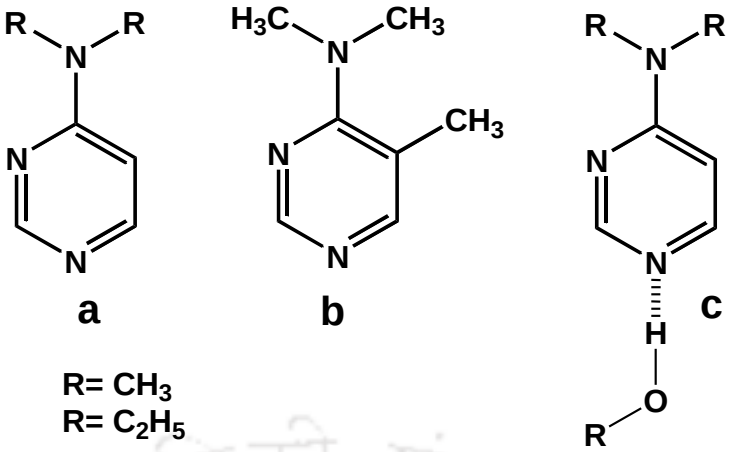

Chart 1.6. Structure of 4-dialkylaminopyrimidines.

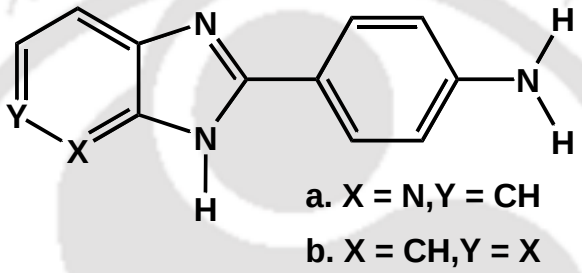

Chart 1.7. Structures of 2-(4'-aminophenyl)-pyridoimidazoles.

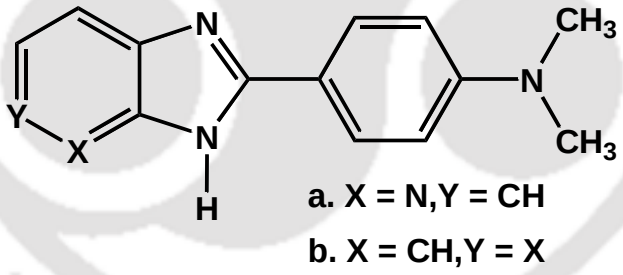

Chart 1.8. Structures of **2**-(4'-*N*,*N*-dimethylaminophenyl)-pyridoimidazoles.

Aminophenylpyridoimidazoles belongs to a special type of TICT exhibiting molecules, where the hydrogen bonding is essential for the ICT emission (**Charts 1.7** and **1.8**). Fasani *et al.* found that the dual emission from 2-(4'-aminophenyl)-pyridoimidazoles only in alcoholic solvents and not in nonpolar or polar aprotic solvents (**Chart 1.7**).[55] They suggested that emissions arise from the locally excited state as well as from tha TICT state. They also hypothesized that the protic solvents form hydrogen bond with hydrogen of the azole nitrogen and the 'NH' hydrogen. This twists the pyridoimidazole moiety perpendicular to form the twisted conformer of the TICT state. But, Fasani model did not assign any role for the pyridyl

nitrogen in the TICT process. But, later studies clearly established both the presence and position of pyridyl nitrogen are crucial for TICT emission in 2-(4'-*N*,*N*-dimethylaminophenyl)imidazo[4,5]pyridines (**Chart 1.8**).[56,57] In addition acceptor twisting model was rejected by studies of Krishnamoorthy and Dogra.[56]

1.3.0. Excited State Proton Transfer

As discussed earlier, excited state PT is one morephoto induced process that also leads to dual emission. PT is more facile in the excited state as acid and base become stronger acid and base in the excited state and are called photo acid and photo base, respectively. Kasha classified the PT phenomena based on their mechanisms as excited state intramolecular proton transfer (ESIPT), concerted biprotonic transfer and proton relay transfer.[58]

1.3.1 Excited State Intramolecular Proton Transfer

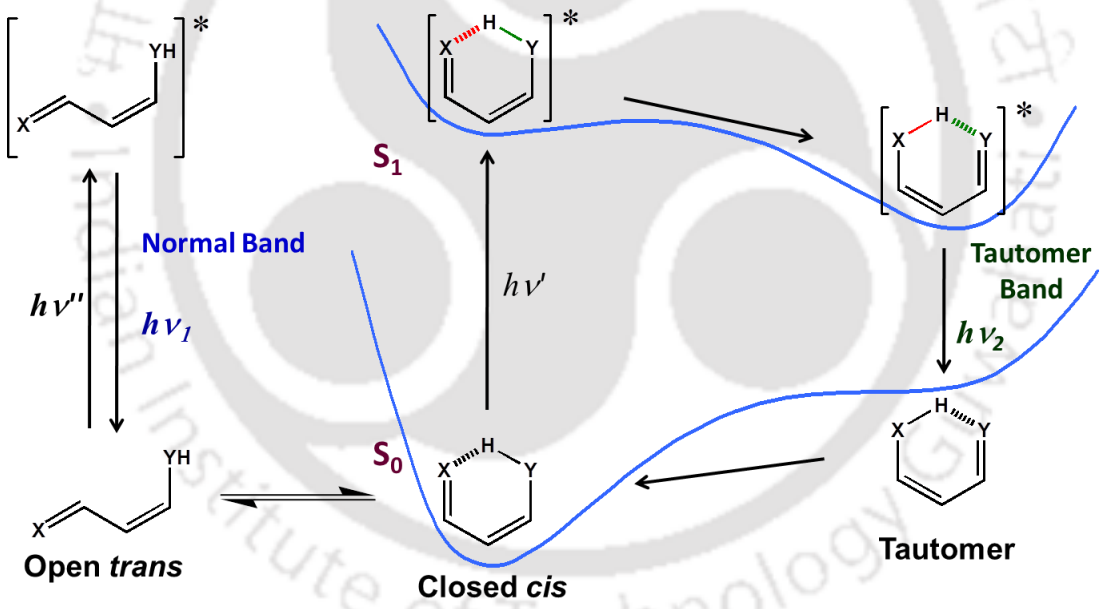

Scheme 1.2. Dual emission due to ESIPT process.

ESIPT has gained special attention among the photochemists and photophysicists owing to its fundamental importance in science and technology. ESIPT is basically a photo tautomerisation in which a proton transfers from a protic acidic group to nearby basic group in electronic excited state of the molecule via intramolecular hydrogen bond.[59,60] This phototautomer generally produces a large Stokes shifted emission, which is the desired feature

to avoid self-absorption and the inner filter effect. The ESIPT leads to dual fluorescence as shown by a cycle (**Scheme 1.2**).

1.3.2. Factors Affecting ESIPT

ESIPT is highly sensitive to the nature of environment. The ESIPT process is poorly dependent on viscosityof the solvents as it follows an intramolecular hydrogen bonded cyclic path (**Scheme 1.2**). However it depends on the polarity and strongly on the protic nature of the solvents.[61-64] The microheterogenious environments also perturbs the ESIPT of several molecules.[65-67] In addition to the effect of solvents, substitution also affects the ESIPT process of several molecules. The effects of solvent and substitution on ESIPT were briefly discussed below.

1.3.3. Effect of Solvents on ESIPT

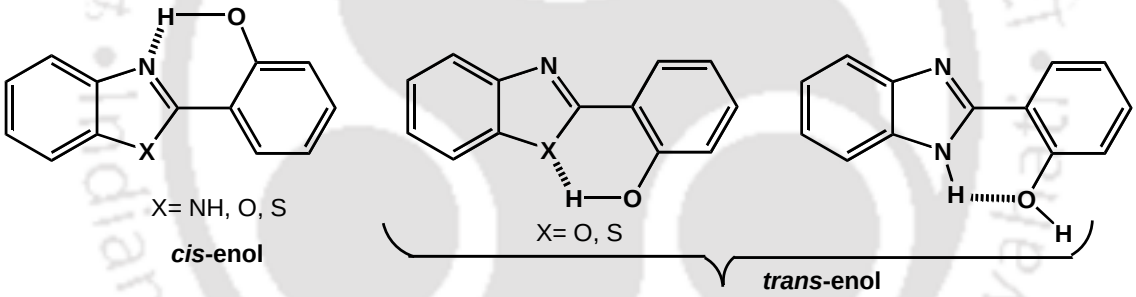

Chart 1.9. *cis*-enol and *trans*-enol conformers of 2-(2'-hydroxyphenyl)benzazole.

The intramolecular hydrogen bond is the main driving force for the ESIPT. Since this intramolecular hydrogen bond is fairly unaffected in aprotic solvents, the ESIPT is more favoured in aprotic solvents. But polarity of the solvent alters the *cis-enol-trans-enol* equilibrium. The relative population of *trans*-enol increases with increase in polarity. On the other hand, in protic solvents the competition between intramolecular hydrogen bonding and intermolecular hydrogen bonding hampers the ESIPT. Therefore, the relative intensities of the normal band and tautomer band change with nature of the solvents. Hence, The ESIPT is highly favoured in nonpolar solvents than in polar or protic solvents. For example, 2-(2'-hydroxyphenyl)benzazole exists as *cis*-enol and *trans*-enol (**Chart 1.9**).[67-72] *Cis*-enol has a hydrogen bond between the hydroxyl group and imidazole nitrogen atom and upon excitation undergoes ESIPT. *Trans*-enol upon excitation produces normal emission. Upon addition of

protic solvents, the intramolecular hydrogen bond that exists in *cis*-enol breaks and equilibrium shifts towords *trans*-enol and intensity of the keto emission decreases.

1.3.4. Effect of Substituents

The proton transfer greatly depends on the acidity of the proton donor group and basicity of the proton acceptor group. It was found that by modifying the molecular structure of the organic molecules, the proton transfer can be controlled/modified. Since the ESIPT behaviour of benzazole derivatives are extensively investigated, the effect of substituents on proton transfer of benzazole derivatives is discussed below.

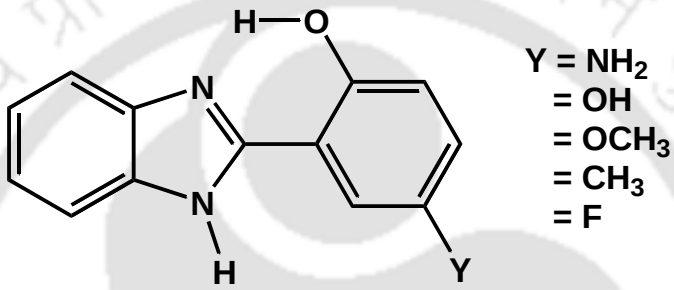

Chart 1.10. Structure of the 2-(2'-hydroxyphenyl)benzimidazole derivatives.

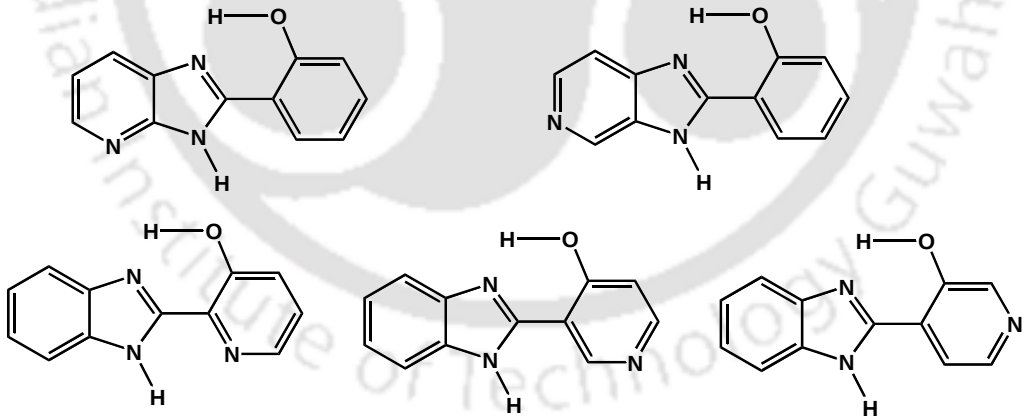

Chart 1.11. Nitrogen substituted analogues of 2-(2' hydroxyphenyl)benzimidazole

Douhal *et al.* proposed that substituion of groups at 5-position (at phenyl moiety) of 2-(2'-hydroxyphenyl)benzimidazole (HPBI) produces a red shift in the absorption and the fluorescence spectra by inducing resonance effect (**Chart 1.10**).[73] Several other reports are also available, where substitution on phenyl as well as benzimidazole moiety alters the spectral properties of HPBI.[74,75] In addition, it was investigated that nitrogen substitution in benzene or

phenolic ring also affects the fluorescence properties of the HPBI (**Chart 1.11**).[76-82] Nitrogen substitutions at benzene ring reduce the quantum yield, whereas substitutions of nitrogen at phenolic ring increase the quantum yield. Zachariasse *et al*. reported the intense tautomer emission from a bridged HPBI even in protic solvents.[83]

2-(2'-aminophenyl)benzimidazole also emits weak tautomer emission. It was found that substitution at amino group affects the proton transfer and proton transfer improved by the substitution of electronegative groups and the maximum enhancement in tautomer emission was observed by the substitution of tosyl group **(Chart 1.12)**.[84-86]

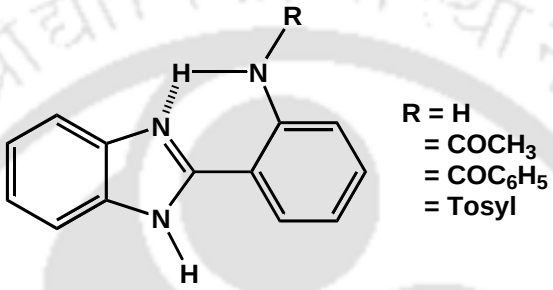

Chart 1.12. Structure of 2-(2'-aminophenyl)benzimidazole and its derivatives.

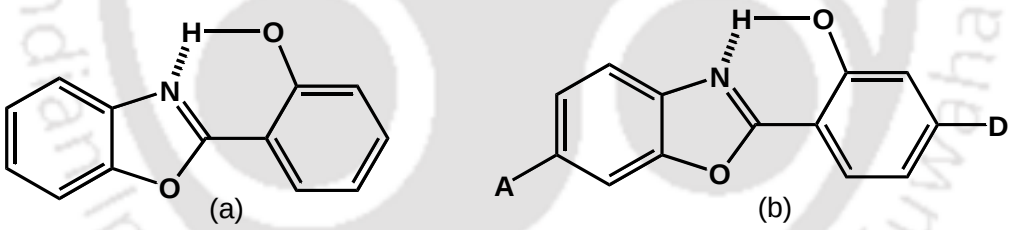

Chart 1.13. Structure of 2-(2'-hydroxyphenyl)benzoxazole and its analogues.

The effect of substitution on the ESIPT of 2-(2'-hydroxyphenyl)benzoxazole (HPBO**, Chart 1.13a**) was also investigated.[87-92] It was found that when HPBO is substituted by methoxy at 3' positionthe fluorescence yield decreases. However, the spectral characteristics of HPBO are almost similar when the methoxy group is substituted at 4'-position.[93] Park *et al.* proposed that the tautomer fluorescence of HPBO is red shifted upon substitution of an electron donor and blue shifted upon substitution electron acceptor group **(Chart 1.13b)**.[94] Recently, Douhal *et al.* reported the photodynamics of two HPBO derivatives, where the benzene ring of benzoxazole substituted by $–NH_2$ group at different positions.[95]

The ESIPT behaviour 2-(2'-hydroxyphenyl)benzthiazole (HPBT, **Chart 1.14a)** and its analogous were also investigated.[96-98] Zhao *et al.* found the spectral properties of HPBT can be modulated by attaching rhodamine moiety to HPBT.[99] Recently Chou *et al.* studied a series of 2-(2′-aminophenyl)-benzothiazoles, where proton donor is $–NH_2$ group (**Chart 1.14b**).[100] They found that 2-(2′-aminophenyl)-benzothiazoles which are incapable to undergo proton transfer, undergo ESIPT upon substitution at amino group. Further, their studies inferred that the electron withdrawing substitution at amino group fastened the proton transfer than the electron donating group. They also found that the substitution at aniline moiety also affects the proton transfer process.

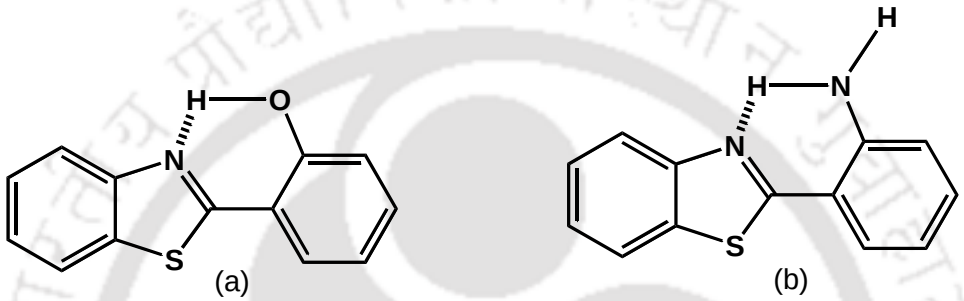

Chart 1.14. Structures of 2-(2'-hydroxyphenyl)benzthiazole and 2-(2′-aminophenyl)-benzothiazole.

1.3.5. Solvent Mediated Proton Transfer

In some cases the itramolecular proton transfer is not possible due to long distance between proton donor and acceptor. But in those cases proton transfer may occurs through solvent molecules. The solvent mediated biproton transfer and relay proton transfer are the two major ways to peruse these processes.

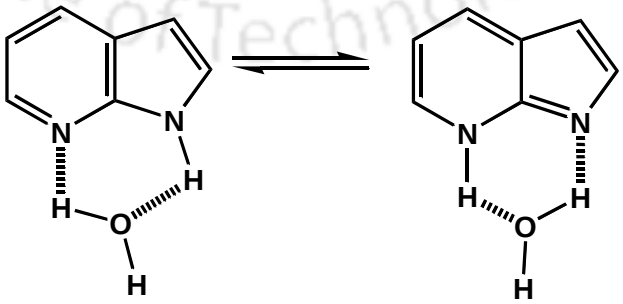

Scheme 1.3. Double proton transfer in 7-azaindole.

The phenomena of biproton transfer is often observed in 7-azaindole in protic solvents, where protic solvent form intermolecular hydrogen bonds with imidazole 'NH' group and pyridyl nitrogen and the undergoes biproton transfer (**Scheme 1.3**).[101,102]

However, in 3-hydroxyquinoline the proton donor and proton acceptor are farther away from each other, where two protic solvent acts as a bridge between them to undergo suitable proton transfer in excited state (**Scheme 1.4**).[103] This is an example of a three proton relay system.

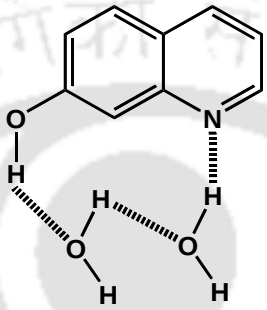

Scheme 1.4. Relay proton transfer in 3-hydroxyquinoline.

1.4.0. ESIPT versus ICT

ESIPT and ICT processes are individually gained attention. Simultaneously, it was found that some structural modification of ESIPT/ICT dyes lead to an interesting photo induced process called coupled proton and charge transfer. The coupling between these two (ICT and PT) processes primarily depends on molecular structures of the fluorophores. Coupled proton and charge transfer reactions play a significant role in many chemical and biological processes. The ICT can either occur prior to PT or after PT.

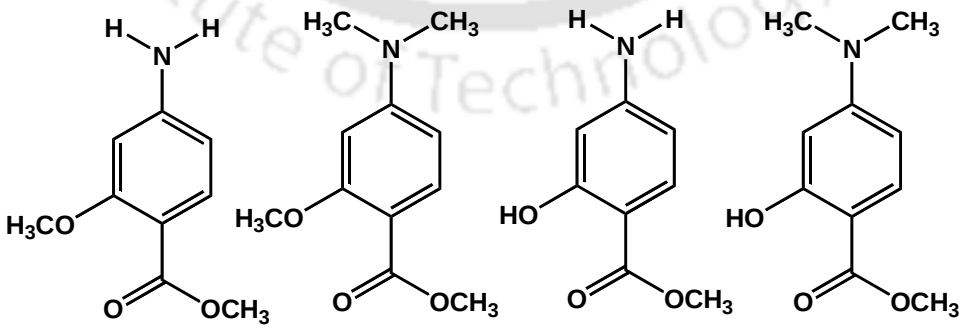

Chart 1.15. Structures of aminosalicylates.

When groups responsible for ESIPT and ICT are combined in the same fluorophores then their photophysical properties become more interesting. Kasha *et al.* illustrated that the emissions can occur from all the three states of *p*-dimethylaminosalicylate, i.e. the locally excited state, the ICT state and the tautomer excited state and compete with each other (**Chart 1.15**).[104-106]

p-*N*,*N*-Dimethylaminobenzoic acid (**Chart 1.16a)** emits only normal emission in nonpolar solvents but Yoon *et al.* found that p-*N*,*N*-dimethylaminosalicylic acid (**Chart 1.16b)** emits ICT emission in nonpolar solvents also.[107,108] Therefore, they proposed that the ESIPT through hydrogen bonding favoured the ICT process. Further they have demonstrated that when the intermolecular hydrogen bonding is supressed by complexation, the ICT emission is enhanced due to intramolecular hydrogen bond that led to ESIPT.

Chart 1.16. Structures of dimethylaminobenzoic and dimethylaminosalicylic acid.

Palit *et al.* reported substituted 1, 3-diketone systems, where proton transfer also directs the charge transfer process (**Chart 1.17**). They observed that in nonpolar solvents ESIPT favours ICT and in polar solvents ESIPT favours TICT.[109]

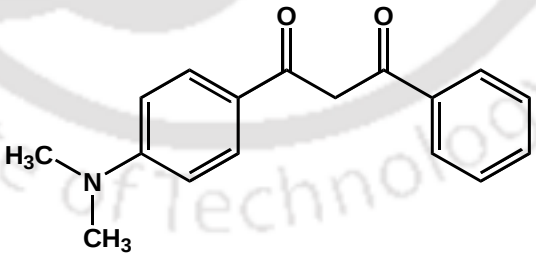

Chart 1.17. Structure of a 1, 3-diketone

Schiff base salicylideneaniline (**Chart 1.18a**) is capable of ESIPT.[110] After the introduction of $-N(C_2H_5)_2$ groups to the salicylideneaniline (**Chart 1.18b**) and it undergoes both proton and charge transfer in excited state. In addition, it was also suggested that the proton transfer is mandatory for charge transfer process.[111] Based on the theoretical investigation it was proposed that the dual emission of a salicylideneaniline derivative, (*E*)-4-

(4-(diethylamino)-2-hydroxybenzylideneamino)benzonitrile (**Chart 1.16c**) is due to charge coupled proton transfer. [112]

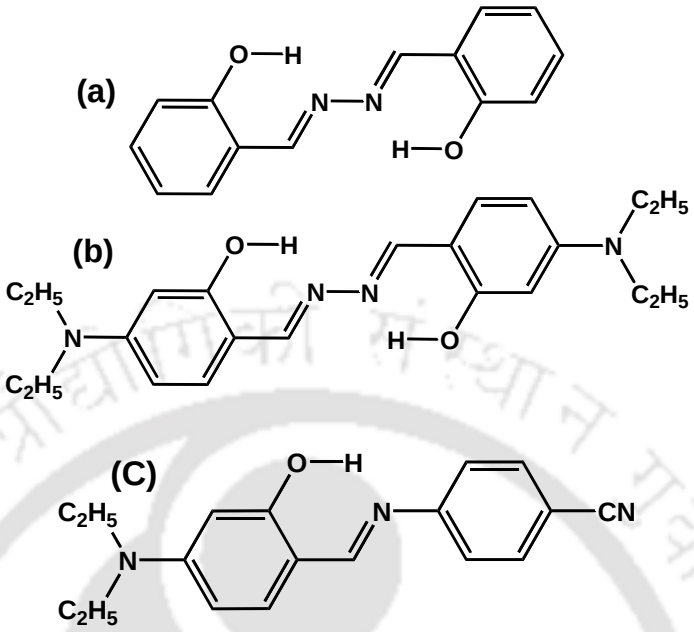

Chart 1.18. Structures of salicylideneanilines.

Rodríguez *et al.* found that 2-(4′-*N*,*N*-diethylamino-2′-hydroxyphenyl)benzimidazole emit normal and tautomer emissions and no ICT emission. However, they proposed ICT from the deprotonated dialkylaminophenol to the protonated benzimidazole in the tautomeric form, but such an ICT process resulted in non-fluorescent tautomer (**Scheme 1.5.**).[113]

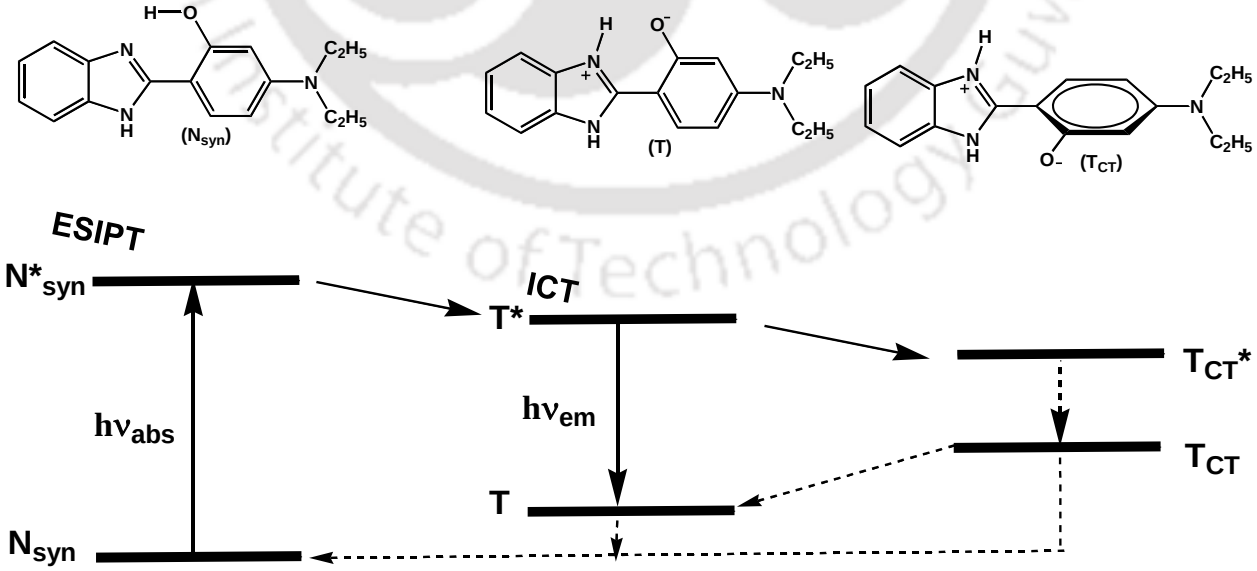

Scheme 1.5. Excited state coupled intramolecular proton and charge transfer of 2-4'-N,N-diethylamino-2'-hydroxyphenyl)benzimidazole.

In addition, the coupled ESIPT-ICT behaviour of some substituted 2'-hydroxyphenylbenzazole also investigated. Chou *et al*. and Park *et al.* reported the coupled proton and charge transfer from a 2'-hydroxyphenylbenzoxazole with an electron withdrawing group to acceptor moiety (**Chart 1.19**) and proposed strong solvatochromic fluorescence from the ICT state created by ESIPT.[64,114]

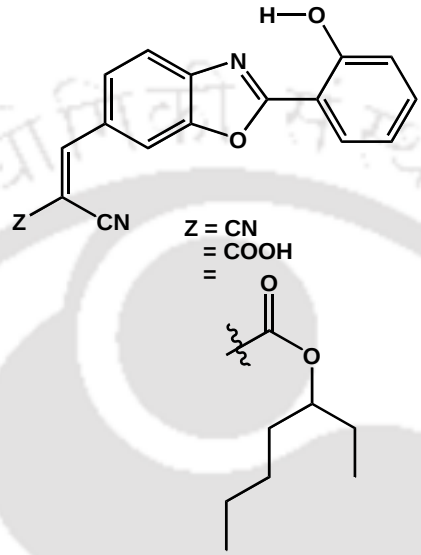

Chart 1.19. Structure of the 2'-hydroxyphenylbenzoxazole derivative.

In 4′-(*N*,*N*-diethylamino)-3-hydroxyflavone and its analogues emissions were observed only from the ICT and phototautomer states, and an equilibrium was established between the two states (**Chart 1.20**).[115-1117] 7-*N*,*N*-Diethylamino-3-hydroxyflavone also emits only dual fluorescence and were observed from ICT and phototautomer states.[118,119] But there was a precursor–successor relationship between the two states (**Scheme 1.6**).

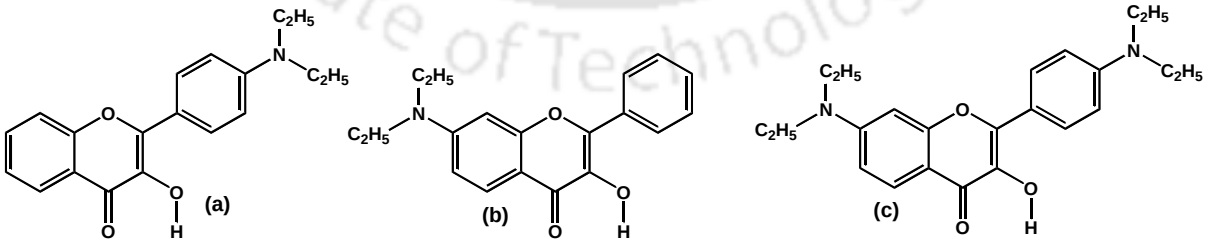

Chart 1.20. Structure of the 3-hydroxyflavones.

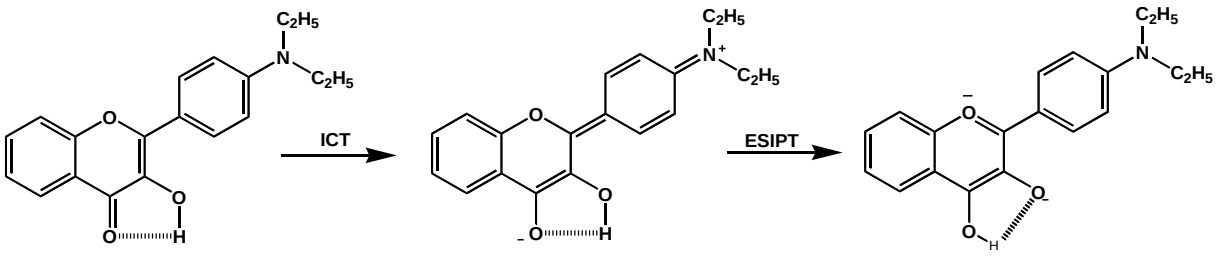

Scheme 1.6. ICT triggered ESIPT in 3-hydroxyflavone.

1.5. Motivation for the Present Work

The motivation for the thesis work is to gain more insight on TICT and ESIPT.

Aminophenylpyridoimidazoles belong to special type of TICT exhibiting molecules (**Charts 1.7 and 1.8**) and protic environment is absolutely essential for the TICT emission of these molecules. The mechanism of TICT of aminophenylpyridoimidazoles is under deep investigation.[55-57] Recently it was ascertained that double proton transfer induced TICT emission of 2-(4'-*N*,*N*-dimethylaminophenyl)imidazo[4,5-b]pyridine (DMAPIP-b, **Charts 1.8a**). In DMAPIP-b only one solvent molecule is sufficient to peruse the double proton transfer.[120] But in 2-(4'-*N*,*N*-dimethylaminophenyl)imidazo[4,5-c]pyridine (DMAPIP-c, **Charts 1.8b**), since the position of pyridyl nitrogen is far away from the imidazole, one protic solvent molecule is not sufficient for the double proton transfer, therefore the studies are performed to understand the TICT emission of DMAPIP-c in protic solvents (**Chapter 3**).

It was investigated that restricted environments modulate the ICT emission of number of dyes.[121-124] In addition, advances in supra molecular chemistry demands suitable host-guest pair for the study. The cucurbit-7-uril (CB-7) is a highly water soluble host among cucurbit-n-uril (CB-n) family and it was also found that the cavity of CB-7 contains some water molecules.[125] Studies revealed that these internal water molecules inside CB-7 cavity is playing a major role for the strong host-guest binding.[125,126] Since, TICT emission of DMAPIP-b and DMAPIP-c is limited only to protic environment; it will be interesting to verify whether DMAPIP-b and DMAPIP-c exhibit TICT emission in CB-7. Such a study will also provide a new insight about the characteristics of internal water molecules of CB-7 cavity. It is reported that the cationic guests have higher binding affinity than the neutral guests towards CB-7.[127,128] However, the effect of CB-7 on the cationic mixture is not investigated. Both DMAPIPs form more than one monocation. Therefore, the studies are extended to investigate the effect of CB-7 on the monocatonic equilibrium of both DMAPIP-b and DMAPIP-c (**Chapter 4**).

As TICT, ESIPT is also an important excited state process that brings dual emission in organic molecules. Current researches focus to modulate the ESIPT behaviour of the dyes by modifying the organic backbone.[129-135] This helps to tune the absorption and emission to longer wavelength. Since, the normal emission is less Stokes shifted it overlaps with the absorption spectrum, therefore it suffers from inner filter effect. Further, as the trans-enol and *cis*-enol are in equilibrium, reduction in the population of *trans*-enol will lead to intense tautomer emission. Therefore, it is good to minimize or completely eliminate the *trans*-enol (which produces normal emission) to obtain exclusive highly Stokes shifted tautomer emission. As stated earlier, the ESIPT behaviour of a benchmark dye HPBI was extensively investigated. To modulate the emissions of HPBI, the ESIPT behaviour of a new HPBI derivative 4-(3-(1H-benzo[d]imidazol-2-yl)-5-tert-butyl-4-hydroxybenzyl)-2-(1H-benzo[d] imidazole-2-yl)-6-tert-butylphenol (*bis*-HPBI) is designed and investigated. The *bis*-HPBI contains two HPBI moieties connected by a methylene linkage and a bulky *tert*-butyl group is substituted at ortho to –OH group in the phenyl ring of HPBI. It is expected the dye emission may affect by these features of *bis*-HPBI. One more interesting option in *bis*-HPBI, it has two HPBI units. Thus it will be interesting to explore whether single unit of HPBI undergo ESPT or both the unit undergo ESIPT. In addition, the effect of acids-bases on the spectral characteristics of *bis*-HPBI is explored (**Chapter 5**).

Some dyes possess weak fluorescence in dilute solution and exhibits intense emission in the aggregate/solid state and the phenomenon is known as aggregation induced enhance emission (AIEE).[136] AIEE earned popularity due to its opposite behaviour to aggregation caused quenching effect. To date variety of AIEE active fluorophores have been designed.[137-145] Recently, AIEE from ESIPT exhibiting fluorophores have gained attention. However, in all those cases not only the tautomer emission, but also the less Stokes shifted normal emission was also observed. Possible AIEE from *bis*-HPBI and its analogues, 4-(3-(benzo[d]oxazol-2-yl)-5-tert-butyl-4-hydroxybenzyl)-2-(benzo[d]oxazol-2-yl)-6-tert-butylphenol (*bis*-HPBO) and 4-(3-(benzo[d]thiazol-2-yl)-5-tert-butyl-4-hydroxybenzyl)-2-(benzo[d]thiazol-2-yl)-6-tert-butylphenol (bis-HPBT) are explored. The main objective was to obtain exclusive AIEE only from the tautomer. In addition, the utility of AIEE in sensing of various cations and anions as well as in cell imaging are investigated (**Chapter 6**).

The phenomena of TICT and ESIPT are individually investigated. As mentioned, recently it was found that coupled TICT and ESIPT processes have also gained interest.[11,113,147-151] The coupled TICT and ESIPT process mainly depends on the molecular structure of the fluorophore and the nature of the environment. 2-(4'-amino-2'-hydroxyphenyl)-*1H*-imidazo-

[4,5-c]pyridine (AHPIP-c) is a newly designed molecule having both charge donor and proton donor groups and is a derivative of 2-(4'-aminophenyl)-*1H*-imidazo-[4,5-c]pyridine (APIP-c). As shown by Fasani *et al.* hydrogen bonding is absolutely essential for APIP-c to emit TICT emission. Therefore, it is interesting to see whether intramolecular hydrogen bonding promote TICT emission or prevent it. To verify this, the spectral characteristics of AHPIP-c are investigated in aprotic and protic solvents. In addition, the characteristics of 2-(4'-amino-2'-methoxyphenyl)-*1H*-imidazo-[4,5-c]pyridine (AMPIP-c, methoxy analogue of AHPIP-c) are also studied to further support the findings on AHPIP-c (**Chapter 7**).

Chapter 2

Materials, Methods and Instrumentations

2.0. Introduction

The details of the chemicals and the solvents used for the work carried out in the present thesis are provided in this chapter. The methodology followed for the syntheses, experiments, theoretical calculations and data analyses were also briefly described in this chapter. In addition, this chapter covers the details of the instruments are used.

2.1.0. Materials

The details of the solvents and chemicals used for the thesis work are listed below:

2.1.1. Solvents

- Acetonitrile (HPLC grade, Spectrochem, India)
- 1-Butanol (HPLC grade, Spectrochem, India)
- Cyclohexane (HPLC grade, Rankem India)
- Diethyl ether (HPLC grade, Spectrochem India)
- Dimethylformamide (DMF), HPLC grade, Rankem India)
- Dimethylsulfoxide (DMSO), HPLC grade, Rankem India)
- 1, 4-Dioxane (HPLC, Spectrochem India)
- Ethanol (ACS grade, Merck)
- Ethyl acetate (HPLC grade, Rankem India)
- Glycerol (AR grade, Rankem India)
- Glycol (AR grade, Rankem India)
- Methanol (HPLC grade, Rankem India)
- 1-Propanol (AR grade, Rankem India)
- 2-Propanol (HPLC grade, Rankem India)
- Tetrahydrofuran (THF), HPLC grade, Rankem)
- Water (Millipore)

The solvents were transparent in the spectral region of interest and were used as received.

2.1.2. Metal Salts

- Cadmium nitrate hydrate, $Cd(NO3)_2.xH_2O$ (Merck)
- Cobalt chloride hexahydrate ($CoCl_2.6H_2O$) (Merck)
- Copper perchlorate hexahydrate, $Cu(ClO_4)_2.6H_2O$, (Sigma Aldrich)
- Iron perchlorate, $Fe(ClO_4)_2.xH_2O$, (Sigma Aldrich)
- Magnesium perchlorate hexahydrate, $Mg(ClO4)_2.6H_2O$ (Sigma Aldrich)

- Mercuric Chloride, $HgCl_2$ (Merck)
- Nickel perchlorate hexahydrate, $Ni(ClO4)_2.6H_2O$ (Sigma Aldrich)
- Sodium perchlorate monohydrate, $NaClO_4.H_2O$ (Sigma Aldrich)
- Zinc perchlorate hexahydrate, $Zn(ClO_4)_2.6H_2O$ (Sigma Aldrich)

2.1.3. Anions

- Tetra-n-butylammoniumacetate, $(CH_3CH_2CH_2CH_2)_4N^+CH_3COO^-$(Sigma Aldrich)
- Tetra-n-butylammoniumchloride, $(CH_3CH_2CH_2CH_2)_4N^+Cl^-$(Sigma Aldrich)
- Tetra-n-butylammonium fluoride, $(CH_3CH_2CH_2CH_2)_4N^+F^-$(Sigma Aldrich)
- Tetra-n-butylammoniumnitrate, $(CH_3CH_2CH_2CH_2)_4N^+NO_3^-$(Sigma Aldrich)
- Tetra-n-butylammoniumperchlorate, $(CH_3CH_2CH_2CH_2)_4N^+ClO_4^-$(Sigma Aldrich)
- Tetra-n-butylammoniumphosphate, $(CH_3CH_2CH_2CH_2)_4N^+PO_4^{3-}$(Sigma Aldrich)

2.1.4. Other Chemicals

- 4-Aminosalicylic acid (Sigma Aldrich)
- 4-Amino-2-methoxybenzoic acid (Sigma Aldrich)
- 4-Aminobenzoic acid (Sigma Aldrich)
- Benzoic acid (Merck India)
- Chloroform-d (Sigma Aldrich)
- Citric acid monohydrate (Merck India)
- 3,4-Diaminopyridine (Sigma Aldrich)
- Diphosphorouspentoxide (Merck India)
- 4-(*N*,*N*-Dimethylamino)benzoic acid (Sigma Aldrich)
- Dimethylsulfoxide-d_6 (Sigma Aldrich)
- Di-sodiumhydrogenphosphate anhydrous (Merck)
- Iodomethane (Merck India)
- Methanol-d_4 (Sigma Aldrich)
- *ortho*-Phenylenediamine (Merck India)
- *ortho*-Phosphoric acid (AR grade, Rankem India)
- Phosphorous oxychloride (Spectrochem)
- Potassium hydroxide (Merck India)
- Silica gel (60-120 mesh) (Merck India)
- Silica gel for thin layer chromatography (Merck India)
- Silica gel GF254 (Merck India)

- Sodium bicarbonate, anhydrous, (Merck India)
- Sodium carbonate, anhydrous (Merck India)
- Sodiumdihydroge phosphate dihydrate (Merck)
- Sodium hydroxide (Merck India)
- Sodium sulfate anhydrous (Merck India)
- Sulfuric acid (AR grade, Rankem India)
- Trisodium citrate dehydrate (Merck India)
- Heavy water (Sigma Aldrich)

2.1.5.0. Synthesis

2.1.5.1. 2-(4'-*N*,*N*-Dimethylaminophenyl)imidazo[4,5-c]pyridine (DMAPIP-c), 2-(4'-aminophenyl)-*1H*-imidazo[4,5-c]pyridine (APIP-c), 2-(4'-amino-2'-hydroxyphenyl)-1H-imidazo-[4,5-c]pyridine (AHPIP-c) and 2-(4'-amino-2'-methoxyphenyl)-*1H*-imidazo-[4,5-c]pyridine (AMPIP-c)

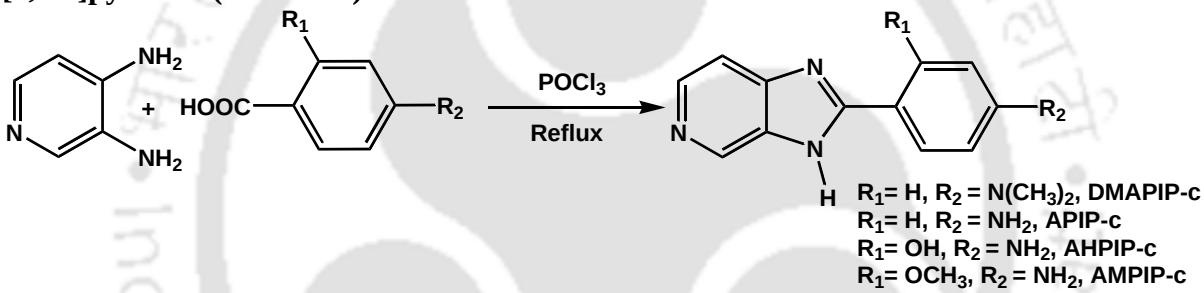

Scheme 2.1. Syntheses of DMAPIP-c, APIP-c, AHPIP-c and AMPIP-c.

2-(4'-*N*,*N*-dimethylaminophenyl)imidazo[4,5-c]pyridine (DMAPIP-c), 2-(4'-aminophenyl)-*1H*-imidazo[4,5-c]pyridine (APIP-c), 2-(4'-amino-2'-hydroxyphenyl)-1H-imidazo-[4,5-c]pyridine (AHPIP-c) and 2-(4'-amino-2'-methoxyphenyl)-*1H*-imidazo-[4,5-c]pyridine (AMPIP-c) were synthesized by refluxing equimolar mixture of 3,4-diaminopyridine and corresponding acids in $POCl_3$ for 6 h (**Scheme 2.1**).[152] After cooling the reaction mixture was added to ice cold water and neutralized with sodium hydroxide. The precipitate thus obtained was purified by column chromatography. The product was confirmed by NMR spectrum and HRMS.

DMAPIP-c: **^{1}H NMR** (400 MHz, $CDCl_3$, ppm) δ 3.11 (6H, s), 6.89 (2H, d), 7.93 (1H, d), 8.20 (2H, d), 8.34 (1H, d), 8.97 (1H, s)
HRMS (ESI) m/z: $[M+H]^+$ Calcd for $C_{14}H_{14}N_4$ 239.1252; Found 239.1301.

APIP-c: **^{1}H NMR** (400 MHz, DMSO-d_6): δ 12.83 (s, 1H), 8.76 (s, 1H), 8.20 (d, 1H), 7.95 (d, 1H), 7.87 (d, 2H), 6.67 (m, 2H), 5.72 (s, 2H).

HRMS (ESI) m/z: $[M+H]^+$ Calcd for $C_{12}H_{10}N_4$ 211.0939; Found 239. 211.097

AHPIP-c: ^{1}H NMR (400 MHz, DMSO-d_6): δ 8.36 (s, 1H), 7.80 (s, 1H), 7.39 (t, 1H), 7.06 (d, 1H), 6.38 (d, 1H), 5.86 d, 1H), 4.9 (br, 3H).

HRMS (ESI) m/z: $[M+H]^+$ Calcd for $C_{12}H_{10}N_4O$ 227.0888; Found 227.0949

AMPIP-c: ^{1}H NMR (400 MHz, DMSO-d_6): δ 12.04 (s, 1H), 8.79 (s, 1H), 8.22 (d, 1H), 8.03 (d, 1H), 7.48 (d, 1H), 6.30 (m, 2H), 5.86 (s, 2H), 3.39 (s,3H)

HRMS (ESI) m/z: $[M+H]^+$ Calcd for $C_{13}H_{12}N_4O$ 241.1045; Found 241.1079

2.1.5.2. *N*,*N*-Dimethyl-4-(5-methyl-5H-imidazo[4,5-c]pyridin-2-yl)benzenamine (DMAPIP-PyMe)

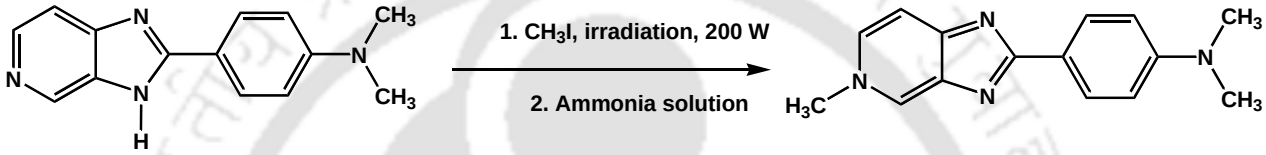

Scheme 2.2. Synthesis of DMAPIP-PyMe.

N,*N*-dimethyl-4-(5-methyl-5H-imidazo[4,5-c]pyridin-2-yl)benzenamine (DMAPIP-PyMe) was synthesized by irradiating the mixture of DMAPIP-c and methyl iodide in a microwave oven at 200W for 4h.[153] After irradiation, the mixture was cooled and then treated with base.[154] The product obtained was purified by preparative thin layer chromatography. The compound was confirmed by HRMS and NMR spectrum.

DMAPIP-PyMe: **^{1}H NMR** (400 MHz, $CDCl_3$, ppm) δ 3.10 (3H, s), 3.53 (6H, s), 4.02 (1H, d), 7.05 (2H, d), 7.08 (2H, d), 7.48 (2H, m)

HRMS (ESI) m/z: $[M+H]^+$ Calcd for $C_{15}H_{16}N_4$ 253.1409; Found 253.1461.

2.1.5.3. *N*,*N*-Dimethyl-4-(1-methyl-1H-imidazo[4,5-c]pyridin-2-yl)benzenamine (DMAPIP-ImMe)

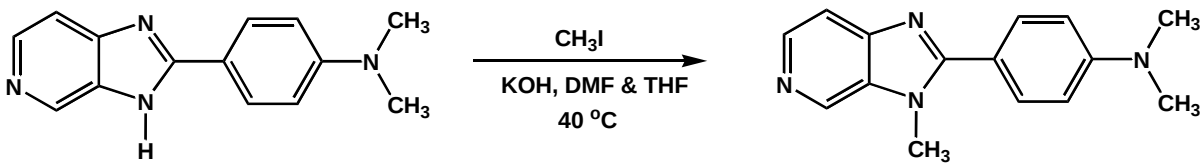

Scheme 2.3. Synthesis of DMAPIP-ImMe

N,*N*-Dimethyl-4-(1-methyl-1H-imidazo[4,5-c]pyridin-2-yl)benzenamine (DMAPIP-ImMe) was synthesized by procedure shown in the **scheme 2.3**. DMAPIP-c, methyl iodide and

KOH (powder) were dissolved in a 3:1 solvent mixture of DMF and THF. The mixture was stirred for 20 h at 40 °C.[155] The product obtained was purified by column chromatography The HRMS and the NMR spectral data confirmed the product.

DMAPIP-ImMe: **^{1}H NMR** (400 MHz, $CDCl_3$, ppm) δ 3.07 (6H, s), 4.11 (3H, s), 6.65 (2H, d), 7.69 (2H, d), 7.77 (1H, d), 8.30 (2H, d)

HRMS (ESI) m/z: $[M+H]^+$ Calcd for $C_{15}H_{16}N_4$ 253.1409; Found 253.1448.

2.1.5.4. 2-(Phenyl)imidazo[4,5-c]pyridine (PIP-c)

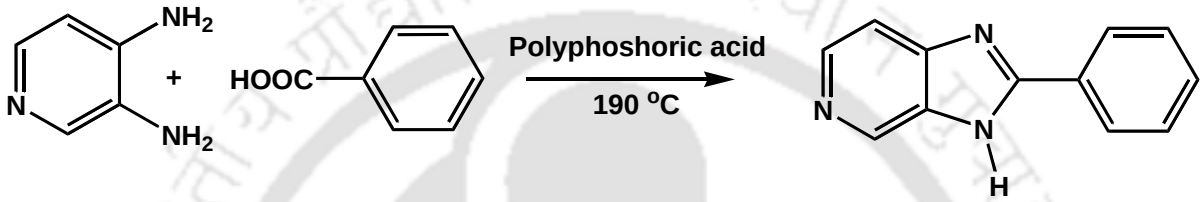

Scheme 2.4. Synthesis of PIP-c.

PIP-c was prepared by refluxing benzoic acid and 3,4-diaminopyridine in polyphosphoric acid at 190°C for 5 h **(Scheme 2.4)**.[156-158] The reaction mixture was cooled and poured into ice cold water. The mixture was neutralized by potassium hydroxide solution. The dried solid product was recrystallized twice in methanol. The product was confirmed by HRMS and NMR spectral data.

PIP-c: ^{1}H NMR (600 MHz, $CDCl_3$, ppm) δ 8.86 (1H, s), 7.36 (4H, m), 8.08 (2H, dd), 8.22 (1H, d)

HRMS (ESI) m/z: $[M+H]^+$ Calcd for $C_{12}H_9N_3$ 196.0830; Found 196.0872.

2.1.5.5. 4-(3-(1H-Benzo[d]imidazol-2-yl)-5-tert-butyl-4-hydroxybenzyl)-2-(1H-benzo[d]imidazol-2-yl)-6-tert-butylphenol (bis-HPBI), 4-(3-(Benzo[d]oxazol-2-yl)-5-tert-butyl-4-hydroxybenzyl)-2-(benzo[d]oxazol-2-yl)-6-tert-butylphenol (bis-HPBO) and 4-(3-(Benzo[d]thiazol-2-yl)-5-tert-butyl-4-hydroxybenzyl)-2-(benzo[d]thiazol-2-yl)-6-tert-butylphenol (bis-HPBT).

The structure of all these molecules are given in the **Chart 2. 1** and molecules were received from Dr. M. Sathiyendiran's (presently at School of Chemistry, University of Hyderabad) Laboratory at Department of Chemistry, University of Delhi, India.[159]

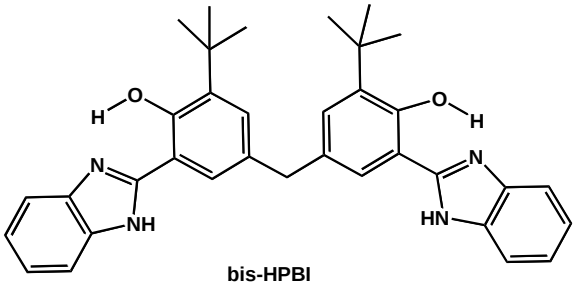

bis-HPBI

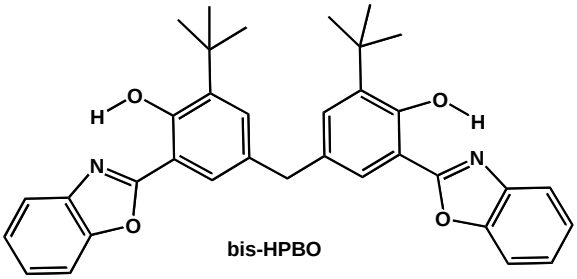

bis-HPBO

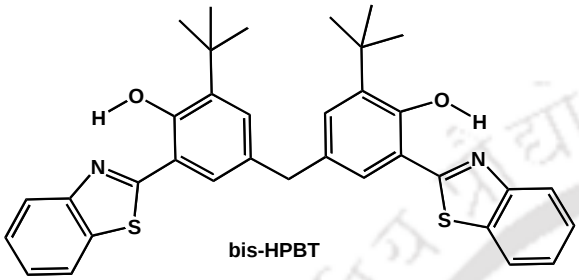

bis-HPBT

Chart 2.1. Structures of bis-HPBI, bis-HPBO and bis-HPBT.

2.2.0. Preparation of Samples

2.2.1. In Solvents

Most of the fluorophores were found to be well soluble in methanol. Therefore, for the spectral measuremnt, a stock solution of the fluorophore was prepared in methanol having solution strength 10^{-3} M. Further, 10^{-4} M of the fluorophore solution was prepared by pipetting out 1 ml of the stock solution to a 10 ml capacity volummetric flask and filling the flask upto the mark by adding methanol. From 10^{-3} M or 10^{-4} M solution, depending upon the requirement 1x 10^{-5} M, 1x 10^{-6} M, 3x 10^{-6} M solutions were prepared in different solvents after drying the pipetted methanol. The solutions were shaken well and sonicated to dissolve the compound completely in the solvents. However, in some cases due to poor solubility of the fluorophores saturated solutions were taken for the spectral measurements. For pH titration, small amount of H_3PO_4/H_2SO_4 or NaOH solution was added to obtain the desired pH. For pK_a studies in aqueous medium due to poor solubilty of bis-HPBI 3% methanol solution was used.

2.2.2. Cucurbit-7-uril Solution

2 x 10^{-3} M stock solution of CB-7 was prepared in a 10 mL capacity volumetric flask by addiing milipore water. Appropriate amount of stock solution was added to the dried fluorophores and diluted to the required volume. The pH solution maintained by using

bicaronate-carbonate, phosphate or citrate buffer (depending on the requiredpH of the solution).

2.2.3. Preparation of Aggregate of bis-HPBT

1 mM stock solution of the dye in THF was prepared. An aliquot of the stock solution was transferred to a 10 mL volumetric flask to obtained 3 μM solutions of the fluorophore in different fractions of water (f_w = 0−90 %). At higher water fractions the clearness of the solutions gradually decreased and a faint milky white colour developed.

Preparation of Solutions of Cations and Anions: 2 mM stock solutions of corresponding cations and anions were prepared in THF. Using the stock solutions 500 μM cation/anion solutions were prepared in 70:30 water/THF (v/v) mixture. Those solutions were used for preparing other required solutions.

Cell Culture and Imaging: HeLa cells were cultured in Dulbecco's Modified Eagle Medium (DMEM, Gibco, USA) supplemented with 10% fetal bovine serum (FBS, Gibco, USA), antibiotics, and 2 mM glutamine. For experimentation, cells were passaged, plated on glass cover slips supplemented with 1% FBS for 24 hrs. Upon cell adherence 200 μL of aggregates were added and placed in an incubator for 2 hrs at 37 °C with 5% CO_2.

2.3.0. Methods

2.3.1. Quantum Yield

Fluorophores upon absorption of photons go to their excited state and are called excited molecules. The fate of the excited molecules depends on the type of the fluorophores and nature of the environment. However, excited fluorophore dissipates its energy by emission or nonradiative ways. Quantum yield of fluorescence (Φ_f) is defined as the ratio of the number of photons emitted to the total number of photons absorbed and this definition leads to following representation of Φ_f

$$\Phi_f = \frac{\text{Number of photons emitted}}{\text{Number of photons absorbed}} \tag{2.1}$$

The quantum yield of a fluorophore can be determined relative to a reference compound whose quantum yield is known. The absorbance(s) of the sample(s) is kept at ~ 0.1 for the

determination of the fluorescence quantum yields. For the work done in this thesis, quinine sulphate in 1N sulphuric acid is used as a standard whose quantum yield is 0.55.[160] The quantum yield is manually calculated by using the following equation:

$$\Phi_S = \Phi_R \frac{n^2}{n_R^2} \times \frac{A_R}{A_S} \times \frac{I_S}{I_R} \quad (2.2)$$

where I_S and I_R represent the area obtained from the emission spectra of the sample and reference, respectively and A_S and A_R denote the absorbance values for the sample and reference, respectively. n_S and n_R are the refractive indices for solvent used for the sample and the reference solutions, respectively.

2.3.2. Determination of Ionization Constant

The acid dissociation constant (K_a) or the pK_a is the measure of the strength of an acid or a base. The pK_a value of the dye gives better idea to understand about nature of the probe and the medium. The most popular Hammett equation given below is employed for the determination of ionization constant of an acid in aqueous medium.

$$BH^+ + H_2O \rightleftharpoons B + H_3O^+ \quad (2.3)$$

$$H_0 = pK_a + \log \frac{[B]}{[BH^+]} \quad (2.4)$$

where $[BH^+]$ and [B] are denotes the molar concentration of conjugate acid and base respectively.

H_0 is called Hammett's acidity function and is defined as follows

$$H_0 = -\log \frac{a_{H^+} f_B}{f_{BH^+}} \quad (2.5)$$

Where f_B and f_{BH^+} are the acidity coefficient of conjugate base and acid respectively. a_{H+} is the activity of the proton. For dilute solution, H_0 is replaced by pH. The plot of pH versus $\log \frac{[B]}{[BH^+]}$ is a straight line with unit slope and the pH = pK_a when $[B] = [BH^+]$. $\frac{[B]}{[BH^+]}$ can be determined from following relation.

$$\frac{[B]}{[BH^+]} = \frac{[A_B - A]}{[A - A_{BH^+}]} \quad (2.6)$$

whereA_{BH}+ and A_B are the absorbance of the pure BH^+ and B respectively and A is absorbance (at same wavelength) of any solution in which BH^+ is partially ionized.

$$\frac{[B]}{[BH^+]} = \frac{[B]}{[C]-[B]} \quad (2.7)$$

where [C] is the molar concentration of the compound in the experimental solution.

$$[B] = \frac{A(\lambda_1)\varepsilon^{+}_{BH}(\lambda_2) - A(\lambda_2)\varepsilon^{+}_{BH}(\lambda_1)}{\varepsilon_B(\lambda_1)\varepsilon^{+}_{BH}(\lambda_2) - \varepsilon_B(\lambda_2)\varepsilon^{+}_{BH}(\lambda_1)} \quad (2.8)$$

ε is the molar extinction coefficient and for the calculation generally two wavelengths were considered (λ_1 and λ_2) at both sides of the isosbestic point of the absorption spectra at different pH.

2.3.3. Quantum Mechanical Calculation

The calculations were performed by using Gaussian 09 programm.[161] Integral equation formalism-polarizable continuum model (IEF-PCM) is used to include the solvent stabilization by choosing methanol as solvent.[162]The configuration interaction with single excitations (CIS) method is used for the optimization of the excited state geometry of the molecules.[163] In recent times for the electronic structure calculations in the excited states time-dependent density functional theory (TDDFT) is the most popular method. The combination of efficiency, that is, computational cost, as well as precision makes TDDFT very popular.[164,165] The TDDFT calculations were performed on the optimized structure to obtain molecular energy. The approach was successful to predict molecular parameters in number of systems.[166,167] Different functions such as Becke's three-parameter hybrid functional B3LYP, Coulomb-attenuating method (CAM)-B3LYP and B3LYP-D3 were used to obtain the molecular energy.[82, 168-171] The 6-31G (d, p) basis set were employed for the calculations.

2.4.0. Instruments

2.4.1. UV-visible Spectrophotometer

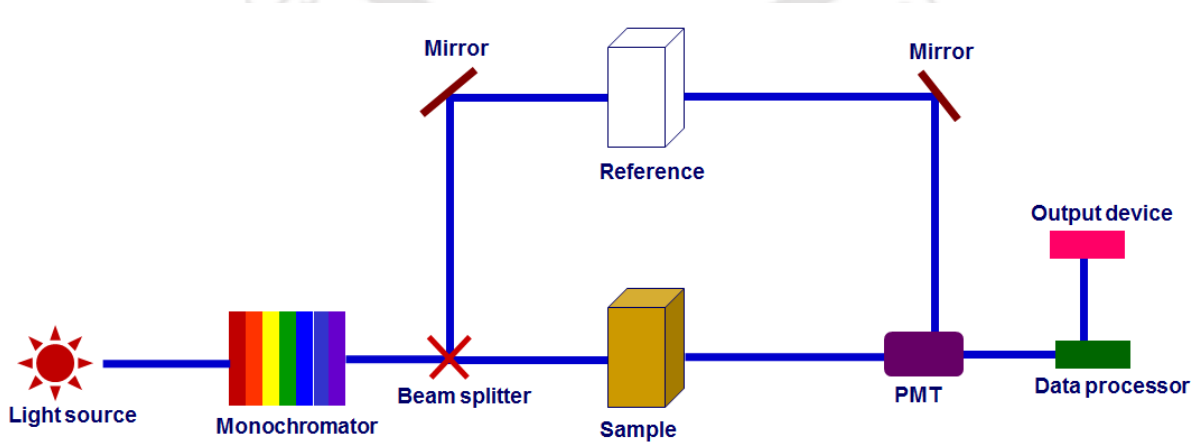

Scheme 2.5. Schematic diagram of a double beam- UV-visible spectrophotometer.

In recent times, absorption measurements are performed by using double beam absorption spectrometers. The block diagram of the double beam UV-visible spectrophotometer is shown in **Scheme 2.5**. The double beam absorption spectrometers consist of following components: light source, monochromator, sample holder, detector, amplifier and recording devices. A beam of polychromatic light from the source is splited into its component wavelengths by the monochromator. Subsequently, each monochromatic beam splits into two sample and reference beams by a half-mirrored device. The sample beam passes through a cuvette containing the sample solution. In the same time, the reference beam passes through an identical cuvette containing the reference solvent. The intensities of these beams are then measured by detectors and compared. In practice, the intensity of the reference beam denoted as $\mathbf{I_0}$ and the intensity of the sample beam is denoted as **I**. Finally the spectrophotometer automatically scans all the component wavelengths very quickly.

For the present thesis work, absorption spectra were recorded with the help of a Cary 100, Perkin Elmer Lambda 25, and Perkin Elmer Lambda 750 double beam spectrophotometers. Deuterium and tungsten lamps are used as light sources and photomultiplier tube (PMT) as detector.

2.4.3. Steady State Spectrofluorimeter

Fluorescence spectral measurements were carried on Jobin Yvon Spex Fluoromax 4 and Fluorolog 3 instruments. The block diagram for steady state fluorimeter is shown in **Scheme 2.6**.

Fluorimeter has xenon arc lamp as a versatile light source. Xenon light provides a continuous emission spectrum with nearly constant intensity in the range from the ultraviolet to the near infrared. Fluorimeters are equipped to record both fluorescence emission and excitation spectra. Two monochromators are used for the selection of the excitation and emission wavelengths. Motorized monochromator is used for automatic scanning of wavelengths. The monochromators are controlled by the electronic devices and the computer. The optical module contains various components: a sample holder, shutters, polarizers (during anisotropy measurement only) and a beam splitter. The beam splitter is fabricated with a quartz plate reflecting a few percentage of the exciting light towards a quantum counter or a photodiode

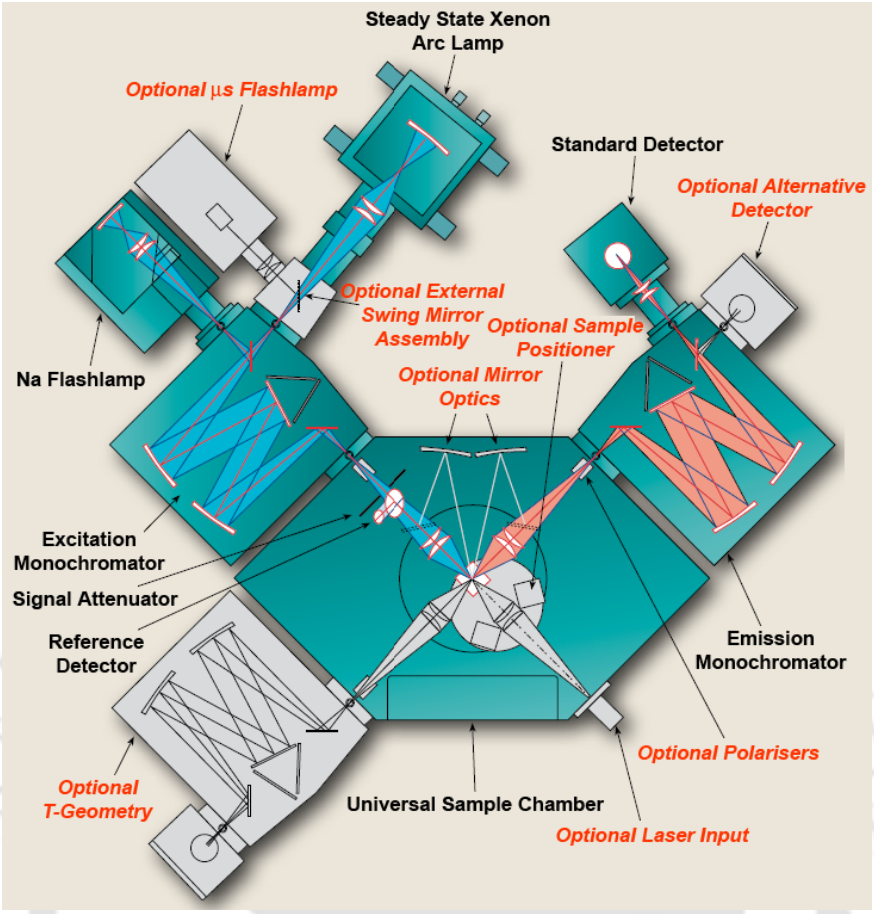

Scheme 2.6. Block diagram of FSP 920 steady state spectrofluorimeter. (Diagram was obtained from the catalogue of Edinburgh instruments FSP 920).

Optical System

The emission spectrum is monitored by fixing the excitation wavelength (λ_{exc}) and it reflects the variations of fluorescence intensity as a function of the wavelength at which the fluorescence is observed (λ_{em}). The excitation spectrum reflects the variations of fluorescence intensity as a function of λ_{exc} with fixed λ_{em}. More conveniently the spectra were recorded as a function of wavelength and not wavenumber. This is because the monochromators of spectrofluorometers are equipped with gratings, thus for a given width of the input and output slits, the monochromators operate at a constant band pass expressed in wavelength.

The fluorescence spectra are distorted mainly by the wavelength dependence of several components of the instrument and required to be corrected.

Correction for Emission Spectra

Basically emission spectrum depends on efficiency of the emission monochromator and the response of the PMT and it is necessary to correct the emission spectra. To obtain a corrected spectrum, the correction factors can be calculated by using a calibrated tungsten lamp or by a standard fluorescence compound whose corrected emission spectrum is known. In General, for all fluorimeters, the correction factors are provided by the supplier.

Correction for Excitation Spectra

Excitation spectra are mainly distorted by the variations of the intensity of the exciting light and of the transmission efficiency of the excitation monochromator. The quantum counter overcomes the wavelength dependence of the sensitivity of the reference photomultiplier. In addition, the ratio of the fluorescence signal from the sample to that from the quantum counter or photodiode (as a function of the excitation wavelength) provides the corrected excitation spectra. However, for more accurate measurements for e.g. comparison of the absorption spectra to the excitation spectra such a correction procedure is not sufficient. This is due to the wavelength dependence of optical parts (e.g. focal length of lenses) may introduce some distortion into the excitation spectrum as it is not same. Thus, the correction factor is obtained by using a known fluorescent compound absorbing in the same wavelength region that of the fluorescent molecule to be studied and whose absorption spectrum should be identical to the corresponding excitation spectrum. The ratio obtained for the excitation spectrum to the absorption spectrum of the reference compound (using the quantum counter) provides the correction factors that can be used. However, the excitation spectra recorded using the photo diode instead of quantum counter is further corrected as the wavelength response of the photodiode is not firmly flat over the complete wavelength range available. But for the fluorometers used in the present thesis instruments the correction files were supplied by the manufacturer.

Fluorolog 3 is equipped with double excitation monochromator and has 450 W Xe lamp as a light source. Other instruments used for the measurements have single excitation monochromator. Fluoromax 4 has 150 W Xe arc lamp as a light source. All these instruments have PMT as detector.

2.4.4. Time Resolved Spectrofluorimeter

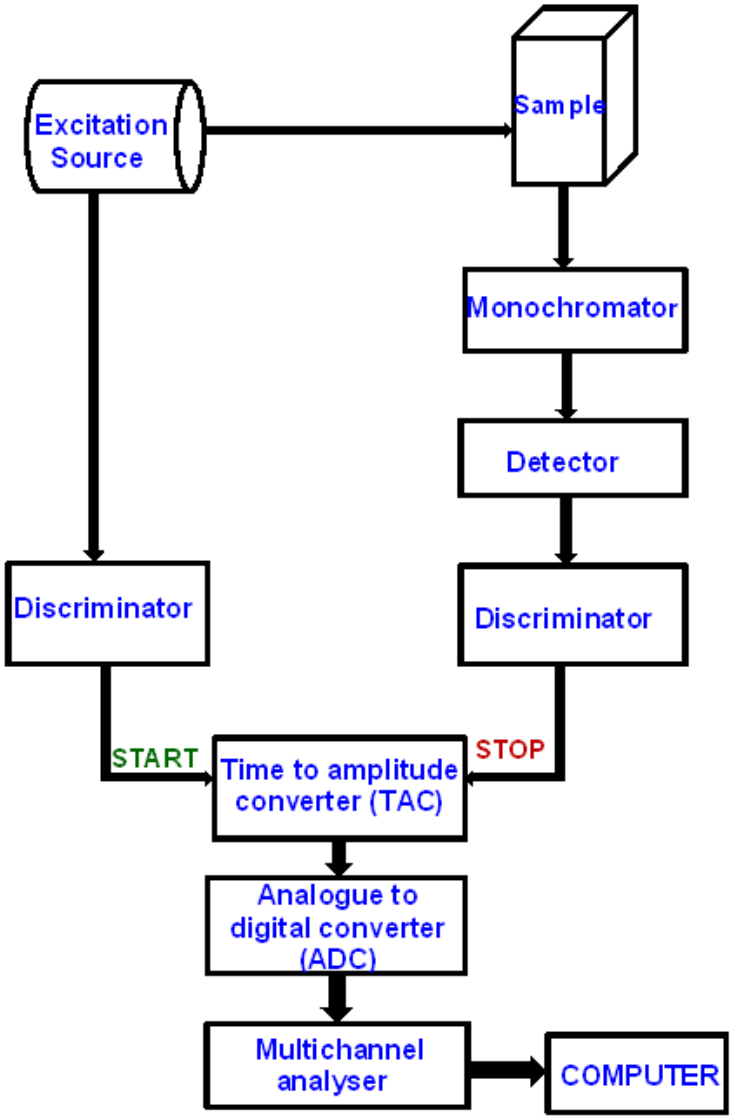

Scheme 2.7. Schematic diagram of time-correlated single photon counting fluorimeter.

Time correlated single photon counting (TCSPC) is the widely used technique in most of the instruments for the determination of fluorescence lifetime. TCSPC method has also been used for the measurement of florescence life time in the present thesis work. A conventional single photon counting instrument sketched in **Scheme 2.7**. In this method the sample to be analysed is excited with a short light pulse from the light source with sufficient delay between pulses. In general, this method uses either a flash lamp, a pulsed laser, a laser diode or a LED as the excitation light source. Upon excitation the molecules emit photons at different relaxation times; thus the decay time of single molecules must have a certain rate rather than occurring at a specific time with excitation. The basic principle of TCSPC method is the detection of single photons and the measurement of their arrival times with respect to

instrument response function (a reference signal from the light source). This method has two pulses namely start signal pulse and the stop signal pulse. The start signal pulse travels to a PMT or micro-channel plate (MCP) photomultiplier that activates the heart of the technique, time-to-amplitude converter (TAC) whereas the stop signal pulse travels through the sample. Then, the growth of ramp signal in TAC is stopped by this pulse. TAC output is amplified using an amplifier, and this analogue pulse of height corresponding to a measured time of the signal goes for further processing to convert to the digital pulse through the analogue to digital converter (ADC). The TCSPC needs a highly repetitive light source to accumulate a sufficient number of photons. The time measurement of the start and stop sequence will be represented by an increase of a memory value in a histogram. Thus, to accumulate sufficient photons in the full range of delays between excitation and emission, this experiment must be repeated several times. The resulting histogram, counts versus the time channels will represent the plot of fluorescence decay profiles. Deconvolution procedure is used to derive the fluorescence temporal profiles with the instrument response using nonlinear least-square fittings.

For the fluorescence lifetime measurements, Edinburgh Instruments Lifespec II instrument is used. Lifespec II employs Hamamatsu MCP detector that has response time of 50 ps. The light sources used to excite the sample were 308 nm, 290 nm and 336 nm LED from PicoQuant and 375 nm laser diode obtained from Edinburgh instruments. Time-resolved data were analysed using the FAST software provided along with the instrument.

2.4.5. pH Meter

The pH of aqueous solutions for present thesis were measured using a standard Jenway (model No 3510) pH meter and where a glass electrode is used. The pH meter was calibrated by using three different standard buffer solutions (pH 4, pH 7 and pH 10) within a range of ± 0.02 pH units to avoid the error.

2.4.6. Other Instruments

High resolution mass spectrometry (HRMS) instruments of Agilent technologies **of Waters Instruments (Q-Tof Premier)** was used for recording the mass spectra. Fourier transform NMR spectra were recorded on Varian instrument of 400 MHz or Bruker 600MHz NMR spectrometers.

The images of the aggregates were obtained by field-emission scanning electron microscopy (FESEM) using a Zeiss (Sigma) instrument. The dried sample was sputter-coated

with gold film using a sputter coater (SC7620 “Mini”, Polaron Sputter Coater, Quorum Technology).

Thermogravimetric analyses (TGA) and differential scanning calorimeter (DSC) analyses were performed on a SDTQ600 thermo gravimetric analyser of TA instruments and on a Q20 differential scanning calorimeter under nitrogen atmosphere respectively.

Chapter 3

Relay Proton Transfer Triggered Twisted Intramolecular Charge Transfer in 2-(4'-*N*,*N*-Dimethylaminophenyl)imidazo[4, 5-c]pyridine†

†*Photochem. Photobiol. Sci.*, 2015, **14**, 2225-223.

3.0. Introduction

The TICT emission of 2-(4'-*N*,*N*-dimethylaminophenyl)imidazo[4,5-c]pyridine (DMAPIP-c, **Chart 3.1**) is an attractive one.[56] Unlike other common TICT emitting molecules, the protic environment is critical for DMAPIP-c to exhibit TICT emission. Even in polar aprotic solvents no TICT emission was observed from DMAPIP-c. Earlier AM1 calculation on DMAPIP-c predicted that under isolated condition, the imidazopyridine ring (the acceptor) is out of plane from the phenyl ring.[56] Further form the calculations it was also predicted that the hydrogen bonding of the imidazopyridine ring (acceptor) with solvent make the imidazopyridine ring coplanar with phenyl ring. This led to the proposition that the planarization through hydrogen bonding increases the charge flow to acceptor from the phenyl ring that results in the TICT state. But *ab intio* calculations on DMAPIP-c suggested that the phenyl and the imidazopyridine rings are planar even under isolated condition.[57] This ruled out the planarization role for the protic solvents in formation of TICT state in 2-(4'-aminophenyl)imidazopyridines. Recently, the mechanism for the TICT emission of 2-(4'-*N*,*N*-dimethylaminophenyl)imidazo[4,5-b]pyridine (DMAPIP-b) was explored and it was found that the double proton transfer via a solvent molecule induced the TICT emission in protic solvents.[120] But, unlike in DMAPIP-b, the proton transfer is not feasible in DMAPIP-c through a single solvent molecule. Therefore, it is interesting to reinvestigate the mechanism of dual emission of DMAPIP-c.

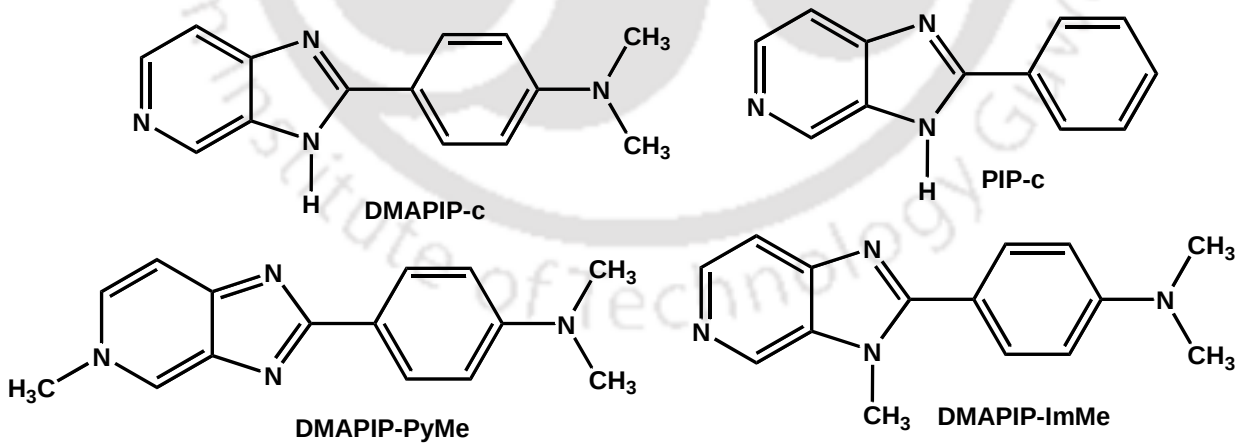

Chart 3.1. Structure of DMAPIP-c, PIP-c, DMAPIP-ImMe and DMAPIP-PyMe.

In this Chapter, the spectral characteristics of DMAPIP-c and related molecules (**Chart 3.1**) were studied to comprehend the mechanism for the dual emission of DMAPIP-c in protic environment.

3.1. Spectral Characteristics of Methyl Derivatives

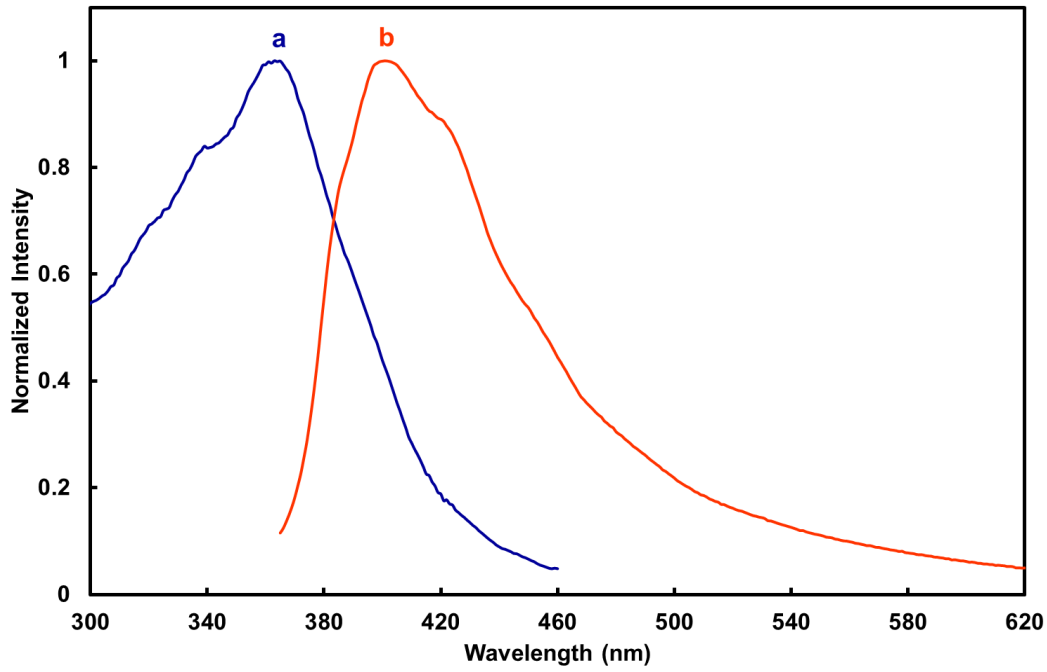

Figure 3.1. Mirror image relationship between the excitation spectrum (a), λ_{em} = 480 nm and emission spectrum (b), λ_{ex} = 355 nm for DMAPIP-PyMe in cyclohexane.

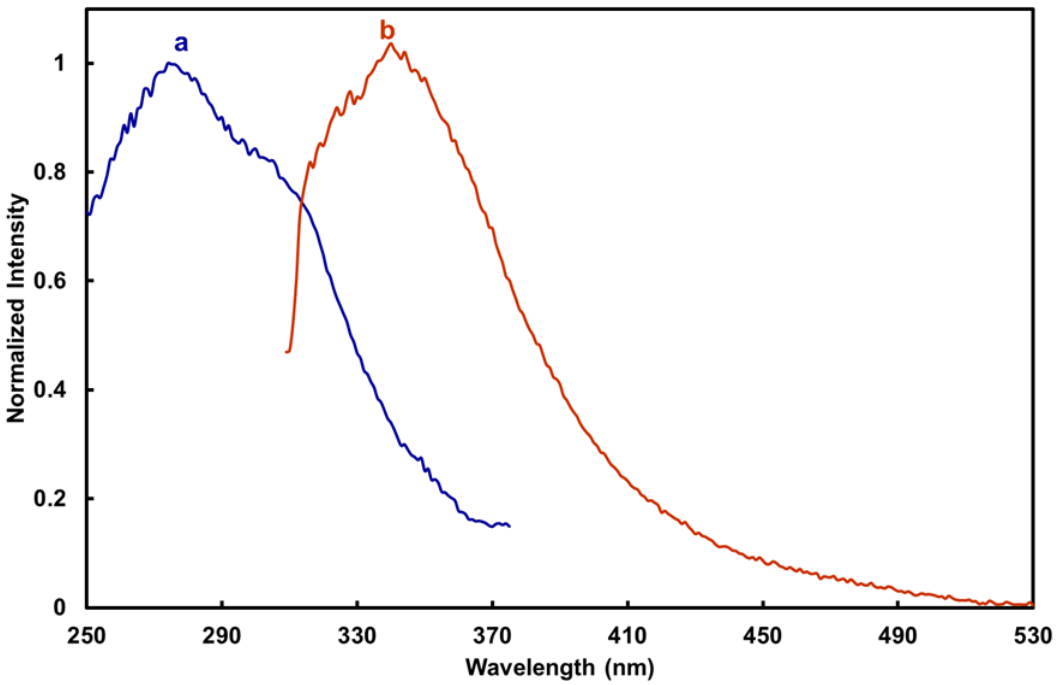

Figure 3.2. Mirror Image relationship between the excitation spectrum (a), λ_{em} = 420 nm and emission spectrum (b), λ_{ex} = 320 nm for DMAPIP-ImMe in cyclohexane.

Table 3.1. Absorption Band Maxima (λ_{max}^{ab}, nm), log ε_{max} (in the parenthesis), Fluorescence Band Maxima (λ_{max}^{fl}, nm) and Fluorescence Lifetimes (τ_f, ns) of DMAPIP-c, DMAPIP-ImMe and DMAPIP-PyMe.

Solvent	DMAPIP-c[a]			DMAPIP-ImMe			DMAPIP-PyMe		
	λ_{max}^{ab} (log ε_{max})	λ_{max}^{fl}	τ_f	λ_{max}^{ab} (log ε_{max})	λ_{max}^{fl}	τ_f	λ_{max}^{ab}	λ_{max}^{fl}	τ_f
Cyclohexane	327, 341	350, 367, 384	-	278, 300	318, 344	2.2	321, 339, 360	397,425, 456	2.2
Tetrahydrofuran	332 (4.45)	380	0.80	322 (4. 25)	411	1.8	351	440	2.4
Acetonitrile	335 (4.45)	391	0.96	314 (4. 28)	424	1.7	349	480	2.5
DMF	336 (4.40)	392	1.41	321 (3. 84)	437	1.9	348	470	3.0
DMSO	340 (4.38)	402	1.45	322 (3. 73)	432	1.9	356	486	3.2
1-Butanol	339 (4.49)	391	0.74	320 (3. 70)	431	1.7	360	484	3.1
1-Propanol	339 (4.49)	393	1.0, 2.4	320 (3. 95)	431	1.6	361	482	3.4
Methanol	341 (4.47)	398, 475	0.35, 1.85	316 (4. 16)	437	1.8	358	490	3.2

[a] Spectral data in Dimethyformaide (DMF) and Dimethylsulphoxide (DMSO) are from present work and in other solvents are from Ref.56

The methyl derivatives of DMAPIP-c were synthesized to ascertain the role of hydrogen bonding of the solvent with imidazole 'NH' hydrogen and pyridyl nitrogen in the longer wavelength emission processes. The emission and the excitation spectra of methyl derivatives in cyclohexane have well resolved vibronic structures with vibrational frequency $2500 \pm 100\ cm^{-1}$ and $1650 \pm 100\ cm^{-1}$ **(Figures 3.1** and **3.2)**. The good mirror image relationship between the excitation and emission spectrum suggests that both the band corresponds to the same electronic transition i.e. S_0-S_1. The spectral data are in different solvents are compiled in **Table 3.1**. The fluorescence emission spectra are supplied in **Figures 3.3** and **3.4**. When polarity and hydrogen bonding capacity of the solvent is increased the spectra are blurred and bathochromic shifts are observed. These features of the methyl derivatives are same as those of DMAPIP-c. However, the solvatochromic shifts in the spectra of the methyl derivatives are less as compared to those of DMAPIP-c.

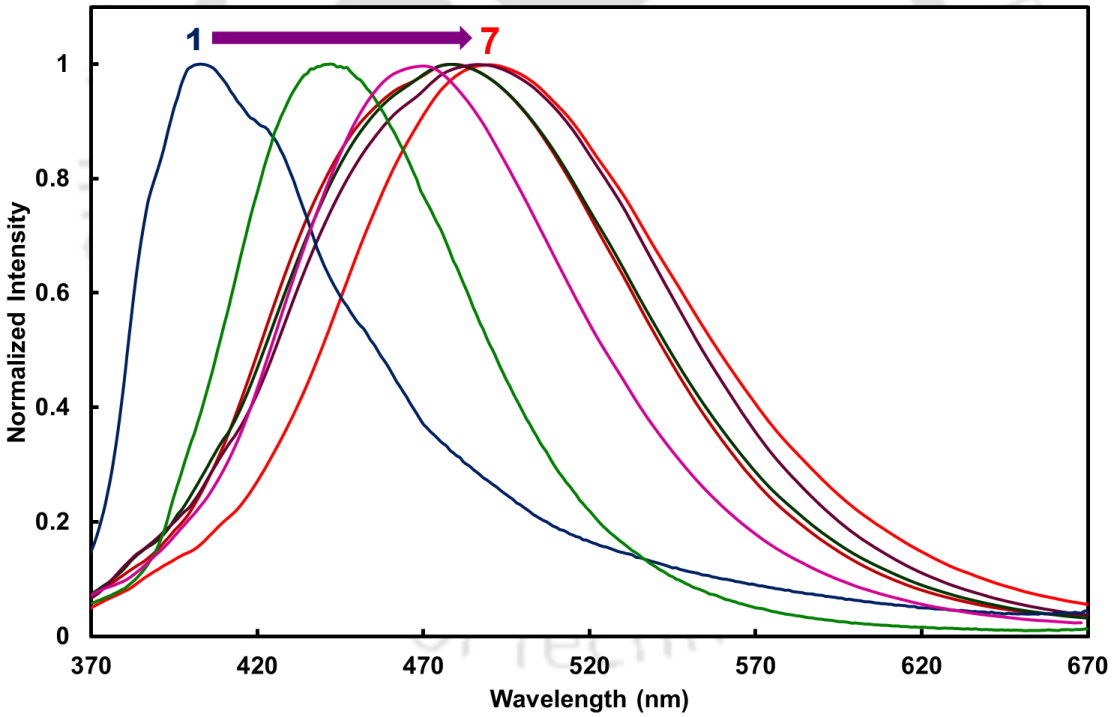

Figure 3.3. Normalised emission spectra of DMAPIP-PyMe in some selected solvents: (1) cyclohexane (2) tetrahydrofuran (3) DMF (4) acetonitrile, (5) butanol, (6) DMSO and (7) methanol, λ_{exc} = 355 nm.

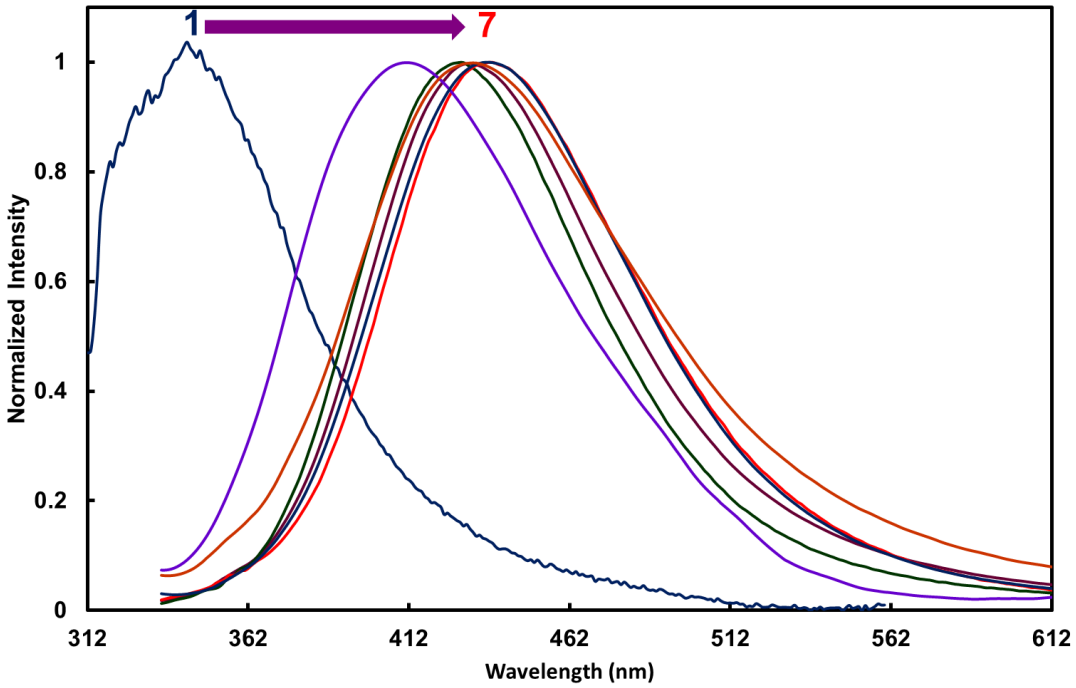

Figure 3.4. Normalised emission spectra of DMAPIP-ImMe in some selected solvents: (1) cyclohexane (2) tetrahydrofuran (3) acetonitrile, (4) DMSO, (5) propanol, (6) methanol and (7) DMF, λ_{exc} = 320 nm.

To explore the polarity effect, the Lippert–Mataga equation used for the analysis of solvent-dependent spectral shifts is given below,[171]

$$\bar{\nu}_{ss} = \left[\frac{2(\mu_e - \mu_g)^2}{hca^3}\right]\Delta f + \text{Constant} \qquad (3.1)$$

Where $\bar{\nu}_{ss} = \bar{\nu}^{ab}_{\max} - \bar{\nu}^{fl}_{\max}$, is the Stokes shift, h is the Planck's constant, c is the speed of light, μ_e and μ_g are the excited state and ground state dipole moments of the dye, respectively and a denotes the Onsagar cavity radius. The orientation polarizability is defined by

$$\Delta f = \left[\frac{\varepsilon - 1}{2\varepsilon + 1} - \frac{n^2 - 1}{2n + 1}\right] \qquad (3.2)$$

where ε and n are the dielectric constant and refractive index of the solvent, respectively.

The μ_e of the methyl derivatives are calculated using Lippert-Mataga plot **(Figure 3. 5)**. The excited state dipole moments of DMAPIP-ImMe, and DMAPIP-PyMe thus obtained are 9.9 and 7.7 D, respectively. Smaller μ_e of methylated derivatives compared to that of DMAPIP-c (12.0 D)[56] indicates that charge transfer process is affected by the methylation of pyridyl nitrogen as well as that of imidazole 'NH' group.

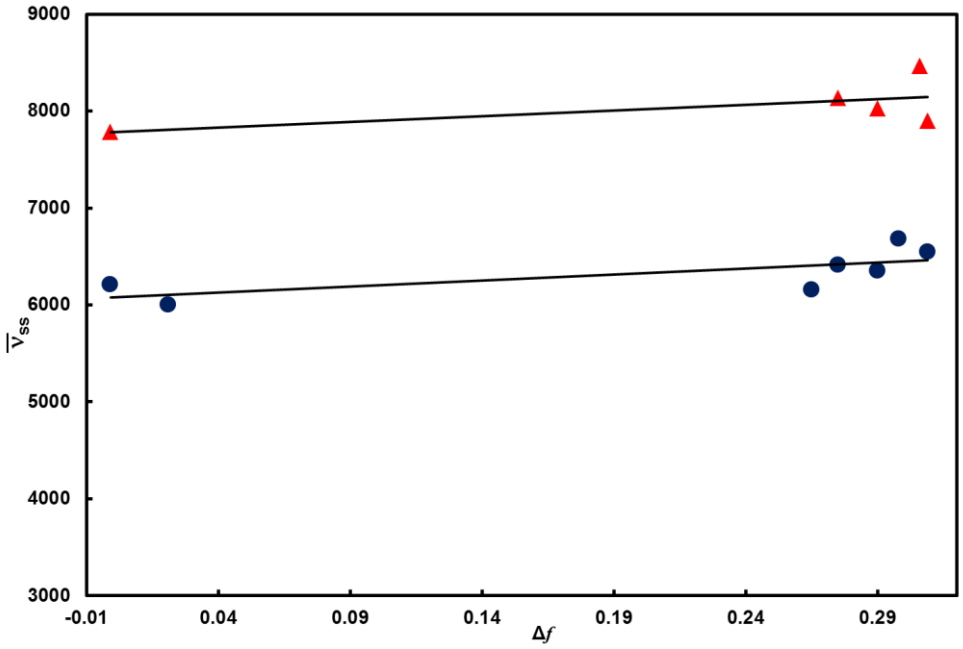

Figure 3.5. Lippert-Mataga plot for DMAPIP-ImMe (▲) and DMAPIP-PyMe (●).

Interestingly, no dual emission is observed form both of the methyl derivatives. However, sometimes a weak emission may be buried underneath the strong normal emission. Even in DMAPIP-c, though clear dual emission is not observed in solvent such as propanol the time resolved studies indicated the weak TICT emission is submerged under the normal emission. Therefore, the fluorescence decays of the methyl derivatives were measured (**Table 3.1**). In aprotic solvents, the fluorescence decay of DMAPIP-c was monoexponential, nevertheless it was double exponential in protic solvents.[56] But the fluorescence decays of methyl derivatives are monoexponential in aprotic as well as protic solvents. This shows that the dual emission is not observed in the methyl derivatives. Due to methylation the hydrogen bonding with pyridyl nitrogen and imidazole 'NH' hydrogen are not feasible in DMAPIP-PyMe and DMAPIP-ImMe, respectively. Therefore, the nonappearance of longer wavelength emission in methyl derivatives specifies that the hydrogen bonding of both azole 'NH' hydrogen and pyridyl nitrogen with the solvent are essential for the dual emission of DMAPIP-c. The proton transfer from the azole 'NH' hydrogen to the pyridyl nitrogen is one such process which requires the hydrogen bonding of solvents at both azole 'NH' hydrogen and pyridyl nitrogen. In the excited state, the transfer of proton from the acidic group to the basic group occurs through hydrogen bonding and it often results in dual emission.[59, 173-176] Usually a negative solvatochromism is observed in the fluorescence of tautomer that formed by proton transfer. However, the longer wavelength fluorescence of DMAPIP-c is a TICT emission and

it exhibits strong positive solvatochromism. A red shift was observed in the longer wavelength emission in water compare to that of methanol and strong blue shift was observed in the longer wavelength emission on moving from the more polar to less polar environment.[56,126,177] Nonetheless in some cases positive solvatochromism is observed when the proton transfer assist the ICT process.[56, 107,111]

3.2. The Relay Proton Transfer

In 7-hydroxyquinoline-8-carbaldehydes the relay proton transfer was reported to take place via ionic form.[178] In DMAPIP-c also the proton transfer might involve deprotonation at imidazole 'NH' proton followed by its addition at pyridyl nitrogen. The effect of deprotonation on the spectral charcteristics of DMAPIP-c in aqueous solution was already investigated.[179] Though the absorption spectrum and the normal emission of the anion are blue shifted compared to neutral molecule no shift was observed in its' longer wavelength emission. But, the intensity of the longer wavelength fluorescence of DMAPIP-c enhanced upon deprotonation. These results suggest that the species responsible for the longer wavelength emission in both anion and neutral species is same. Therefore, it may be hypothesized that the molecule that was deprotonated in the ground state to form anion and was again protonated in the excited state. If reprotonation occurs at same site, one should expect no shift in the nomal emission also. The blue shift in the normal emission of the anion with respect to neutral form indicates that reprotonation did not occur at same site. Further, the enhancement in the longer wavelength emission suggests that the depronation is one of the steps that lead to the longer wavelength emitting state. In DMAPIP-c single solvent molecule is not sufficient to produce the biproton transfer and this should occur via solvent network. To verify the relay proton transfer hypothesis, DMAPIP-c was deprotonated using with fluoride anion in acetonitrile. Since acetonitrile is an aprotic solvent whose polarity similar to that of methanol it is expected to prevent the relay proton transfer without hindering the charge transfer process. Upon addition of fluoride the absorption and the fluorescence spectra are blue shifted due to formation of anion (**Figures 3.6** and **3.7**). However, no longer wavelength fluorescence is observed in presence of fluoride.

Similar study with chloride ion (relatively weaker base) does not produce any shift in the absorption and fluorescence spectra of DMAPIP-c (**Figures 3.8a** and **3.8b**). This confirms the fact that the spectral shift observed upon addition of fluoride ion is not due to the effect of ionic strength but due to formation of anion.

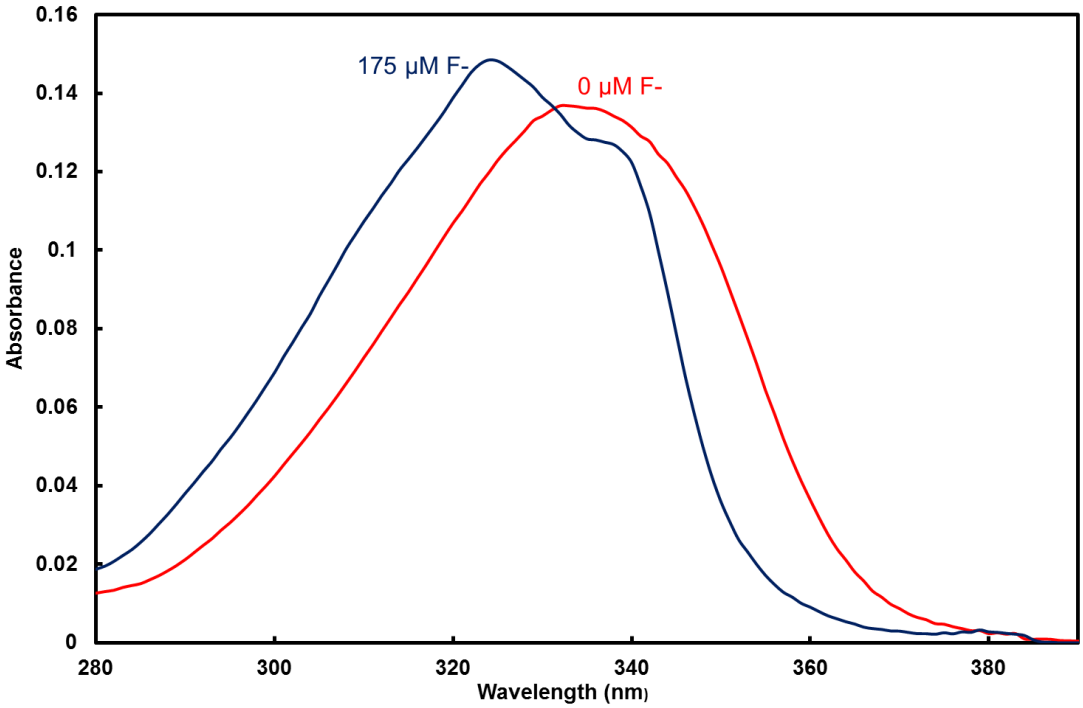

Figure 3.6. Absorption spectra of DMAPIP-c in neutral (0µM F^-) and anion (175µM F^-) forms in acetonitrile.

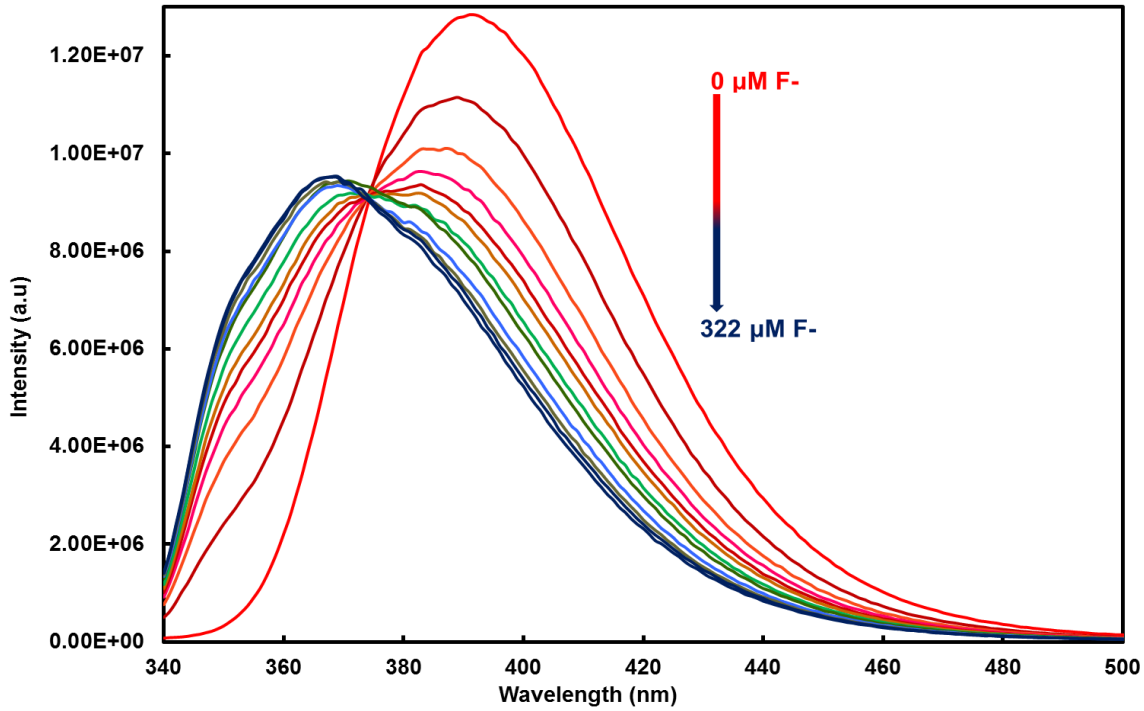

Figure 3.7. Fluorescence spectra of DMAPIP-c at different fluoride ion concentration in acetonitrile, λ_{exc} = 330 nm.

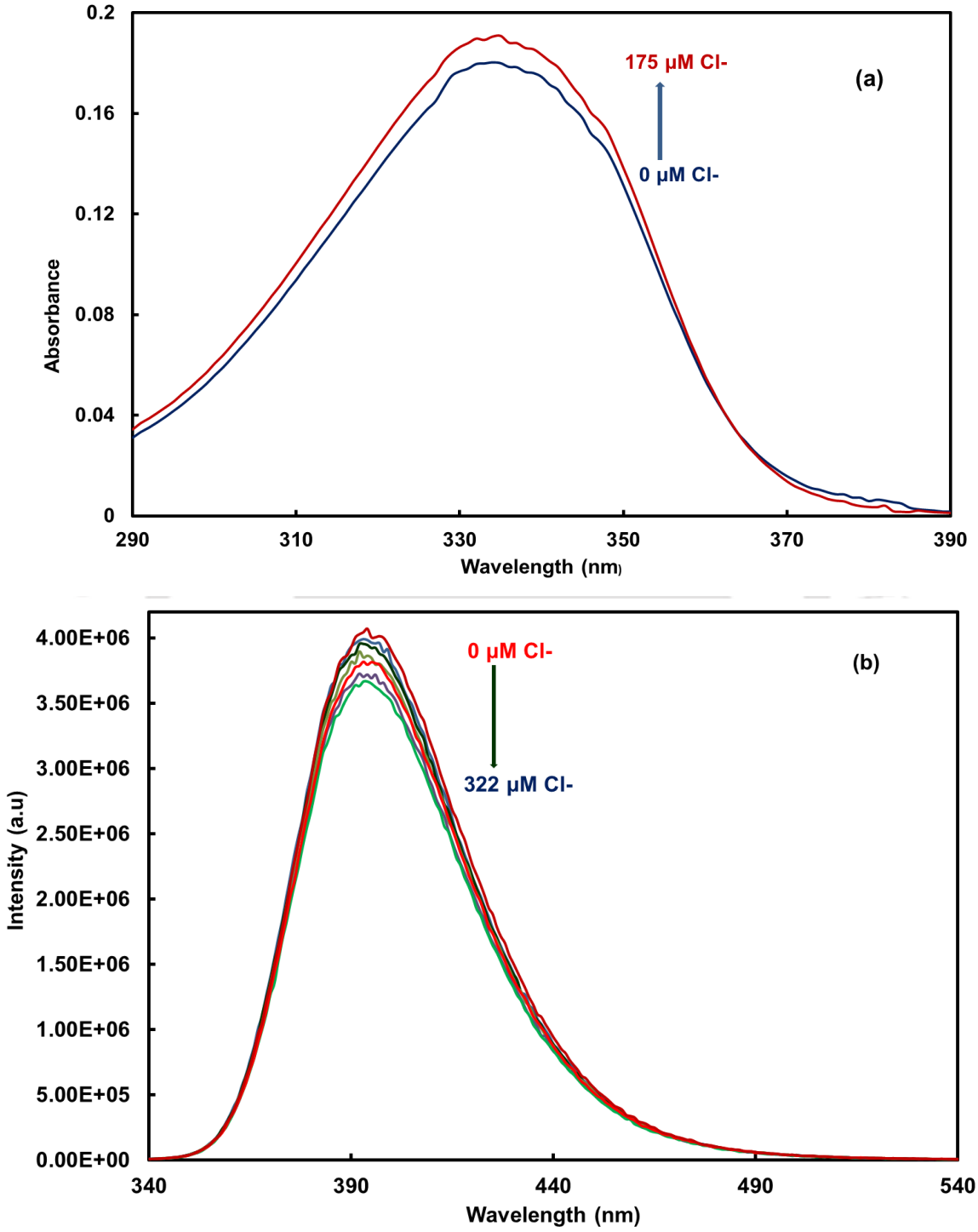

Figure 3.8. (a) Absorption spectra and (b) Fluorescence spectra at λ_{exc} = 330 nm of DMAPIP-c at different chloride ion concentration in acetonitrile.

The results are summarized below: (i) the non-appearance of longer wavelength emission in methyl derivatives shows that the hydrogen bonding of the solvents with both azole 'NH' hydrogen and pyridyl nitrogen play the essential roles in formation of TICT state (ii) the enhancement in TICT emission upon deprotonation in aqueous medium and its absence upon deprotonation in polar aprotic solvent signifies the role of relay proton transfer in the process. (iii) Strong positive solvatochromism advocates that the relay proton transfer leads to a TICT state. Based on these, a scheme for the formation of TICT state is proposed (**Scheme 3.1**). The scheme was substantiated by the fact that the TICT emission for both neutral and anion is same. This relay proton transfer is a paramount interesting process and it can mimick proton relay in vital biosystems.[180]

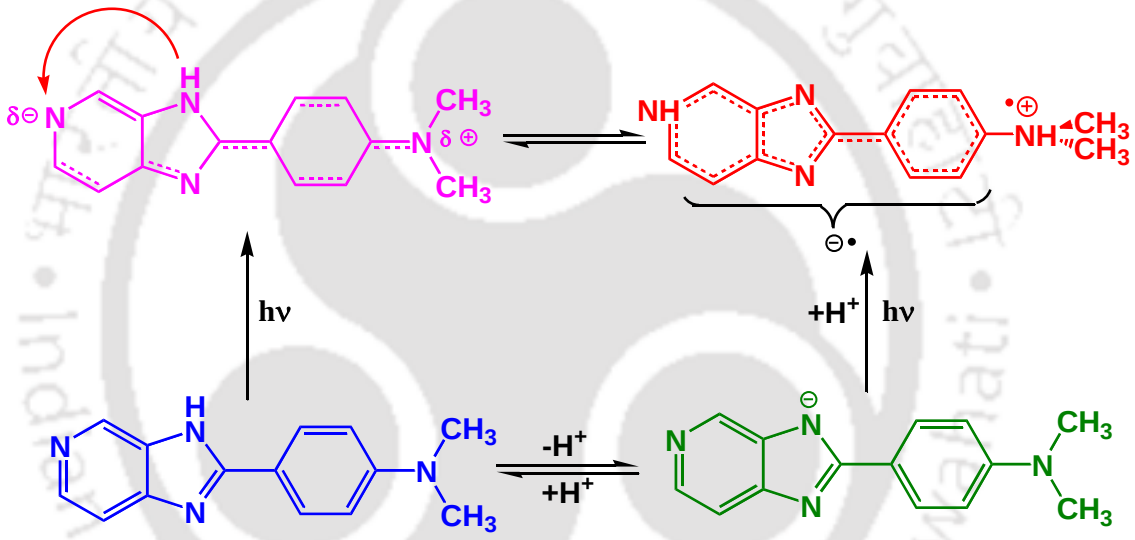

Scheme 3.1. The path for the formation of the TICT state.

3.3. Binary Solvent Mixture and Stochiometry

The spectral characteristics of DMAPIP-c in neat solvents were reported else where.[56] A bathochromic shift was observed in the absorption spectra with increase in polarity and hydrogen bonding capacity of the solvents except in water. Here, the effect of acetonitrile-methanol binary solvent mixture on the absorption spectrum of DMAPIP-c is investigated (**Figure 3.9**). Successive addition of methanol to acetonitrile shifts the absorption spectrum of DMAPIP-c towards longer wavelength. This red shift is the consequence of hydrogen bonded complex formation between DMAPIP-c and methanol.

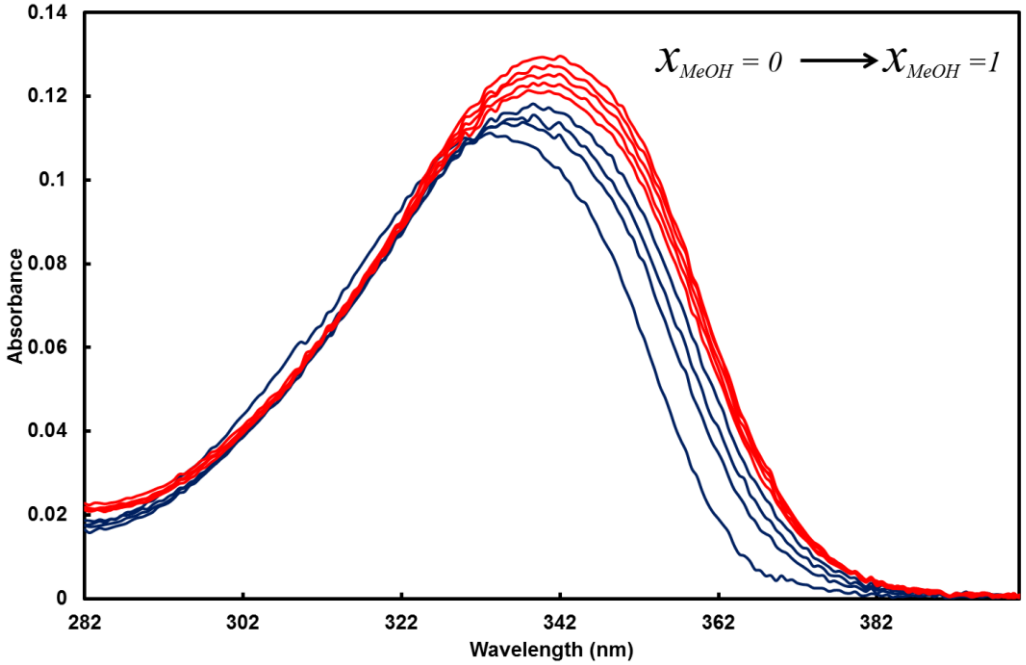

Figure 3.9. Absorption spectra of DMAPIP-c in acetonitrile-methanol mixture.

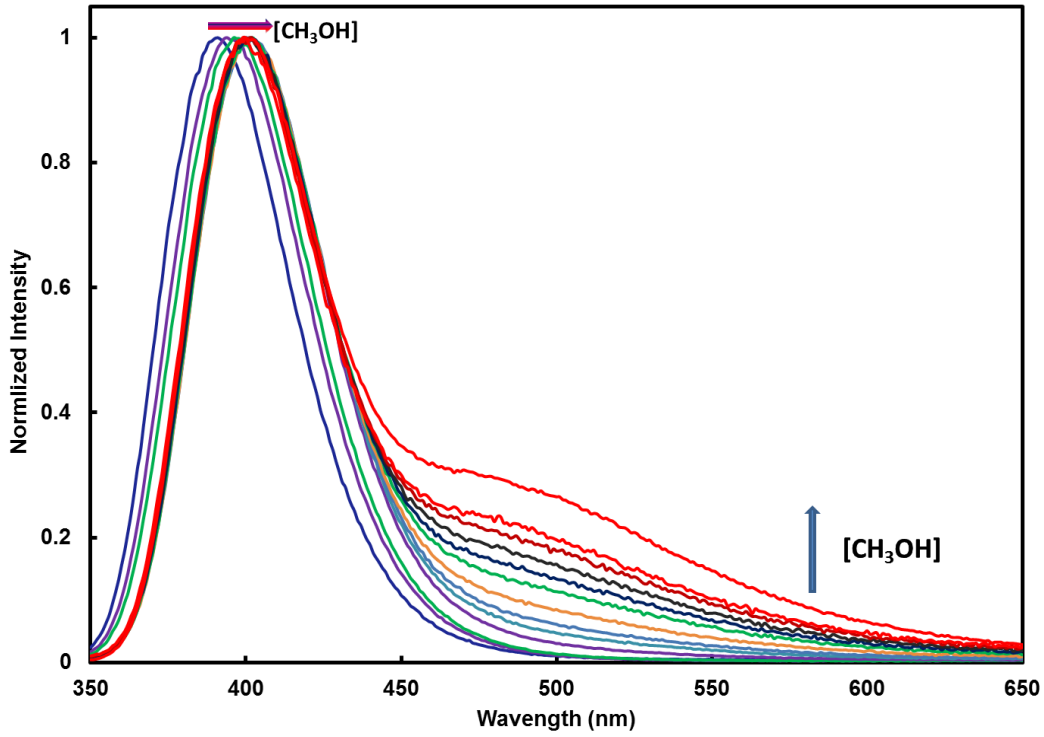

Figure 3.10. Normalized fluorescence spectra of DMAPIP-c in acetonitrile-methanol mixture, λ_{exc} = 340 nm.

The relay proton transfer process involves cylic hydrogen bonding network of fluorophore and solvent molecules. For *e.g.*, relay proton transfer of 7-hydroxyquinoline and 3-hydroxyxanthone involves cylic network of two and three solvent molecules,

repectively.[103,181] Therefore, to determine the number of methanol molecules those act as bridge connecting the 'NH' group and pyridyl nitrogen in the relay transfer, the fluorescence characteristics are investigated in acetonitrile-methanol mixture. DMAPIP-c emits a single emission at 390 nm in acetonitrile and is consistent with the earlier work.[56] Gradual addition of methanol leads to formation of an additional band at longer wavelength. The relative intensity of the longer wavelength band increases with increases in quantity of methanol (**Figure 3.10**). Though at low methanol concentration, the longer emission band is not clear, the band is well devepoled with sequential addition of methanol. The emission spectrum of DMAPIP-c in neat methanol matches with the literature report.[56]

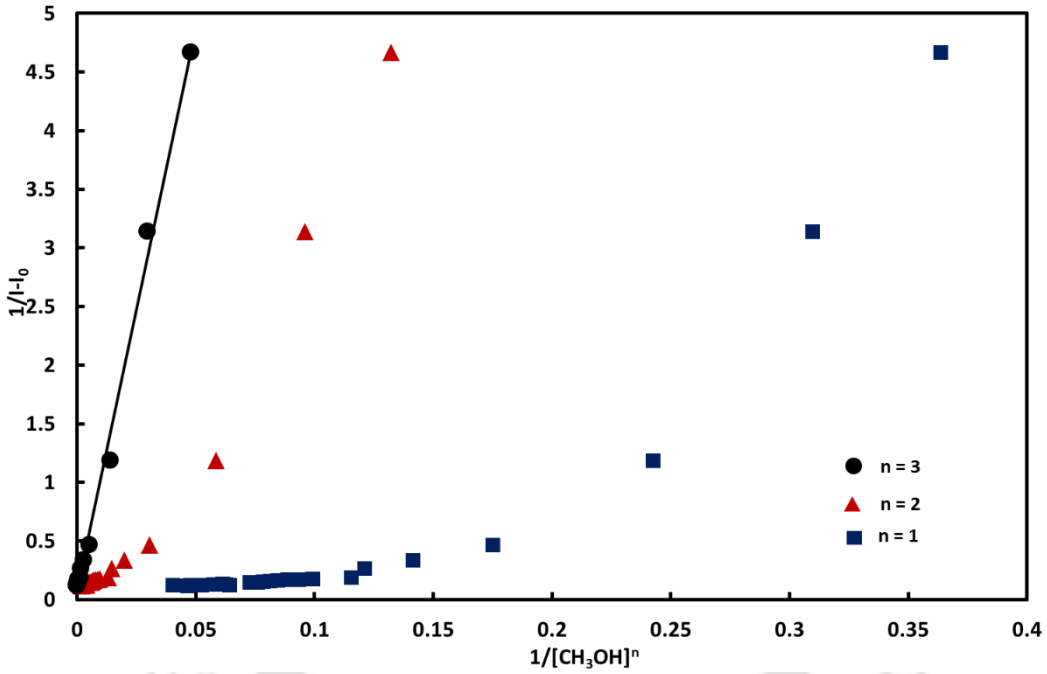

Figure 3.11. Benesi-Hilderbrand plot showing 1:3 binding of DMAPIP-c and methanol (measured at TICT band).

The stoichiometric ratio of DMAPIP-c and methanol is estimated from the Benesi-Hildebrand plot **(Figure 3.11)**.[182] Since, it is interested to determine the stoichiometry of complex responsible for the TICT emission the fluorescence intensities at 550 nm is used for calculations. The general form of Benesi-Hilderbrand equation for a 1: n complex formed between dye and methanol is presented below:

$$\frac{1}{I - I_0} = \frac{1}{I_\infty - I_0} + \frac{1}{K[M]^n\{I_\infty - I_0\}} \qquad (3.3)$$

where [M] represents the concentration of methanol, I_0 and I are the fluorescence intensities in absence and presence of alcohol respectively, I_∞ is the limiting intensity of fluorescence, *n* is the number of methanol molecules and *K* is the binding constant. The plots of $\frac{1}{I-I_0} Vs \frac{1}{[M]}$ and $\frac{1}{I-I_0} Vs \frac{1}{[M]^2}$ did not yield straight lines. However, the plot of $\frac{1}{I-I_0} Vs \frac{1}{[M]^3}$ results in a straight line (r^2 = 0.995, **Figure 3.11**). This advocates that three methanol molecules are involved in the proton transfer process. The multiple proton-transfer systems are rare compared to single or two proton transfer and typically entail molecular self-assembly or assembly of solvent molecules.

Strong positive solvatochromism clearly suggests that the longer wavelength emission is TICT emission. Still to rule out that the emission is not due to relay proton transfer without charge transfer, the spectral characteristics of 2-phenylimidazo[4,5-c]pyridine (PIP-c) are studied in acetonitrile-methanol mixture. The longer wavelength emission is observed neither in acetonitrile-methanol mixture nor in pure solvents (**Figure 3.12**). Unlike in DMAPIP-c with addition of methanol only a blue shift is observed even in normal emission of PIP-c. Thus, the conclusion that the longer wavelength is due to emission of the TICT state is further substantiated.

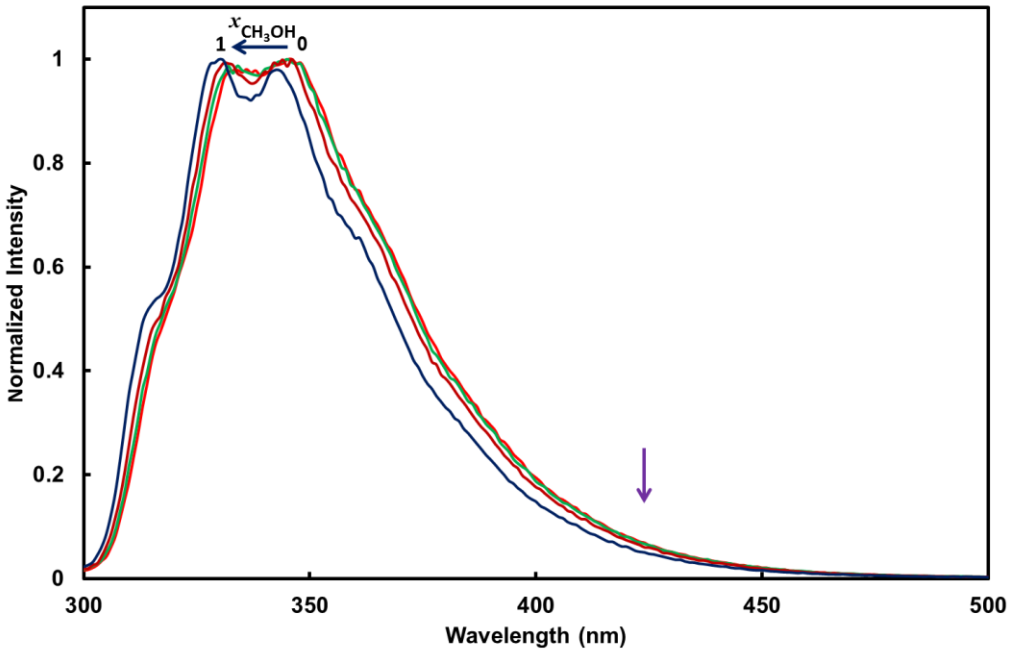

Figure 3.12. Normalized fluorescence spectra of PIP-c in acetonitrile-methanol mixture, λ_{exc} = 290 nm.

3.4. Quantum Mechanical Calculations

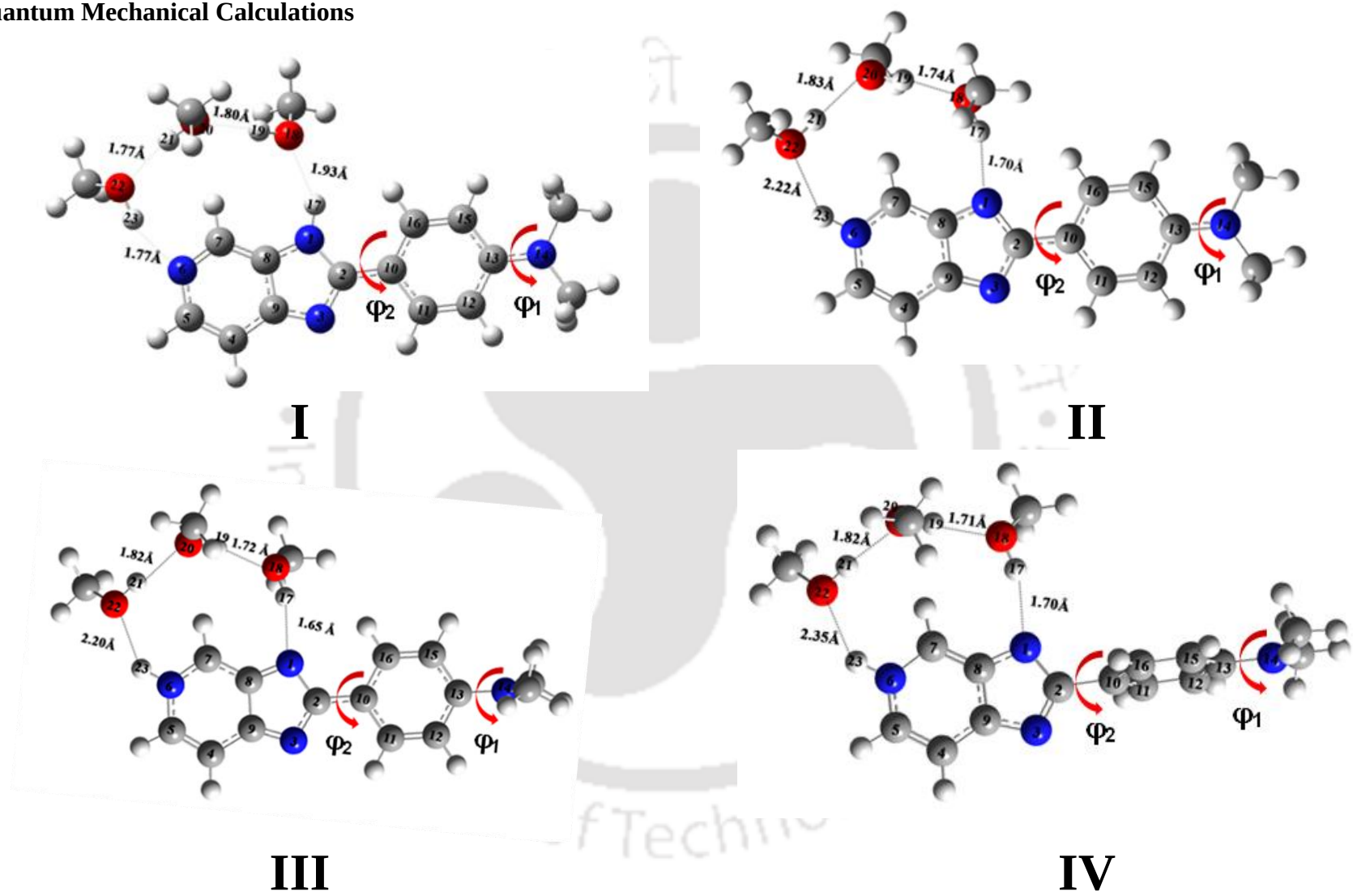

Figure 3.13. Excited state optimized structures of different forms of DMAPIP-c. $(CH_3OH)_3$ complex.

Table 3.2. Calculated Energy (eV) Obtained for the Normal Emission

Methods	Functional	Normal Emission
CIS/TDDFT	B3LYP	3.45
CIS/TDDFT	CAM-B3LYP	3.70
CIS/TDDFT	B3LYP- D3	3.43
TDDFT	B3LYP	3.21
TDDFT	CAM-B3LYP	3.41
TDDFT	B3LYP-D3	3.20

Experimental Value for Normal Emission is 3.13 eV

As mentioned earlier, the structure of the complex (**Figure 3.13**) were optimized in the excited state by CIS and TDDFT methods and the emission energy of the normal emission is calculated by TDDFT method using different functions (**Table 3.2**). The normal emission predicted from the TDDFT (with B3LYP-D3 function) optimized structure is in better agreement with the experimental value. Therefore, this procedure was followed for the excited state optimization of different forms of DMAPIP-c.$(CH_3OH)_3$ complex (**Figure 3. 13**). The calculations also suggest that three methanol molecules are required to form the cyclic hydrogen bond structure. In the normal form complex the $H_{17}\cdots O_{18}$ and $H_{23}\cdots N_6$ hydrogen bond lengths are 1.93 Å and 1.77 Å, respectively. In $H_{17}\cdots O_{18}$ hydrogen bond the hydrogen atom of the imidazole 'NH' group acts as the hydrogen bond donor and the oxygen atom of the methanol acts as the hydrogen bond acceptor. In $H_{23}\cdots N_6$ hydrogen bond, the hydrogen atom of the methanol acts as the hydrogen bond donor and the pyridyl nitrogen acts as the hydrogen bond acceptor. The H_{17}-O_{18} and H_{23}-N_6 bond distances shrink to form covalent bonds and the $N_1\cdots H_{17}$ and $O_{22}\cdots H_{23}$ bond distances elongate as hydrogen bond to form tautomer. In tautomer-$(CH_3OH)_3$ complex $N_1\cdots H_{17}$ and $O_{22}\cdots H_{23}$ hydrogen bonds are 1.70 Å and 2.22 Å respectively. In all the complexes, the N-H$\cdots$O hydrogen bonds are little longer than O-H$\cdots$N hydrogen bonds. In other words, methanol formed a shorter bond when it acts as hydrogen bond donor than when it acts as hydrogen bond acceptor. The intermolecular hydrogen bonds between methanol molecules (O-H$\cdots$H hydrogen bond) are shorter than 2 Å. The intermolecular hydrogen bonds between methanol molecules are also affected by the formation of tautomer. The cone angles of tautomer-$(CH_3OH)_3$ complex are $\angle N_1\cdots H_{17}$-O_{18} = 166º, $\angle O_{18}\cdots H_{19}$-$O_{20}$ = 176º, $\angle O_{20}\cdots H_{21}$-$O_{22}$ = 174º, $\angle O22\cdots H_{23}$-N_6 = 131º and those of normal-$(CH_3OH)_3$ complex are $\angle N_1$-$H_{17}\cdots O_{18}$ = 148º, $\angle O_{18}$-$H_{19}\cdots O_{20}$ = 177º, $\angle O_{20}$-$H_{21}\cdots O_{22}$= 173º, $\angle O_{22}$-$H_{23}\cdots N_6$ = 158º. Twisting of dimethylamino group shortens these hydrogen bonds. In other words, the formation of TICT strengthened the hydrogen bonds of the imidazo pyridine ring (acceptor). But still the hydrogen bond is little shorter when methanol acts as donor than

when it acts as acceptor. The bond distances and cone angles are suitable for the hydrogen bond formation in both complexes.[183]

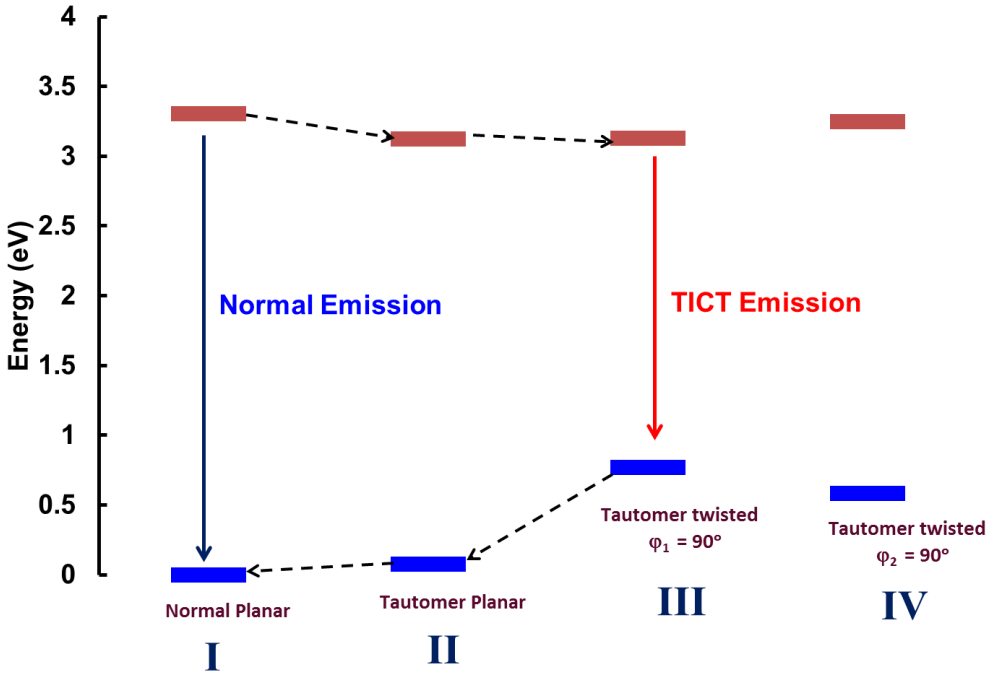

Scheme 3.2. Energy level diagram of different forms of DMAPIP-c.$(CH_3OH)_3$ complex shown in Figure 3.13.

The emission energy obtained from the theoretical calculations are sketched in **Scheme 3.2.** The calculations predict that the energy of normal hydrogen bonded structure is lowest in the ground state. But in the excited state, the energy of the normal form is higher than that of the tautomer. This suggests that the relay proton transfer through solvent molecule is energetically favoured in the excited state. From the tautomer, twisting of the dimethylamino group or the dimethylaminophenyl group should lead to TICT state. Therefore, the energies of both the excited states were calculated. In the S_1 state, the energy of the dimethylamino twisted conformer is less than that of the dimethylaminophenyl twisted conformer. Thus, it can be inferred that it is the dimethylamino group that is twisted to form the TICT state in DMAPIP-c. The energy predicted by the calculation for the TICT emission (2.41 eV) is also concord with the experimental value (2.61 eV) in methanol.[56] The frontier molecular orbitals involved in this transition are shown in **Figure 3.14**. The charge is localized on the dimethylamino group in the highest occupied molecular orbital (HOMO) and on the other part of the molecule in the

lowest unoccupied molecular orbital (LUMO). These decoupled orbitals (very little overlap between the orbitals) are consistent with TICT model.[1]

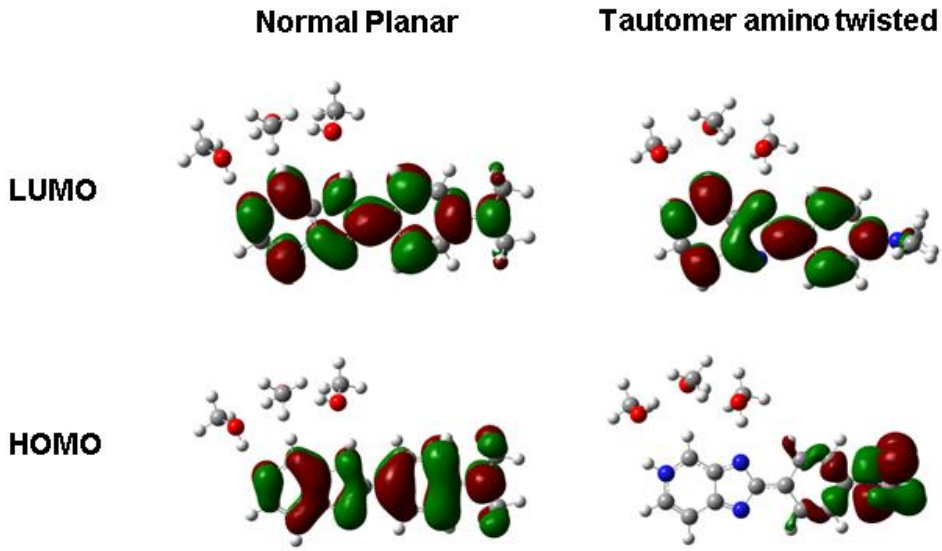

Figure 3.14. The frontier molecular orbitals of DMAPIP-c, normal planar form and the dimethylamino twisted conformer of tautomer form.

The proton transfer induced charge transfer that lead to nonradiative process was reported in number of molecules.[107, 184] Similar proton transfer enhanced/induced TICT emission was reported from 4-amino- and 4-*N*,*N*-dimethylamino- salycylic acids.[108] But in salylic acids the proton transfer is an intramolecular process. In DMAIP-b, it is an intermolecular process involving just one solvent molecule, but the salient feature in DMAPIP-c that it is an intermolecular process involves relay of four proton transfer which leads to TICT emission.

3. 5. Conclusion

No dual emission is observed when pyridyl nitrogen or imidazole 'NH' of DMAPIP-c can not form hydrogen bond. The binary solvent study reveals that three solvent molecules are involved in the formation of TICT state. No TICT emission is observed upon deprotonation in acetonitrile. Comparison of characteristics of anionic form in protic and aprotic solvents indicates that the formation of TICT state occurs via monoanionic form, but the anion does not emit TICT emission in aprotic solvent. The relay transfer of proton from the imidazole hydrogen to the nitrogen at pyridyl ring induces the TICT emission in DMAPIP-c. In contrast to Fasani *et al*. model, the dimethylamino group of DMAPIP-c is twisted to form the TICT

state. The theoretical calculations support the proposed mechanism and the transition energy predicted by the calculation is in good agreement with the experimental value.

Chapter 4

Intermolecular Proton Transfer Induced Twisted Intramolecular Charge Transfer Inside Cucurbit-7-uril Cavity: Role of Internal Water

4.0. Introduction

Supramolecular systems for designing new systems with improved host-guest interaction have been a topic of growing research interest. Further these host-guest bindings are used to modulate the photophysical and photochemical properties of the various organic dyes.[185-187] Todate variety of organic host systems including cyclodextrins (CDs), calixarenes, octa-acids, cucurbit[n]urils (CB-n)etc. are used to encapsulate guest molecules.[187-192] Among the various kind of supramolecular host systems, CB-ns have gained fame in recent years.[125,192-194] CB-ns are highly water soluble macrocylic host, which are having different glycoluril units connected by a pair of methylene linkers. CB-ns are classified into different types such as CB-5, CB-6, CB-7 etc. depending upon the n value 5, 6, 7 etc. respectively.[125] They have fairly rigid hydrophobic cores of different sizes and are blessed with fairly low polarity and polarizability. Furthermore, on-going research on host-guest chemistry with CB-n shows that the release of the high energy water molecules from CB-n cavity in aqueous solution upon binding with guests is one of the major driving forces for encapsulation.[125,126,195] However, for higher members of CB-n, the energy of internal molecules decreases due to improved hydrogen-bonding possibilities between guest and CB-n through hydrogen bond network.[125,195]

Among the CB-n family, cucurbit -7-uril (CB-7) has been established as an excellent water-soluble host, with high binding affinity with various guests.[196-200] CB-7 also shows high binding affinity for cationic guest molecules such as milrinone, N-alkylated pyridines, imidazolium-based compounds etc.[127,128,201-202] It is well studied that the CB-7 forms inclusion complex with guest molecules through charge-dipole and hydrogen bonding interactions at the carbonyl oxygen present at the opening of CB-7 cavity and through hydrophobic interaction at inside CB-7 cavity. CB-7 is also recognized to modify the photophysical characteristics of chromophoric guest molecules.[199,200,203,204] Modulations of the acid– base behaviour of encapsulated molecules contribute surplus interest to understand the host–guest interactions.[205-207] Bhasikuttan *et al.* investigated the modulation of ICT to TICT state upon interaction of coumarin derivative with CB-7.[123] Recently, Bhattacharya *et al.* reported that *N*,*N*-dimethylaminonaphthyl-(acrylo)-nitrile has high binding affinity with CB-7 compared to that of β-CD.[124]

In this chapter the interactions of DMAPIP-b and DMAPIP-c with CB-7 are investigated. The chapter is divided into two sections. First section contains interaction of the CB-7 with neutral DMAPIP-b and DMAPIP-c. Second section focuses the effect of the CB-7 on the monocationic equilibrium of DMAPIP-b and DMAPIP-c.

4.1.0. Interaction of the CB-7 with Neutral DMAPIP-b and DMAPIP-c

Though studies of ICT/TICT probes are investigated in CB, studies of DMAPIP-b and DMAPIP-c inside CB is much more interesting as for these molecules protic environment is essential to exhibit TICT emission. As described in previous chapter TICT emission of DMAPIP-b and DMAPIP-c induced by double proton transfer and relay proton transfer, respectively. Therefore studies of DMAPIP-b and DMAPIP-c in CB will provide new insight about the characteristics such as proton transferring ability of the internal water present inside CB.

4.1.1. Absorption Spectra of the Neutral DMAPIP-b and DMAPIP-c in CB-7

The absorption spectra of DMAPIP-b and DMAPIP-c in presence of CB-7 are depicted in **Figures 4.1 and 4.2**, respectively. The spectral data in presence of CB-7 along with aqueous medium and cyclodextrin media are provided in **Table 4.1**. It was reported that the neutral DMAPIP-b and DMAPIP-c in aqueous solution possess longest wavelength absorption band at 345 nm and at 335 nm, respectively.[57,179] With gradual addition of CB-7, a very little blue shift is observed in the absorption spectra of DMAPIP-b. The absorbance decreases for the initial addition of CB-7. The absorbance as well as the absorption band maximum remains unchanged after addition of 66 μM of CB-7. On the otherhand, the absorption spectrum of DMAPIP-c in CB-7 is distinctly blue shifted by ~ 5 nm with decrease in absorbance. Although not clear, a quasi-isosbestic point is observed at ~ 321 nm in the absorption spectra of DMAPIP-c. The variations in absorption spectra infer that the interaction of fluorophores and CB-7 and might be due to formation of host-guest inclusion complexes. It was reported that the neutral probes bind with CB-7 through hydrogen bonding at carbonyl portal region and mainly through hydrophobic interaction inside the CB cavity.[124] Therefore, these two interactions are primarily responsible for changes in the absorption spectral profile. The spectral shift observed in presence of CB-7 is just opposite to that observed in presence β-CD, where the spectrum is red shifted upon complexation with β-CD.[121,122] The difference in absorption profile may be due to the structural difference between CB -7 and β-CD, which might have provided different binding opportunity.

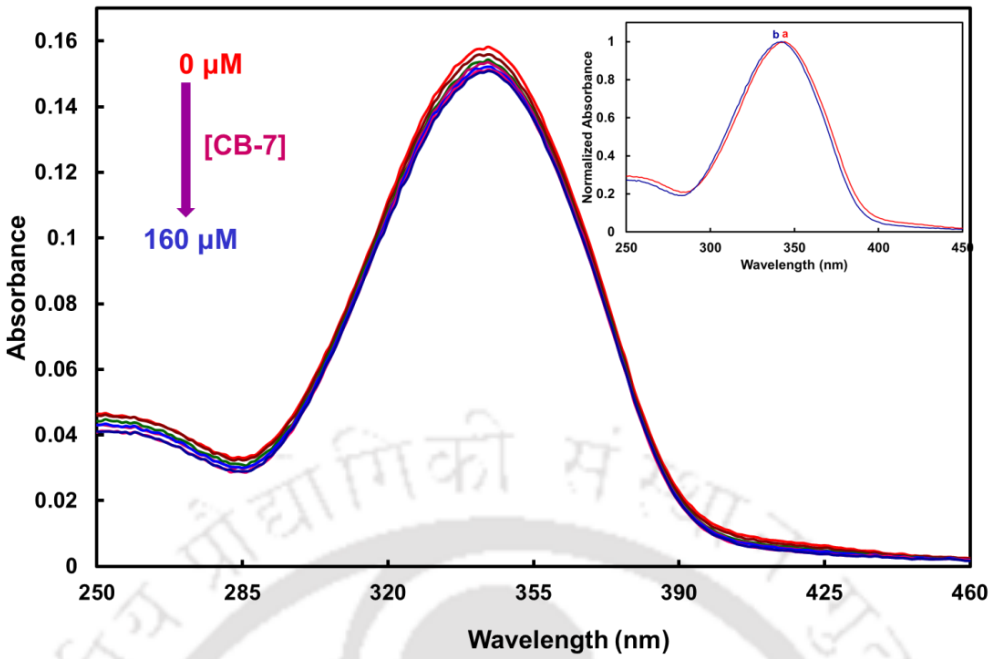

Figure 4.1. Absorption spectra of neutral DMAPIP-b at various concentration of CB-7 (Inset (a) 0 µM and (b) 160 µM showing blue shift of the spectra upon binding with CB-7).

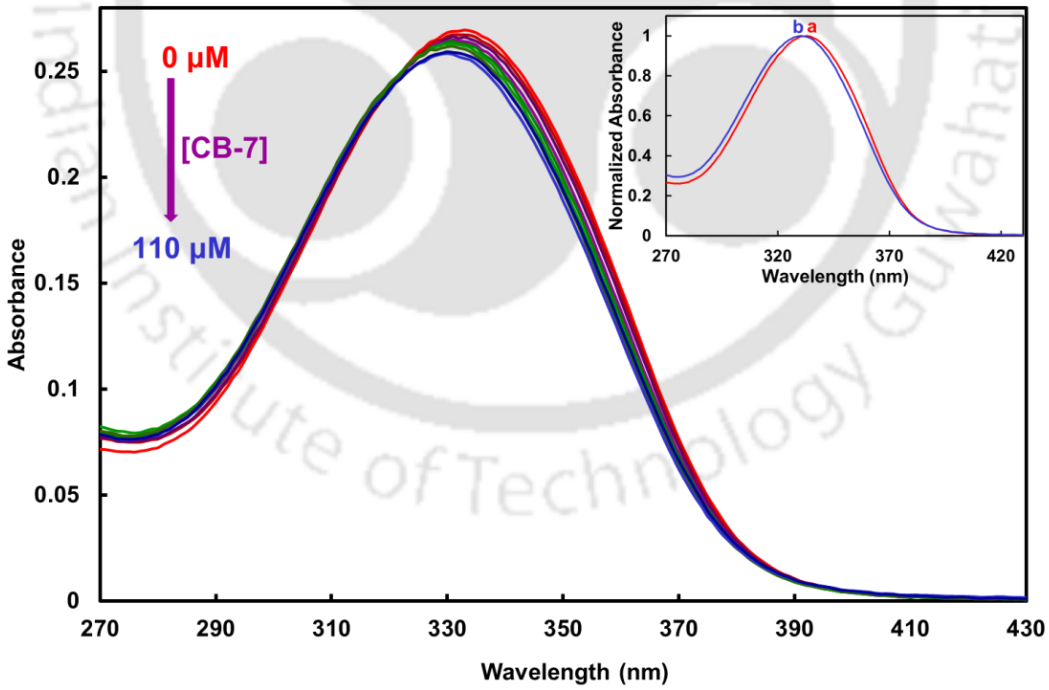

Figure 4.2. Absorption spectra of neutral DMAPIP-c at various concentration of CB-7 (Inset (a) 0 µM and (b) 110 µM showing blue shift of the spectra upon binding with CB-7).

Table 4.1. Absorption Band Maximum (λ_{max}^{ab}, nm), Fluorescence Band Maximum (λ_{max}^{fl}, nm) and Fluorescence Lifetimes (τ, ns) of Neutral DMAPIP-b and DMAPIP-c in Different Media.

Molecule	Medium	λ_{max}^{ab}	λ_{max}^{fl}		τ^a	
			N	TICT	N	TICT
DMAPIP-b	Water (pH 9.0)[b]	345	451		0.16 (98.75)	2.12 (1.25)
	β-CD (pH 9.0)[b]	350	424		0.61 (79.54)	2.04 (20.46)
	CB-7 (pH 9.5)	344	448		0.23 (96.14)	2.70 (3.86)
DMAPIP-c	Water (pH 9.0)	335	414	505	0.17 (89.80)	1.47 (10.20)
	β-CD (pH 9.0)[c]	340	397	460	0.54	1.74
	CB-7 (pH 9.5)	331	407	510	0.29 (74.83)	2.52 (25.87)

[a]Relative amplitudes of the species in the biexponential decays are present in parenthesis.[b]From ref. 121.[c]From ref. 122.

4.1.2 Fluorescence Spectra of DMAPIP-b and DMAPIP-c in CB-7

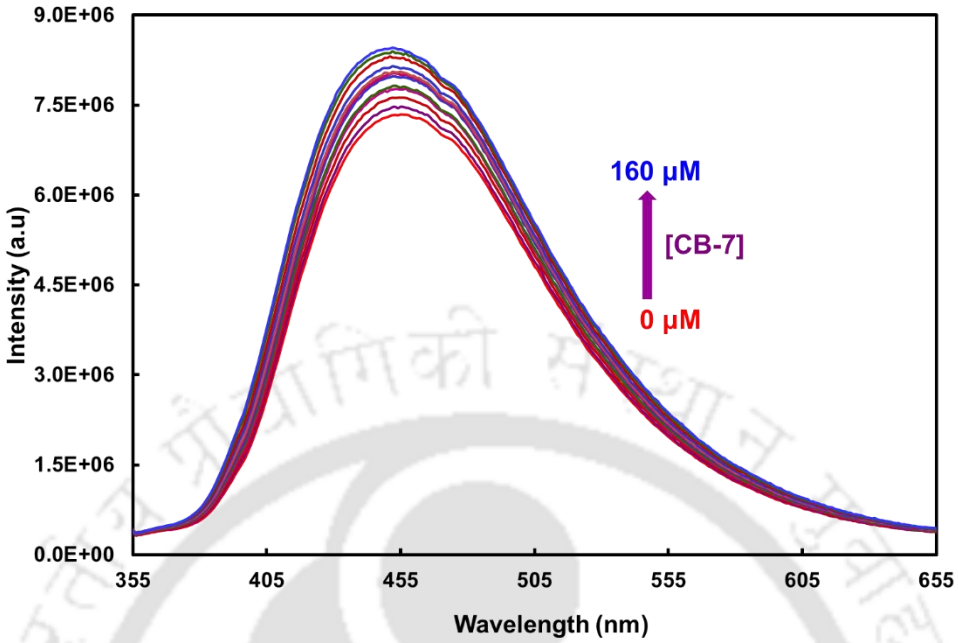

Figure 4.3. Fluorescence spectra of neutral DMAPIP-b with varying concentration of CB-7, λ_{exc} = 345 nm.

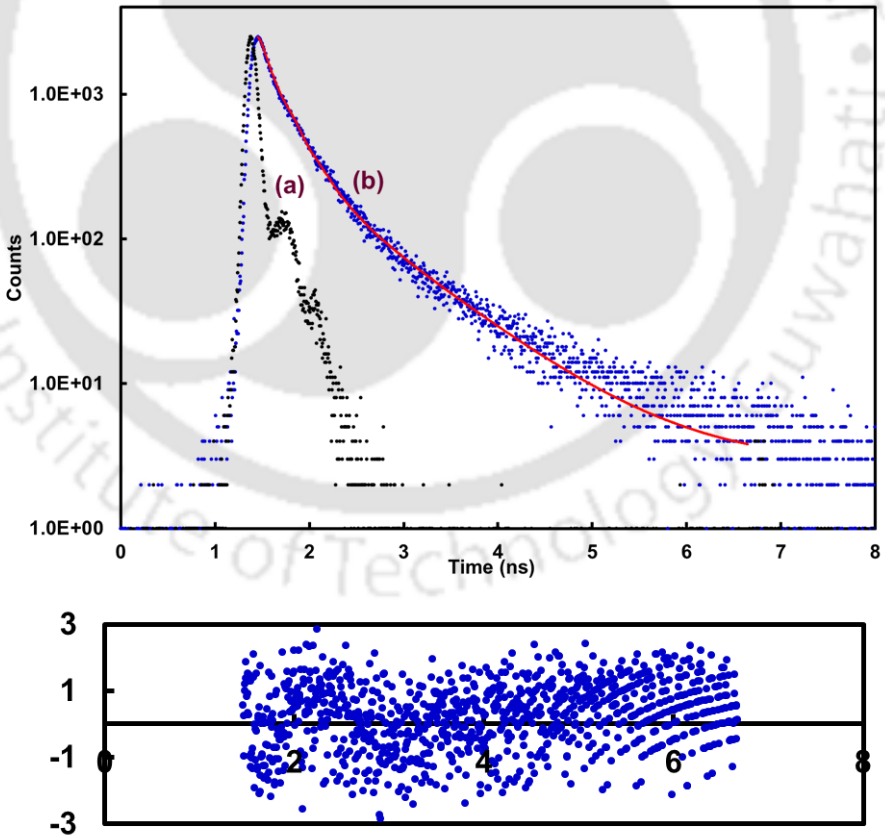

Figure 4.4.(a) Instrument Response function and (b) fluorescence decay of neutral DMAPIP-b in 160 μM CB-7, along with fitted curve and residue plot at λ_{exc} = 375 nm and λ_{em}= 450 nm.

In addition to absorption study, the fluorescence study of both the molecules is studied with CB-7. Upon, addition of the CB-7, the fluorescence spectra of DMAPIP-b undergoes a gradual blue shift with increase in intensity (**Figures 4.3)**. However, no clear TICT band appears in presence of CB-7. The TICT emission of DMAPIP-b in water is also very weak and is present underneath the sturdy normal emission.[57] The biexponential decay in water illustrated the dual emission of the DMAPIP-b in water. Therefore, the fluorescence decay was measured in CB-7 solution **(Figure 4.4)**. The biexponential fluorescence decay obtained in CB-7 (**Table 4.1**) indicates the presence of TICT emission in CB-7 environment also. The blue shifts in the fluorescence spectrum are much small compared to that in *β*-CD. Though the relative amplitude of TICT emission increases in CB-7 compared to aqueous medium, like the spectral blue shift it is also relative small compared to that in presence of *β*-CD.

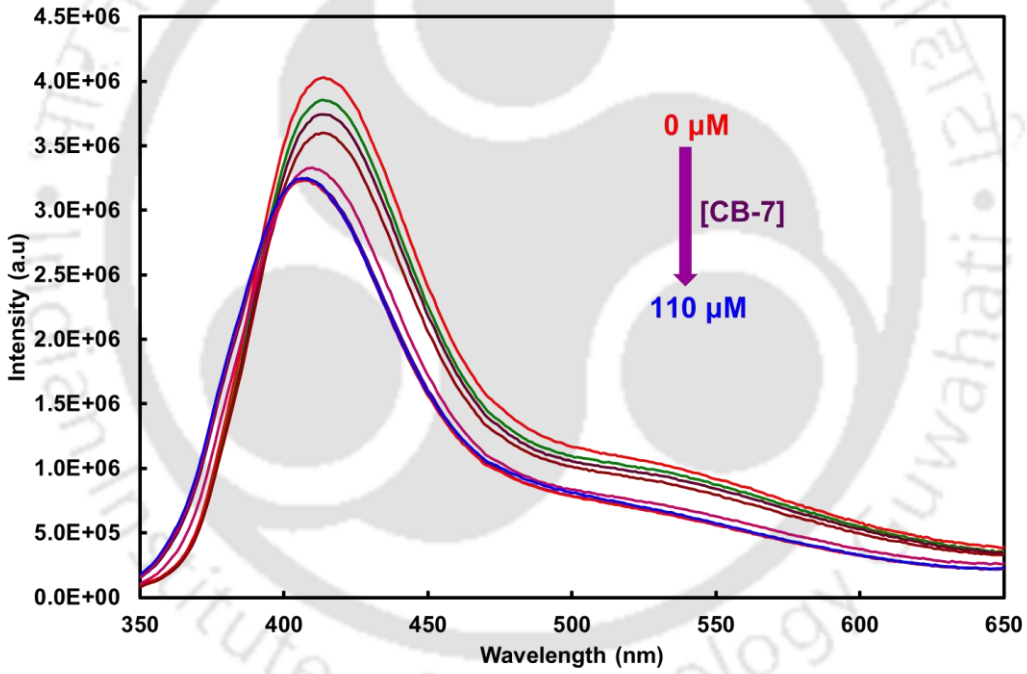

Figure 4.5. Fluorescence spectra of neutral DMAPIP-c with varying concentration of CB-7, λ_{exc} = 335 nm.

The changes in the fluorescence spectra of DMAPIP-c in presence of CB-7 are more significant than those of DMAPIP-b (**Figure 4.5**). Nevertheless, like those of DMAPIP-b the blue shift is less compared to the effect of *β*-CD on DMAPIP-c (**Table 4.1**). The noted difference between the effect of CB-7 on fluorescence of DMAPIP-b and DMAPIP-c is the reduction in fluorescence intensity of DMAPIP-c with increase in CB-7 concentration. Whereas, the fluorescence of DMAPIP-c also increases upon complexzation with CDs.[122]

Unlike that of DMAPIP-b, the TICT band of DMAPIP-c is clearly visible in water. With addition of CB-7 though the fluorescence intensities of both normal and TICT bands of DMAPIP-c decrease, the relative amplitude of the TICT emission increases (**Table 4.1** and **Figure 4.6**).

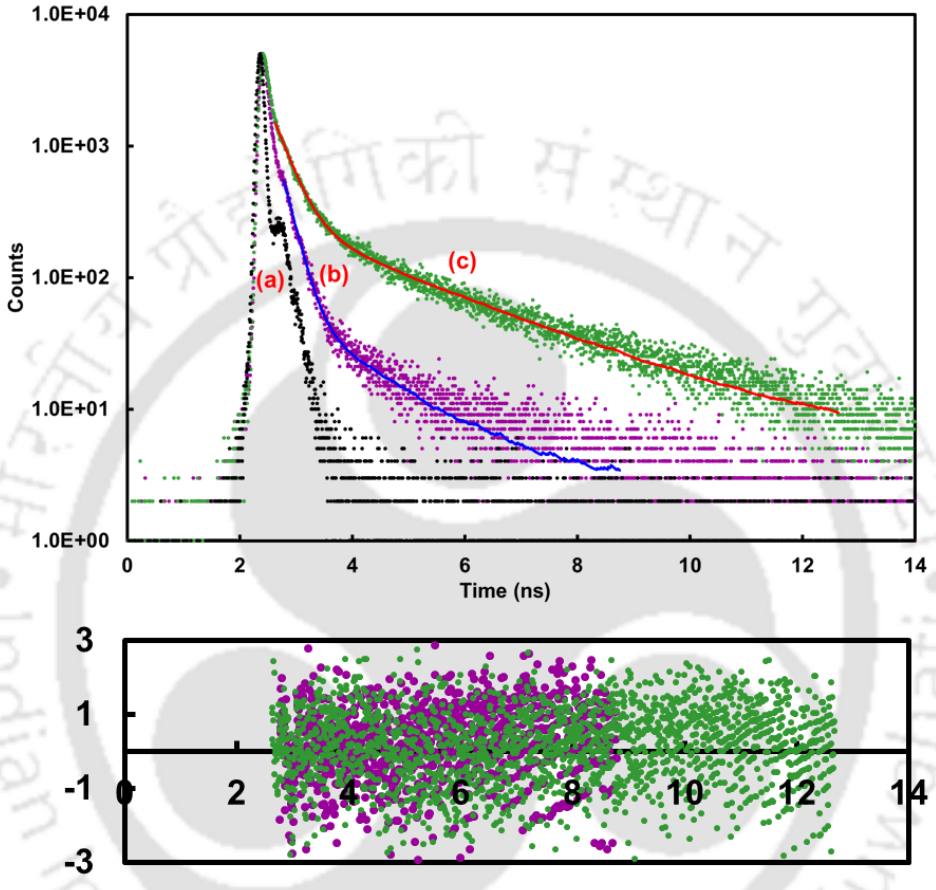

Figure 4.6. (a) Instrument response function, (b) fluorescence decay of neutral DMAPIP-c, absence of CB-7 and (c) presence of CB-7, λ_{em}= 510 nm along with fitted curve and residue plot at λ_{exc} = 375 nm.

As mentioned earlier, both DMAPIP-b and DMAPIP-c emit dual emission in protic environment.[57,208] The dual emission are the normal emission and the proton transfer induced TICT emission. In general, the polarity experienced by the guest inside the CB cavity depends upon the local polarity, partial encapsulation of the probe, number of water molecules confined inside the cavity, freedom of movement etc. It was also reported that the polarity of CB-7 is comparable to ethanol or octanol.[125,209] Therefore, in hydrophobic CB-7 cavity the guest is expected to experiences a less polar microenvironment than water. The excited state dipole

moments of DMAPIP-b and DMAPIP-c are higher than their respective dipole moments in the ground state. Hence, the reduction of polarity increases the energy gap between the ground state and more polar excited state of the guest molecules; as a result the spectra of the guests are blue shifted compared to aqueous medium. The blue shift observed in the fluorescence spectra of both guest molecules suggests that both of them are encapsulated inside the CB-7 cavity. However, the fluorescence of DMAPIP-c decreases upon complexzation with CB-7 and this may be due to dipole-dipole interaction between electron rich carbonyl portal of CB-7 and lone pair electron of pyridyl N of DMAPIP-c. Theoretical calculations also predict that the position of pyridyl nitrogen is closer to carbonyl portal of CB-7 (see later). The fluorescence lifetime of guest molecules are longer inside the CB cavity than those in aqueous medium. Interestingly, the lifetimes of the normal emission in CB-7 cavity are shorter than those in *β*-CD complex but the lifetimes of the TICT emission in CB-7 are longer than those in *β*-CD complex. This may be due to difference in orientation of the guest molecules inside CB-7 cavity than in *β*-CD inclusion complexes (see later).

4.1.3. Stoichiometry and Binding Constant

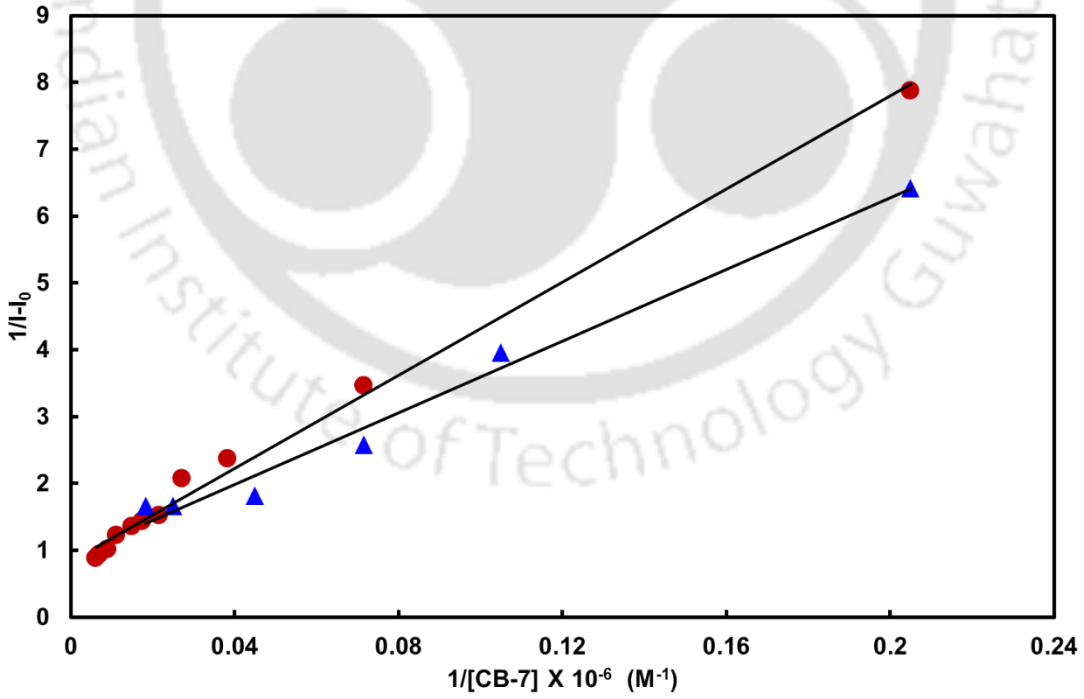

Figure 4.7. Double reciprocal plot for (a) DMAPIP-b (●) and (b) DMAPIP-c (▲).

Since, the fluorescence spectra are more sensitive than the absorption spectra the association constants of these guest molecules with CB-7 have been determined using fluorescence intensities. The Benesi-Hildebrand equation (**Equation 3.3, Chapter 3**) is used for the calculation. The double reciprocal plots of $\frac{1}{I - I_0}$ versus $\frac{1}{[CB-7]}$ are depicted in **Figure 4.7** for DMAPIP-b and DMAPIP-c, respectively. The linear plots with good correlation coefficient (r^2 = 0.99) show the formation of 1: 1 inclusion complexes between these guest molecules and CB-7. The binding constants obtained for CB-7 complexes much greater than the CD complexes of these molecules reported earlier (**Table 4.2**).[121,122] This shows that binding affinity of the guest molecules with CB-7 is more than with β-CD. Varieties of other guest molecules also have greater binding affinity towards CB-7 than CDs.[124,196,210,211]

Table 4.2. Binding Constants (K_a, M^{-1}) of DMAPIP-b and DMAPIP-c.

Host	K_a	
	DMAPIP-b	**DMAPIP-c**
β-CD[a]	4.1×10^2	3.9×10^2
CB-7	2.7×10^4	3.3×10^4

[a]From ref.121 and122

4.1.4. Mode of Encapsulation of Guests inside CB-7

Apart from the spectral changes, the dimensions of CB-7 and the size of the guests will give a better picture for the mode of encapsulation. As mentioned earlier, CB-7 is a barrel shaped molecule having cavity parameters as shown in the **Figure 4.8**.The optimised geometries of the DMAPIP-b and DMAPIP-c are also provided in the **Figure 4.9**. The dimensions of both the molecules are nearly same.

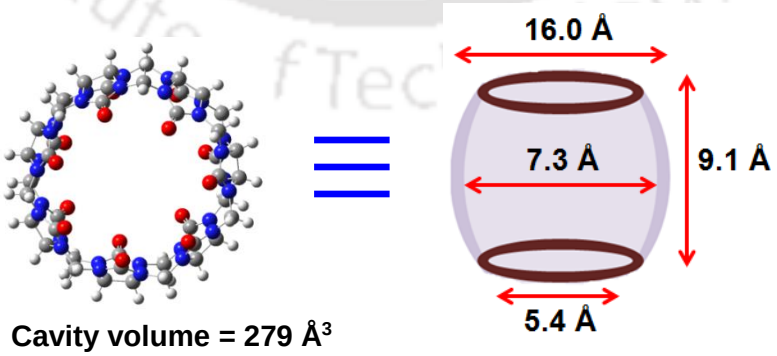

Figure 4.8. Different representations of CB-7 (from Ref. 192).

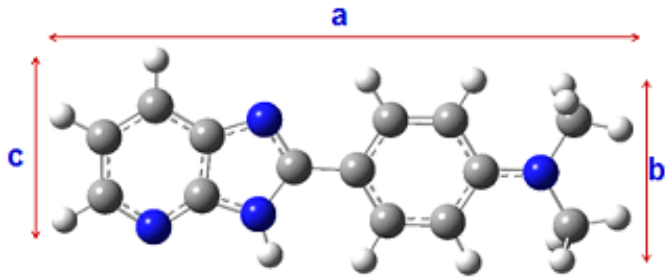

(DMAPIP-b)

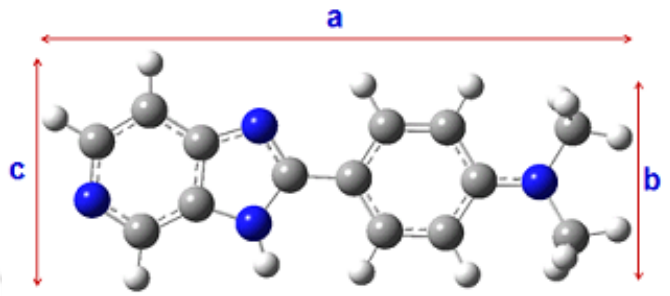

(DMAPIP-c)

	a (Å)	b (Å)	c (Å)
DMAPIP-b	12.86	4.12	3.96
DMAPIP-c	12.85	4.10	4.96

Figure 4.9. Dimensions of DMAPIPs.

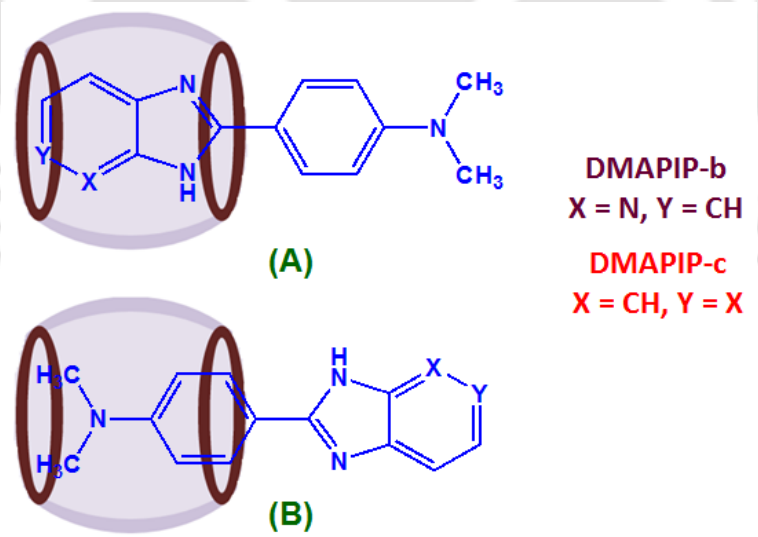

Scheme 4.1. Orientations of the guests inside CB-7.

By taking into account the stoichiometry and the dimensions of host and guest molecules, it can be inferred that both guests are encapsulated only partially inside the host. Two different orientations are possible for guest molecules as shown in the **Schemes 4.1 (A)** and **(B)**. In orientation (**A**), the imidazopyridyl ring of the guest resides inside the CB-7 cavity

and the other part of the molecule resides outside the cavity. While, in orientation (**B**) the dimethylaminophenyl ring of the guest exist inside CB-7 and other part of the molecule is present outside the cavity.

In DMAPIP-b and DMAPIP-c hydrogen bonding with the imidazopyridine (the charge acceptor) increases the charge flow to the acceptor which produces red shift in the spectra. On the other hand, the hydrogen bonding with dimethylamino group (charge donor) reduces the charge flow from the donor which leads to the blue shift in the spectra. The absorption spectrum of both guest molecules are blue shifted compared to that in water. This suggests that both guests form complexes with CB-7 in such a way that the hydrogen bonding with the imidazopyridine moiety is eliminated. In other words, the guest molecules form the inclusion complexes as shown in orientation (**A**). In this orientation, the imidazopyridine present inside the CB-7, as a result of the hydrogen bonding interaction is eradicated (**Scheme 4.1 A**). The blue shifts of the CB-7 complexes are less and these suggest that the hydrogen bonding with imidazopyridine through reduced but not completely eliminated. With CD, these imidazopyridines form complexes in such a way that the dimethylamino groups were present inside the CD cavity and the imidazopyridine rings were present in water and red shifts were observed in the absorption spectra of theses guests upon complexzation with CD.

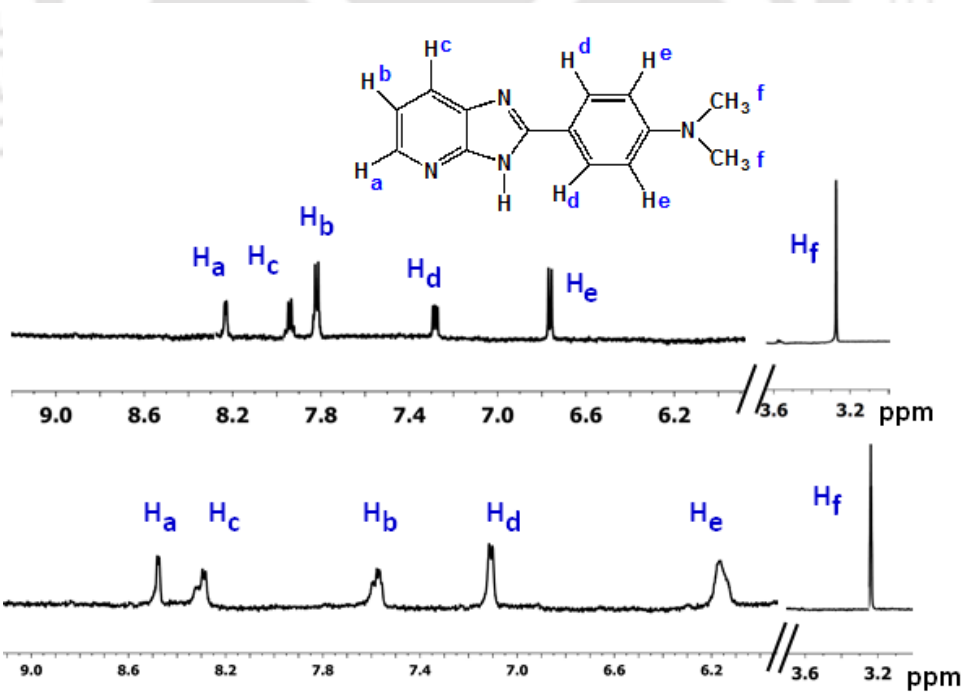

Figure 4.10. ^{1}H NMR spectra of DMAPIP-b (a) without CB-7 and (b) with CB-**7** in D_2O**.**

Table 4.3. ^{1}H NMR Spectral Data of DMAPIP-b (Proton labels, Figure 4.10)

Proton	D_2O	CB-7+D_2O	Δδ shift
H_a	8.23 (brs, 1H)	8.52 (brs, 1H)	– 0.29
H_b	7.28 (dd, 1H)	7.58 (brs, 1H)	–0.30
H_c	7.93 (d, 1H)	8.30 (brs, 1H)	–0.37
H_d	7.82 (d, 1H)	7.12 (brs, 1H)	
		6.99 (brs, 1H)	+ 0.77
He	6.76 (d, 2H)	6.08 (brs, 2H)	+ 0.68
H_f	3.24 (s, 6H)	3.27 (s,6H)	– 0.03

^{1}H NMR measurements provide useful details about molecular orientation in inclusion complexes.[121,124,199,212] Thus, NMR spectra were recorded. **Figure 4.10** depicts the NMR spectra of DMAPIP-b in the absence and in the presence of CB-7 and the data are compiled in **Table 4.3.** The peaks are better resolved in D_2O than earlier work, but the values are very close to reported values.[121] The better resolution may be due to higher frequency (600 MHz) of the spectrometer used in the present work. All the peaks broaden upon addition of CB-7. It is reported that the hydrophobic interaction of guest and host produce an upfield shift in the ^{1}H NMR spectrum.[123] Therefore, the peaks of protons which reside inside the cavity are shifted to upfield and protons nearer to the carbonyl portal shifted to downfield upon interaction with CB.[128,213] Since, the H_d and H_e protons are outside the cavity nearer to carbonyl portal of the CB-7, they experience a down field effect. Only small downfield effect in the peak of H_f protons (dimethylamino protons) is observed.

Table 4.4. ^{1}H NMR Spectral Data of DMAPIP-c (for Proton Labels, see Figure 4.11)

Proton	D_2O	CB-7 + D_2O	Δδ shift
H_a	8.37 (s, 1H)	9.26 (s, 1H)	– 0.89
H_b	8.05 (d, 1H)	8.67 (brs, 1H)	– 0.62
H_c	7.43 (d, 1H)	8.25 (brs,1H)	– 0.82
H_d	7.11(d, 2H)	7.22 (brs, 2H)	– 0.11
He	6.14 (d, 2H)	6.08 (brs, 2H)	+ 0.06
H_f	2.64 (s, 6H)	2.84 (s,6H)	– 0.20

Similarily, the data of ^{1}H NMR spectra of DMAPIP-c in the absence and in the presence of CB-7 are compiled in **Table 4.4** and **Figure 4.11** depicts the NMR spectra. Same as earlier, the peaks of the imidazopyriyl protons of DMAPIP-c are shifted upfield. But the shifts in the peaks of protons of phenyl ring are relatively small and the downfield shifts in peak of dimethylamino protons are higher than that of DMAPIP-b. This effect may be due to better charge transfer in DMAPIP-c than in DMAPIP-b upon encapsulation by CB-7. As a consequence of this, the upfield shift in the peaks of H_e protons are less than that in DMAPIP-b and that of H_d protons is also shifted downfield though to a smaller extent. Therefore, it is clear that small change in position of pyridyl nitrogen made large change in the complexzation.

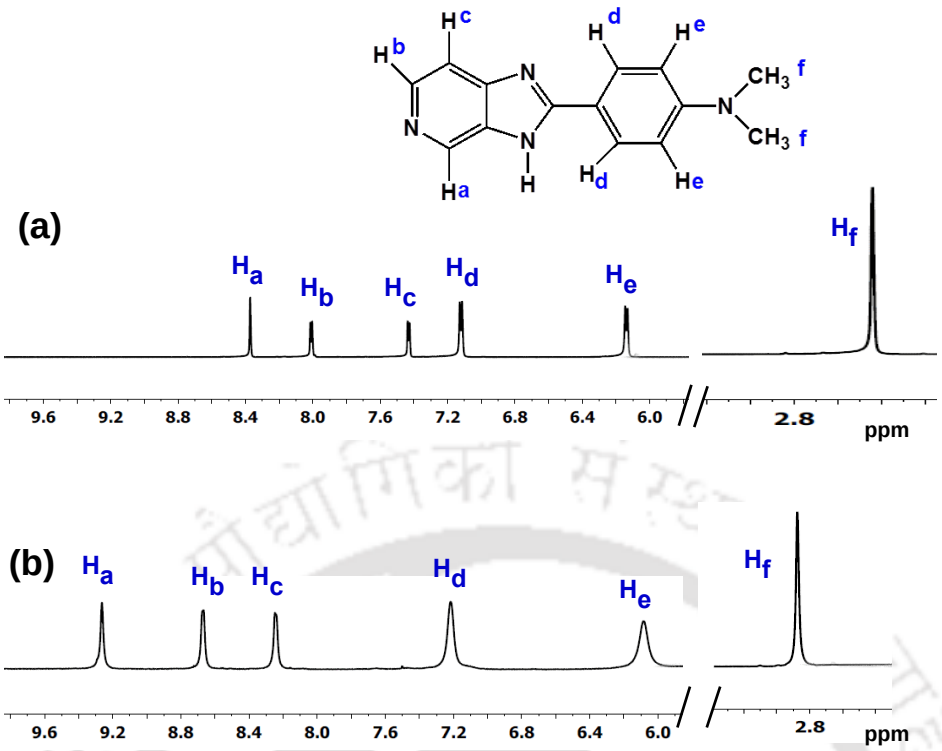

Figure 4.11. ^{1}H NMR spectra of DMAPIP-c in (a) the absence and (b) the presence of CB-7 in D_2O.

4.1.5. Quantum Mechanical Calculations on Host-Guest Complex

It is evident from the experimental findings that a 1:1 complex is formed between guests and CB-7 as shown in orientation **(A)**. To gain further insight about the complex, the structure of the complex is optimized by Gaussian 09 using B3LYP-D3 functional. The optimized geometries of the complexes are provided in the **Figures 4.12** and **4.13**. In the optimized structure, the guests are only partial encapsulation in CB-7. The pyridoimdazole moiety present inside the CB-7 in such a way that the pyridyl nitrogen and imidazole nitrogen and azole'NH' group present in close proximity to the carbonyl portals at openings of CB-7. The optimized structures of uncomplexed DMAPIP-b and DMAPIP-c suggest that the imidazo pyridine ring and the aminophenyl ring are coplanar before forming the complex. Even upon forming inclusion complex with CB-7 two ring of DMAPIP-c retains the coplanarity. In contrast, the angle between the two rings of DMAPIP-b increases to ~ 25° upon complex formation. This decreases the charge flow from the phenyl ring to imidazopyridine of DMAPIP-b. Kim *et al*. also hypothesized that the increase in planarity

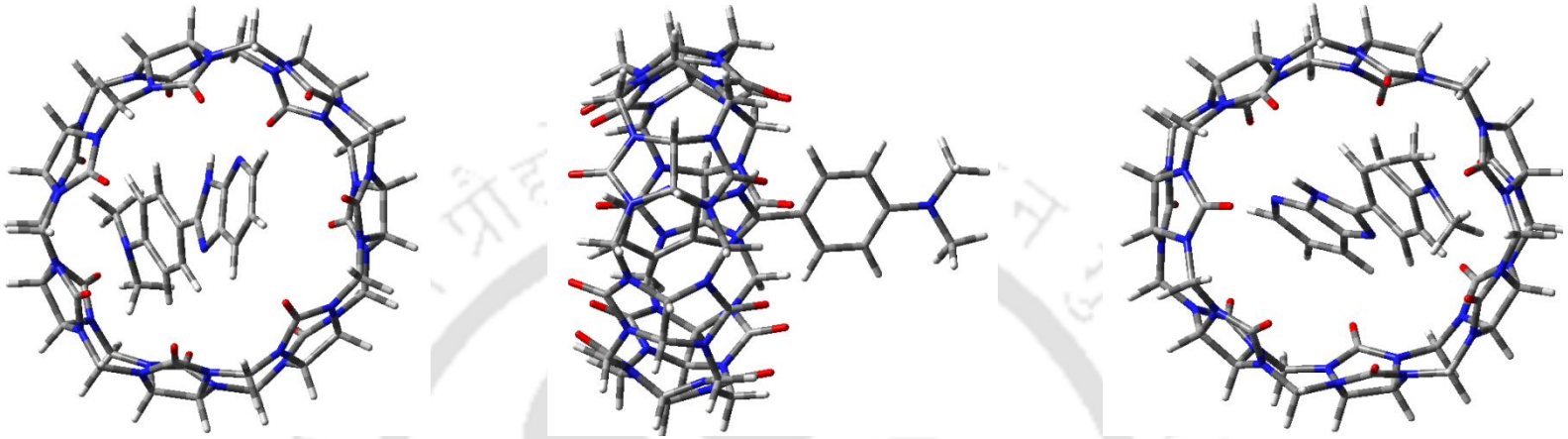

Figure 4.12. Optimized geometry of DMAPIP-b and CB-7 complex (Snapshots from different view).

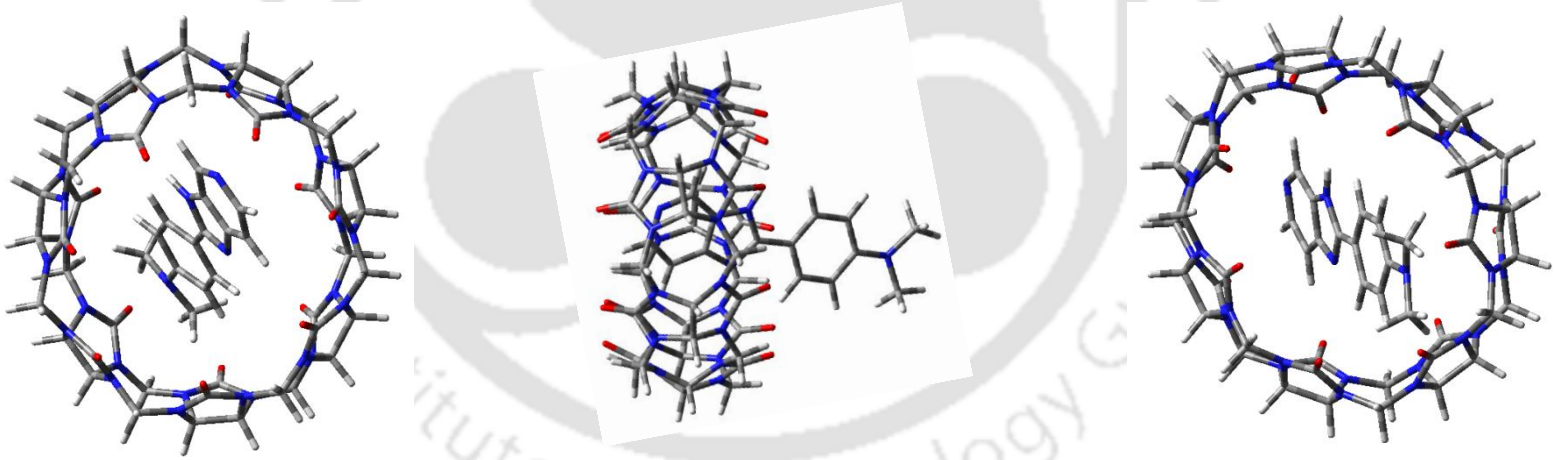

Figure 4.13. Optimized geometry of DMAPIP-c and CB-7 complex (Snapshots from different view).

between the spacer (phenyl ring) and the acceptor moiety increases the charge flow in diethylaminobenzoic acid.[214] This also corroborates with the NMR spectral finding that the charge transfer is better in DMAPIP-c than in DMAPIP-b upon complexation with CB-7.

The stabilization energies (E_s) of host−guest complexes were calculated by using the following equation:

$$E_s = E_{complex} - [E_{host} + E_{guest}] \quad (4.1)$$

Where E_{host}, E_{guest} and $E_{complex}$ are the energy of the host, guest and complex obtained from the DFT optimized structures. The stabilization energy obtained for DMAPIP-c and CB-7 complex is -165 kJ/mol and -167 kJ/mol for DMAPIP-b and CB-7 complex. The high negative value of stabilization energies signifies that the complex formation is much reliable and energy release takes place through hydrogen bonding and other interactions.

4.1.6. Proton Transfer Induced TICT Emission in CB-7

TICT emission of both DMAPIPs are lesser in aqueous medium compared to those in alcohols.[57,208] This was attributed to increase in non-radiative decays to the lowlying states due to decrease in the energy gap by greater stabilization in more polar protic water. ICT is more in DMAPIP-b than in DMAPIP-c, due to change in position of the pyridyl nitrogen. Therefore, the TICT state of DMAPIP-b will be stabilized more than that of DMAPIP-c in aqueous medium. Consequently, the TICT emission of DMAPIP-b is very weak in water compared to that of DMAPIP-c. When DMAPIP-b or DMAPIP-c enter the CB-7 cavity, will experience a less polar environment which reduces the nonradiative decay due increase in the energy gap between the TICT state and lowlying states. Due to this in CD medium also the relative intensity of the TICT emissions of these molecules are enhanced.[121,122] But the observation of TICT emissions of DMAPIPs in CB-7 is much more interesting than that in CD. This is because of the fact that the TICT emissions of DMAPIPs are special cases and they are induced by proton transfer. Since these proton transfers are intermolecular processes, hydrogen bonding with protic solvent is an essential requirement. In CD inclusion complexes of DMAPIPs the dimethylaminophenyl groups were present inside the cavity and the imidazopyridines were present in bulk water, which make the hydrogen bonding with bulk water feasible. But, in CB-7 both DMAPIPs enter through imidazopyridine rings and only the dimethylaminophenyl rings are projected outside. Therefore, the hydrogen bonding with external water is not feasible. It is reported that the cavity of CB-7 is occupied with some water molecules (7 to 8), termed as internal water molecules.[126,126] The energy of these water molecules are generally high than the

bulk water due to the effect of confined environment. When guest approaches to the CB cavity, the high energy water molecules releases from the cavity or they form suitable hydrogen bonding with guest through hydrogen bond network and are in fact act as a driving force for the complex formation.[125,195] The observation of TICT emission from DMAPIP-b complex implies the presence of at least an internal water molecule inside the CB cavity. The TICT emission from DMAPIP-c complex advocates not only the presence of a few internal water molecules but also indicates that they will involve relay transfer of proton.

4.1.7. Conclusion

The fluorescence intensity of DMAPIP-b increases in CB-7, but that of DMAPIP-c is reduced in CB-7. The spectral data confirms the formation of 1:1 inclusion complex between CB-7 and DMAPIPs. The NMR spectral data also substantiate the formation of inclusion complexes. In CB-7 cavity both the guests are only partially encapsulated. The imidazopyridines reside inside the CB-7 cavity and the dimethylamino phenyl rings are present outside in bulk water. This orientation of these guests in CB-7 is just opposite to that of these guests in CD complexes. The association constants with CB-7 are also higher compared to those with β-CD. Interestingly the TICT emission is observed from both the guest molecules. The internal water molecules are present inside the CB-7 cavity and make hydrogen bonding with the guest molecules in CB-7 medium. The hydrogen bonding network ensured not only the double proton transfer induced TICT emission from DMAPIP-b but also the relay proton transfer induced TICT emission from DMAPIP-c. Though, both the molecules are planar before complexzation, upon complex formation only DMAPIP-c retains the planarity but the dimethylamino phenyl ring of DMAPIP-b is twisted with respect to imidazopydine ring.

4.2.0 Effect of the CB-7 on the Cationic Equilibria of DMAPIP-b and DMAPIP-c

It was reported CBs show higher affinity to host the cationic guests than the neutral guests.[127,128,201-202] The interactions of single cations with CB-7 were investigated. [127,128,201-202] Therefore, the effect of CB-7 on the cationic mixture will be very much interesting and such a study is not reported so far. Both DMAPIPs have three basic centres and possess very interesting cationic equilibrium. DMAPIP-b exists as MC2 in water and MC2 and MC3 β-CD or micelle in the ground as well as the excited state.[57,121,215] Though, it is also possible for DMAPIP-c to form three monocations (**Chart 4.1**), not in a single medium, DMAPIP-c exists in all three monocationic forms. In water, β-CD and micelle, DMAPIP-c exists as MC1 and MC3 in the ground state and as MC2 and MC3 in the excited state. On the other hand, in aerosol

OT reverse micelle before addition of external water it exists as MC2 and MC3 in both the ground as well as the excited states. After addition of external water again it present as MC1 and MC3 in the ground state and as MC2 and MC3 in the excited state. Thus, monocationic equilibrium is medium dependent and the prototropic behaviour of the fluorophore is also affected by the formation of inclusion complex. Therefore, the effect of CB-7 on the monocationic equilibrium of DMAPIP-b and DMAPIP-c are explored in details in this section.

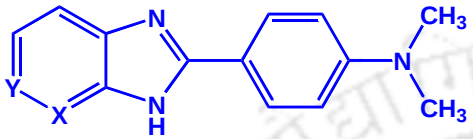

DMAPIP-b, X = N, Y = CH
DMAPIP-c, X = CH, Y = N

Protonation site	Monocation (MC)
Dimethylamino nitrogen	MC1
Imidazole nitrogen	MC2
Pyridyl nitrogen	MC3

Chart 4.1 DMAPIPs and their monocations.

4.2.1.0. Prototropic Equilibrium of DMAPIP-b

4.2.1.1. The Acid Dissociation Constant in CB-7

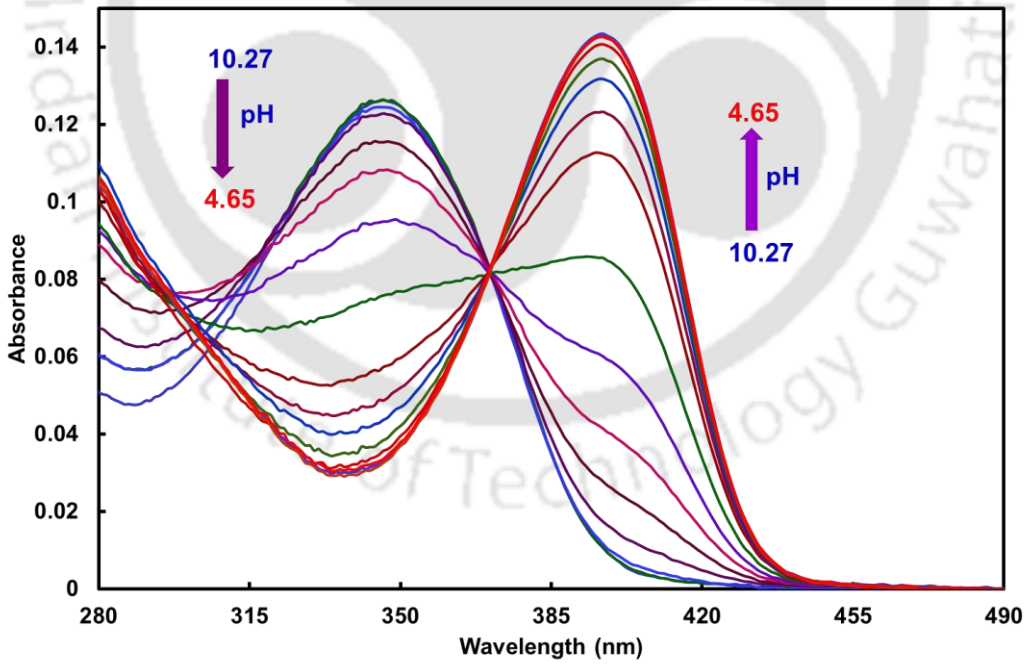

Figure 4.14. Absorption spectra of DMAPIP-b in 200 μM CB-7 at different pH.

Since, the acid dissociation constant of guest molecules are influenced by the formation of inclusion complex, the prototropic behaviour of DMAPIP-b has been investigated in 200

μM of CB-7. The effect of pH on the absorption spectra of DMAPIP-b is depicted in **Figure 4.14**. The absorbance of the band at 344 nm slowly decreases with formation of red shifted absorption band of monocation with a quasi-isosbestic point at ~ 370 nm. This specifies the equilibrium between N and MCs. The pK_a value for the neutral-monocation equilibrium is calculated in CB-7 environment is 7.7. In β-CD, the pK_a (4.8) decreases compared to water (5.4).[57,121] But in CB-7, it is much higher than that in water and interestingly it is even little higher than that in anionic micelle sodium dodecysulphate (7.3). This signifies the higher affinity of the cations towards CB-7. In β-CD, the pK_a values decreases compared that in water. This substantiates the different in orientation of DMAPIP-b in β-CD and CB-7, where pyridyl nitrogen is present near the carbonyl portal. In other pyridyl guest molecules also it was reported that when pyridyl nitrogen resides closer to the carbonyl portals of the CB-7 the pK_a value of the guest increases.[127,211]

4.2.1.2 The Monocations in Water and CB-7

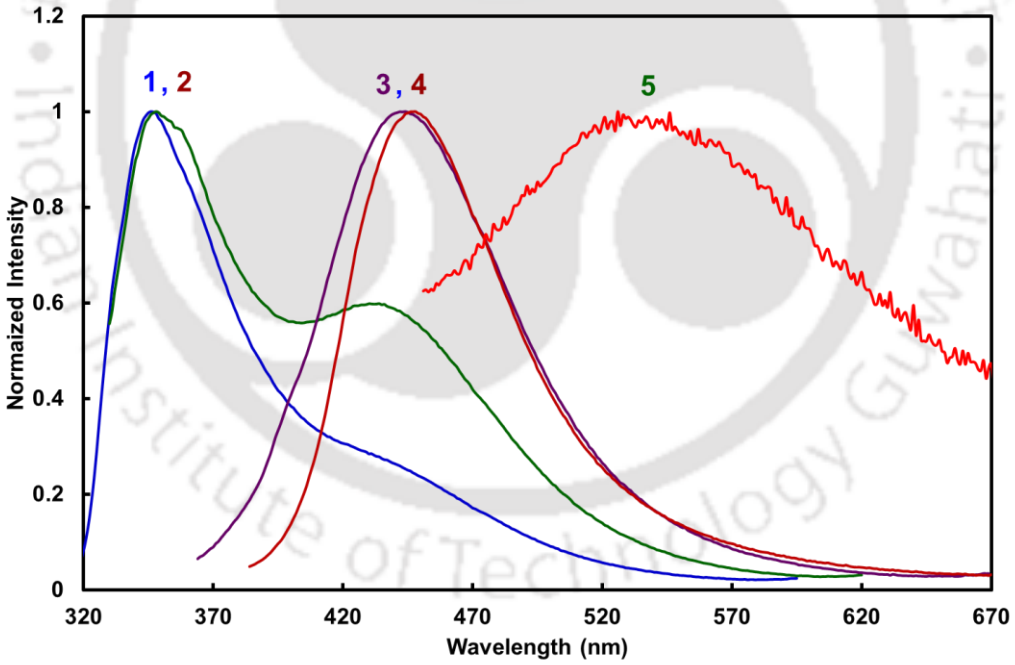

Figure 4.15. Normalized fluorescence emission spectra of MCs (at pH 4. 3) of DMAPIP-b in aqueous solution, (1) λ_{exc} = 305 nm, (2) λ_{exc} = 320 nm, (3) λ_{exc} = 350 nm, (4) λ_{exc} = 380 nm and (5) λ_{exc} = 440 nm.

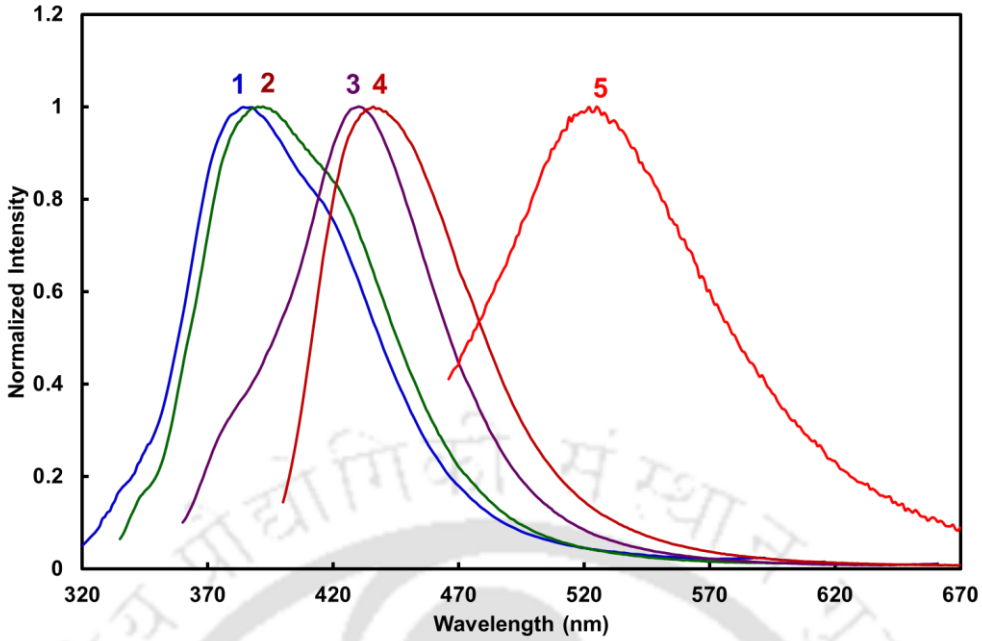

Figure 4.16. Normalized fluorescence emission spectra of MCs of DMAPIP-b at different excitations in 200 μM CB-7, (1) λ_{exc} = 305 nm, (2) λ_{exc} = 320 nm, (3) λ_{exc} = 350 nm, (4) λ_{exc} = 390 nm and (5) λ_{exc} = 440 nm.

The absorption spectra did not provide the information about the number of monocations present in the solution. As mentioned earlier, three different monocations are possible for DMAPIP-b. In such a complicated case, the fluorescence excitation and emission spectra are often useful to identify the species. The absorption spectrum of monocation at 385 nm is dominated by MC2 and excitation at 385 nm resulted in 451 nm band, due to emission of MC2.[57] Based on those results it was suggested that MC2 is present in water. But the fluorescence lifetime was not measured. As reported earlier, sometime a weak fluorescence band might present underneath a strong emission and fluorescence decay measurements will better reveal the number of species present in the system. Therefore, the fluorescence decay is measured in water by excited at 370 nm and is monitored at much longer wavelength at 500 nm. The decay thus obtained yield two different lifetimes, τ_1 = 0.11 (93.52) and τ_2 = 1.18 (16.48). This shows the presence of more than one monocation. To ensure the number of monocations, the emission spectra were recorded by exciting at different wavelengths (**Figure 4.15**). The emission spectra clearly show the presence of three monocation. When excited at 305 or 320 nm a band is observed at 350 nm with a shoulder at 435 nm. Upon excitation at 350 or 380 nm the band at 435 nm becomes strong with a long tailing at longer wavelength. Excitation at 440 nm yields a new band at 535 nm. The spectral data are compiled in **Table 4.5**.

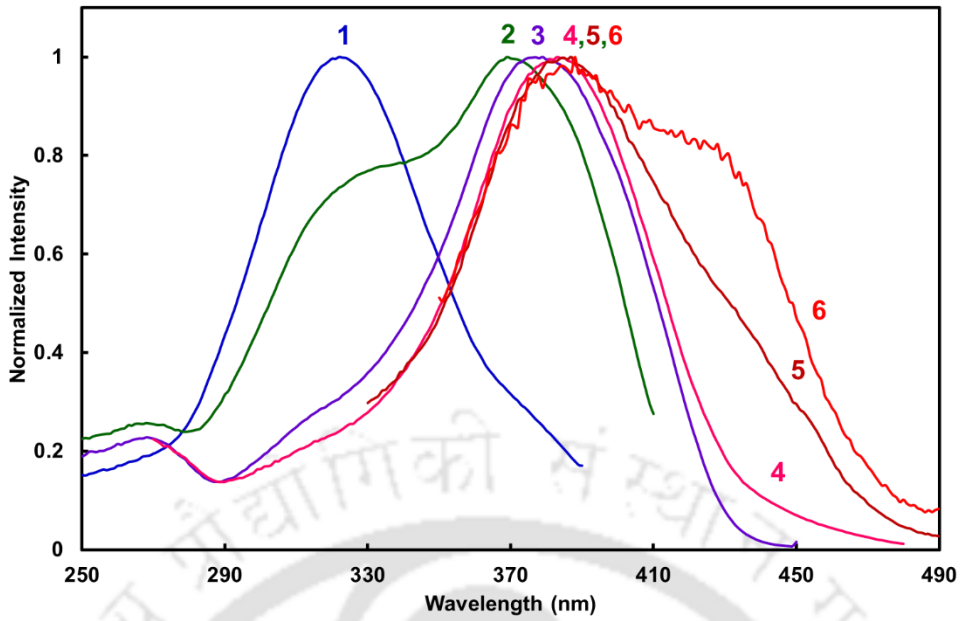

Figure 4.17. Normalized fluorescence excitation spectra of MCs of DMAPIP-b at different emissions in 200 μM CB-7 (1) λ_{em} = 400 nm, (2) λ_{em} = 420 nm, (3) λ_{em} = 440 nm (4) λ_{em} = 500 nm and (5) λ_{em} = 540 nm and (6) λ_{em} = 600 nm.

The fluorescence spectra of monocations of DMAPIP-b in 200 μM of CB-7 at pH 4.5 at different excitation are given in **Figure 4.16**. Excitation at shorter wavelength results in a band at 385 nm and a shoulder at ~ 430 nm. Upon exciting at longer wavelength the relative intensity of the 385 nm band decreases and that of the ~ 430 nm increases. Excitation at 440 nm produces a large Stoke shifted band at 522 nm. The excitation spectra were also recorded at different λ_{em} and depicted in **Figure 4.17**. The fluorescence excitation spectra at λ_{em} = 400 nm has a main band at 320 nm and has a small hump around 385 nm. The relative intensity of ~ 385 nm band raises than that of the 320 nm band shrinks with λ_{em} till 460 nm. When monitored at longer wavelength ($\lambda_{em} \geq$ 480 nm) a band emerges at ~ 430 nm along with 385 nm band. This indicates like in water in CB-7 also all three monocations are present and the data are also compiled in **Table 4.5**.

Table 4.5. The Excitation Band Maximum (λ_{max}^{exc}, nm) and the Emission Band Maximum (λ_{max}^{em}, nm) and the Fluorescence Lifetime (τ, ns) of the MCs of DMAPIP-b in Water and CB-7.

MCs	In water			In CB-7		
	λ_{max}^{exc}	λ_{max}^{em}	τ	λ_{max}^{exc}	λ_{max}^{em}	τ
MC1	320	350	0.96	321	385	1.8
MC2	375	435	0.05	380	430	0.4
MC3		535	2.97	425	522	1.2

The absorption and the emission spectra of DMAPIP-b were red shifted upon formation of monocation than in neutral molecule in respective medium. [57,121,215] Addition of proton at pyridyl nitrogen produced more bathochromic shift relative to protonation at azole nitrogen due to higher conjugation.[179] Accordingly, in water the newly found emission band at longer wavelength (535 nm) can be assigned to MC3 (**Chart 4.1**). Other assignment of blue shifted band at 321 nm and the corresponding emission band at 385 nm to MC1 (**Chart 4.1**) and the excitation bands at 380 nm and emission band at 430 nm to MC2 (**Chart 4.1**) are already made.[121,215] As protonation at dimethylamino nitrogen reduces the conjugation and that at azole nitrogen increases the conjugation the assignment aremade based on the shift in spectra. By analogy the emission bands at 380 nm, 430 nm and 522 nm and the corresponding excitation spectral bands at 321 nm, 380 nm and 425 nm in CB-7 may be assigned to MC1, MC2 and MC3. Three distinct fluorescence lifetimes are found for the MCs are compiled in **Table 4.5**.

4.2.1.3. Effect of CB-7 on Monocationic Equilibrium

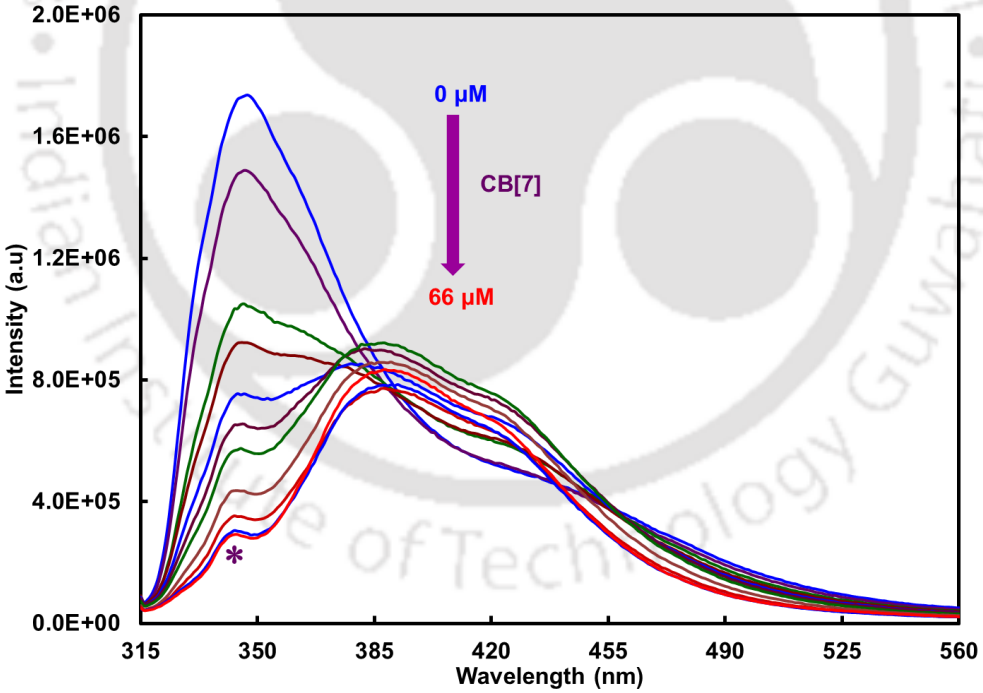

Figure 4.18. Effect of CB-7 on the fluorescence spectra of MC1, λ_{exc}= 305 nm (* indicates the water Raman).

With increases in CB-7 concentration the fluorescence intensity of MC1 decreases (**Figure 4.18**) and those of MC2 (**Figure 4.19**) and MC3 (**Figure 4.20**) increases. From this it can be inferred that addition CB-7 shifts the equilibrium more towards MC2 and MC3 from

MC1. Among the three monocations, MC1 is the most polar and MC2 is the least polar.[215] Since, CB-7 is less polar than water, addition of CB-7 move the equilibrium in favour of MC2 and MC3 from MC1. The association constant of MC2 and MC3 with CB-7 are 100 x 10^4 M^{-1} and 8.0 x 10^4 M^{-1}, respectively.

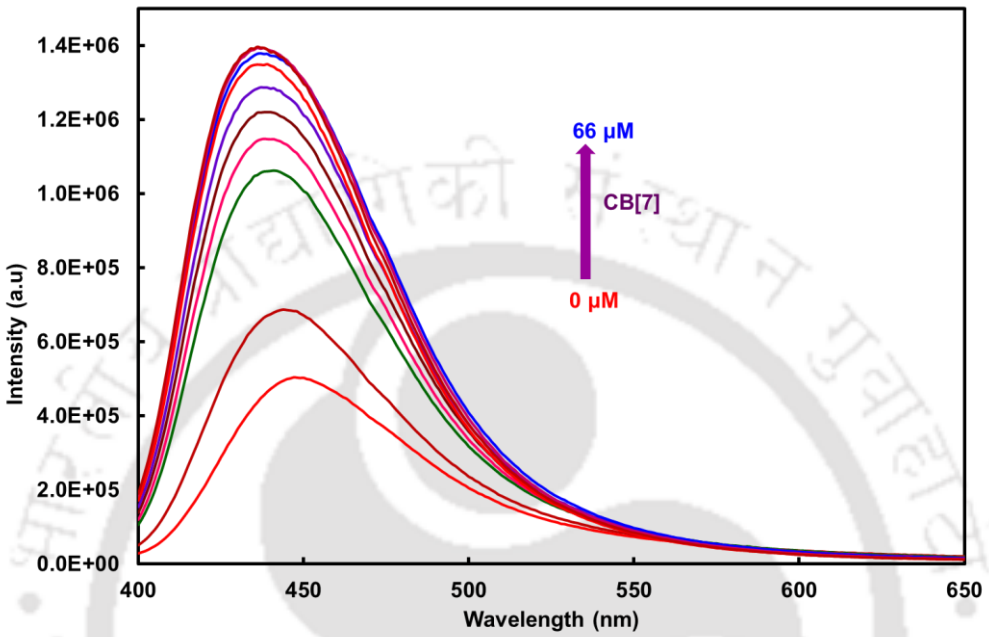

Figure 4.19. Effect of CB-7 on the fluorescence spectra of MC2, λ_{exc}= 390 nm.

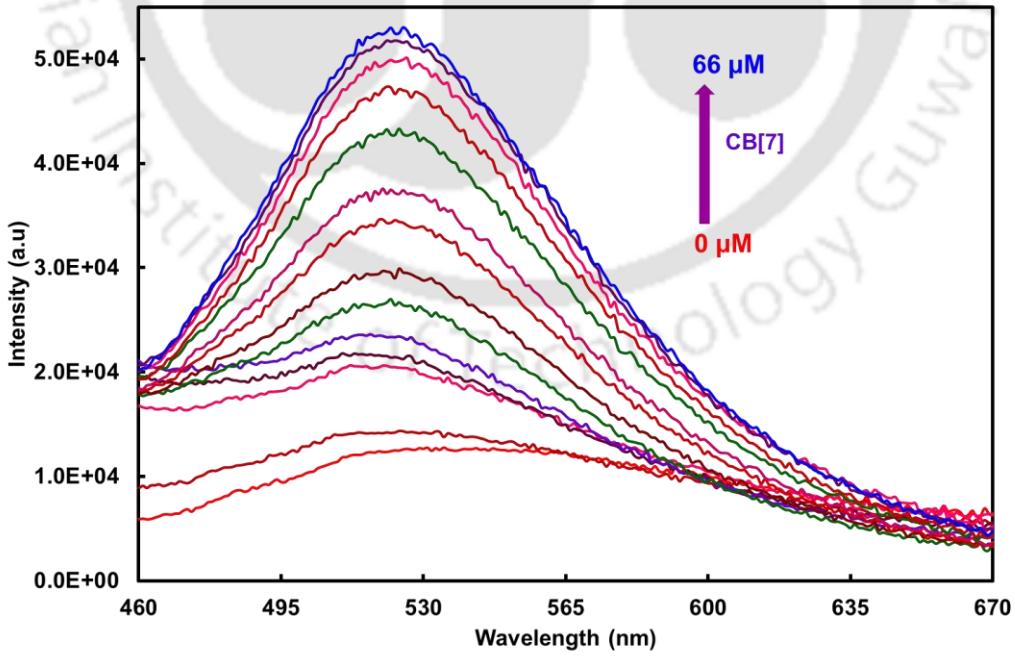

Figure 4.20. Effect of CB-7 on the fluorescence spectra of MC3, λ_{exc} = 440 nm.

4.2.2.0. Prototropic Equilibrium of DMAPIP-c

4.2.2.1. The Acid Dissociation Constant in CB-7

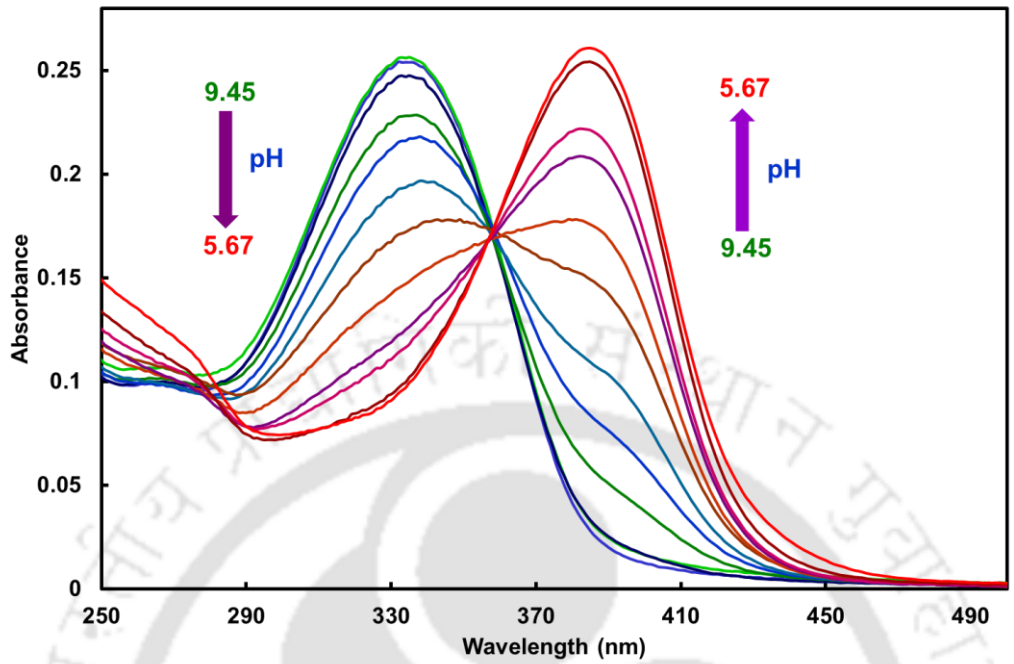

Figure 4.21. Absorption spectra of DMAPIP-c in 200 μM CB-7 at different pH.

The absorption spectra of DMAPIP-c in 200 μM CB-7 at different pH are investigated (**Figure 4.21**). As that of DMAPIP-b, the absorption spectrum of DMAPIP-c also red shifted upon reducing the pH with a quasi isosbestic point at 358 nm. A new band emerges at ~ 390 nm. The pK_a value for neutral-monocation equilibrium determined in CB-7 is 7.55. Like DMAPIP-b, the pK_a observed for DMAPIP-c is also higher than the p*K*a obtained in water and *β*-CD (6.45).[122] But unlike the pK_a of DMAPIP-b it is less than that in anionic sodium dodecylsuphate micelle (9.0).[216] This difference may be due to the difference in position of the pyridyl nitrogen.

4.2.2.2. The Monocations of DMAPIP-c in CB-7

To explore the monocations of DMAPIP-c in CB-7, the fluorescence excitation spectra in 200μM CB-7 at pH 5.8 were also recorded at different λ_{em} and are shown in **Figure 4.22**. When monitored at shorter wavelengths two bands are observed one at 305 nm and one at ~ 365 nm. Upon shifting towards the longer wavelengths, 365 nm band is gradually replaced by a band at 388 nm and 305 nm band also diminishes slowly. The presence of three distinct excitation spectral maxima indicates the presence of all three

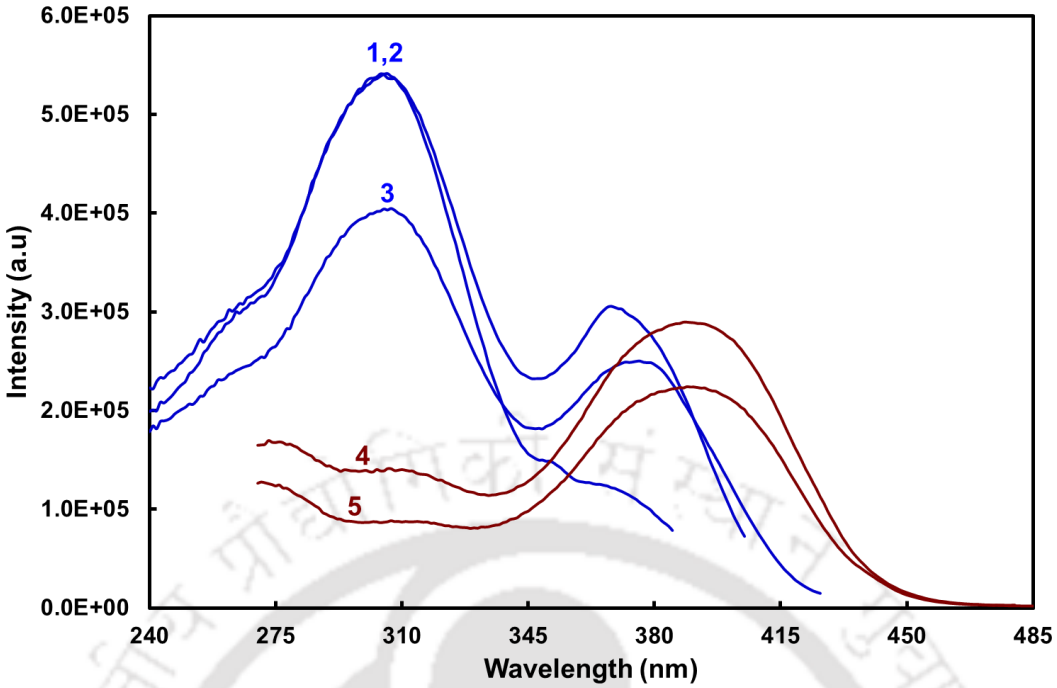

Figure 4.22. The fluorescence excitation spectra of MCs of DMAPIP-c at different emissions in 200 μM CB-7, (1) λ_{em} = 400 nm, (2) λ_{em} = 420 nm, (3) λ_{em} = 440 nm (4) λ_{em} = 500 nm and (5) λ_{em} = 520 nm.

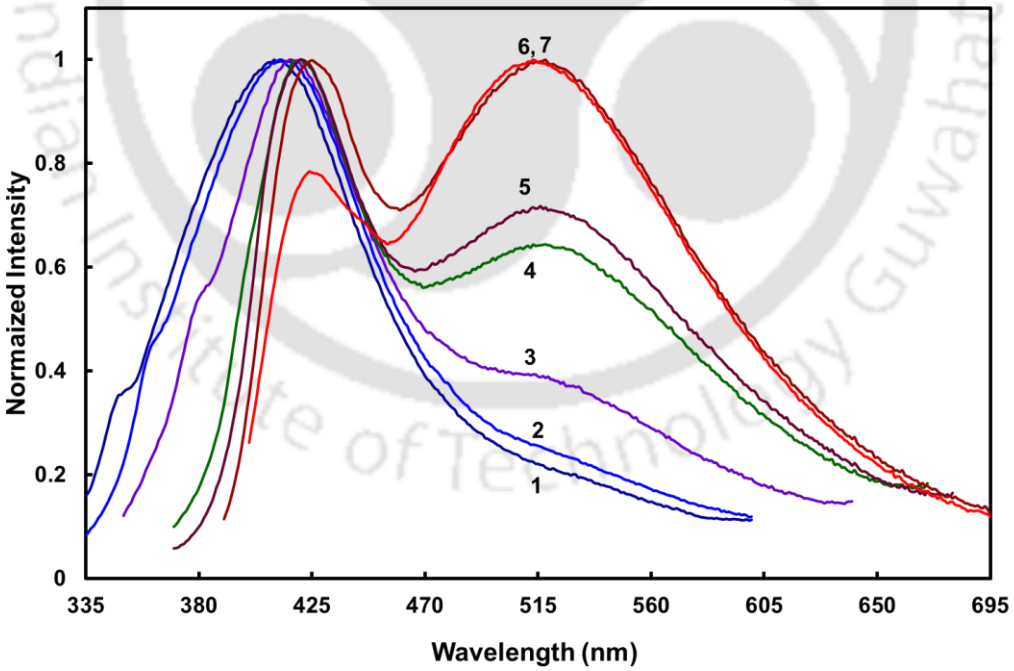

Figure 4.23. Normalized fluorescence emission spectra of MCs of DMAPIP-c at different excitations in 200 μM CB-7, (1) λ_{exc} = 310 nm, (2) λ_{exc} = 320 nm, (3) λ_{exc} = 335 nm, (4) λ_{exc} = 350 nm, (5) λ_{exc} = 357 nm, (6) λ_{exc} = 378 nm and (7) λ_{exc} = 387 nm

monocations in the ground state. A band at ~ 365 nm was not observed in water.[179] The 365 nm band and 388 nm bands are bathochromically shifted compared to absorption band of neutral DMAPIP-b (331 nm). From the extent of red shift the 365 nm and 388 nm can be assigned to absorption band of MC2 and MC3, respectively. Since the other band at 305 nm is hypsochromically shifted the band can be assigned absorption band of MC1. Whereas, the emission spectra are two bands system and the bands are at ~ 420 nm and ~ 515 nm (**Figure 4.23**). When at shorter wavelength, the ~ 420 nm band dominates and when excited at longer wavelength the 515 nm band is the prominent band. As both the bands are red shifted they are due to the emission from monocations formed by the protonation of ring nitrogens. Since, the shorter wavelength excitation produces ~ 420 nm band and the longer wavelength excitation produces ~ 515 nm band, they are assigned the emission of MC2 and MC3, respectively. Distinct lifetimes are observed for both MC2 and MC3 in water as well as in CB-7 (**Table 4.6**).

Table 4.6. The Excitation Band Maximum and the Emission Band Maximum and the Fluorescence Lifetime of the MCs of DMAPIP-c in Water and CB-7.

MC	In water			In CB-7		
	λ_{max}^{exc}	λ_{max}^{em}	τ	λ_{max}^{exc}	λ_{max}^{em}	τ
MC1	310			310		
MC2		416	0.99	365	420	0.30
MC3	380	525	1.07	390	515	2.60

4.2.2.3. The effect of CB-7 on Cationic Equilibrium

The effect of CB-7 on the fluorescence spectra of monocations are depicted in **Figure 4.24** and **4.25**. As reported in literature,[179] excitation of MC1 at 310 nm produced a band at ~ 420 nm which corresponds to the emission spectrum of MC2. Upon addition of CB-7 only a small enhancement in fluorescence was observed. This indicates that even in CB-7 the MC1 dissociates in the excited state and the molecule undergoes phototautomerism to form MC2. The excitation spectra monitored at 420 nm is interesting (**Figure 4.24** Inset). Initially before addition of CB-7 a single band is observed at 305 which correspond to MC1. With addition of CB-7 a new band of MC2 started to appear at ~ 365 nm and slowly gains intensity with addition of CB-7. This is consistent with the observation of previous section. Excitation at 390 nm produces two bands at ~ 420 nm and ~ 520 nm. The intensities of both the band rise with addition of CB-7. The binding constants of MC2 and MC3 with CB-7 are 2.7 X 10^3 M^{-1} and 5.6 X 10^3 M^{-1}, respectively. The binding constant MC2 of DMAPIP-b is nearly 10 times higher

than MC3 of DMAPIP-b. On the other hand, association constant MC3 of DMAPIP-c was nearly 2 times higher than MC2 of DMAPIP-b.

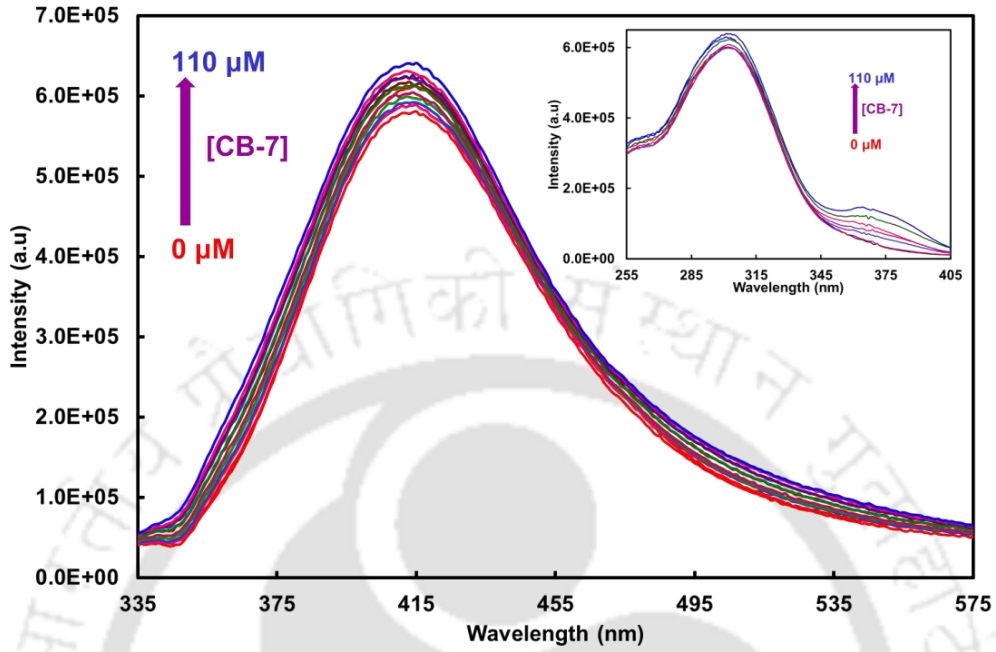

Figure 4.24. Fluorescence spectra of DMAPIP-c in different CB-7 concentration at pH ~ 5.5, λ_{exc} = 310 nm. Inset shows the excitation spectra of the same solutions, λ_{em} = 420 nm.

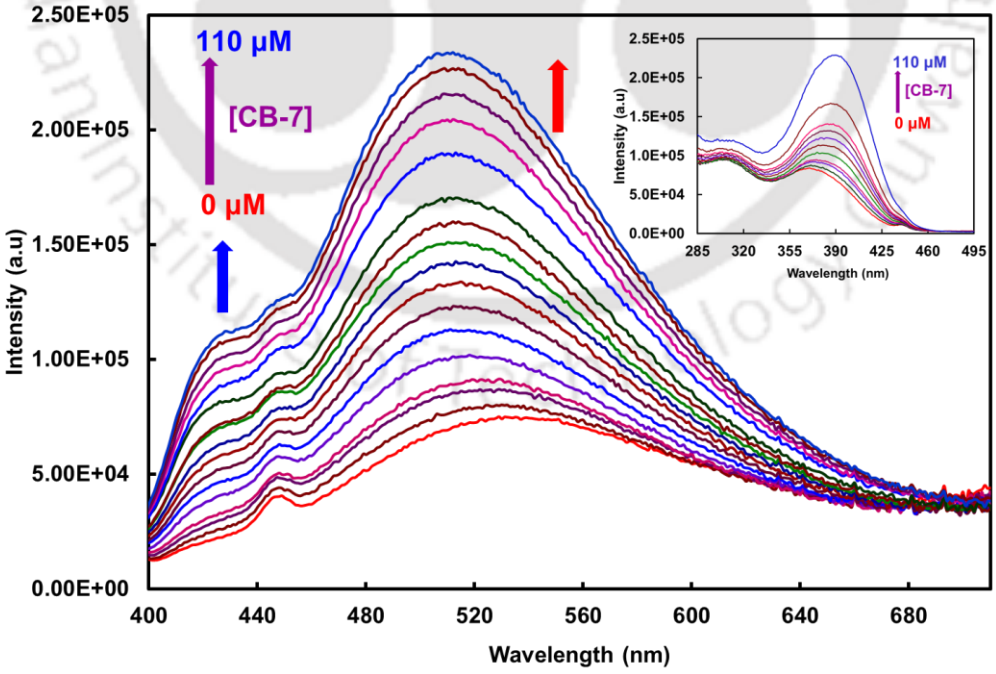

Figure 4.25. Fluorescence spectra of DMAPIP-c in different CB-7 concentration at pH ~ 5.5, λ_{exc} = 390 nm. Inset shows the excitation spectra of the same solutions, λ_{em} = 490 nm.

Upon excitation of MC1, due to more charge flow from the dimethylamino group, the protonated dimethylamino group behaves like a photoacid and dissociates to produce a proton which attacked the azole nitrogen to form MC2 as in to other media.[179] As revealed earlier, at monocationic pH, DMAPIP-c exists as MC1 and MC3 in the ground state and as MC2 and MC3 in the excited state.[179] MC2 is formed in the excited state from MC1 by phototautomerism by relay transfer of proton.[179] MC1 is more polar than MC3 which is more polar than MC2 of DMAPIP-c. Therefore, the decrease in polarity is expected to shift the equilibrium towards less polar MC2. The most the exciting feature in CB-7 is the existence of all three monocations of DMAPIP-c i.e MC1, MC2 and MC3 in the ground state. But, unlike the MC2 of DMAPIP-b, the MC2 of DMAPIP-c was observed in CDs or aqueous micelles.[121,177] Though, MC2 was found in aerosol OT/n-heptane reverse micellar solution before the addition of external water. However, in that solution MC1 was not observed, only MC2 and MC3 were present in the ground state.[177] Interestingly, all three monocations are present in the ground state in CB-7 and it provides the unique environment for the survival of all three monocations in the ground state. The other interesting aspect is though inclusion complexes are formed with both nonpolar hosts CDs and CB-7 but MC2 is observed in the ground state in CB-7 only. This can be attributed to the difference in orientation of DMAPIP-c inside these host molecules (**Scheme 4.1**). In CD-complexes of DMAPIP-c, the dimethylaminophenyl ring resides inside the cavity and the imidazopyridine ring was present outside the cavity. But in CB-7 complex of DMAPIP-c, the imidazopyridine ring present inside the cavity and therefore the azole nitrogen is present inside the hydrophobic cavity. Thus, MC2 exist in CB-7, whereas it fails to exist in CDs. The enhancement in the fluorescence intensity with addition of CB-7 is less with excitation at 310 nm whereas, significant enhancements are observed in both the bands with addition of CB-7 when excited at 390 nm. This is due to fact that both MC1 and MC2 form MC2 in the excited state. With addition of CB-7 the relative population of MC1 decreases and that of MC2 increases due to reduction in polarity of the environment. The reduction in MC1 (ground precursor for MC2 in the excited sate) population decreases the MC2 population in the excited state. This is compensated by the formation of MC2 in the ground state (which upon excitation gives excited MC2). Therefore, only small enhancement in fluorescence intensity is observed when excited at 310 nm. On the other hand, when excited at 390 nm both MC2 and MC3 are excited. Therefore, their respective fluorescence intensity also increases.

4.2.3. Conclusion

The p*K*a values of both DMAPIP-b and DMAPIP-c are higher in CB-7 compared to water and CDs. In water all three monocations of DMAPIP-b are present in the ground as well as the excited states. Addition of CB-7 shifts the equilibrium towards MC2. On the other hand DMAPIP-c which exists only as MC1 and MC3 in water exists as MC1, MC2 and MC3 in CB-7. The difference in orientation of fluorophore inside CB-7 ensures the existence of MC2. However, in the excited state, like in water and β-CD, MC1 undergoes phototautomerism to form MC2 in CB-7 too. Addition of CB-7 shifts the equilibrium from polar MC1 to relatively less polar MC2 and MC3. The association constant of MC2 of DMAPIP-b is higher than that of MC3 of DMAPIP-b. But that of MC3 of DMAPIP-c is higher than that of MC2 of DMAPIP-c.

Chapter 5

Excited State Intramolecular Proton Transfer of 4-(3-(1H benzo[d]imidazol-2-yl)-5-tert-butyl-4-hydroxybenzyl)-2-(1H-benzo[d]imidazol-2-yl)-6-tert-butylphenol: Effect of Solvent and pH†

† *RSC Adv.*, 2016, **6**, 59708-59717.

5.0. Introduction

ESIPT of hydroxyphenylbenzazoles such as 2-(2′-hydroxyphenyl)benzimidazole (HPBI), 2-(2′-hydroxyphenyl)benzoxazole (HPBO), 2-(2′-hydroxyphenyl)benzothiazole (HPBT) and their derivatives have been extensively studied.[59,71,75,81,96, 217-220] Undoubtedly, these dyes are good candidates for the study because of their efficient ESIPT fluorescence, easy synthetic modulations and wide varieties of applications.[60,173,221-226] In recent times also, these dyes are used for the study as a tailoring molecule with different organic back bone.[64,99,98,129,130,132,133] The idea behind these studies to tune the absorption or emission to a longer wavelength or to obtain a largely Stoke shifted emission. The acidity and basicity of the groups are affected by the substitutions there by the rate of proton transfer is also altered.

In the first report on HPBI, Dogra *et al.* studied the spectral properties of HPBI in organic as well as aqueous media and established the ESIPT in HPBI.[68] Later HPBI became a prototype and ESIPT behaviour of HPBI was investigated both experimentally and theoretically.[75,87,92,217,227] However, HPBI emits the normal emission along with tautomer emission. Currently, research is focussed to avert the normal emission which overlaps with the absorption. As a consequence the dye will emit only tautomer emission that may help to avoid the fluorescence quenching due to self-absorption (inner filter effect) etc. This can be achieved by eliminating the presence of *trans*-enol, which is the cause for normal emission. Having a hope to peruse this, ESIPT behaviour of a new HPBI derivative, 4-(3-(1H-benzo[d]imidazol-2-yl)-5-tert-butyl-4-hydroxybenzyl)-2-(1H-benzo[d]imidazol-2-yl)-6-tert-butylphenol (bis-HPBI), **Chart 5.1** is investigated. The special features of bis-HPBI are that it contains a bulky *tert*-butyl group ortho to –OH groups and also have two HPBI moieties which are not in conjugation.

Like HPBI, the proton transfer behaviour of HPBO was also investigated.[218,219] In addition to single proton transfer of HPBO, the double proton transfer behaviour of bis-3,6-(2-benzoxazolyl)-pyrocatochol is also reported, where two HPBO moieties are in same plane and also in conjugation.[228] Studies revealed that apart from normal and tautomer emissions, the emission is observed form the diketo due to ESIPT of monoketo tautomer which is present in the ground state. Based on the experimental studies only one proton transfer is reported from bis-2,5-(2-benz oxazolyl)hydroquinone (which has two HPBO groups).[228] On the contrary, recently Hoffmann *et al.* based on theoretical calculations reported that both single and double proton transfer is possible in bis-2,5-(2-benzoxaroiyl)hydroquinone.[229] Unlike these systems, in bis-HPBI the two HPBI groups are not in conjugation.

The goal of the work is to find out (i) whether a single or double proton transfer is taking place (ii) the effect of bulky substitution at ortho to –OH group on the emission characteristics of the dye (iii) the effect of acids and bases on the spectral characteristics of the bis-HPBI. The chapter is divided into two sections. In first section, the photophysical properties of bis-HPBI investigated in various organic solvents and theoretical calculations are also performed. In second section, the effects of bases and acids on spectral characteristics of bis-HPBI are studied in aqueous medium. The results of bis-HPBI are also compared with that of HPBI.

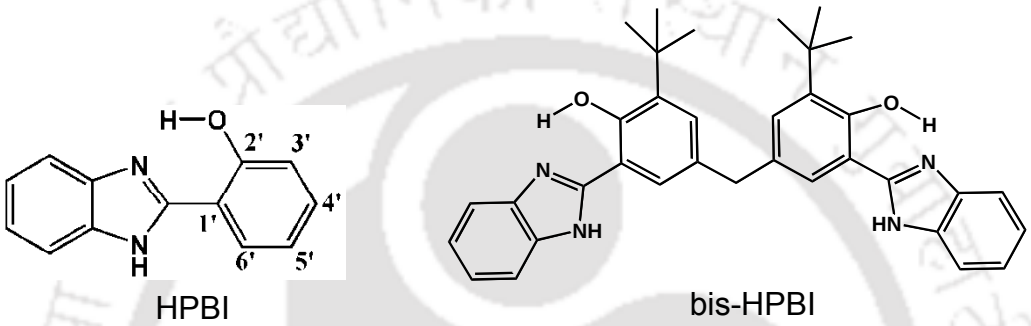

Chart 5.1. Structures of HPBI and bis-HPBI.

5.1.0. Effect of Solvents on the ESIPT of bis-HPBI

5.1.1. Absorption Study

The absorption spectra of bis-HPBI in few selected solvents are provided in **Figure 5.1** and the complete data are compiled in **Table 5.1**. Like HPBI,[68] the absorption spectra of bis-HPBI are structured and blue shifted with increase in polarity and hydrogen bond capacity of the solvent. However, bis-HPBI absorbs at a longer wavelength than HPBI and the molar extinction co-efficient obtained for bis-HPBI is also higher than that of HPBI in corresponding solvents. This suggests that the alkyl substitution at 3' and 5' positions have some effect on the transition.[95] Douhal *et al.* also reported a red shift in the absorption spectra in 5'- substituted HPBI derivatives.[73] A tailing towards longer wavelength was found in the absorption spectra of bis-HPBI in protic solvents and it may be due to small amount of anions (phenoxide ion) present in the ground state.[73,76]

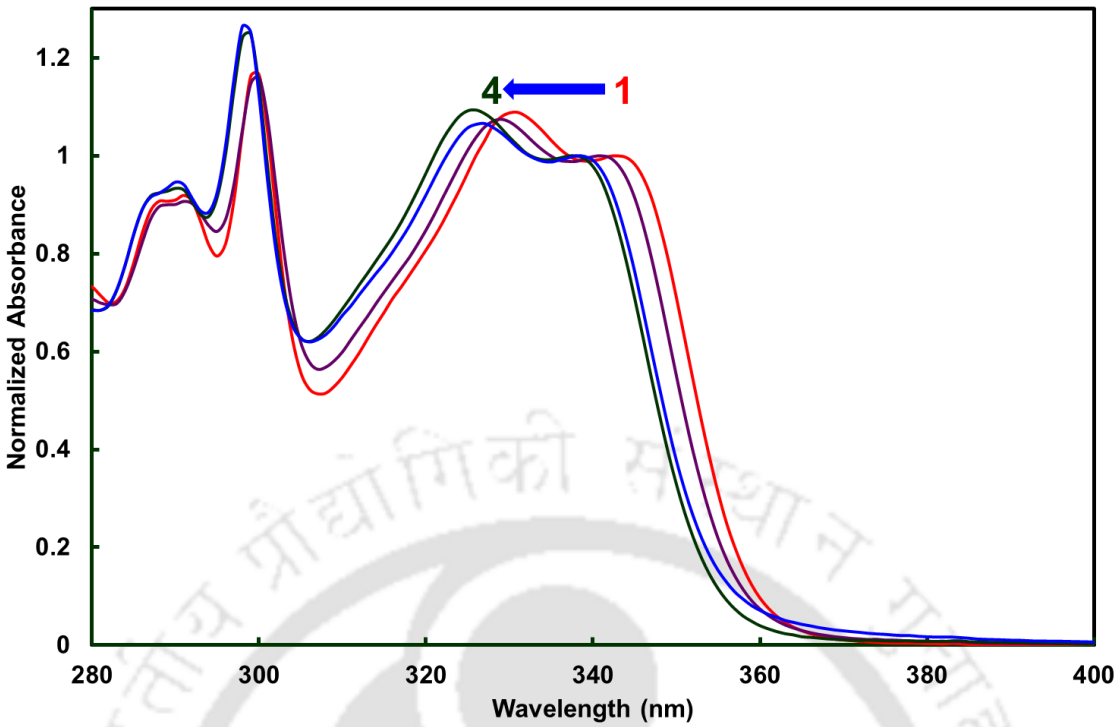

Figure 5. 1. Absorption spectra of bis-HPBI in selected solvents (1) cyclohexane, (2) dioxane (3) acetonitrile, and (4) methanol.

Table 5.1. Absorption Band Maxima (λ_{max}^{ab}, nm), log ε_{max} (in the Parenthesis), Fluorescence Band Maxima (λ_{max}^{fl}, nm) and Stoke Shift (cm^{-1}) of bis-HPBI in Different Solvents.

Solvents	λ_{max}^{ab} (log ε_{max})	λ_{max}^{fl}		Stokes shift
		Normal Emission	Tautomer Emission	
Cyclohexane	332 (4.28), 343 (4.20)		482	8408
1,4-Dioxane	329 (4.91), 341 (5.03)		480	8361
Diethyl Ether	328 (4.89), 341 (5.06)		479	8449
Ethylacetate	327 (4.87), 340 (5.04)		477	8449
Tetrahydrofuran	329 (4.95), 341 (5.06)		477	8361
Acetonitrile	326 (4.89), 339 (4.90)	385	478	8490
DMF	327 (4.95), 340 (5.04)		481	8623
DMSO	328 (4.95), 341 (5.06)		478	8405
Butanol	328 (4.98), 341 (5.04)		471	8139
2-Propanol	328 (4.94), 340 (5.07)		471	8135
1-Propanol	328 (4.95), 340 (5.07)		470	8180
Ethanol	328 (4.95) 340 (5.07)		472	8180
Methanol	327 (4.93), 338 (5.08)		470	8309
Glycol	327 (4.95), 340 (5.08)	393	477	8447

5.1.2. Steady State Fluorescence Measurements

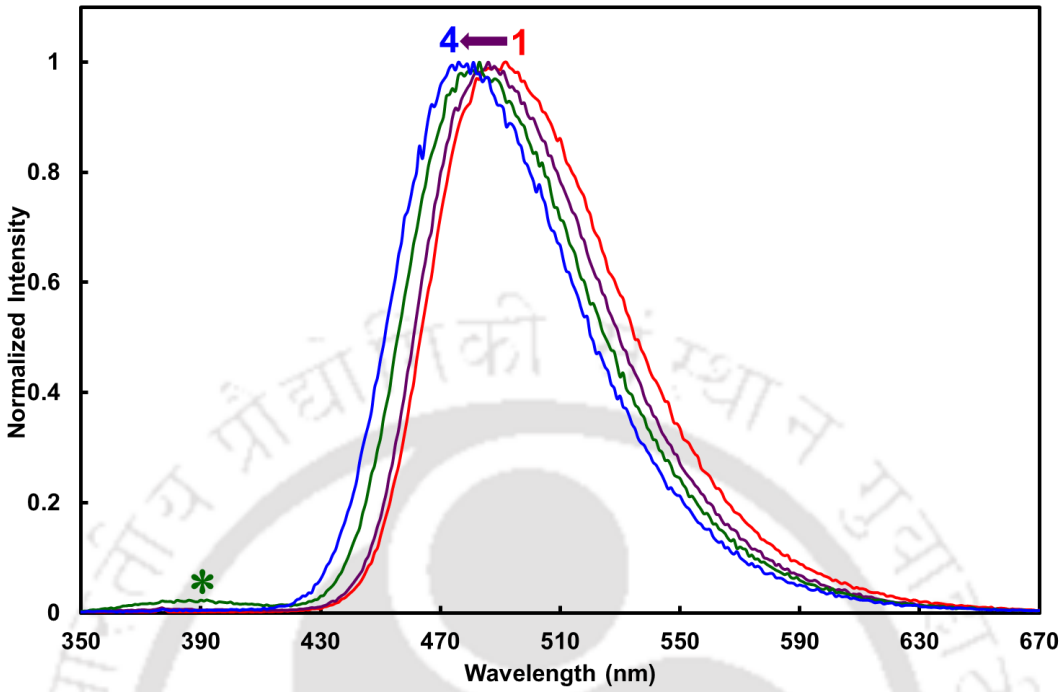

Figure 5. 2. Fluorescence spectra of of bis-HPBI in selected solvents (1) cyclohexane, (2) dioxane, (3) acetonitrile and (3) methanol, λ_{exc} = 340 nm. ('∗' denotes normal band in acetonitrile).

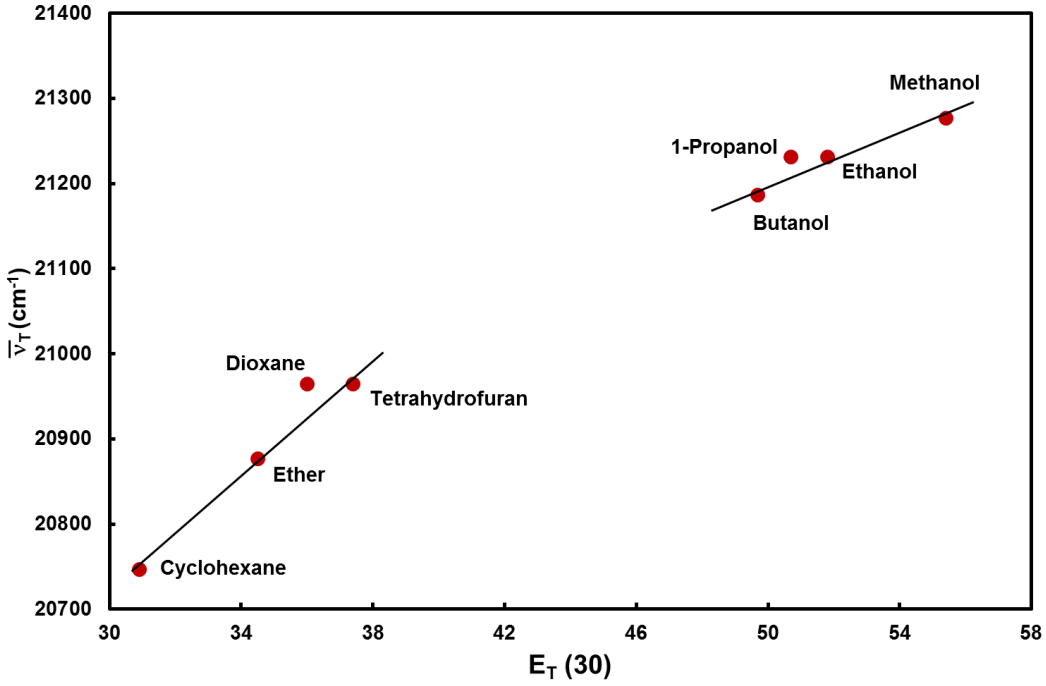

Figure 5.3. Plot of tautomer band maximum versus $E_T(30)$ of the solvents.

In most of the solvents, bis-HPBI exhibits almost exclusively single emission (**Figure 5.2** and **Table 5.1**). In acetonitrile and glycol a very weak shorter wavelength emission is observed along with a strong longer wavelength emission. Except in few nonpolar solvents, HPBI emits two emissions in most of the solvents.[68] The shorter wavelength emission is the normal emission from the excited *trans*-enol and the longer wavelength emission is from the tautomer which is formed by ESIPT.[68] As mentioned earlier, the tautomer emission has high Stokes shift. The Stokes shift calculated for bis-HPBI is higher than that of normal emission of HPBI and comparable to that of tautomer emission. Therefore, it can be inferred that the single emission at longer wavelength of bis-HPBI is the tautomer emission. Following points substantiate this assignment, (i) The second weak emission in acetonitrile and glycol is observed at shorter wavelength indicates that it is the normal emission and the strong longer wavelength emission is the tautomer emission. (ii) The longer wavelength emission band is blue shifted with increase in polarity and hydrogen bonding capacity of the solvent (**Table 5.1**). This is a characteristic of tautomer emission. But the normal emission undergoes a bathochromic shift with rise in polarity and hydrogen bonding capacity of the solvents. The blue shift in the tautomer emission is due to smaller dipole moment of the tautomer in the excited state compared to that in the ground state. Therefore, upon increasing the polarity and hydrogen bond capacity of the solvent, the excited state is less stabilized than the ground state. This leads to increase in the energy gap between these states. Thus, a negative solvatochromism is observed (**Figure 5.3)**. But the extent of blue shift in bis-HPBI is less than that in HPBI. However, the tautomer emission of bis-HPBI is red shifted compared to that of HPBI in the same solvent. For example, in methanol it is 34 nm red shifted to that of HPBI. These changes indicate the effect of substitution.

5.1.3. Tautomer Lifetime and Quantum Yield

Since bis-HPBI has two HPBI units, it is possible to form monoketo upon ESIPT of one unit of HPBI and diketo upon ESIPT of both the units of HPBI. bis-HPBI exhibits single longer wavelength emission indicating the presence either monoketo or diketo. Sometimes if one emission is very weak and buried underneath the other then it is very difficult to distinguish the single emission and the dual emission. In those cases, the time resolved emission is handy to detect the existence of weak emission that is hidden beneath a strong emission.[230] Therefore, the fluorescence decays of tautomer emission are recorded in different solvents. A single exponential decay is observed in all the solvents and the lifetimes thus obtained are compiled in **Table 5.2**. It clearly tells that only one species is responsible for the tautomer emission. The

fluorescence lifetimes of bis-HPBI in methanol and acetonitrile are less and this indicates that non-radiative channel become active in these solvents.

Table 5.2. Lifetime (τ_T, ns), Quantum Yield (Φ_T), Radiative Rate Constant (k_r, $10^7 s^{-1}$) and Non-radiative Rate Constant (k_{nr}, $10^7 s^{-1}$) of Tautomer emission of bis-HPBI in Different Solvents.

Solvents	τ_T	Φ_T	k_r	k_{nr}
Cyclohexane	4.0	0.82	20.50	4.50
1,4-Dioxane	3.8	0.41	10.78	15.52
Diethyl Ether	4.2	0.51	12.14	11.67
Ethylacetate	3.7	0.39	10.54	16.48
Tetrahydrofuran	3.8	0.40	10.52	15.79
Acetonitrile	2.6	0.26	9.62	27.40
DMF	4.0	0.48	12.00	13.00
DMSO	4.3	0.51	11.86	11.40
Butanol	3.8	0.41	10.78	15.52
2-Propanol	3.6	0.39	10.83	16.95
1-Propanol	3.5	0.39	11.14	17.43
Ethanol	3.2	0.29	9.06	22.18
Methanol	2.2	0.17	7.72	37.73
Glycol	3.9	0.51	13.07	12.56

Since, almost exclusive tautomer emission is observed the quantum yield of tautomer emission as well as the radiative and the nonradiative rates are calculated in different solvents (**Table 5.2**). The quantum yield of tautomer emission is less in methanol and acetonitrile relative to other solvents. Therefore, the radiative rate constants are low and the nonradiative rate constants are high in these solvents. In HPBI and related molecules the torsional rotation around phenolic/azole rings of keto in the excited state leads to a nonemissive ICT state which acts as a major nonradiative channel.[82,89,167,231-232] Such a process is expected to be high in polar nonviscous solvents like methanol and acetonitrile. Grellinann *et al*. observed a relatively intense tautomer emission when the *cis-trans* conversion of keto tautomer is practically disabled by bridging the bezinmidazole and phenolic ring of HPBI in a bridged HPBI.[83] In bis-HPBI, the rotation of the phenolic ring is difficult due to bulky substitution, but, the rotation of benimidazole ring is not hampered that much. As a result torsional rotation of the keto tautomer is feasible. However, the torsional rotation of excited keto of HPBI is also predicted to be retarded by viscosity of the medium.[233] The quantum yields of bis-HPBI are higher in relatively more viscous solvents like DMF, DMSO and glycol despite their higher polarity. Similarly, the fluorescence lifetimes are also longer in these solvents.

Table 5.3. Optimized Parameters of Different Conformers of bis-HPBI in Acetonitrile.

		cis-cis-enol	*cis-trans*-enol	*trans-trans*-enol	Monoketo	Diketo
S_0 State						
	E (eV)	0.00	0.34	0.60		
	μ (D)	6.8	9.3	8.3		
	Transition energy ($S_0 \rightarrow S_1$)/nm	331 (339)	329 (326)	314		
S_1State						
	E (eV)		3.76		3.11	3.36
	μ (D)		9.2		7.7	
	Transition energy ($S_1 \rightarrow S_0$)/nm		378 (385)		493 (477)	

E (relative energy with respect to most stable *cis-cis*-enol energy -46940.30 eV)

5.1.4. Ground State and Excited State Species

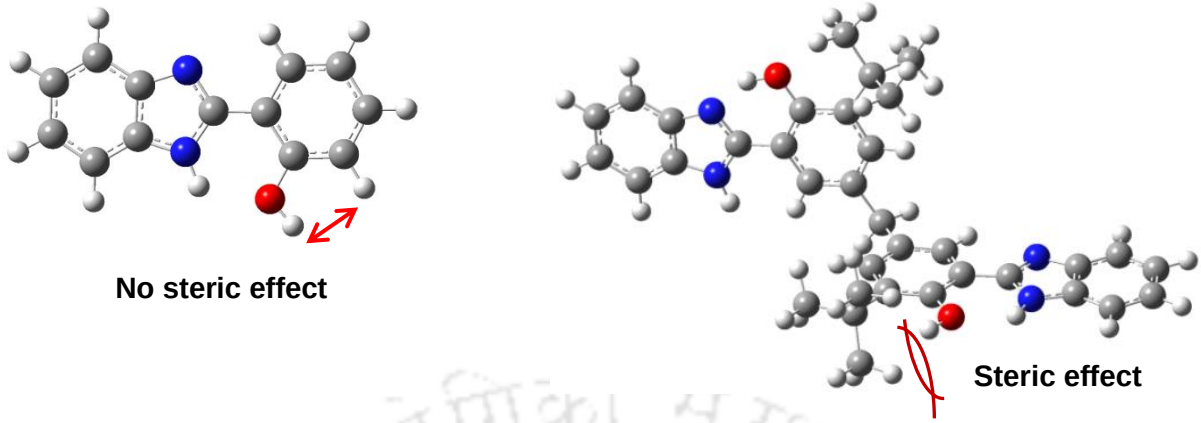

Figure 5. 4. Presence and absence of steric effect in *trans*-enol's of bis-HPBI and HPBI

HPBI exists as *cis*- and *trans*-enol in the ground state.[68] Due to the presence of two HPBI units, three conformers are possible for the enol form of HPBI. The optimized structures of different forms are presented in **Chart 5.2** and the data are compiled in **Table 5.3**. The *cis,cis*-enol is more stable than *cis,trans*-enol by 0.34 eV which more stable than *trans,trans*-enol by 0.26 eV. *cis,trans*-enol or *trans,trans*-enol is required to produce normal emission from excited *trans*-enol. As *cis,cis*-enol has very high stability than other two conformers and bis-HPBI is present almost exclusively as *cis,cis*-enol in ground state. This explains the negligible presence of normal emission in acetonitrile and its almost complete nonexistence in other solvents. Unlike in bis-HPBI, in HPBI the normal emission is significant in polar and protic solvents.[68] In bis-HPBI, the substitution of bulky *tert*-butyl group ortho to –OH group helped in suppressing the population of the *trans* conformer. Unlike that of HPBI, in the *trans-enol* conformer of bis-HPBI has steric hindrance between the hydrogen atom of the –OH group and hydrogen atom of the *tert*-butyl group (**Figure 5.4**). Consequently, the population of *cis,trans*-enol is negligible and almost no existence of *trans,trans*-enol is there in the ground state. Excitation of the *cis*-enol will result in *keto* tautomer in the excited state. Both, *cis,cis*-enol and *cis,trans*-enol has *cis*-enol conformer. As mentioned earlier, bis-HPBI can form monoketo or diketo. The excitation of *cis* conformer of *cis,cis*-enol and *cis,trans*-enol can lead to monoketo. Whereas, excitation on both *cis* conformer of *cis,cis*-enol may lead to diketo. As suggested by the calculation bis-HPBI exist primarily as *cis,cis*-enol. Therefore, both one proton transfer and two proton transfers are probable. However, in nonconjucated system like bis-HPBI at least one of the *cis*-enol of *cis,cis*-enol has to be excited to form monoketo and

both the *cis*-enols have to be excited to form diketo. Such an excitation of two chromophores has to be a two photon absorption processes. To find the dependence of fluorescence intensity on excitation intensity, using a set of neutral density filters the excitation intensity is attenuated. The relative spectral areas of bis-HPBI fluorescence spectrum with no filter (F_0) to with different filters (F) are obtained. Similarly, the relative spectral areas of standard quinine sulfate solution in 1 N sulphuric acid with no filter (I_0) to with different filters (I) are measured. A linear fit with a slope of 0.96 ± 0.05 was obtained for the plot of relative fluorescence of both the solutions (**Figure 5.5**). This shows that the formation of keto tautomer is a single photon processes. Therefore, it can be inferred that the emitting species of bis-HPBI is the monoketo tautomer. This is further substantiated by the theoretical calculation which suggests that the formation of monoketo is energetically favored over diketo (**Table 5.2**). The calculated excitation and emission energies are in good aggrement with the experimental values (**Table 5.2**). The tautomer emission is observed along with the anion emission even after the deprotonation of one of the –OH group of bis-HPBI (see **Section 5.2.1**). This further supports assignment of tautomer band to emission form monoketo formed by single proton transfer.

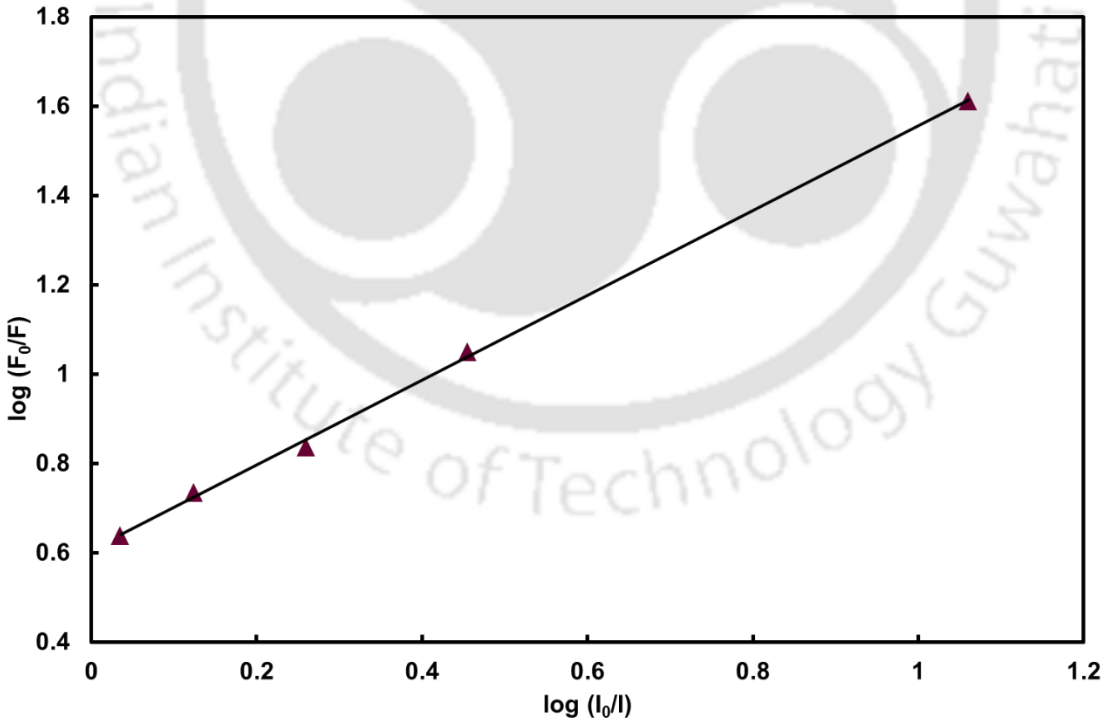

Figure 5.5. Logarithmic plot of relative fluorescence intensity (F_0/F) of bis-HPBI in acetonitrile versus relative excitation intensity log (I_0/I), λ_{exc} = 330 nm.

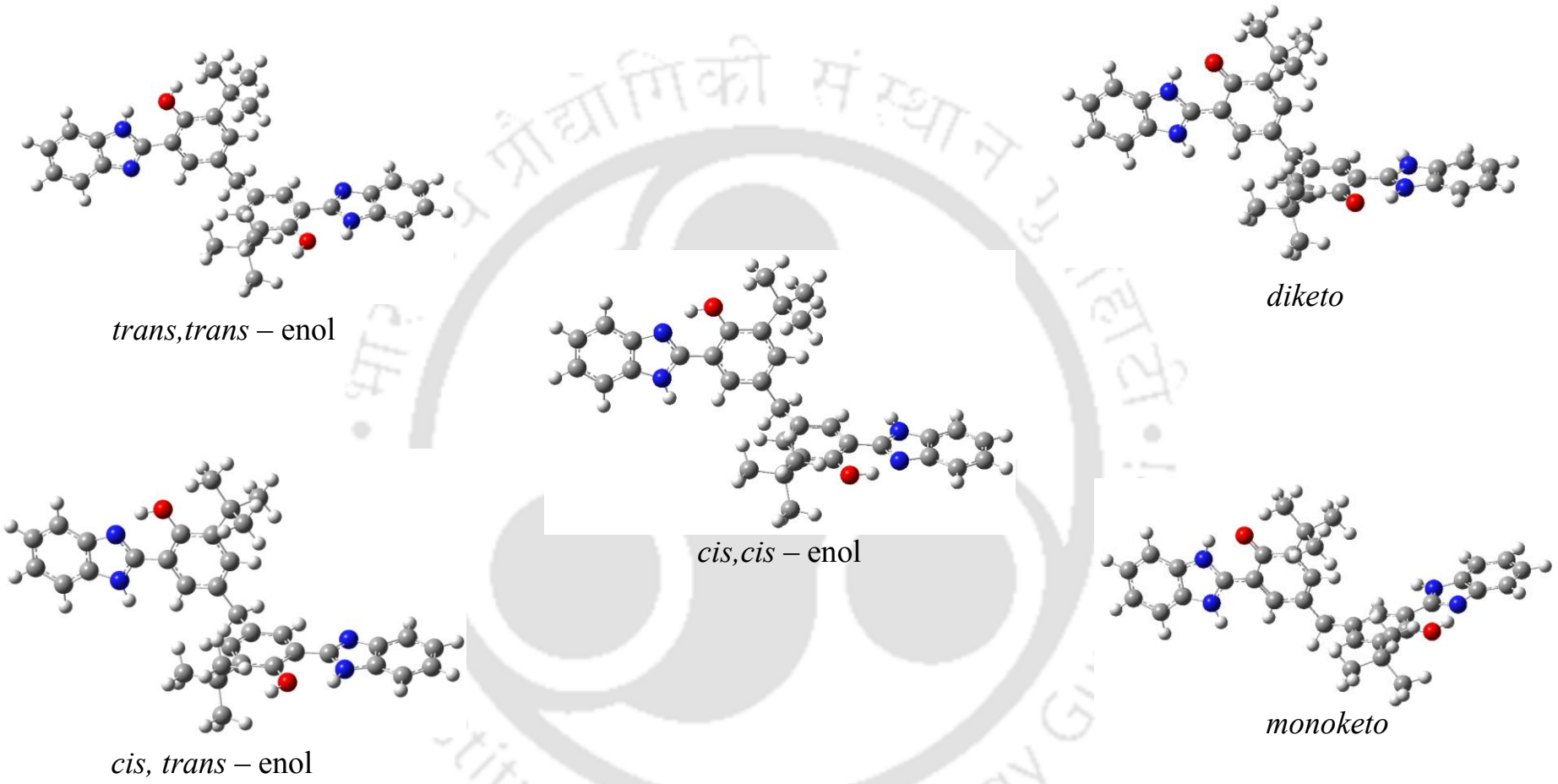

Chart 5.2. DFT optimized geometries of the different conformers of the bis-HPBI.

5.1.5 Conclusion

The absorption and emission spectra of bis-HPBI are bathochromically shifted than HPBI. Unlike HPBI, bis-HPBI emits almost exclusively intense tautomer emission even in protic solvents. The presence of bulky *tert*-butyl group ortho to –OH group hindered the formation of *trans*-enol which is responsible for normal emission. Though bis-HPBI has two HPBI units the tautomer emission of bis-HPBI is due to only single proton transfer. The theoretical calculation also supports this result.

5.2.0. Effect of Bases and Acids on ESIPT

Besides the ESIPT process, the acid-base chemistry of bis-HPPBI will be an interesting one as it has two HPBI moieties. The variation in hydrogen ion concentrations is expected to modulate the spectral characteristics due to the presence of acidic and basic groups in bis-HPBI.

5.2.1. Effect of Base

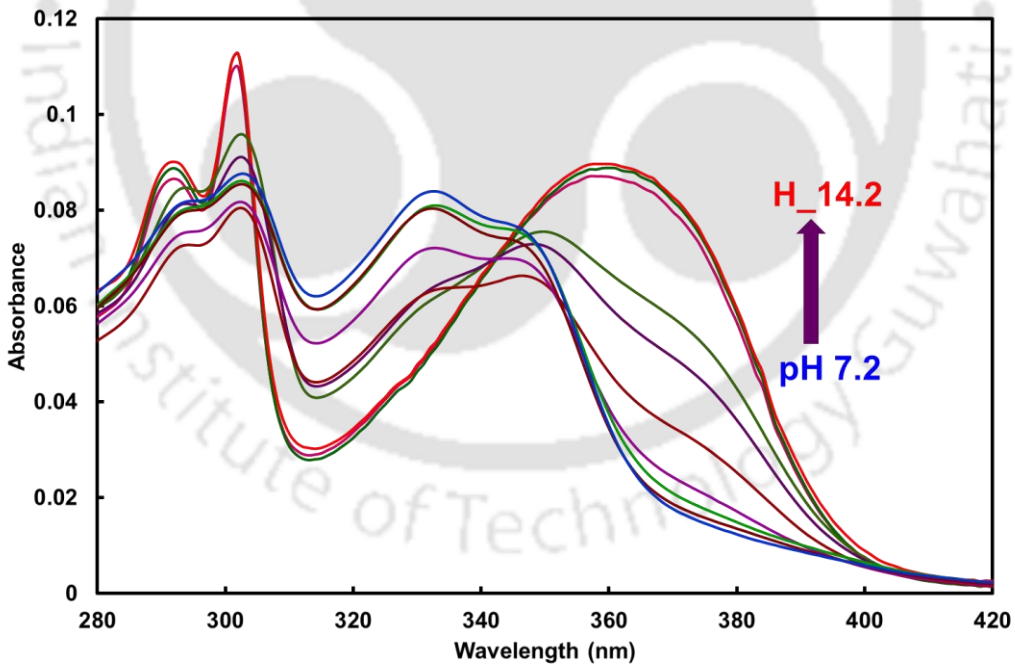

Figure 5.6. Absorption spectra of bis-HPBI in aqueous medium in pH /H_ range 7.2 to 14.2.

bis-HPBI exists in neutral form at pH 7.2. Upon increasing the pH, a new band starts to appear on the red side of the neutral band of the bis-HPBI **(Figure 5.6)**. The new band at ~ 360 nm co-exists with neutral band upto pH ~12.5. Nonetheless, with further rise in pH, the

molecular band totally disappeared and a single band at ~360 nm is observed around pH ~12.9 to H_ ~14.2 **(Figure 5.6)**. The red shift illustrates the increase in conjugation due to deprotonation of hydroxyl group.[68]

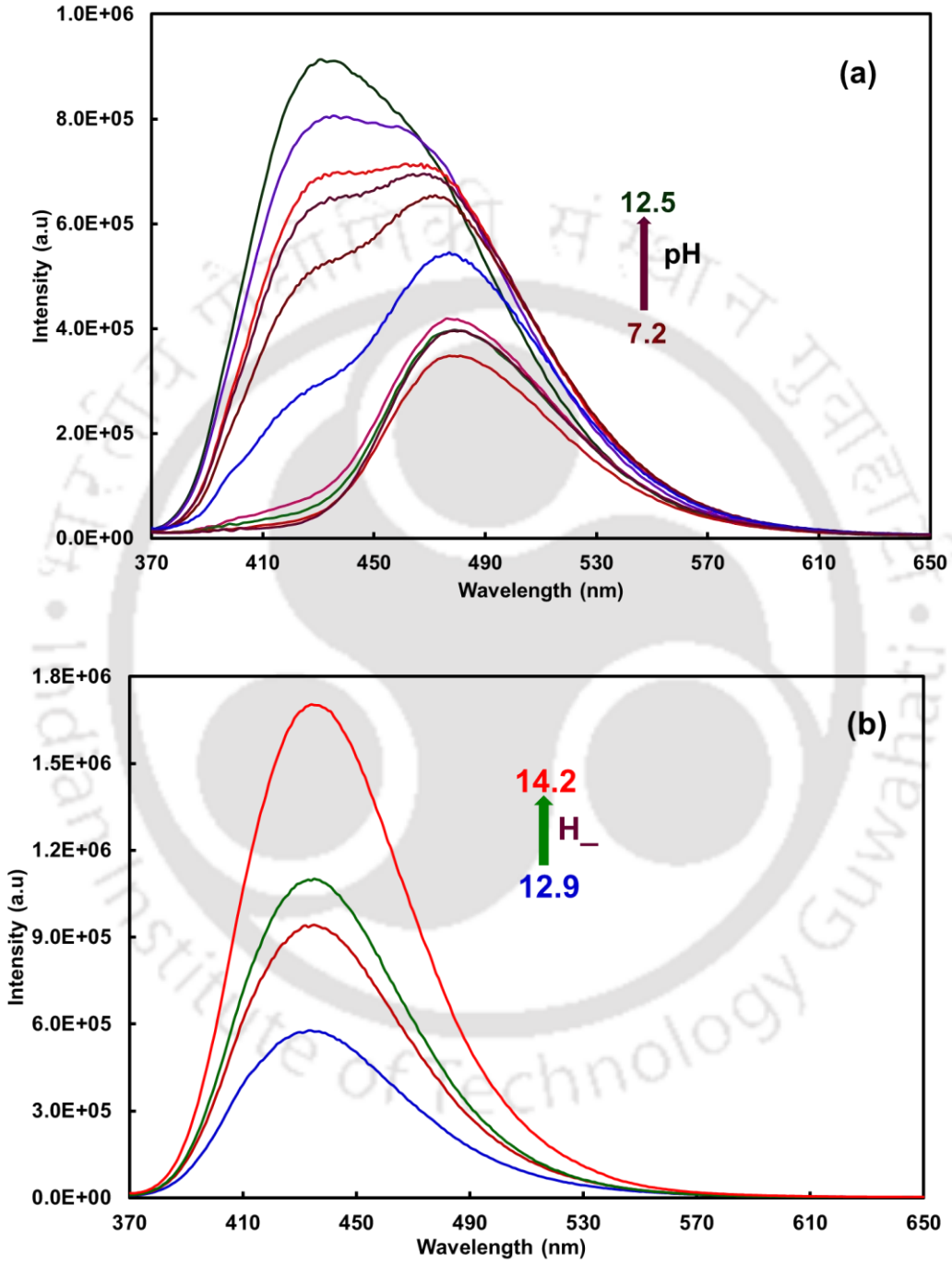

Figure 5.7. Fluorescence spectra of bis-HPBI under basic media , λ_{exc} = 360 nm.

The emission spectrum of bis-HPBI in water at pH 7.2 is also having predominantly a single emission around 475 nm. Therefore the emitting species in aqueous medium is also the tautomer **(Figure 5.7a)** and the fluorescence lifetime is 1.64 ns. Upon addition of the base, the

fluorescence intensity increases and a new band appear at shorter wavelength (~435 nm). But the intensity of the tautomer also increases with base concentration till pH 12.5 along with the band at 435 nm **(Figure 5.7a)**. In contrast, it was reported that the tautomer emission of HPBI decreases and that of its anion increases upon addition of base to aqueous solution.[68] This difference in behaviour is due to the presence of two HPBI units in bis-HPBI. The step wise deprotonation is taking place in bis-HPBI for initial addition of base only one units of –OH group is deprotonated to form anion. Since, the other HPBI unit possess the –OH group and it can undergo ESIPT. As a result, the tautomer emission is also observed along with the emission from the anion. At higher concentration of base both the –OH groups are deprotonated and bis-HPBI exhibits only single emission **(Figure 5.7b)**. The single exponential decay is also obtained for bis-HPBI at H_ 14.2 (**Table 5.4**). Such an enhancement in lifetime is also obtained for HPBI upon deprotonation of –OH group compared to that of tautomer (the fluorescence lifetimes of tautomer and anion in aqueous solution are 1.86 ns and 2.95 ns, respectively).[61]

Table 5.4. Fluorescence Wavelength Maximum (λ_{max}^{fl}, nm) and Lifetimes (τ, ns) of bis-HPBI in Aqueous Medium at Different Conditions.

Conditions	λ_{max}^{fl}	τ (ns)
H_ 14.2	435	3. 97
pH 11.0	435	0.31
	470	2.52
pH 7.2	475	1.64
pH 1.0	388	0.38
	360	1.89
H_0 -7.3	388	0.28
	455	2.88
H_0 -10.0	388	1.18

5.2.2. Effect of Acid

Under acidic condition, the vibrational structure in the absorption spectrum of bis-HPBI is lost and the absorbance of the longer wavelength emission band decreases and that of shorter wavelength increases (**Figure 5.8)**. In other words, the addition of acid brings minimal changes in the absorption spectrum of bis-HPBI in aqueous medium. This shows the interaction of protons with bis-HPBI in the ground state, but no clear picture emerges from the absorption studies. However, the emission spectra gave a clear picture about the interactions. As mentioned earlier, neutral bis-HPBI emits the tautomer emission at 475 nm. For initial addition of acids, the intensity of the tautomer emission decreases (**Figure 5.9a)**. When acidity of the solution increased a new band appeared at a shorter wavelength at 388 nm and the tautomer emission also recovered its fluorescence partially (**Figure 5.9b)**. Interestingly, both the bands

co-exist up to H_0 -7.8. However, with further increase in acid concentration, the two band system slowly moves toward a single band system. The emission at 388 nm gains the intensity and the tautomer emission intensity diminishes. In a strongly acidified solution (~H_0 -10.0) the tautomer band totally vanishes and bis-HPBI exclusively emits only 388 nm emission (**Figure 5.7c)**. The fluorescence lifetimes of bis-HPBI in aqueous medium at different conditions are summarized in **Table 5.4**.

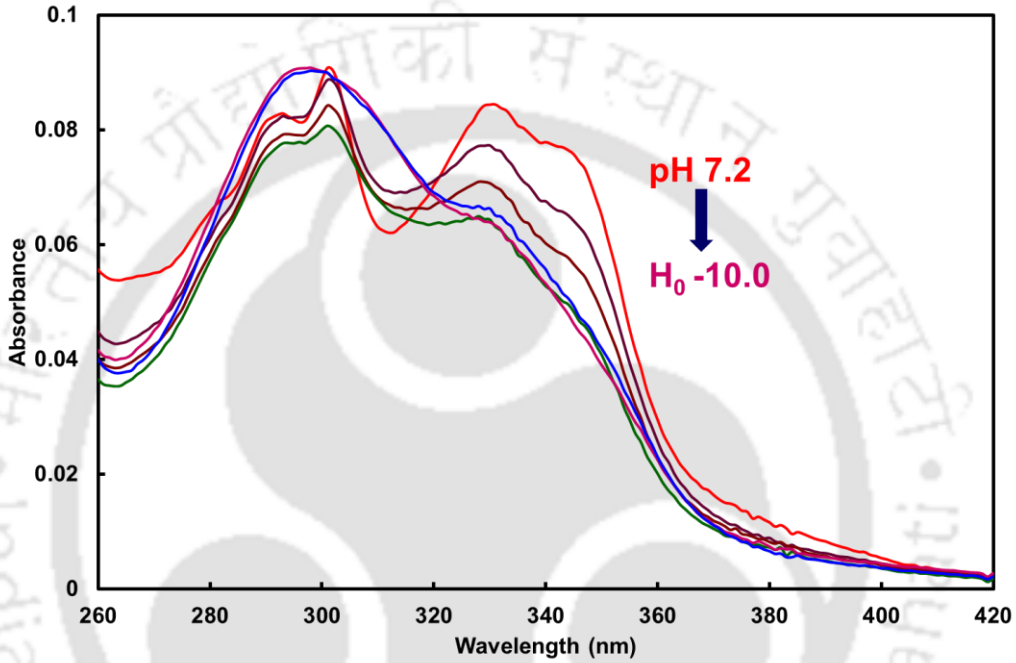

Figure 5.8. Absorption spectra of bis-HPBI in aqueous medium in pH /H_0 range 7.2 to -10.

The initial decrease in tautomer emission suggests weaker hydrogen bonding type interaction of protons with bis-HPBI. Such hydrogen bond induced quenching of tautomer emission was observed in several other dyes also.[234,235] The recovery of tautomer emission and appearance of new band at 388 nm are due to protonation of imidazole nitrogen of one of the HPBI unit. The emission band at 388 nm can be assigned to emission of cation formed by the protonation of imidazole nitrogen. The appearance of neutral tautomer emission along with cationic emission is due to dissociation of proton from the –OH group of cation which reorganizes to form tautomer in the excited state. Rodrı´guez-Prieto *et al.* also reported that in aqueous acidic solution (pH~3), the cation of HPBI upon excitation emits the neutral keto

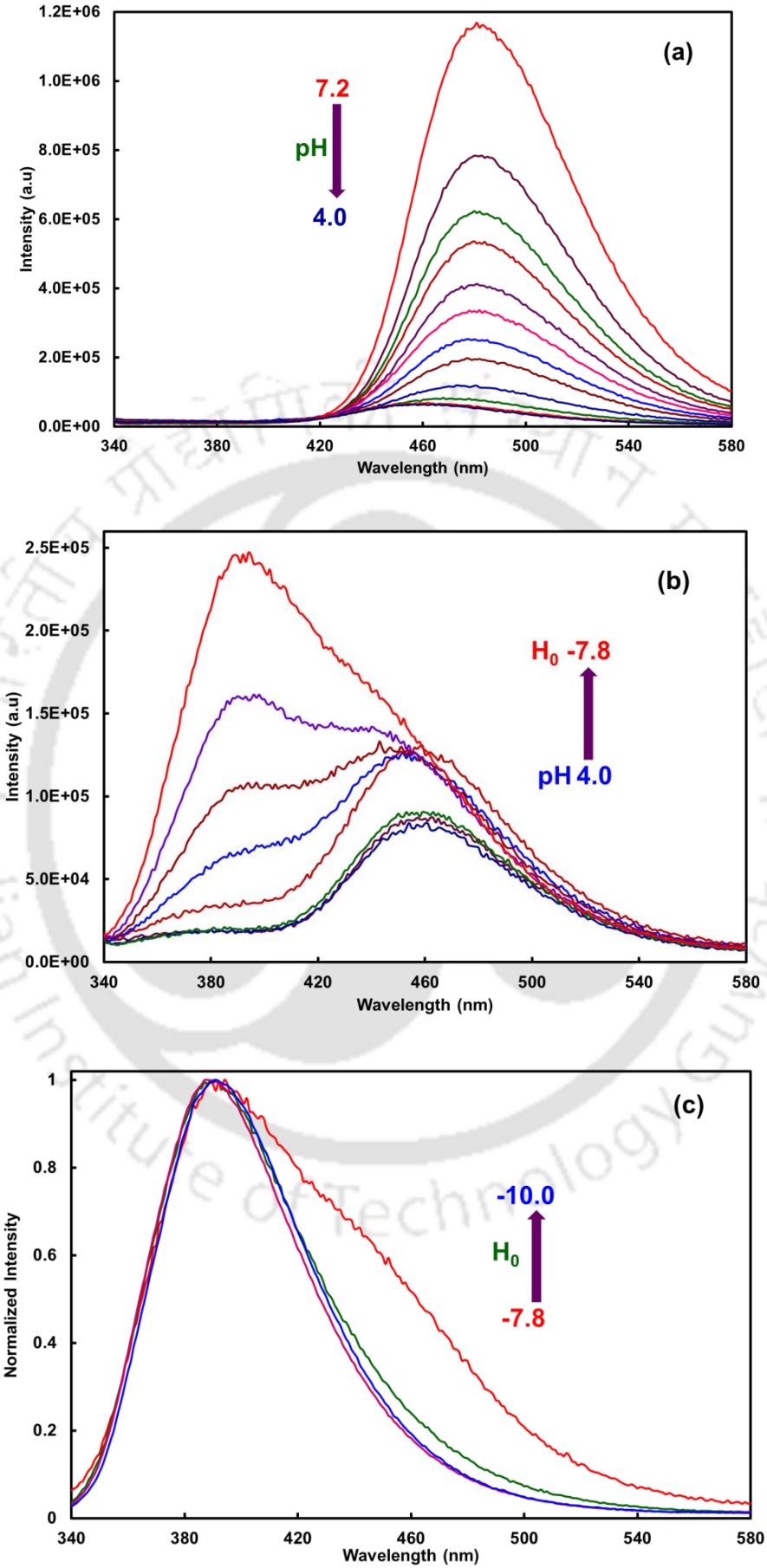

Figure 5.9. Fluorescence spectra of bis-HPBI under acidic media, λ_{exc} = 300 nm.

emission.[61] Similar events are also encountered by HPIP-b in water.[151,236] However, Rodrı´guez-Prieto *et al.* observed the two emission of HPBI in acidified ethanol, due to excited state cation and the neutral tautomer produced from cation.[61] The results of bis-HPBI in acidified aqueous solution is little similar to results of HPBI in acidified ethanol rather than acidified aqueous solution. Recently, Rodrı´guez-Prieto *et al.* demonstrated that when electron donating amino group was substituted in HPBI, the excited cation was unable to transfer its –OH proton to solvent, due to electron donating nature of $–NH_2$ group.[237] In bis-HPBI, the electron donating alkyl groups are substituted, but as the electron donating ability is less than that of amino group, bis-HPBI exist in both cationic form and neutral tautomeric form. As, the deprotonation is prevented in strongly acidic solution emission is observed only from the cationic form of bis-HPBI

5.2.3. Conclusion

Enhancement of tautomer band intensity upon deprotonation of single –OH also supports the single proton transfer hypothesis in bis-HPBI. On the other hand, the tautomer emission decreases in acidic solution with initial addition of acid due to quenching by hydrogen bonding. When the imdazole nitrogen is protonated the tautomer emission is partially recovered due to dissociation of proton of –OH group and reorganization of cation. In strongly acidic solution the dissociation of –OH group from cation is prevented and emission is observed only from cation of bis-HPBI.

Chapter 6

Aggregation Induced Enhance Emission of 4-(3-(benzo[d]thiazol-2-yl)-5-tert-butyl-4-hydroxybenzyl)-2-(benzo[d]thiazol-2-yl)-6-tert-butylphenol†

†*Faraday Discuss.*, 2016, DOI:10.1039/C6FD00171H.

6.0. Introduction

In recent times molecular self-assembly of organic dyes have gained much attention in science and technology because of their potential use in optoelectronic and photonic applications.[238-248] But, due to aggregation caused quenching most of the organic molecules which are otherwise highly fluorescent in dilute solution become weakly emissive or non-emissive in self-assembly or in solid state. However, the pioneering work of Tang *et al*. opened up a new avenue of aggregation-induced emission (AIE) and aggregation induced emission enhancement (AIEE) mechanisms. Tang *et al*. first reported the aggregation-induced emission (AIE) phenomenon of silole molecule, which is just opposite to aggregation caused quenching effect.[134] Successively, the AIE and AIEE properties of variety of luminophores were investigated.[134-143] The noncovalent intermolecular forces such as hydrogen bonding, van der Waals interaction, π-π stacking, hydrophobic interaction etc. control these self-assembly.[249,250] Several mechanisms such as restricted internal rotation, J-aggregation formation, restriction of TICT emission etc were proposed to explain the AIE and AIEE of dyes. [251,252] After the design of AIE/AIEE molecules, now many reports are available on the high-tech applications of the AIE/AIEE not only optoelectronic but also in sensing and detection.[252-256] More recently cell imaging application of aggregated structure and the ion sensing ability of AIEE self-assembly got attentation.[257-262] With time ESIPT dyes were developed to show AIEE.[263-270] In the present scenario ESIPT dyes offers a better platform due their abnormal large Stokes shift, which helps to avoid the self-absorption and brings the intense emission by ESIPT. Recently the AIEE active ESIPT dyes, *N*,*N*′-di[3-Hydroxy-4-(2′-benzothiazole)phenyl]isophthalic amide (DHIA) and *N*,*N*′-di[3-Hydroxy-4-(2′-benzothiazole)phenyl]5-tert-butyl-isophthalic amide (DHBIA) were investigated by Yang *et al*.[264] In these fluorophores two 2-(2'-hydroxyphenyl)benzthiazole moieties were attached to a phenyl spacer through amide linkage. Based on theoretical calculation Yang et al. hypothesized that, DHIA and DHBIA emit weak fluorescence in diluted solution but high fluorescence in aggregates due to inhibition of twisted intramolecular charge transfer (TICT) of the enol conformer in the excited state.[144] They suggested formation of TICT state by C-N bond of the amide linkage that suppress the ESIPT process. Later, they also showed AIEE in the fluorophore with one 2-(2'-hydroxyphenyl)benzthiazole but possess the amide group connecting to phenyl ring.[265] In most of the systems including the present thesis work (see later **Chapter 7**), it is observed that the ESIPT suppresses the C-N rotation route that lead to TICT emission. Rather in ESIPT exhibiting 2-hydroxyphenylazoles it was predicted that the torsional rotation of C-C bond

connecting the azole ring and the phenyl ring from the keto tautomer leads to ICT state and that opened a channel for non radiative decay.[82,89,167,213,232] Therefore to understand the cause of AIEE in ESIPT fluorophores, 4-(3-(benzo[d]thiazol-2-yl)-5-tert-butyl-4-hydroxybenzyl)-2-(benzo[d]thiazol-2-yl)-6-tert-butylphenol (bis-HPBT) **(Chart 6.1)** is investigated. In bis-HPBT, the phenyl ring with amide linkage were replaced with simple methylene group to completely eliminate the option of C-N twisting. In addition, bis-HPBT has a smaller less interacting spacer which may reduce the flexibility of the system. As a consequence, more enhancements in AIEE may be achieved. In the last chapter, it is shown that the less Stoke shifted normal emission can be suppressed by substituting *tert*-butyl group at ortho position to phenolic OH group. Therefore, *tert*-butyl group was substituted at ortho position to phenolic OH group in bis-HPBT. In this chapter, the possible AIEE from not only that of bis-HPBT but also those of 4-(3-(benzo[d]oxazol-2-yl)-5-tert-butyl-4-hydroxybenzyl)-2-(benzo[d]oxazol-2-yl)-6-tert-butylphenol (bis-HPBO) and 4-(3-(1H-benzo[d]imidazol-2-yl)-5-tert-butyl-4-hydroxybenzyl)-2-(1H-benzo[d]imidazol-2-yl)-6-tert-butylphenol (bis-HPBI) **(Chart 6.1)** are explored. The applications of AIEE in sensing of metal ions, anions and imaging of cells are also examined.

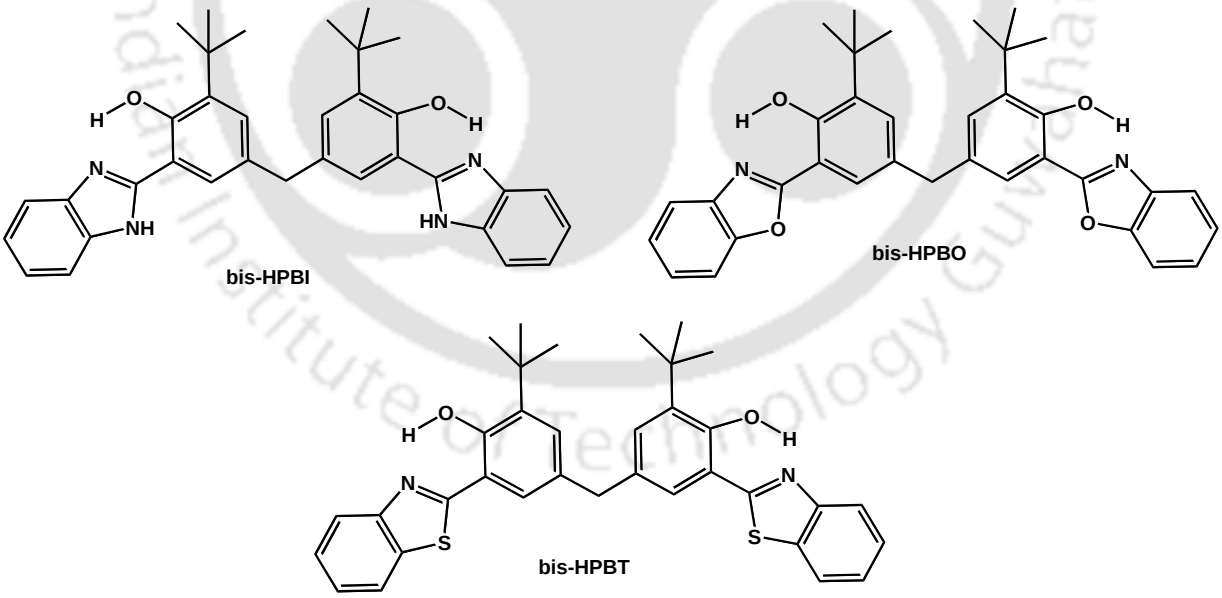

Chart 6.1. Structures of the bis-HPBI, bis-HPBO and bis-HPBT.

6.1. Solubility Testing

bis-HPBI and bis-HPBO are well soluble in most of the organic solvents (**Table 6. 1**). On other hand bis-HPBT is insoluble in most of the organic solvents except in THF, DMF and DMSO (**Table 6. 1**). It is insoluble in water also. Therefore, it can be inferred that by a small change in molecular substitution, the solubility can also be changed.

Table 6.1. Solubility of bis-HPBI, bis-HPBO and bis-HPBT in Different Solvents. (Soluble: S, Insoluble: S_i and Sparingly Soluble: S_p).

Solvents	bis-HPBI	bis-HPBI	bis-HPBT
Cyclohexane	S	S	S_p
Dioxane	S	S	S_p
Ethylacetate	S	S	S_i
THF	S	S	S
Acetonitrile	S	S	S_i
DMF	S	S	S
DMSO	S	S	S_p
Butanol	S	S	S_i
Ethanol	S	S	S_p
Methanol	S	S	S_i
Water	S_p	S_p	S_i

Since bis-HPBT is insoluble water and soluble in THF, the molecular aggregation of bis-HPBT studied in THF/water mixture.

6.2. Molecular Aggregation of bis-HPBT

The absorption spectrum of bis-HPBT exhibits two main absorption bands in THF **(Figure 6.1)**. The absorption spectra in THF is structured having vibrational frequency equal to 1000 ± 40 cm^{-1}. The higher energy bands around 315 nm are for benzthiazole moiety and the lower energy bands around 360 nm corresponds to the π-π* transition of the coupling between benzthiazole and the hydroxyphenyl moieties.[264,265] To study the molecular aggregation the absorption spectra of bis-HPBT in different mixtures of water/THF (v/v) are recorded. From the absorption spectra, it can be clearly seen that the spectral pattern of the dye in water-THF mixtures remains same up to 60% volume fraction of water (f_w), only the absorbance of the dye decreases compared to that in pure THF, which indicates that the dye has no apparent structural changes up to f_w = 60%. The decrease in absorbance may be due to different solubility of the fluorophores in water/THF mixture than pure THF owing to the change in dielectric constant of the solution.[271] But, after f_w = 60%, rapid bathochromic shift is observed with spectral broadening and a long tailing. This sudden spectral changes may be due

to change in homogeneity of the solution.[272] The emergence of level-off tails in the absorption spectra indicates the formation of aggregated structure in higher water fraction (> 60%).[264] Similar level - off tail is also obtained due the Mie scattering of the aggregated structure .[273,274] The red shifts in the spectrum are due to the weak π–π stacking interaction of the dye in its aggregated structure and attributed for the J-aggregation formation.[265] Usually, in J-aggregation the absorption band is red shifted, which is intense and narrow as compared to the monomer.[275] But, the weak and broad absorption spectra of bis-HPBT may be due to the less optimal J-aggregation way alignment of molecules.

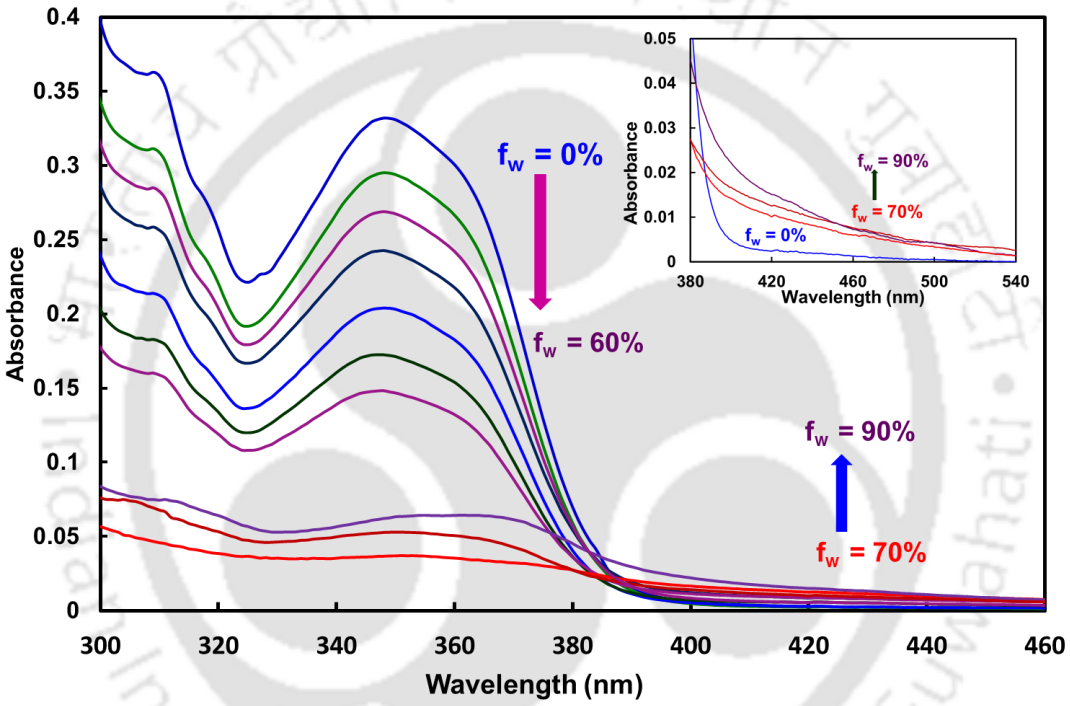

Figure 6.1. Absorption changes of bis –HPBT in different fractions of water/THF. The inset shows level-off tails owing to Mie scattering at higher water content..

Field emission scanning electron microscope (FESEM) images were obtained to verify the observed spectral changes. Fibrous aggregated structures having width ~300 nm were found from the f_w = 70% solution, whereas in pure THF no such aggregated morphology was found (**Figure 6.2**).

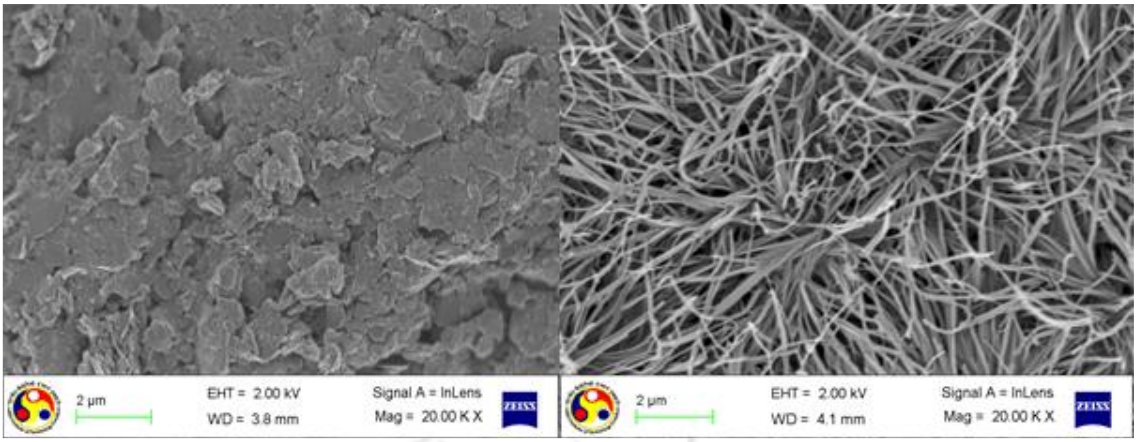

Figure 6.2. FESEM images of bis-HPBT in pure THF (left) and in f_w = 70% water/THF mixture (right).

6.3. Enhanced Fluorescence

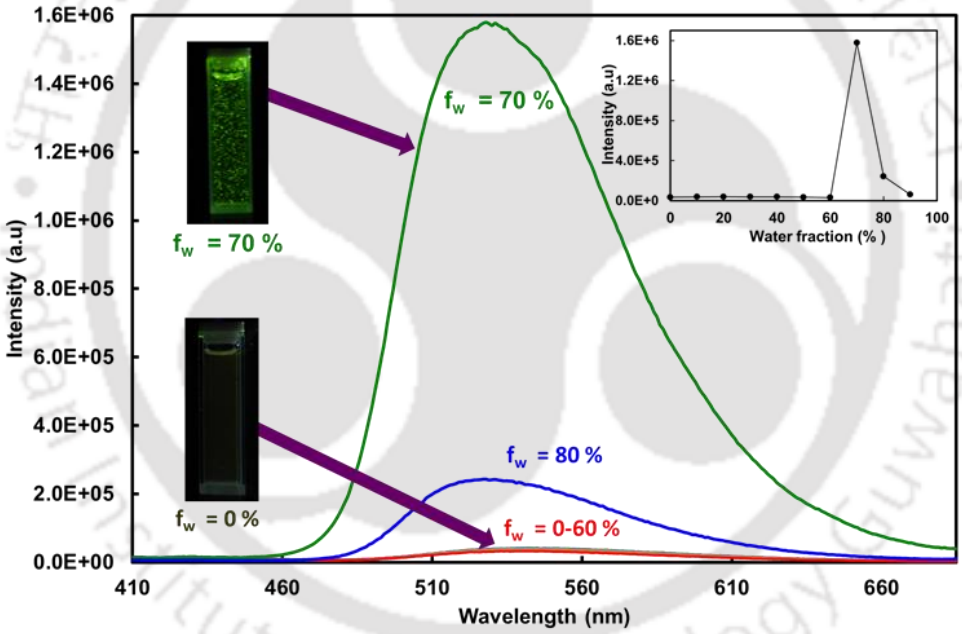

Figure 6.3. Fluorescence spectra of bis-HPBT in different water/THF (v/v) mixtures, λ_{exc} = 365 nm. Inset showing variation of fluorescence intensity with increase in water fraction.

The fluorescence emission spectrum of bis-HPBT in THF was monitored by exciting the solution at 365 nm (**Figures 6.3**). In THF solution, bis-HPBT emits two distinct emissions one at ~ 410 nm and other at ~ 530 nm (**Figure 6.3**). By analogy with HPBT the dual emissions of bis-HPBT in THF can be attributed to normal emission (410 nm) and keto emission (~ 530 nm) after ESIPT.[264] The normal emission of bis-HPBT is weak and structured in THF having vibrational frequency 1400 ± 50 cm^{-1}. But the THF solution of bis-HPBT is weakly fluorescent

and poorly soluble in water. With addition of water to THF solution of the bis-HPBT, the fluorescence may enhance due to aggregation formation. To verify this phenomenon, different amount of water (f_w) are added to the THF solutions of bis-HPBT. As a result, small enhancement in fluorescence was observed at f_w = 20% and remain constant up to f_w = 60%. At f_w = 70%, a sudden boost in the green fluorescence is observed **(Figure 6.4**.). The fluorescence yield (Φ_F) of the tautomer band increases ~300 times in aggregation (Φ_F = 0.3885) than that in THF (Φ_F =0.0013). This increase in fluorescence intensity can be attributed to the AIEE effect. The increase in fluorescence yield is much impresive as compared to those obtained for DHIA (21 times enhancement) and DHBIA (112 times enhancement).[264] This infers more facile AIEE in bis-HPBT than in DHIA and DHBIA. The other foremost advantage of bis-HPBT is that the less Stokes shifted normal emission is completely eleminated and only AIEE of highly Stokes shifted tautomer emission is observed. After reaching a maximum intensity at f_w = 70% the fluorescence intensity of the dye decreases at higher water fractions i.e f_w = 80% and f_w = 90% **(Figure 6.3)**. This type of change in fluorescence intensity is observed in other AIEE systems also.[272] It is attributed to the fact that aggregation is much more facile at high water contents and emission is probably due to the molecules attached on the surface of these highly aggregated particles together with aggregated structure. This may results in drop of original fluorescence of the aggregated structure.[272,277]

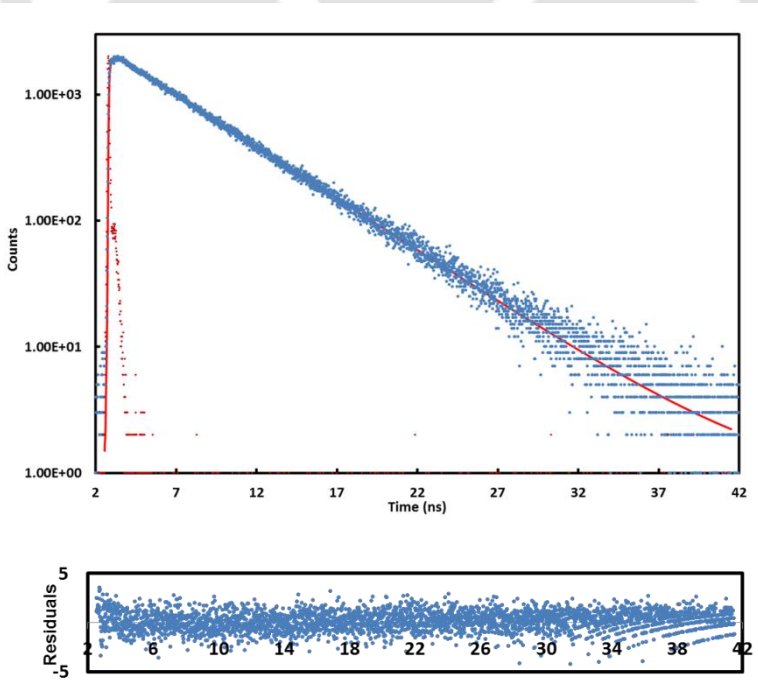

Figure 6.4. The instrument response function and the fluorescence decay of bis-HPBT in fw = 70% along with fitted curve and residue plot.

The fluorescence lifetime of bis-HPBT in pure THF is short (0.89 ns). However, the decay lifetime of the dye in f_w = 70% is as long as 5.3 ns **(Figure 6.4)**. The longer fluorescence decay time reveals that the nonradiative processes of the electronically excited state of the dye are substantially reduced due to molecular aggregation. To further substantiate this fluorescence decay was monitored in solid state. The longer life time obtained for solid bis-HPBT (5.1 ns) also corroborates with the conclusion.

6.4. The Cause for AIEE

To confirm the role of RIR in AIEE of bis-HPBT, the effect of viscochromism and thermochromism on the dye emission are scrutinized. Since, the RIR process is expected to affect by the viscosity of the mediun, the fluorescence of bis-HPBT is recorded in glycol/THF mixtures. The fluorescence of the dye is enhanced with an increase in the viscosity of the solvent mixture **(Figure. 6.5)**. In addition to tautomer emission, the normal emission also increases. This is due to breaking of intramolecular hydrogen bond of the *cis*-enol by the intermolecular hydrogen bond of protic glycol. This shifts the *cis*-enol-*trans*-enol equilibrium towards *trans*-enol. Regardless of the decrease in *cis*-enol population that the tautomer emission increases, this shows the strong RIR due to enhanced viscosity.

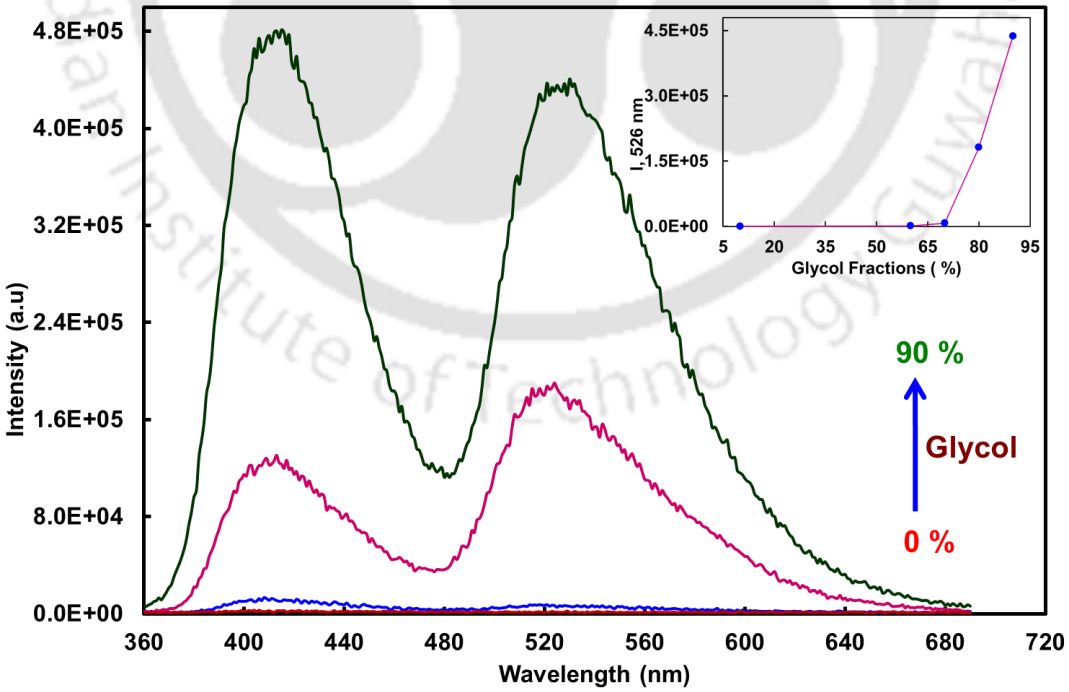

Figure 6.5. Fluorescence spectra of bis-HPBT in glycol/THF mixture.

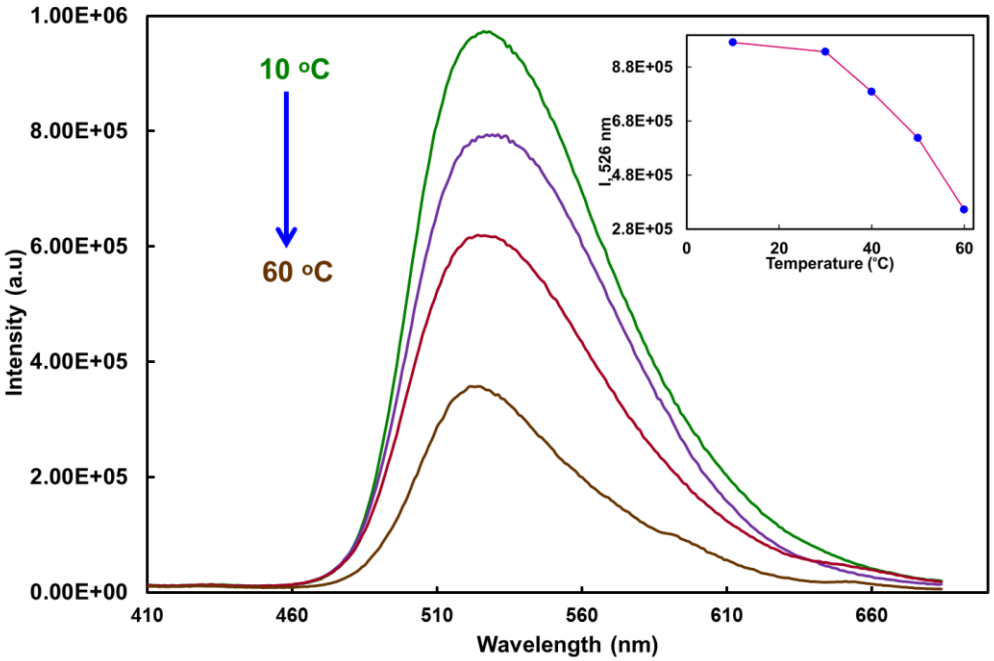

Figure 6.6. Fluorescence spectra of bis-HPBT in different temperature.

The effect of temperature on the fluorescence spectrum of f_w = 70% solution is depicted in the **Figure 6.6**. The fluorescence maximum is virtually unaffected by the temperature. The fluorescence intensity of the system decreases with rise in temperature **(Figure. 6.6)**. This indicates that with increase in temperature the flexibility of the aggregate increases, which reduces the RIR. The results of viscochromism and thremochromism, suggested that the RIR is responsible for AIEE of bis-HPBT.[278]

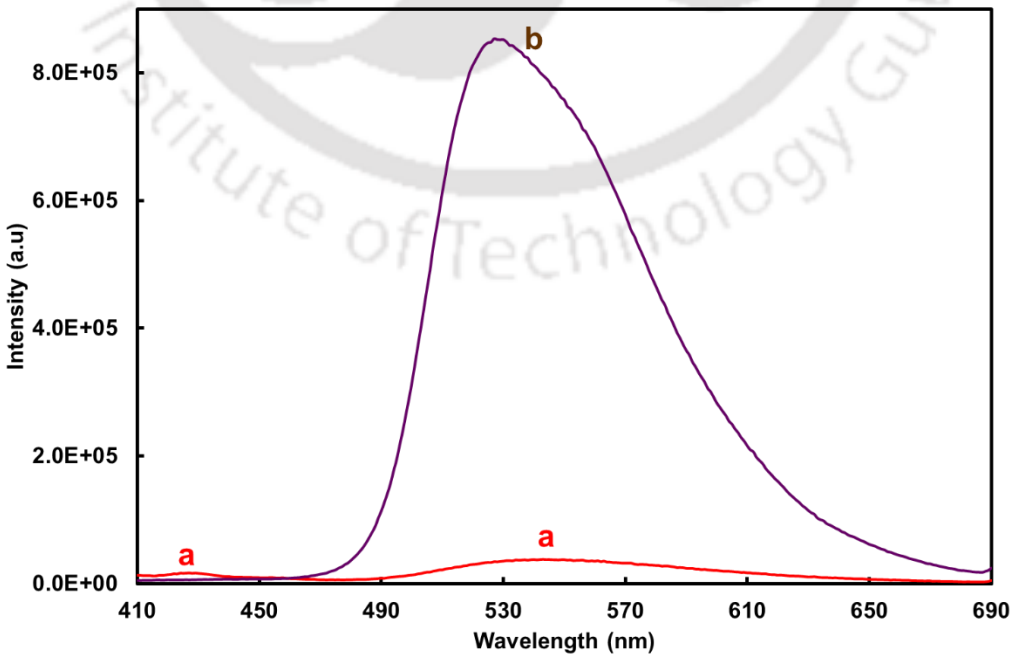

Figure 6.7. Fluorescence spectra of bis-HPBT in (a) THF and (b) solid state, λ_{exc} = 365 nm.

Table 6.2. Absorption Band Maxima (λ_{max}^{ab}, nm), Fluorescence Band Maxima (λ_{max}^{fl}, nm) and Fluorescence Yield (Φ_F) of bis-HPBT in THF, f_w = 70% and Solid State.

	λ_{max}^{ab}	λ_{max}^{fl}	τ_{fl}	Φ_F
THF	348, 360	542	0.89	0.0013
f_w = 70%	353, 368	527	5.30	0.3885
Solid		527	5.10	-

As mentioned earlier, Yang *et al*. proposed that the weak emission of DHIA and DHBIA in diluted solution is due to non-emissive TICT formed by C-N rotation. They hypothesized the high fluorescence of DHIA and DHBIA in aggregates is due to inhibition of non-emissive TICT of the enol conformer in the excited state.[144] In bis-HPBT there is no C-N bond, therefore the hypothesis that RIR of C-N which led to non-emissive TICT state of enol is ruled out. Hence, the enhancement of fluorescence intensity in aggregated state is due to restriction of RIR of C-C single bond connecting hydroxyphenyl and benzthiazole moieties of bis-HPBT. As discussed earlier, subsequent to ESIPT the keto form of 2-(2'-hydroxyphenyl)azoles undergo torsional rotation which led to nonradiative de-excitation of the excited states. [82,89,167,213,232] But aggregation of bis-HPBT leads to close packing of the molecules which provide structural rigidity to molecular rotation. bis-HPBT is also highly emissive in solid state than its diluted solution which infers that molecule is highly emissive in its closed pack structure **(Figure 6.7**). The fluorescence spectra of bis-HPBT is blue shifted in the solid state and aggregated state than in THF solution **(Figures 6.3 and 6.7, Table 6.2)**. This spectral blue shift clearly suggests that rigidity of the system increases by aggregation as it obeys the principle of rigidochromism.[279] The intarmolecular hydrogen bonding, the weak van der Waals interaction and hydrophobicity provided by the *tert*-butyl groups and the partial (head to tail) π-π stacking interactions may be responsible for the formation of aggregation in water-THF mixture.

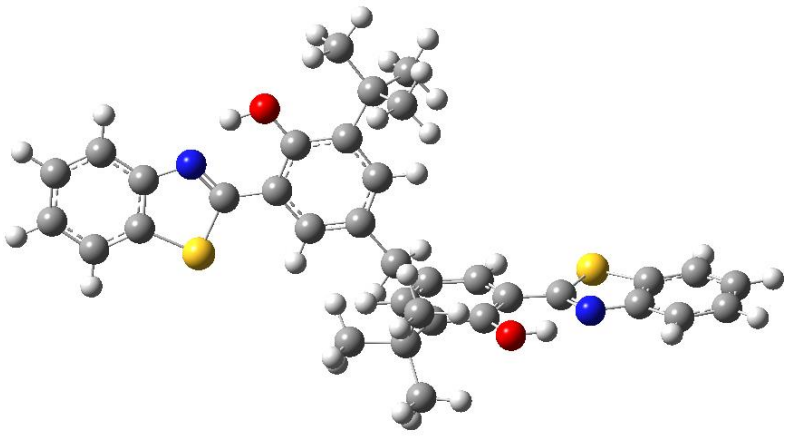

Figure 6.8 DFT optimized structure of bis-HPBT.

To gain more insight the structure of the bis-HPBT is optimized using Gaussian 09 by employing Becke's three-parameter hybrid functional B3LYP with 6-31G (d, p) as basis set at DFT level and the optimized structure has nonplanar geometry (**Figure 6.8**).[161] The presence of two bulky *t*-butyl groups prevents the full face to face arrangement due to steric reasons. Absence of full face to face arrangement of aromatic moieties reduces the π-π stacking interactions, which leads to fluorescence quenching. It appears that RIR plays a predominant role than other factors in aggregated state (f_w = 70%). When f_w > 70%, the solubility of bis-HPBT in the solvent mixture decreases further to yield more insoluble particles and thus, expected to decrease the number of emitting molecule. In other way it can be interpretted that in the mixture with medium water content (here at f_w = 70%), molecules of bis-HPBI steadily gather to form fibrous aggregates and lead to an enhancement in the fluorescence intensity. However, it is very difficult to control the uniform formation of aggregation at high water fraction. Thus, no uniformity is observed and the fluorescence intensity drops at high water content.[277,280,281]

The advantage of AIEE of bis-HPBT over DHIA or DHBIA is not only limited to more enhancement than those fluorophores. In most of the ESIPT fluorophores in the aggregate solution both normal and tautomer emission are observed. However, the less Stoke shifted normal emission is almost completely eliminated and bis-HPBT almost exclusively emit highly keto emission. Despite the fact that in THF the relative intensity of normal emission is not negligible and water is a protic solvent. Here it can be hypothesized that the presence of two bulky *tert*-butyl groups at ortho position has reduced the population of trans-enol by providing steric hindrance as well as more hydrophobicity to the aggregates.

6.5. Thermal Stability

The AIEE behaviour of bis-HPBT, motivated to investigate the thermal properties of the dye. Fortunately the dye is thermally stable. It can be inferred from differential scanning calorimetry (DSC) the melting temperature of bis-HPBT is ~ 245 ºC **(Figure 6.9)** and from thermal gravimetry analysis (TGA) it is found that there is no weight loss up to ~ 300 **(Figure 6.10)**. It is obvious that the stability and lifetime are affected by these thermal properties. The high thermal stability renders that bis-HPBT can be used in optical devices such as OLED.

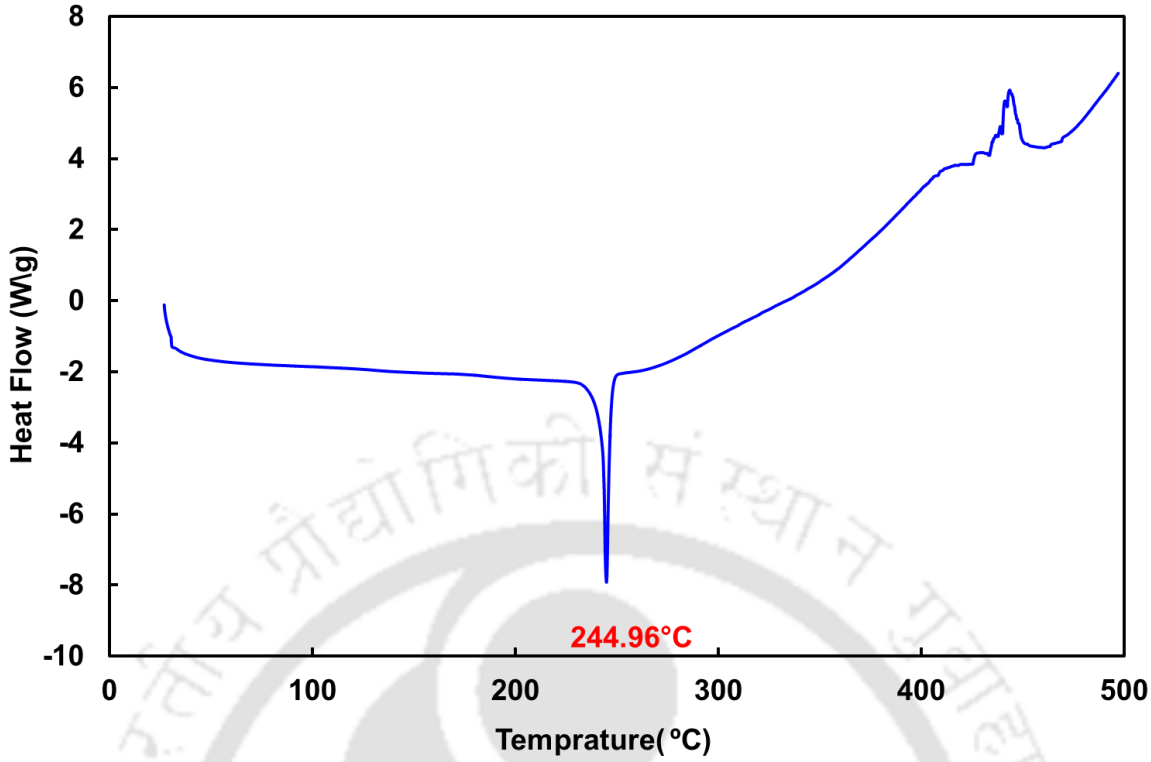

Figure 6.9. DSC plot showing heat change of bis-HPBT.

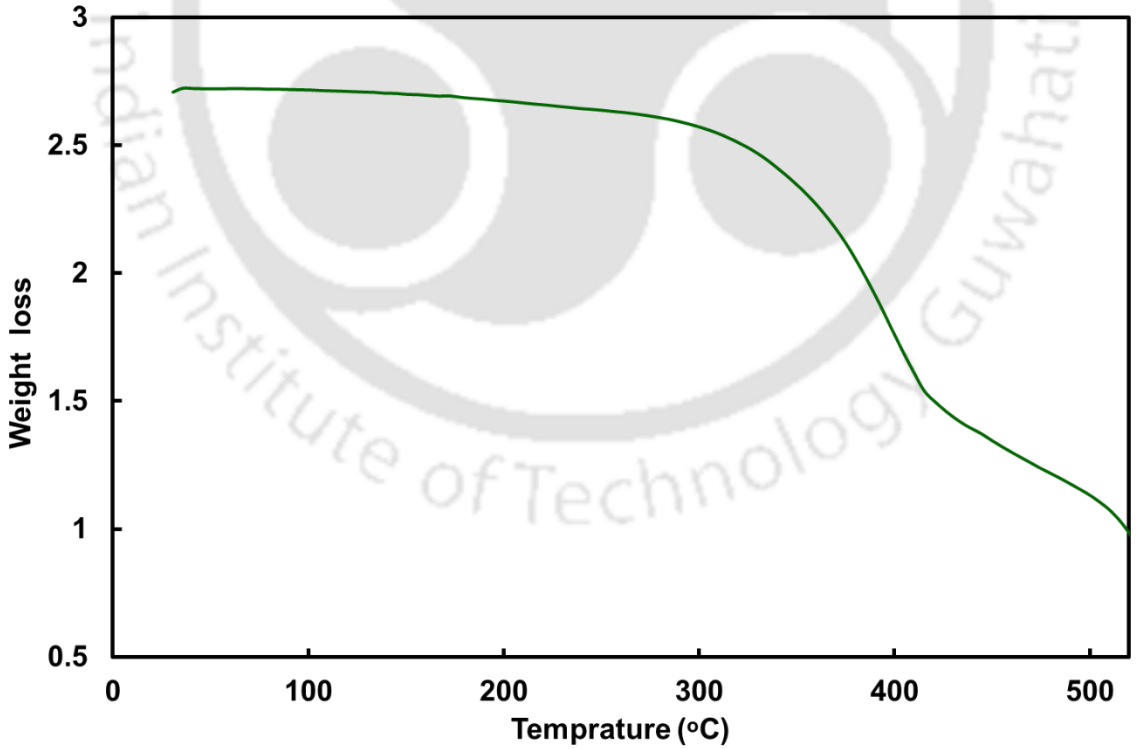

Figure 6.10. TGA plot showing weight loss of bis-HPBT.

AIEE molecules recently used for the ion sensing and cell imaging.[252-256] To further enhance the utility of the AIEE of bis-HPBT, the sensing ability of aggregates have been investigated with various metal ions and anions. The effect of different metal ions on fluorescence intensities is depicted in **Figure. 6.11**. Significant quenching of aggregates fluorescence is observed with metal ion such as Cu^{2+}, Fe^{2+}, Co^{2+}, Cd^{2+}, Hg^{2+}, Mg^{2+} and Na^{+}. Only in the case of Zn^{2+} and Ni^{2+} the quenching is lesser extent with addition of ~ 12 μM of metal ions. But the fluorescence is nearly completely quenched at around 170 μM in case of Zn^{2+}, Ni^{2+}, Mg^{2+} and Na^{+} and at around 100 μM additions of other tested transition metal ions. The interaction of Zn^{2+} ion on AIEE is presented in **Figure 6.12** as a representative plot. The studies indicate that AIEE is hampered by the addition of metal ions and therefore, it can be used for metal ion sensing. From the quenching it can be inferred that the aggregation is hampered by these metal ions due to binding of metal ions with monomers which breaks the aggregation.

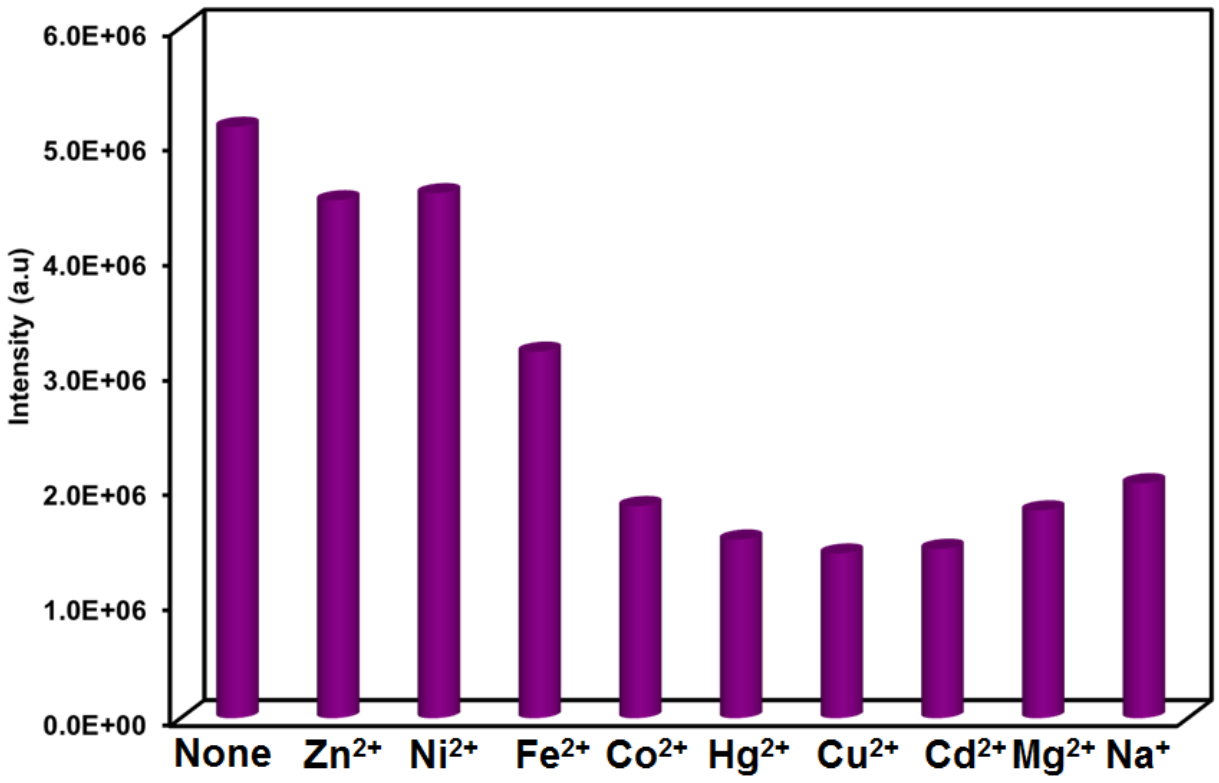

Figure 6.11. The histogram plot for the cation sensing of the aggregated structure. (12 μM metal ion concentration).

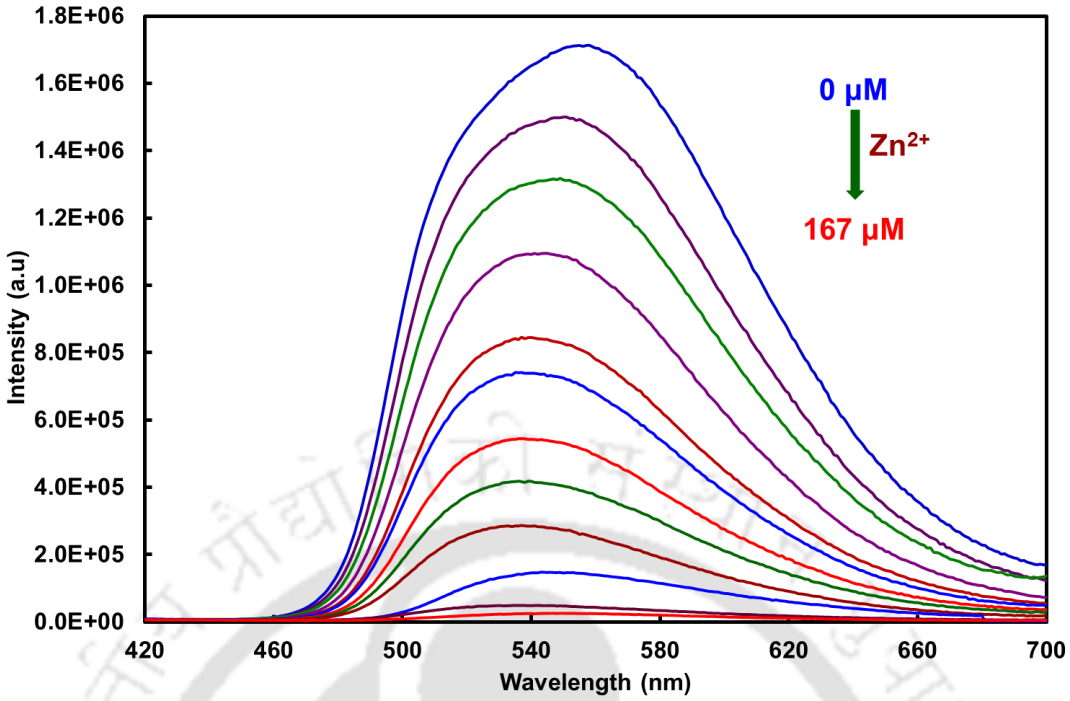

Figure 6.12. Effect of Zn^{2+} on the AIEE.

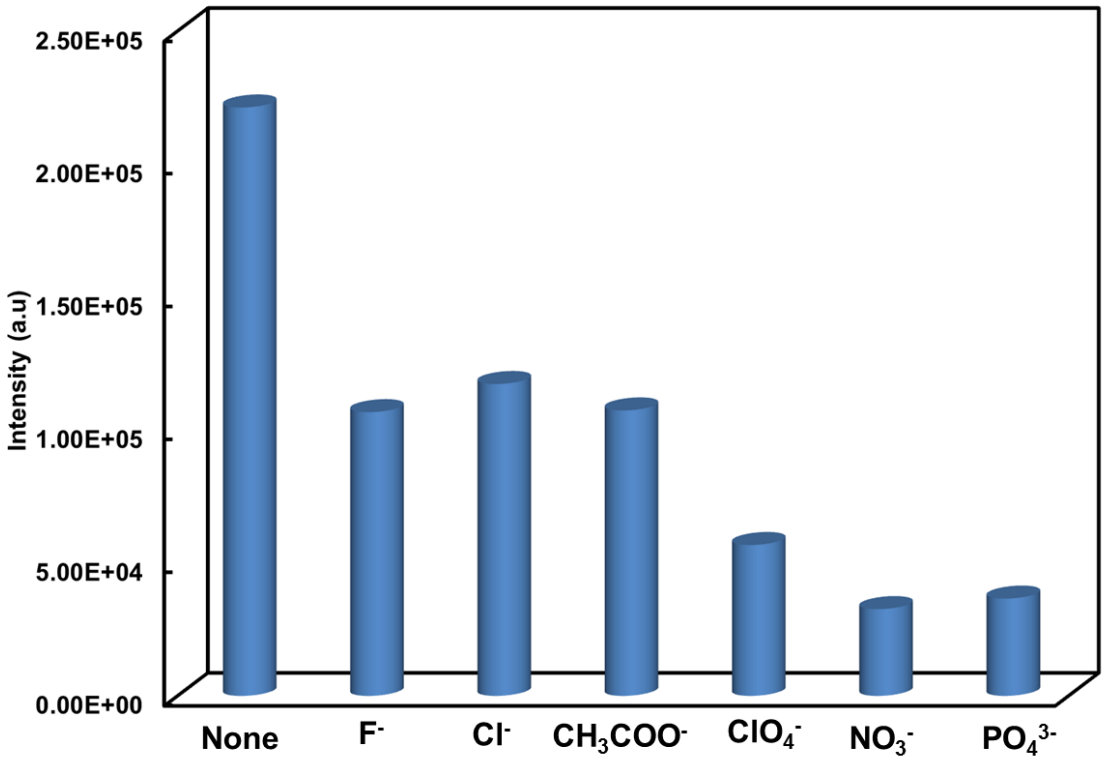

Figure 6.13. The histogram plot for the anion sensing of the aggregated structure (~12 μM anion concentration is considered.

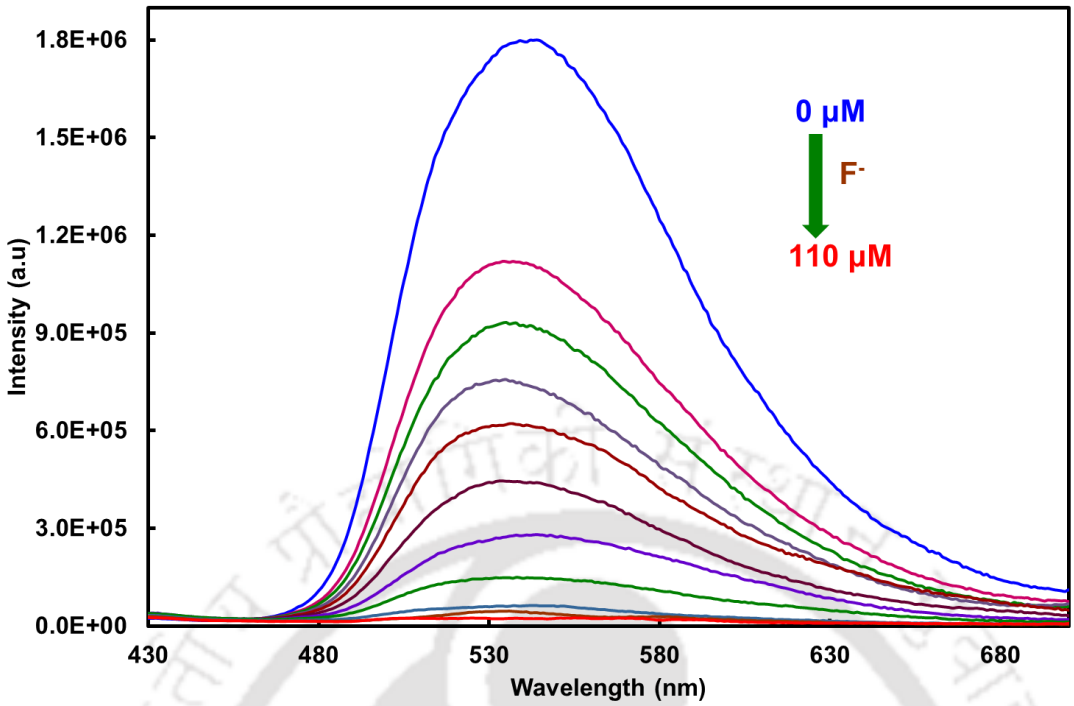

Figure 6.14. Effect of F^- on the AIEE.

Similarly the interaction of the aggregates with different anions such as F^-, Cl^-, CH_3COO^-, NO^{3-}, PO_4^{3-} and ClO^{4-} are e also evaluated. With addition of anions at ~ 12 µM cause a drop in fluorescence intensity **(Figure 6.13)**, successive addition of anions continue the decrease of fluorescence and the fluorescence is almost quenched at higher anion concentration. $NO^{3-}$and PO_4^{3-} are more efficient in quenching. On the other hand F^- and Cl^- are relatively less interacting. The interaction of F^- ion on aggregates is presented in **Figure 6.14** as a representative plot. ~ 130 µM of anions is sufficient enough to completely brake the aggregated structure. Thus, like the metal ions, the anions also quench the aggregation therefore may be used for sensing.

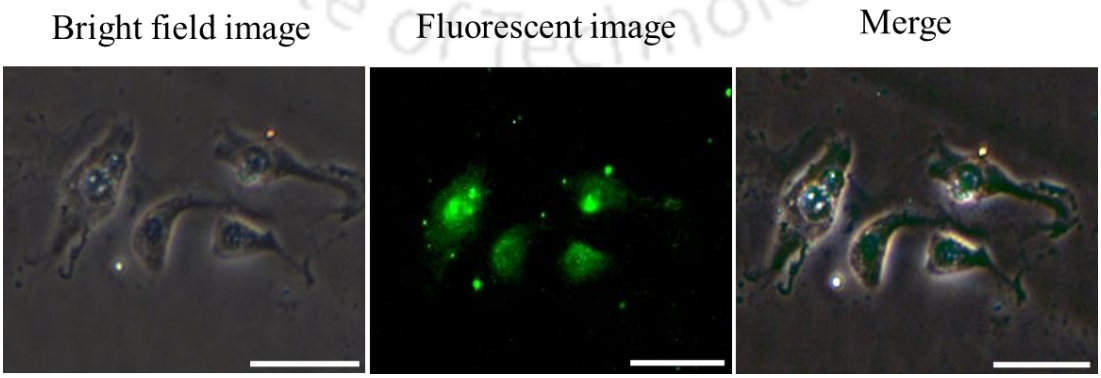

Figure 6.15. Representative phase and fluorescent images showing HeLa cells treated with f_w = 70% and aggregate formed after 2 hrs. Scale bar represents 50 microns.

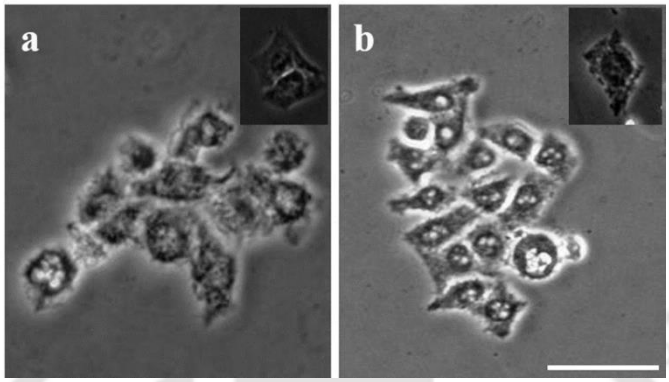

Figure 6.16. Representative images showing morphology of HeLa cells (a) Control (without treatment) and (b) after 8 hrs of THF treatment. Scale bar represents 50 microns.

The application of aggregated structure for imaging living cells is also explored using HeLa cells. Green emission of aggregates is also observed inside cell and this observation relates to the fluorometric studies done with f_w = 70% (**Figure 6.15**). This suggest that the aggregates are cell permeable and in addition there was no morphology alteration within cells treated with aggregated structure (f_w = 70%) upto 8 hrs (**Figures 6.16a** and **6.16b**). From the results obtained, it may be inferred that the bis-HPBT aggregate is useful for shorter incubation studies (**Figure 6.16b**). As in published reports, all incubation studies for *in vitro* imaging are performed for only shorter duration (minimum 1-2 hrs and maximum 4-5 hrs).[261,262] Thus, the bis-HPBT aggregate may be useful as biomedical sensing probe for future *in vitro* and *in vivo* application.

6.9. Conclusion

AIEE is observed from bis-HPBT whereas it is absent in other two derivatives i.e bis-HPBI and bis-HPBO. Bis-HPBT is weakly fluorescent in THF solution and highly fluorescent aggregates are obtained at f_w = 70% due to aggregation. The enhancement of fluorescence due to aggregation bis-HPBT is much impressive than other similar ESIPT fluorophores. Added advantage of AIEE of bis-HPBT is almost exclusive highly Stokes shifted tautomer emission. The high fluorescence in aggregate state is due to RIR of C-C single bond connecting the benzthiazole and hydroxyphenyl ring. The aggregate structure ruptures by the addition of ions.

The aggregated structure acts as a good fluorescence chemosensor for metal ions as well as anions. The AIEE also observed inside the HeLa cell.

Chapter 7

Photophysics of 2-(4'-Amino-2'-hydroxyphenyl)-*1H*-imidazo-[4,5-c]pyridine and Its Analogues: Effect of Solvents†

†*J. Phys. Chem. B*, 2015, **119**, 2330–2344.

7.0. Introduction

No doubt TICT and ESIPT processes have earned popularity due to their contribution in science and technology. As mentioned earlier, in recent times, the coupled proton and charge transfer process received major attention.[109,145-150] When groups responsible for ESIPT and ICT are combined in the same fluorophore then their photophysical properties become more interesting. In **Chapter 3** it is shown that in DMAPIP-c relay proton transfer induces the TICT emission in protic solvents and it is applicable also for APIP-c. Therefore, AHPIP-c **(Chart 7. 1**) was synthesized where both proton donating and electron donating groups are attached in the single fluorophore. So far in the combined ESIPT-ICT system those reported in the literature, the intermolecular hydrogen bonding is not absolutely essential for ICT molecules to emit ICT emission.[104-109,113,115-119,235,182,283] Hence, AHPIP-c is the first molecule of this kind. The effect of solvent on AHPIP-c was investigated. Besides, for better understanding, the spectral characteristics of AMPIP-c and PIP-c are also investigated **(Chart 7.1)**.

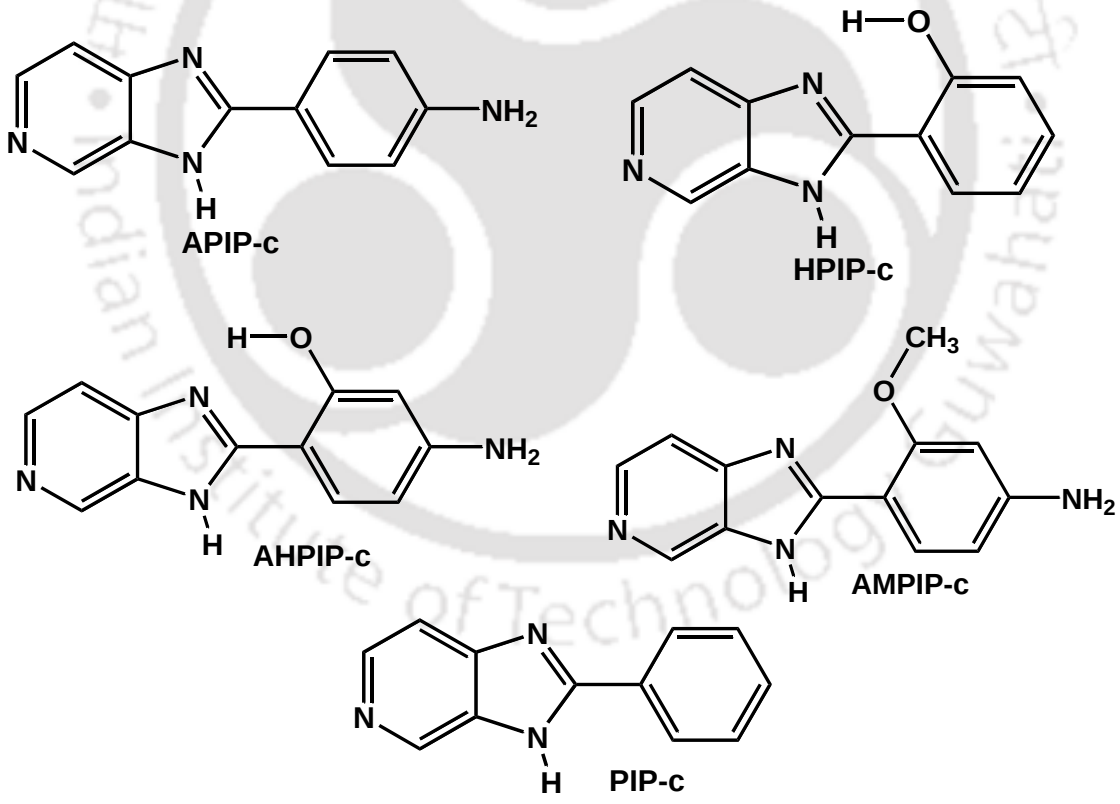

Chart 7.1. Structures of APIP-c, HPIP-c, AHPIP-c, AMPIP-c and PIP-c.

7.1.0. Effect of Solvents on Spectral Charateristics

The main objective of the study is to ascertain the roles of intermolecular hydrogen bond, intramolecular hydrogen bond and proton transfer in the ICT process and to find whether intramolecular hydrogen bond or proton transfer is competent to promote ICT. Further, the studies in protic solvents will be more interesting to determine the dominating process (ICT/ESIPT) in protic solvents.

7.1.1. Spectral Characteristics of APIP-c

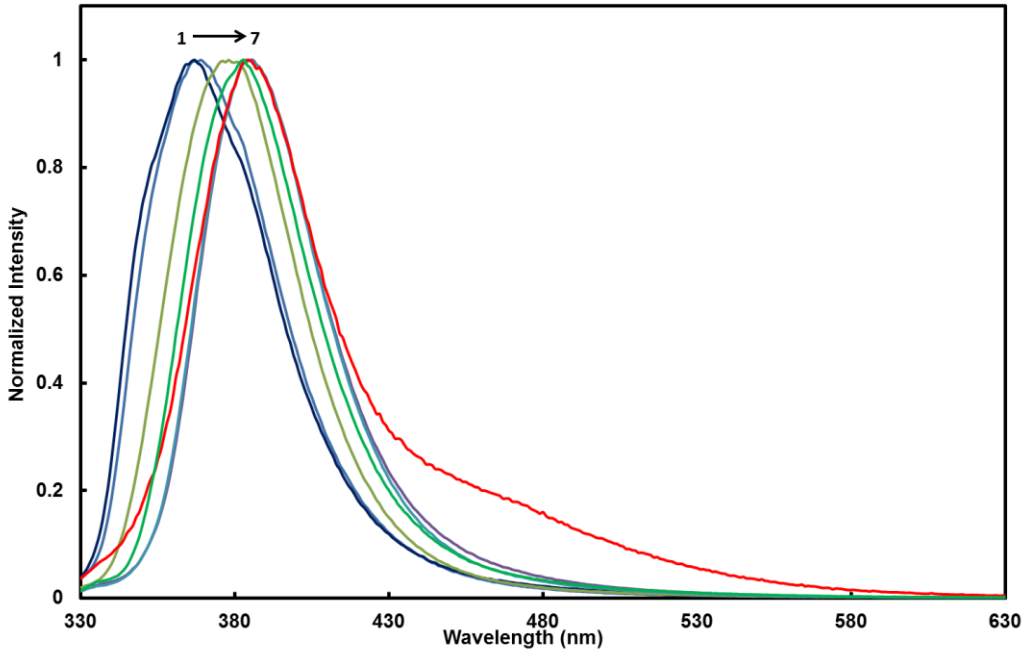

Figure 7.1. Fluorescence spectra of APIP-c in (1) ethylacetate, (2)dioxane, (3) acetonitrile, (4) dimethylformamide, (5) 2-propanol, (6) butanol and (7) methanol, λ_{exc} =320nm.

Fasani *et al.* studied only the steady state spectral characteristics of APIP-c in few selected solvents.[55] For a better comparative study the steady state spectral characteristics of APIP-c in more solvents are measured. The data are presented in **Table 7.1** and the fluorescence spectra in few solvents are depicted in **Figure 7.1**. APIP-c exhibits only normal emission in aprotic solvents. In methanol TICT emission is observed at longer wavelength. The results are well reproducible and in good agreement with the spectral maxima reported by Fasani *et al.* The fluorescence spectra of APIP-c are recorded in more protic solvents. In all these solvents though no clear band appears (as in methanol), but long tailings are observed. In addition, time resolved fluorescence measurements are also performed in some solvents (**Table 7.2**). The fluorescence decay in propanol is shown as representative plot (**Figure 7.2**). Single

exponential decays were detected when decays were monitored at 380 nm, in all aprotic as well as protic solvents except in methanol. However, when monitored at 460 nm, a biexponential decay was observed in all the protic solvents. The short lifetimes match with the lifetimes obtained at shorter wavelength. Therefore they can be assigned to normal emission. The long lifetime components are due to TICT emission and their relative amplitude increases with protic nature of the solvents. Thus, not only methanol but also other protic solvents induce the TICT emission. The absence of dual emission in polar aprotic solvents and its presence in protic solvents suggest the realy proton transfer induces TICT emission in APIP-c also (as discussed in **chapter 3** for DMAPIP-c).

Table 7.1. Absorption Band Maxima (λ_{max}^{ab}, nm), Fluorescence Band Maxima (λ_{max}^{fl}, nm of APIP-c in Different Solvents.

Solevent	λ_{max}^{ab}	λ_{max}^{fl}	
		Shorter Wavelength	Longer Wavelength
Methylcyclohexane		366, 394, 415	
Dioxane	309	367	
Ether	311	371	
Ethylacetate	310	369	
Tetrahydrofuran	313	375	
Acetonitrile	314	378	
Dimethylformamide	314	384	
Dimethylsulphoxide	317	385	
Butanol	316	383	
2-Propanol	316	384	
1-Propanol	318	383	
Ethanol	318	384	
Methanol	319	384	470

Table 7.2. Fluorescence Lifetime of APIP-c in Different Solvents Along With the Corresponding Chi Square (χ^2) (Values in the Parentheses are the Relative Amplitudes).

Solvent	λ_{em} = 380 nm		λ_{em} = 460 nm		
	τ	χ^2	τ_1	τ_2	χ^2
Dioxane	1.0	1.0			
Acetonitrile	1.2	1.0			
2-Propanol	1.3	1.0	1.1 (52.59)	2.7 (47.41)	1.0
Butanol	1.3	1.0	1.1 (46.34)	2.9 (53.66)	1.0
1-Propanol	1.3	1.0	1.0 (38.28)	2.8 (61.72)	1.0
Methanol	0.5	1.4	0.4 (27.43)	2.2 (72.57)	1.0

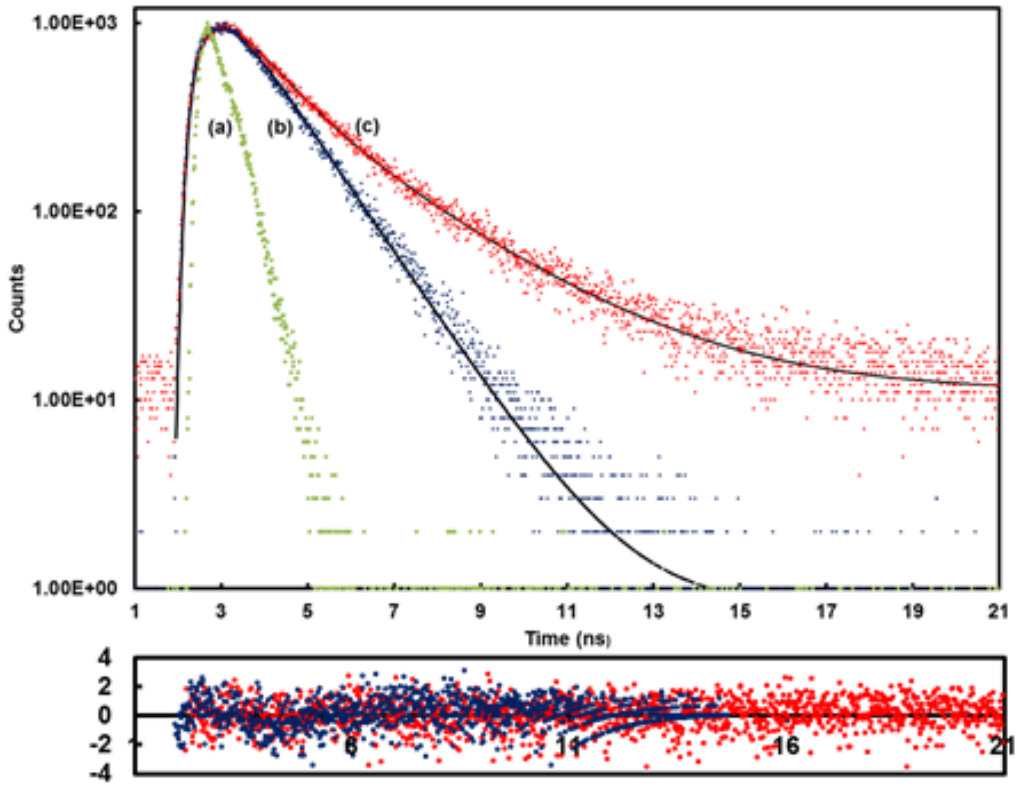

Figure 7.2. The instrument response function (a) and the fluorescence decays of APIP-c in propanol (b) λ_{em} = 380 nm and (c) λ_{em} = 460 nm along with fitted curve and residue plot , λ_{exc} = 308 nm.

The electronic transition dipole moment (M_{flu}) for the charge transfer state can be determined using following expression,[284]

$$k_f = \frac{64\pi^4}{3h}(n\bar{\nu}_{flu}^{TICT})^3 \left|M_{flu}\right|^2 \qquad (7.1)$$

Where k_f is the radiative rate constant, h is the Planck's constant and n is the refractive index. Since clear dual emission is observed only in methanol, calculation of quantum yield is more reliable in methanol. Therefore, the M_{flu} is estimated in methanol. The quantum yield, radiative rate constant, nonradiative rate constant and electronic transition dipole moment for the longer wavelength emission are 0.039, 1.8 X 10^7 s^{-1}, 4.4 X 10^8 s^{-1} and 1.5 D.The small values of the electronic transition dipole moments corresponding to the longer wavelength emission suggest a small overlap between the donor and the acceptor orbitals. This supports the TICT model.[285-287]

7.1.2. Spectral Characteristics of AHPIP-c

The absorption spectra of AHPIP-c were recorded in different solvents and the data are compiled in **Table 7.3**. Absorption spectra in all the solvents consist of one band at ~ 300 nm and another band at ~ 345 nm. The longer wavelength absorption band maxima of AHPIP-c are red shifted compared to those of APIP-c and HPIP-c. This may be due to greater conjugation in AHPIP-c which has both hydroxyl and amino groups. Upon increasing the polarity and hydrogen bonding capacity of the solvents a small blue shift is observed in the longer wavelength absorption band maximum whereas, it produces a red shift in the absorption spectrum of APIP-c**.** However, a blue shift was found in the absorption maximum of HPIP-c.[76]

Table 7.3. Absorption Band Maxima (λ_{max}^{ab}, nm) and Fluorescence Band Maxima (λ_{max}^{fl}, nm) of AHPIP-c in Different Solvents.

Solevent	λ_{max}^{ab}	λ_{max}^{fl}	
		Shorter Wavelength	Longer Wavelength
Methylcyclohexane	287, 327, 353	390, 420	474
Dioxane	296, 346	389	472
Ether		389	473
Ethylacetate	300, 346	388	465
Tetrahydrofuran	310, 347	388	464
Acetonitrile	297, 344	386	460
Dimethylformamide	300, 344	376	462
Dimethylsulphoxide	304, 443	379	462
Butanol	310, 346	384	455
2-Propanol	309, 346	382	451
1-Propanol	305, 345	389	452
Ethanol	307, 345	389	452
Methanol	303, 342	379	451

Fluorescence spectral data of AHPIP-c in different solvents are compiled in **Table 7.3**. **Figure 7.3** shows the representative spectra of AHPIP-c in selected solvents. Unlike APIP-c, in AHPIP-c dual emission is observed in both aprotic and protic solvents. The fluorescence decays were monitored at both bands and were found to be single exponentials **(Table 7.4)**. The fluorescence lifetime of the shorter wavelength emitting species is shorter than that of the longer wavelength emitting species.

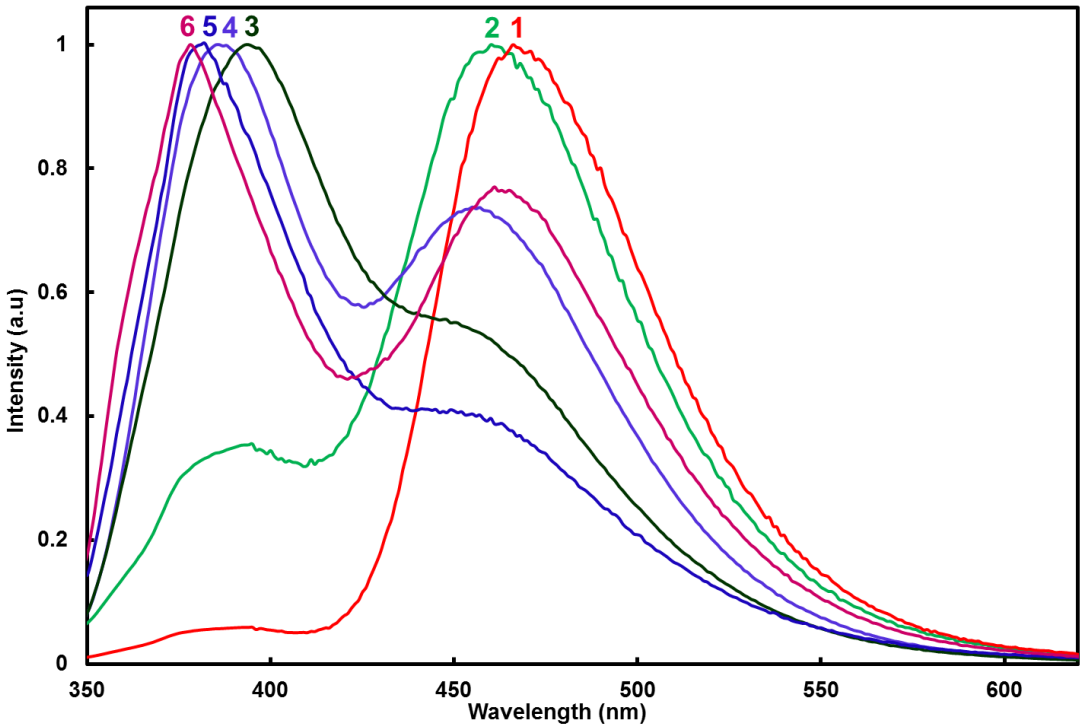

Figure 7. 3. Fluorescence spectra of AHPIP-c in (1) ethylacetate, (2) acetonitrile, (3) 1-propanol, (4) butanol, (5) methanol and (6) dimethyformamide, λ_{exc}=340 nm.

Table 7.4. Fluorescence Lifetime of Shorter Wavelength Emission (τ_S , ns) and Longer Wavelength Emission (τ_L , ns) of AHPIP-c in Different Solvents Along With the Corresponding Chi Square (χ^2).

Solvents	τ_S	χ^2	τ_L	χ^2
Dioxane			3.0	1.0
Ethylacetate	1.2	1.0	3.9	1.2
Acetonitrile	1.2	1.1	3.1	1.0
Butanol	1.3	0.9	2.8	1.0
2-Propanol	1.4	1.0	3.2	1.0
1-Propanol	1.3	1.0	2.8	1.0
Ethanol	1.3	1.0	2.6	1.0
Methanol	1.1	1.0	2.3	1.0

Dogra *et al*. established that HPIP-c exists in both *cis* and *trans* enol forms.[76] *Cis*-enol upon excitation undergoes ESIPT to form a keto tautomer and the emission occurs from the tautomer, whereas the *trans*-enol upon excitation emits the normal emission. The shorter and the longer wavelength emissions were assigned to normal emission (from *trans* enol) and tautomer emission (from the tautomer formed by ESIPT from *cis*-enol), respectively. In APIP-c only a single emission is observed in aprotic solvents. But, Yoon *et al*. hypothesized that the activation energy for the ICT processes is lowered by the ESIPT through the intramolecular hydrogen bonding in 4-aminosalicylic acid.[107] Park *et al.* also described a consecutive

ESIPT/ICT process that led to dual emission when different acceptors were substituted in the ESIPT exhibiting 2-(2'-hydroxyphenyl)benoxzazole.[64,88]

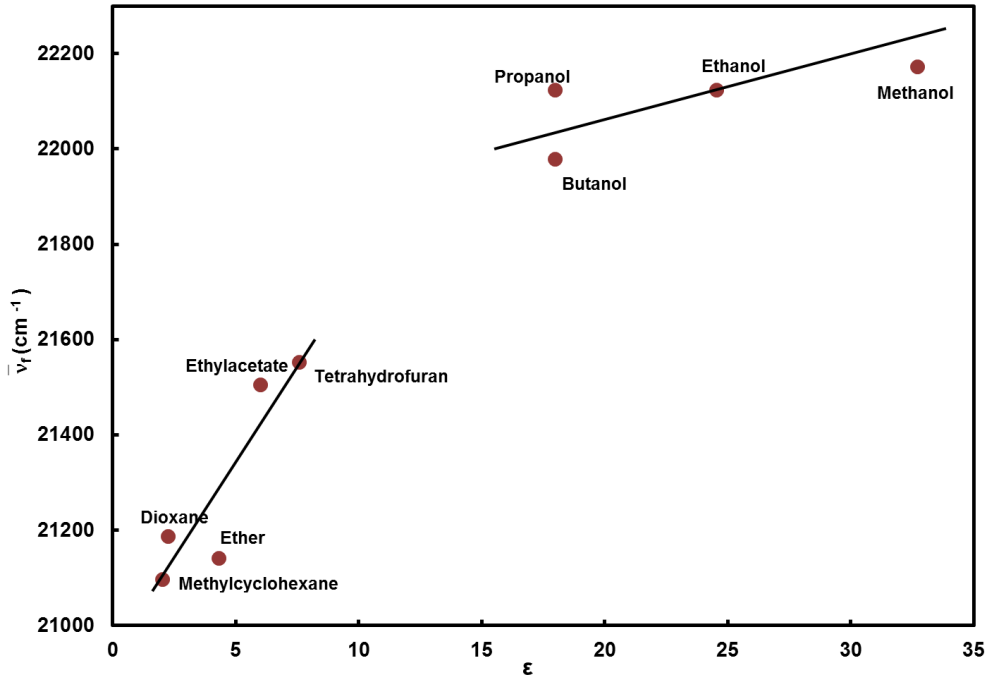

Figure 7.4. Plot of tautomer band maximum against the dielectric constant of aprotic and protic solvents.

ESIPT yields a phototautomer whose dipole moment is lesser than the ground state. Therefore, upon increasing the polarity of the solvent, the excited state is less stabilized than the ground state. This lead to increase in the energy gap between the states, thus, a negative solvatochromism is experienced. On the other hand, ICT in the excited state generates a highly polar TICT state whose dipole moment is much higher than the ground state.[1,2,33,288] Consequently, the excited state is more stabilized with increase in polarity which decreases the energy gap. Accordingly, it produces a red shift in the fluorescence spectra upon increasing the polarity of the environment. In AHPIP-c the longer wavelength emission is blue shifted with increase in solvent polarity **(Table 7.3)**. In other words a negative solvatochromism is observed **(Figure 7.4)**. Hence, it can be concluded that the longer wavelength emission of AHPIP-c in aprotic solvents is due to ESIPT. Guchhait *et al*. found that in some Schiff bases the proton transfer assist the ICT process.[111] It was also reported that the ICT emission is at shorter wavelength than the tautomer emission. But the solvatochromic shift of the shorter wavelength emission is small to assign the shorter wavelength as ICT band. In addition the shorter

wavelength band is blue shifted with respect to the ICT emission of APIP-c **(Tables 7.1 and 7.3)**. Therefore, the shorter wavelength and the longer wavelength emission from AHPIP-c in aprotic solvents can be assigned to normal and tautomer emission, respectively. This conclusion is further substantiated from the single emission observed in aprotic solvents from the methoxy derivative of AHPIP-c (see later).

TICT process is responsible for the longer wavelength emission of the 4-aminophenyl derivatives of imidazopyridines in protic solvents.[55-57,120] But, in protic solvents also the longer wavelength emission of 2-hydroxyphenyl derivative is due to ESIPT process.[76] Protic solvents break the intramolecular hydrogen bond in *cis* enol which is perquisite for the ESIPT process. This decreases the tautomer intensity. In contrast, the intermolecular hydrogen bond with the charge acceptor favours the formation of ICT state thereby enhances the ICT emission.[55-57,120] Therefore, the effect of protic solvents is further more exciting. The single exponential decays of both emissions clearly suggest that in protic solvents also AHPIP-c exhibits only dual fluorescence and not the triple fluorescence. Therefore, it is clear that one of the processes (TICT or ESIPT) is suppressed by the other in AHPIP-c. The longer wavelength fluorescence of AHPIP-c may be due to ESIPT or ICT process. The longer wavelength emission maxima in protic solvents also show negative solvatochromism **(Figure 7.4).** The longer wavelength band maxima in methanol is blue shifted compared to nonpolar solvents **(Table 7.3).** This indicates that the longer wavelength emission is the tautomer emission. The intermolecular hydrogen bonding is essential for the ICT emission in APIP-c. In AHPIP-c, the ESIPT process completely prevents the ICT process in protic solvents also despite the fact that protic solvents favour the intermolecular hydrogen bonding. In 4-(diethylamino)-2-hydroxybenzaldehyde also the ICT process is supressed by ESIPT process.[235] But the nature of 4-(diethylamino)benzaldehyde is different unlike in APIP-c, the protic environment is not essential for the ICT process in 4-(diethylamino)benzaldehyde. Rodríguez *et al.* illustrated though nonemissive ICT is observed in 2-(4′-*N*,*N*-diethylamino-2′-hydroxyphenyl)benzimidazoles no ICT emission is found in aprotic or protic solvents.[113] But unlike AHPIP-c, 2-(4′-*N*,*N*-diethylamino-2′-hydroxyphenyl)benzimidazole does not have pyridyl nitrogen which plays a crucial role in the intermolecular proton transfer induced TICT emission of 2-(4'-aminophenyl)imidazopyridines.[55-57,120] In AHPIP-c despite the presence of the pyridyl nitrogen the TICT emission is suppressed by ESIPT.

The fluorescence excitation spectra of AHPIP-c monitored at both emission maxima are different **(Figure 7.5)**. This suggests that the ground state precursors for both the emissions are different. As mentioned earlier, HPIP-c and related molecules exist as *cis*-enol and *trans*-

enol conformers. Accordingly, in AHPIP-c also the two different ground state species can be assigned to *cis*- and *trans*- enols **(Chart 7.2)**. Subsequently, two different lifetimes obtained for the normal and the tautomer emissions can be assigned to the lifetime of the excited *trans*-enol and the tautomer, respectively. The fluorescence lifetimes of both species of AHPIP-c are longer than those of respective forms of HPIP-c.[76] Such enhancements in radiative lifetimes are observed in ESIPT molecules also upon increasing conjugation.[76,111] The increase in polarity and hydrogen bonding capacity of the environment shifts the *cis*-enol-*trans*-enol equilibrium towards *trans*-enol. Therefore, the intensity ratio of the tautomer emission to normal emission decreases with increase in polarity and hydrogen bonding capacity of the solvent **(Figure 7.6)**. The ratio is less in protic solvents than in aprotic solvents and, it decreases with the protic nature of the solvent. As the intermolecular hydrogen bond breaks the intramolecular hydrogen bond in *cis*-enol, the completion between the intramolecular and intermolecular hydrogen bond decreases the relative population of *cis*-enol in protic solvents.[76] In other words, the ESIPT process is hindered by intermolecular hydrogen bonding and it is evident from **Figure 7.6.**

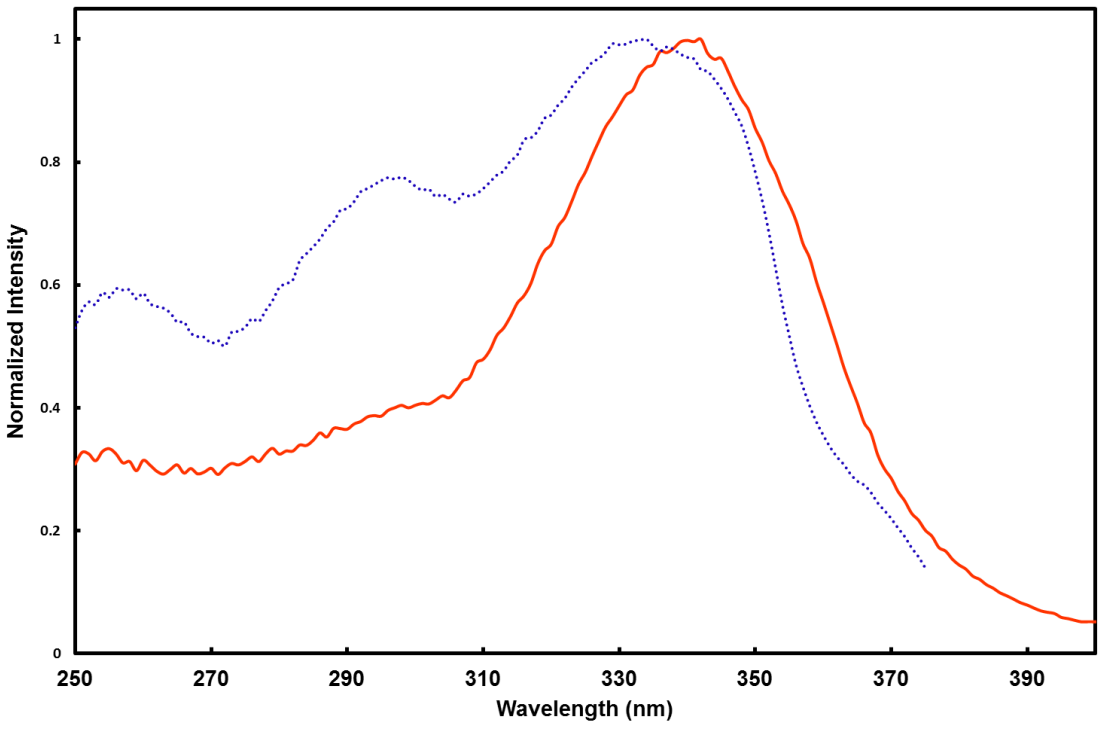

Figure7.5. Fluorescence excitation spectra of AHPIP-c monitored at normal band maximum (dotted line) and tautomer band maximum (solid line) in methanol.

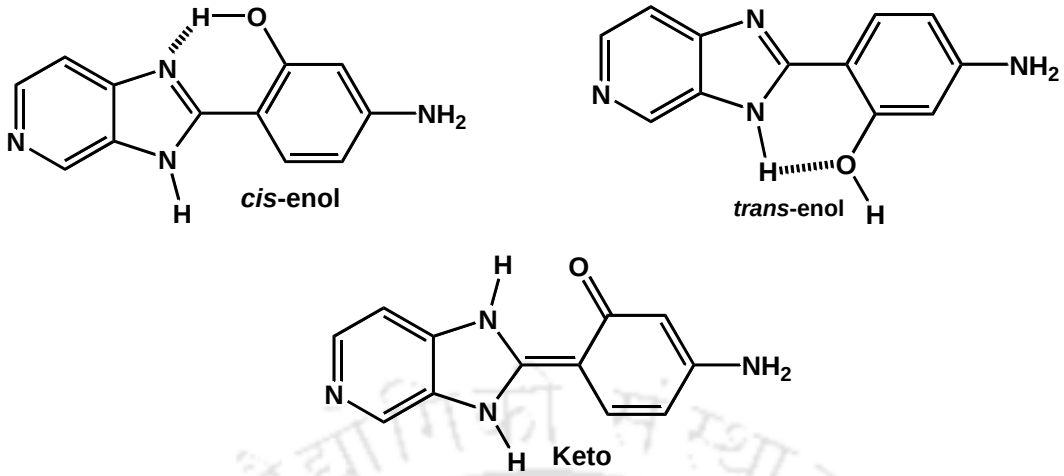

Chart 7.2.*cis*-enol, *trans*-enol and keto forms of AHPIP-c.

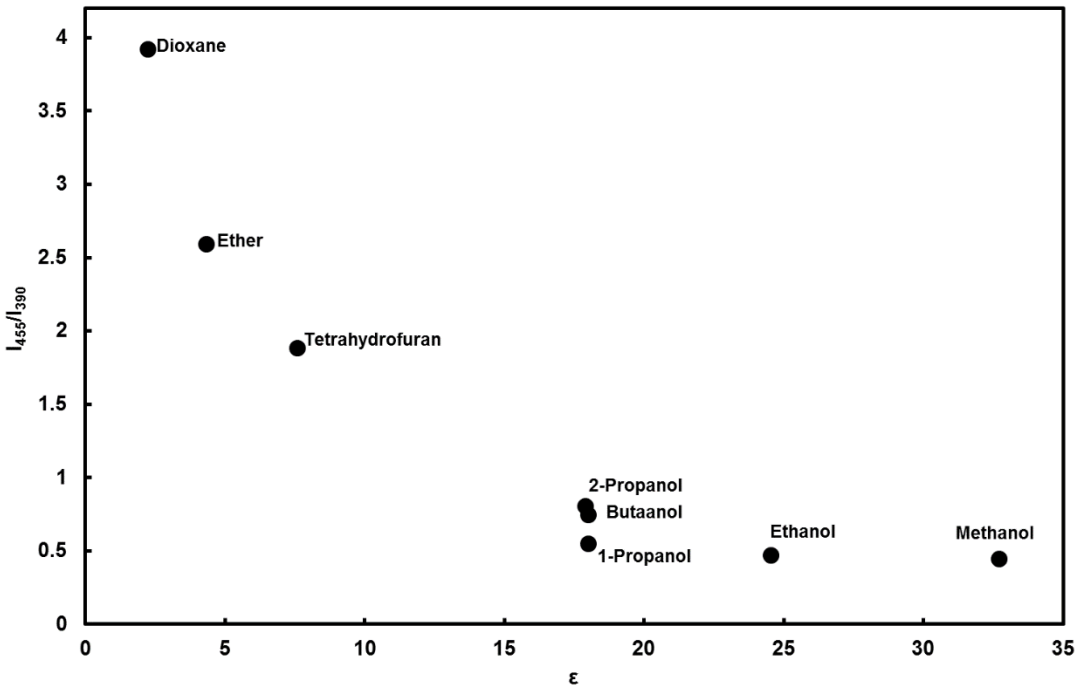

Figure 7. 6. Plot of I_T/I_N versus dielectric constant (ε).

7.1.3. Spectral Characteristics of AMPIP-c

To understand the role of ESIPT in suppressing the ICT process of AHPIP-c, the spectral properties of methoxy derivative AMPIP-c are further investigated **(Chart 7.1)**. Upon enhancing the polarity and the hydrogen bonding capacity of the solvents, though, little smaller than APIP-c, a bathochromic shift is observed in the absorption spectrum of AMPIP-c **(Table 7. 5)**. This behaviour of AMPIP-c is different from that of methoxy derivative of HPIP-c. Dogra

et al. reported that the absorption maxima of MPIP-c are nearly insensitive to nature of the solvents.[289] Therefore, it is clear that the substitution of electron donating amino group make it sensitive to environment and characteristics of AMPIP-c are more closer to APIP-c than those of MPIP-c.

Table 7.5. Absorption Band Maxima (λ_{max}^{ab}, nm) and Fluorescence Band Maxima (λ_{max}^{fl}, nm) of AMPIP-c in Different Solvents.

Solevent	λ_{max}^{ab}	λ_{max}^{fl}	
		Shorter Wavelength	Longer Wavelength
Methylcyclohexane	297, 321, 334	339, 355, 374	
Cyclohexane	298, 320, 334	341, 356, 374	
Dioxane	300, 328	371	
Ether	301, 327	371	
Ethylacetate	302, 328	370	
Tetrahydrofuran	301, 328	373	
Acetonitrile	301, 329	373	
Dimethylformamide	302, 334	383	
Dimethylsulphoxide	304, 337	384	
Butanol	301, 336	381	
2-Propanol	301, 333	383	
1-Propanol	302, 336	383	
Ethanol	301, 336	383	
Methanol	302, 336	383	450

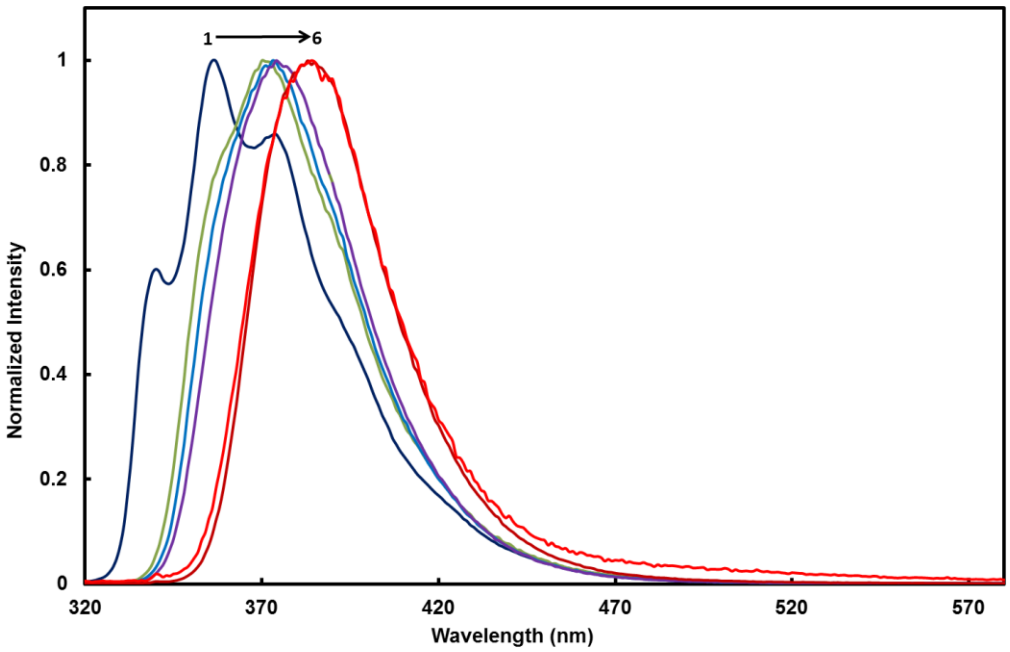

Figure 7.7. Fluorescence spectra of AMPIP-c in (1) cyclohexane, (2) ethylacetate, (3) dioxane, (4) acetonitrile, (5) 1-propanol and (6) methanol, λ_{exc} =310 nm.

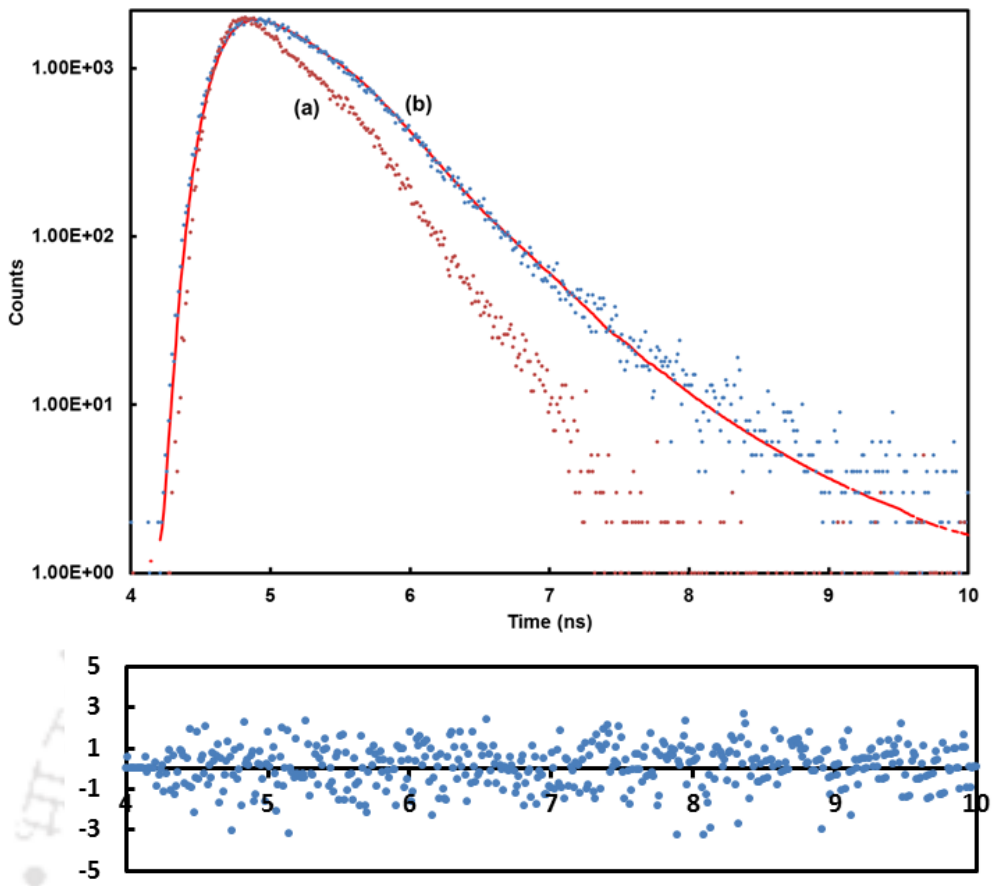

Figure7. 8. The instrument response function (a) and the fluorescence decays of AMPIP-c in methanol (b) along with fitted curve and residue plot, λ_{em} = 385 nm.

The fluorescence maxima of AMPIP-c are also more sensitive to the solvent polarity **(Figure 7.7 and Table 7.5)**. Same as in APIP-c a positive solvatochromism is observed. But the charge transfer is less in AMPIP-c than in APIP-c. This is substantiated by the lower dipole moment of AMPIP-c than APIP-c (see later). The TICT emission of AMPIP-c is not as prominent as in APIP-c only long tail is found in methanol **(Figure 7.1 and Figure 7.7)**. The excited decays of AMPIP-c measured in all solvents except methanol are single exponentials **(Table 7.6).** Attempt to fit the single exponential decay to the fluorescence decay in methanol resulted in poor fit with high chi square (χ^2). But the biexponential fit yields good results with two different lifetimes which further substantiate the presence of two different emitting species **(Figure 7.8 and Table 7.6)**. By analogy with APIP-c they may be assigned to normal and TICT emitting species. In other protic solvents even when monitored at 465 nm single exponential decays are observed. The fluorescence lifetime also matches with the fluorescence lifetime obtained by monitoring at 385 nm. This shows that except methanol other alcohols do not induce TICT emission in AMPIP-c.

Table 7.6. Fluorescence Lifetime of AMPIP-c in Different Solvents Along With the Corresponding Chi Square (χ^2), λ_{em} = 385 nm (Values in the Parentheses are the Relative Amplitudes).

Solvent	Single exponential decay		Biexponential decay		
	τ	χ^2	τ_1	τ_2	χ^2
Cyclohexane	1.1	0.9			
Dioxane	1.1	1.1			
Ether	1.2	1.0			
Ethylacetate	1.3	1.1			
Acetonitrile	1.3	1.1			
Butanol	1.4	1.1			
2-Propanol	1.4	1.0			
1-Propanol	1.4	1.1			
Ethanol	1.3	1.1			
Methanol	1.3	1.6	0.2 (82.72)	0.7 (17.28)	1.0

Table 7.7. DFT Optimized Parameters for AHPIP-c, AMPIP-c and APIP-c.

Parameters	APIP-c	AHPIP-c	AMPIP-c
Energy (eV)	-18563.43	-20610.75	-21679.54
μ_g (D)	7.84	6.98	7.08
Dihedral angle between imidazole moiety and phenyl ring (°)	0.01	0.03	37.13
Dihedral angle between amino group and phenyl ring (°)	0.01	0.09	22.39

Therefore, it is clear that the TICT emission of AMPIP-c is weak due to substitution of methoxy group at ortho position. It may be the substitution of methoxy group at ortho position twists the acceptor imidazopyridine out of plane from the phenyl ring. To substantiate this, the geometries of APIP-c, AHPIP-c and AMPIP-c were optimized by DFT method using Gaussian 09.[161] The optimized structural parameters are summarized in **Table 7. 7**. APIP-c and AHPIP-c are planar molecules. The imdazopydridine ring and the phenyl ring are out of plane by 37.1° in AMPIP-c. Such a twisting should reduce the charge flow from the phenyl ring to acceptor. Yoon *et al.* also proposed that the planarization of the benzene ring with acceptor favours the TICT processes owing to large charge flow from the phenyl ring to acceptor.[214,290] In APIP-c and AMPIP-c the TICT state is formed by the twisting of the amino group induced by relay proton transfer (**Chapter 3**). The reduced TICT emission from AMPIP-c also suggests that the TICT state is not formed by the twisting of the imidazopyridine as proposed by Fasani *et al.*[55] Like AHPIP-c, 2-(4′-*N*,*N*-diethylamino-2′-hydroxyphenyl)benzimidazoles also undergo ESIPT and no ICT emission was observed. But unlike the methoxyderivative of 2-(4′-*N*,*N*-diethylamino-2′-hydroxyphenyl)benzimidazoles, AMPIP-c emits ICT emission in methanol.

7.1.4. Solvatochromismic Approach

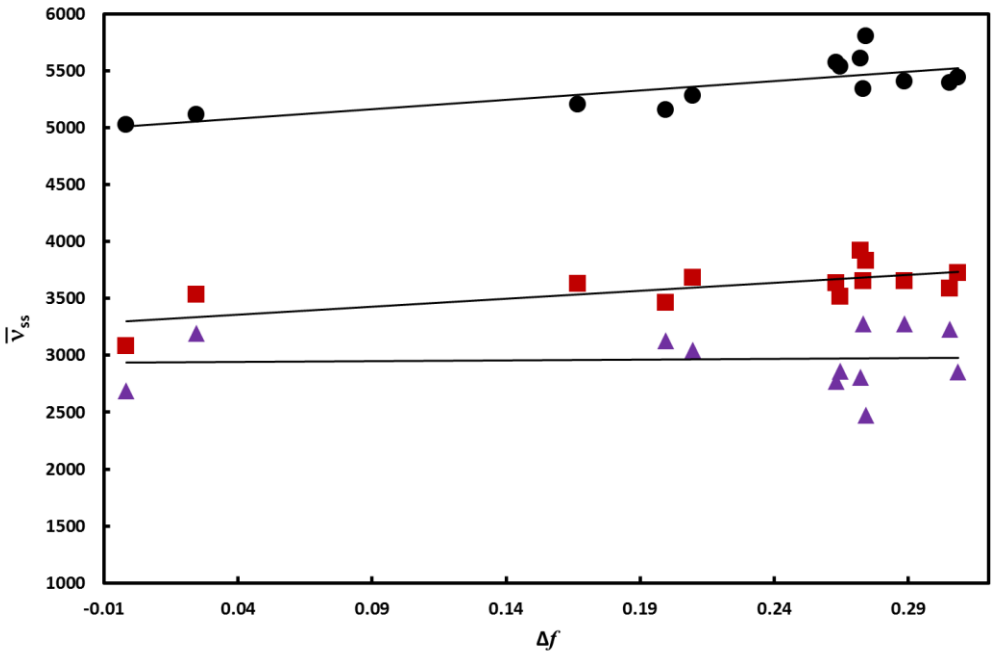

Figure 7.9. Lippert-Mataga plot using normal emission of APIP-c (●), AMPIP-c (■), and AHPIP-c (▲).

Lippert-Mataga analysis **(Chapter 3, Equation 3.1)** is employed to estimate the excited state dipole moments of the molecule to verify the charge transfer characteristics in the excited state. The Lippert-Mataga plot is constructed for normal emissions of APIP-c, AMPIP-c and AHPIP-c **(Figure 7.9)**. Using the slope obtained from Lippert plot and the Onsager radius and the ground state dipole moments obtained from the DFT calculations, the excited state dipole moments are calculated. The excited state dipole moment, thus estimated for APIP-c, AMPIP-c and AHPIP-c (*trans*-enol) are 11.9 D, 10.8 D and 10.8 D, respectively. The ground state dipole moments of APIP-c, AMPIP-c and AHPIP-c (*trans*-enol) are 7.1 D, 7.8 D and 9.6 D, respectively. Thus, it can be interpreted that the charge transfer is enhanced in the excited state. The enhancement in excited state charge transfer is more in APIP-c than in AMPIP-c, which is higher than that in AHPIP-c.

The dipole moments for the normal emissions suggest appreciable charge transfer from the donor to acceptor in all the molecules. Unfortunately, the longer wavelength emission is observed from AMPIP-c only in methanol. Therefore estimating the dipole moment of the longer wavelength emitting state by solvatochromic approach is not viable. Even the longer

wavelength emission of APIP-c is buried under the normal emission (expect in methanol). The spectral characteristics of PIP-c, the fluorophore without the charge donor (amino group) are studied and summarized in **Table 7.8** and the fluorescence spectra are presented in **Figure 7.10**. As it is found in methanol- acetonitrile (**Chapter 3**) no dual emission is observed in PIP-c in not only in aprotic solvents but also in protic solvents. On the other hand, when the electron donating ability of the donor is higher the longer wavelength emission induced by protic solvents increases (intensity ratio of longer wavelength to shorter wavelength is 0.18 in methanol for APIP-c and the same for the dimethyl derivative of APIP-c, DMAPIP-c is 0.30 in methanol (**Chapter 3**). This is consistent with our assignment that the longer wavelength emission is the TICT emission. In APIP-c analogue, DMAPIP-b also dual emission observed only in protic solvents. Since DMAPIP-b, emits clear dual emission in other protic solvents, the dipole moment was estimated using longer wavelength emission by solvatochromic approach. The estimated dipole moments (μ_e = 12.0 D (normal) 24.6 D (TICT)) substantiated the assignment of the longer wavelength emission as the TICT state.[56,230]

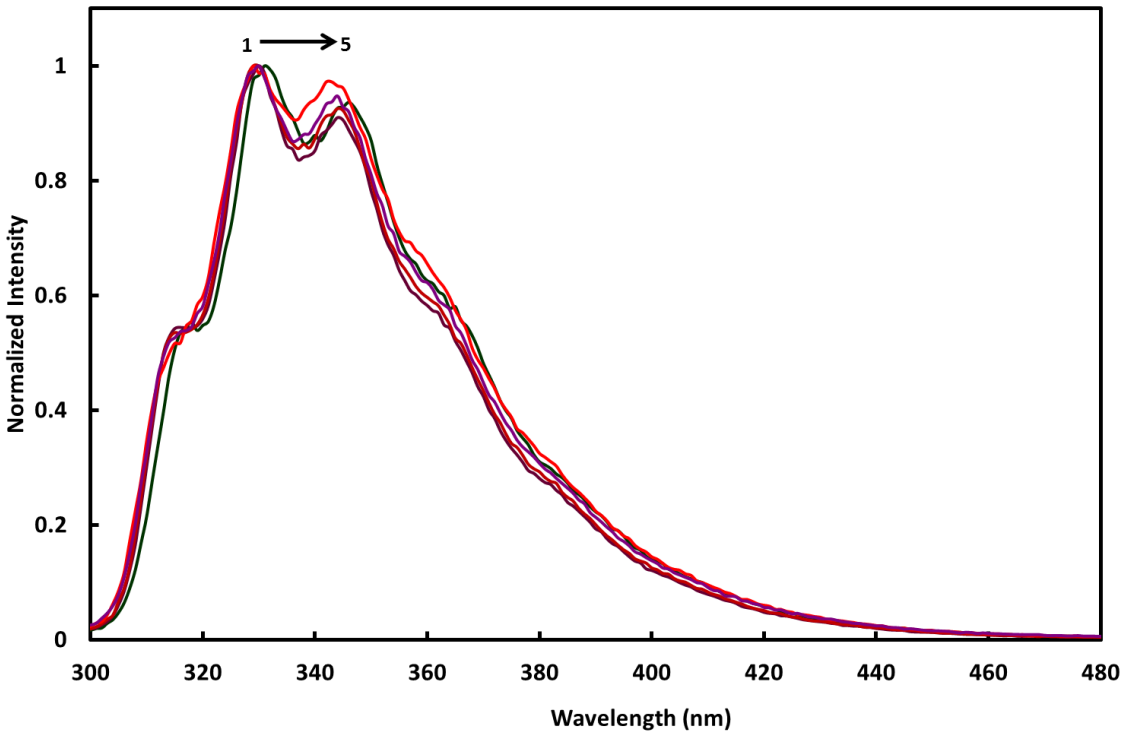

Figure 7.10.Fluorescence spectra of PIP-c in different solvents : (1) ether, (2) butanol, (3) 1-propanol, (4) ethanol and (5) methanol, λ_{exc} = 290 nm.

Table 7.8. Absorption Band Maxima (λ_{max}^{ab}, nm) and Fluorescence Band Maxima (λ_{max}^{fl}, nm) of PIP-c.

Solvent	λ_{max}^{ab}	λ_{max}^{fl}
Cyclohexane	292, 311	316, 331, 345, 364
Dioxane	293, 312	319, 334, 347, 366
Ether	292, 309	317, 331, 346, 362
Butanol	291, 308	315, 329, 343, 361
2-Propanol	292, 308	315, 329, 343, 360
1-Propanol	291, 308	315, 329, 343, 361
Ethanol	290, 307	315, 329, 343, 361
Methanol	290, 307	315, 329, 344, 362

Kamlet Taft solvatochromic method is widely used to understand the interaction between the solute and solvent molecules.[291] This multi-parametric approach separates the effects of polarity and hydrogen bonding, and provides useful information. According to multiple linear regression analysis approach the spectral band energy (in cm^{-1})

$$\bar{\nu} = \bar{\nu}^0 + s\pi^* + a\alpha + b\beta \quad (7.2)$$

where π^*, α and β are the polarity/polarizability, hydrogen bond donating ability and hydrogen bond accepting capacity of the solvents, respectively. The sensitivity to each individual parameter were given as *s*, *a* and *b* coefficients. The fits obtained using the absorption spectral data are presented below:

$$\bar{\nu}(\text{APIP-c}) = 32589 - 863\pi^* - 750\alpha - 24\beta \ (r = 0.89) \quad (7.3)$$

$$\bar{\nu}\,(\text{AHPIP-c}) = 28364 + 880\pi^* + 306\alpha - 57\beta \ (r = 0.93) \quad (7.4)$$

$$\bar{\nu}(\text{AMPIP-c}) = 31205 - 1167\pi^* - 713\alpha - 260\,\beta \ (r = 0.89) \quad (7.5)$$

The $\bar{\nu}^0$ values obtained in all the molecules are in good agreement with the values in nonpolar solvent. The negative and positive values of coefficients indicate the stabilization and destabilization of the system by individual parameter. Not only the polarity parameter but also the hydrogen bond donating ability of the solvent has positive coefficient for the hydroxyl derivative. The hydroxyl derivative has strong intramolecular hydrogen bond which stabilizes the system. Therefore, any intermolecular hydrogen bonding through solvents destabilizes it. On the other hand, when there was no intramolecular hydrogen bond the intermolecular hydrogen bond stabilizes the molecules. Therefore, the intermolecular hydrogen bonding stabilizes APIP-c and AMPIP-c. In other words, when the intramolecular hydrogen bonding

that leads to ESIPT is prevented and the intermolecular hydrogen bonding dominates which allows TICT to prevail.

Less sensitivity of the fluorescence maxima toward the solvent results in a poor correlation for AHPIP-c. However, reasonably good correlations were obtained for APIP-c and AMPIP-c and are shown below:

$$\bar{\nu}(\text{APIP-c}) = 27514 - 1203\pi^* - 863\alpha - 243\beta \quad (r = 0.82) \qquad (7.5)$$

$$\bar{\nu}(\text{AMPIP-c}) = 27982 - 1507\pi^* - 825\alpha - 552\beta \quad (r = 0.91) \qquad (7.6)$$

Like the ground state, the excited state is also stabilized by both polarity and hydrogen bonding parameters. The solvatochromic approach clearly shows that the intermolecular hydrogen bonding plays an important role in the stabilization of APIP-c and AMPIP-c. The ESIPT prevents the TICT processes of AHPIP-c in protic solvents also and blocking of ESIPT in AMPIP-c opens the TICT channel due to strong intermolecular hydrogen bonding.

7.1.5. Conclusion

APIP-c exhibits dual emission only in protic solvents. Dual fluorescence is observed from AHPIP-c in all solvents. The shorter wavelength emission is the normal emission from the excited *trans*-enol. Unlike in APIP-c the longer wavelength emission of AHPIP-c is the tautomer emission. Like in HPIP-c, the radiative lifetime of the tautomer emission is longer than normal emission. But the lifetime of both normal and tautomer emissions of AHPIP-c are longer than the respective lifetimes of HPIP-c. The intensity ratio of the tautomer emission to the normal emission is sensitive to nature of the solvent. Not only in aprotic solvents but also in protic solvents the ESIPT process suppresses the TICT process. When the intramolecular hydrogen bond is blocked, the methoxy derivative of AHPIP-c, AMPIP-c emits normal emission in most of the solvent. But it exhibits the TICT emission in methanol. The TICT emission of AMPIP-c is weaker than the TICT emission of APIP-c. The substitution of bulky methoxy group twisted the imidazopyridine out of plane from the benzene ring and thereby reduced the ICT from the benzene ring to imidazopyridine ring.

Chapter 8

Summary and Scope for Future Work

8.1 Summary of the Present Thesis Work

In the present thesis, intramolecular processes such as TICT and ESIPT are explored and the outcome of the works is summarized below:

In the family of TICT exhibiting systems, DMAPIP-b and DMAPIP-c are the unique ones. They emit TICT emission only in protic medium. Unlike in DMAPIP-b, the pyridiyl nitrogen is far away from imidazole nitrogen in DMAPIP-c. Hence, one solvent molecule is not sufficient enough for the proton transfer induced TICT emission. To comprehend the mechanism for the TICT emission of DMAPIP-c, DMAPIP-c and related molecules were synthesized and studied. Based on the experimental studies a relay transfer of proton from the imidazole hydrogen to the nitrogen at pyridyl ring induced TICT emission is proposed. Three protic solvent molecules are involved in the relay proton transfer process. The proposed mechanism was further corroborated by the theoretical calculations.

The inclusion complex formation of CB-7 with DMAPIP-b and DMAPIP-c is investigated to find the effect of CB-7 and the role of internal water molecules on the TICT emission of these fluorophores. DMAPIPs forms 1:1 complex with CB-7. They enter the CB-7 reverse form the way they form the complexes with CD. In the inclusion complex the pyridoimidzole ring is present inside the cavity and the dimethylaminophenyl ring is present outside. TICT emission is observed from the inclusion complex indicating that the internal water molecules participate in the proton transfer process. Despite the fact that CB has higher binding affinity towards cations than neutral guests the effect of CB on the mixture of cations are not investigated. Therefore, the effect of CB-7 on the monocationic equilibrium of DMAPIP-b and DMAPIP-c are explored. Both the imidazopyridines forms all three monocations in CB-7 in the ground state. However, addition of CB shifts the monocationic equilibrium towards MC2 and MC3 and the relative population of these monocations increases over MC1. In the excited state, DMAPIP-b exists in all three monocationic forms. But, DMAPIP-c is present only as MC2 and MC3 in the excited state. Upon excitation MC1 undergoes biprotonic phototautomerization to MC2 in CB-7 also.

In an effort to obtain self-quenching free emission, the spectral characteristics of a newly designed derivative of HPBI derivative (bis-HPBI) was investigated. The absorption and emission spectra of bis-HPBI are bathochromically shifted compared to that HPBI. This is due to the effect of substitution at 3' and 5' position of HPBI. Unlike HPBI, bis-HPBI emits almost exclusively intense tautomer emission even in protic solvents. The tautomer emission of bis-HPBI is due to only single proton transfer and is supported by the theoretical calculation. Enhancement of tautomer band intensity upon deprotonation of single –OH also supports the

single proton transfer hypothesis in bis-HPBI. Conversely, the tautomer emission decreases in acidic solution with initial addition of acid due to quenching by hydrogen bonding. When the imdazole nitrogen is protonated the tautomer emission is partially recovered due to dissociation and reorganization of cation. In strongly acidic solution the dissociation of –OH group from cation is prevented and emission is observed only from cation of bis-HPBI.

AIEE studies of bis-HPBI, bis-HPBO and bis-HPBT reveal that only bis-HPBT experiences AIEE. bis-HPBT is weakly fluorescent in THF solution and highly fluorescent aggregates are obtained at f_w = 70% in water/THF solution. The fluorescence quantum yield is enhanced nearly 300 times. Added advantage is the AIEE emission is free of less Stokes shifted normal emission. Therefore, it does not suffer self quenching. In addition, the mechanism for the RIR in ESIPT exhibiting molecules is revealed. It is due to restriction on the torsional rotation of the keto tautomer around C-C bond connecting the two rings. The AIEE of bis-HPBT can be used for sensing the ions and Hela cell imaging.

It is revealed that when intramolecular hydrogen bond is introduced in AHPIP-c, not only, it does not aid TICT emission but also suppress TICT emission even in protic solvents. When the intramolecular hydrogen bond is blocked, the methoxy derivative of AHPIP-c, AMPIP-c emits normal emission in most of the solvent. But it exhibits the TICT emission in methanol. The TICT emission of AMPIP-c is weaker than the TICT emission of APIP-c due to non-planarity of the benzene ring and imidazopyridine ring due to the substitution of bulky methoxy group.

8.2 Scope for the Future Work

In the present thesis the relay proton transfer induced TICT emission of DMAPIP-c in protic solvent is investigated. The TICT emission of DMAPIP-c can also be studied by replacing pyridine moiety with pyrimidine. As a result the electron withdrawing capacity of the acceptor group will be increased, which may facilitate the charge flow from donor to acceptor.

The ESIPT behaviour of bis-HPBI is studied in different solvents at room temperature. The study can be extended to investigate the effect of temperature on the photophyics of bis-HPBI.

Though the spectral characteristics of the AHPIP-c are studied, a complete theoretical study can be performed to gain insight on the proton transfer and charge transfer characteristics of AHPIP-c. In addition, the spectral characteristics of AHPIP-c can be explored in the microhetrogenous media such as cylodextrins, curcurbit-*n*-uril, proteins, DNA etc. Besides the

acid-base chemistry of AHPIP-c can be explored to find out the different prototropic species involved in prototropic equilibrium. The spectral characteristics of different prototropic species may provide further insight for the charge suppressing ESIPT emission to induce TICT emission.

Studies revealed that the position of pyridyl nitrogen alters the charge transfer and it is greater in APIP-b than in APIP-c. Therefore, the position of pyridyl nitrogen may be changed in AHPIP-c to verify whether that can lead to TICT emission. In addition, the amino group can be replaced by better charge donating dialkylamino to study the influence.

It was found that binding of metal ion to pyridyl nitrogen induces the TICT emission. Therefore, the work can be extended to study the effect of metal ions on the TICT emission of DMAPIP-c.

All these fluorophores DMAIP-c, bis-HPBI, bis-HPBT and AHPIP-c interacts with protons. Thus, they may bind with metal ions. Only the effect of metal ions on bis-HPBT aggregates is explored. All these molecules emit dual fluorescence, so they can act as ratiometric sensors. The interaction and metal ions sensing ability of all the molecules can be investigated.

~References~

1. Z. R. Grabowski, K. Rotkiewicz and W. Rettig, *Chem. Rev.*, 2003, **103**, 3899-4031.

2. W. Rettig, *Angew. Chem. Int. Ed. Engl.*, 1986, **25**, 971-988.

3. B. Valeur, Molecular fluorescence principles and applications. Wiley-VCH: Weinheim, 2002.

4. V. Martínez-Martínez, J. Lim, J. Bañuelos, I. López -Arbeloa and O. Š. Miljanić, *Phys. Chem. Chem. Phys.*, 2013, **15**, 18023-18029.

5. E. Ishow, R. Guillot, G. Buntinx and O. Poizat, *J. Photochem. Photobiol., A*, 2012, **234**, 27-36.

6. W. Schuddeboom, S. A. Jonker, J. M. Warman, U. Leinhos, W. Kuhnle and K. A. Zachariasse, *J. Phys. Chem.*, 1992, **96**, 10809-10819.

7. A. L. Sobolewski and W. Domcke, *Chem. Phys. Lett.*, 1996, **250**, 428-436.

8. N. Chattopadhyay, C. Serpa, M. M. Pereira, J. S. de Melo, L. G. Arnaut and S. J. Formosinho, *J. Phys. Chem. A*, 2001, **105**, 10025-10030.

9. C. Zhong, *Phys. Chem. Chem. Phys*., 2015, **17**, 9248-9257.

10. K. A. Zachariasse, *Chem. Phys. Lett.*, 2000, **320**, 8-13.

11. M. Dekhtyar, W. Rettig and W. Weigel, *Chem. Phys.*, 2008, **344**, 237-250.

12. W. Weigel, W. Rettig, M. Dekhtyar, C. Modrakowski, M. Beinhoff and A. Dieter Schlu1ter, *J. Phys. Chem. A*, 2003, **107**, 5941-5947.

13. A. Muller, H. Ratajczak, W. Junge and E. Diemann, Electron and proton transfer in chemistry and biology, Elsevier, Amsterdam, 1992.

14. C. E. Crespo-Hernández, B. Cohen, P. M. Hare and B. Kohler, *Chem. Rev.*, 2004, **104**, 1977-2020.

15. R. L. Cukier, *J. Phys. Chem.*, 1994, **98**, 2377-2381.

16. M. Wikstrom, *Nature*, 1989, **338**, 776-778.

17. S. Jana, S. Dalapati, S. Ghosh and N. Guchhait, *J. Photochem. Photobiol. A*, 2013, **261**, 31-40.

18. B. K. Paul, A. Samanta, S. Kar and N. Guchhait, *J. Luminesc.*, 2010, **130**, 1258-1267.

19. E. Ragnoni, M. D. Donato, A. Iagatti, A. Lapini and R. Righini, *J. Phys. Chem. B*, 2015, **119**, 420-432

20. L. - H. Ma, Z. - B. Chen and Y. - B. Jiang, *Chem. Phys. Lett.*, 2003, **372**, 104-113.

21. K. Dahl, R. Biswas, N. Ito and M. Maroncelli, *J. Phys. Chem. B*, 2005, **109**, 1563-1585.

22. R. J. Visser, C. A. G. O. Varma, J. Konijenberg and P. C. M. Weisenborn, *J. Mol. Struct.*, 1984, **114**, 105-112.

23. A. Nag, T. Kundu and K. Bhattacharyya, *Chem. Phys. Lett.*, 1989, **160**, 257-260.

24. R. A. Marcus and N. Sutin, *Biochim. Biophys. Acta*, 1985, **811**, 265-322.

25. W. Siebrand, *J. Chem. Phys.*, 1971, **55**, 5843.

26. A. Siemerczuk, Z. R. Grabowski, M. Asher and M. Ottolenghi, *Chem. Phys. Lett.*, 1977, **51**, 315-320

27. J. M. Hicks, M. T. Vandersall, E. V. Sitzmann and K. B. Eisethal, *Chem. Phys. Lett.*, 1987, **135**, 413-420.

28. J. M. Hicks, M. Vandersall, Z. Babarogic and K. B. Eisethal, *Chem. Phys. Lett.*, 1985, **116**, 18-24.

29. S. Tazuke, R. K. Guo and T. Ikeda, *J. Phys. Chem.*, 1990, **94**, 1408-1413.

30. R. M. Yusop, A. Unciti-Broceta and M. Bradley, *Bioorg. Med. Chem. Lett.*, 2012, **22**, 5780-5783.

31. K. A. Al-Hassan, *Chem. Phys. Lett.*, 1991, **179**, 195-198.

32. P. Changenet, P. Plaza, M. M. Martin and Y. H. Meyer, *J. Phys. Chem. A*, 1997, **101**, 8186-8194.

33. F. A. S. Chipem, A. Mishra and G. Krishnamoorthy, *phys. Chem. Chem. Phys., 2012*, **14**, 8775-8790.

34. C. Cazeau-Dubroca, A. Peirigua, M. B. Brahim, G. Nouchi and Ph. Cazeau, *Chem. Phys. Lett.*, 1989, **157**, 393-397.

35. C. Cazeau-Dubroca, A. Peirigua, M. B. Brahim, G. Nouchi and Ph. Cazeau, *Proc. Indian Acad. Sci. (Chem. Sci.)*, 1989, **104**, 209-217.

36. C. Cazeau-Dubroca, G. Nouchi, M. B. Brahim, M. Pesquer, D. Gorse and Ph. Cazeau, *J. Photochem. Photobiol. A*, 1994, **80**, 125-133.

37. C. Cazeau-Dubroca, A. Peirigua, S. Ait-Lyazidi, G. Nouchi, P. Cazeau and R. Lapouyade, *Chem. Phys. Lett.*, 1986, **124**, 110-115.

38. K. A. Al-Hassan and T. Azumi, *Chem. Phys. Lett.*, 1988, **146**, 121-124.

39. C. Cazeau-Dubroca, S. A. Lyazidi, P. Cambou, A. Peirigua, Ph. Cazeau and M. Pesquer, *J. Phys. Chem.*, 1989, **93**, 2347-2358.

40. T. Kobayashi, M. Futakami and O. Kajimoto, *Chem. Phys. Lett.*, 1986, **130**, 63-66.

41. J. Herbich, Z. R. Grabowski, H. Wójtowicz and K. Golankiewicz, *J. Phys. Chem.*, 1989, **93**, 3439-3444.

42. J. Herbich, J. Karpiuk, Z. R. Grabowski, N. Tamai and K. Yoshihara, *J. Lumin.*, 1992, **54**, 165-175.

43. S. I. Druzhinin, V. A. Galievsky, A. Demeter, S. A. Kovalenko, T. Senyushkina, S. R. Dubbaka, P. Knochel, P. Mayer, C. Grosse, D. Stalke and K. A. Zachariasse, *J. Phys. Chem. A,* 2015, **119**, 11820-11826.

44. M. Zakharov, O. Krauss, Y. Nosenko, B. B. Brutschy and A. Dreuw, *J. Am. Chem. Soc.*, 2009, **131**, 461-469.

45. M. J. Kamlet, C. Dickinson and R. W. Taft, *Chem. Phys. Lett.*, 1981, **77**, 69-72.

46. K. Rechthaler and G. Köhler, *Chem. Phys.*, 1994, **189**, 99-116.

47. E. Krystkowiak, K. Dobek and A. Maciejewski, *Int. J. Mol. Sci.*, 2014, **15**, 16628-16648

48. E. Krystkowiak, R. A. Bachorz and J. Koput, *Dyes and Pigments*, 2015, **112**, 335-340.

49. W. -M. Kwok, M. W. George, D. C. Grills, C. -S. Ma, P. Matousek, A. W. Parker, D. Phillips, W. T. Toner and M. Towrie, *Angew. Chem. Int. Ed. Engl.*, 2003, **42**, 1826-1830.

50. G. Zhao and K. Han, *J. Comput. Chem.*, 2008, **29**, 2010-2017.

51. S. Mishina, M. Takayanagi, M. Nakata, J. Otsuki and K. Araki, *J .Photochem. Photobio. A*, 2001, **141**, 153-158

52. J. Herbich and J. Waluk, *Chem. Phys.*, 1994, **188**, 247-268.

53. A. Demeter, V. Mile and T. Bérces, *J. Phys. Chem. A*, 2007, **111**, 8942-8949.

54. I. Szydłowska, J. Kubicki and J. Herbich, *Photochem. Photobiol. Sci.*, 2005, **4**, 106-112.

55. E. Fasani, A. Albini, P. Savarino, G. Viscardi and E. Barni, *J. Heterocycl. Chem.*, 1993, **30**, 1041-1044.

56. G. Krishnamoorthy and S. K. Dogra, *Spectrochim. Acta. A*, 1999, **55**, 2647-2658.

57. N. Dash, F. A. S. Chipem, R. Swaminathan and G. Krishnamoorthy, *Chem. Phys. Lett.*, 2008, **460**, 119-124.

58. M. Kasha, J. *Chem. Soc., Faraday Trans. 2*, 1986, **82**, 2379-2392.

59. J. E. Kwon and S. Y. Park, *Adv. Mater.*, 2011, **23**, 3615-3642.

60. J. Zhao, S. Ji, Y. Chen, H. Guo and P. Yang, *Phys. Chem. Chem. Phys.*, 2012, **14**, 8803-8817.

61. M. Mosquera, J. C. Penedo, M. C. R. Rodríguez and F. Rodríguez-Prieto, *J. Phys. Chem.* 1996, **100**, 5398-5407.

62. D. A. Yushchenko, V. V. Shvadchak, A. S. Klymchenko, G. Duportail and V. G. P. Y. Mély, *J. Phys. Chem. A*, 2007, **111**, 10435-10438.

63. P. Chou, D. McMorrow, T. J. Aartsma and M. Kasha, *J. Phys. Chem.* 1984, **88**, 4596-4599.

64. J. Seo, S. Kim and S. Y. Park, *J. Am. Chem. Soc.*, 2004, **126**, 11154-11155.

65. S. K. Das, A. Bansal and S. K. Dogra, *Bull. Chem. Soc. Jpn.*, 1997, **70**, 307-313.

66. S. K. Das and S. K. Dogra, *J. Chem. Soc., Faraday Trans.*, 1998, **94**, 139-145.

67. N. Sarkar, K. Das, S. Das, A. Datta, D. Nath and K. Bhattacharyya, *J. Phys. Chem.*, 1995, **99**, 17711-17714.

68. H. K. Sinha and S. K. Dogra, *Chem. Phys.*, 1986, **102**, 337-347.

69. K. Das, N. Sarkar, D. Majumdar and K. Bhattacharyya, *Chem. Phys. Lett.*, 1992, **198**, 443-448.

70. R. Wang, D. Liu, K. Xu and J. Li, *J. Photochem. Photobio. A*, 2009, **205**, 61-69.

71. O. K. Abou-Zied, R. Jimenez, E. H. Z. Thompson, D. P. Millar and F. E. Romesberg, *J. Phys. Chem. A*, 2002, **106**, 3665-3672.

72. T. Iijima, A. Momotake, Y. Shinohara, T. Sato, Y. Nishimura and T. Arai, *J. Phys. Chem. A*, 2010, **114**, 1603-1609.

73. A. Douhal, F. Amat-Guerri, M.P. Lillo and A. U. Acuña, *J. Photochem. Photobiol. A*, 1994, **78**, 127-138.

74. V. S. Padalkar, P. Ramasami and N. Sekar, *J. Fluoresc.*, 2013, **23**, 839-851.

75. Y. Houari, S. Chibani, D. Jacquemin and A. D. Laurent, *J. Phys. Chem. B*, 2015, **119**, 2180-2192.

76. M. M. Balamurali and S. K. Dogra, *J. Photochem. Photobiol. A*, 2002, **154**, 81-92.

77. G. Krishnamoorthy and S. K. Dogra, *J. Lumin*., 2001, **92**, 91-102.

78. G. Krishnamoorthy and S. K. Dogra, *J. Lumin.*, 2001, **92**, 103-114.

79. M. Mosquera, M. C. R. Rodríguez and F. Rodríguez-Prieto, *J. Phys. Chem. A*, 1997, **101**, 2766-2722.

80. M. C. R. Rodríguez, M. Mosquera and F. Rodríguez-Prieto, *J. Phys. Chem. A*, 2001, **105**, 10249-10260.

81. F. Rodriguez Prieto, M. C. R. Rodriguez, M. M. Gonzalez and M. A. R. Fernandez, *J. Phys. Chem.*, 1994, **98**, 8666-8672.

82. F. A. S. Chipem, N. Dash and G. Krishnamoorthy, *J. Chem. Phys.*, 2011, **134**, 104308.

83. J. S. Stephan, C. R. Rodriguez, K. H. Grellinann and K. A. Zachariasse, *Chem. Phys.* 1994, **186**, 435-446.

84. S. Santra, G. Krishnamoorthy and S. K. Dogra, *J. Phys. Chem. A.*, 2000, **104**, 476-482.

85. S. Santra, G. Krishnamoorthy and S. K. Dogra, *Chem. Phys. Lett.* 1999, **311**, 55-61.

86. C. J. Fahrni, M. M. Henary and D. G. VanDerveer, *J. Phys. Chem. A*, 2002, **106**, 7655-7663.

87. P. Purkayastha and N. Chattopadhyay, *Phys. Chem. Chem. Phys.*, 2000, **2**, 203-210.

88. C. H. Kim, J. Park, J. Seo, S.Y. Park and T. Joo, *J. Phys. Chem. A*, 2010, **114**, 5618-5629.

89. S. R. Vázquez, M. C. R. Rodríguez, M. Mosquera and F. Rodríguez-Prieto, *J. Phys. Chem. A*, 2007, **111**, 1814-1826.

90. H. Roohi, F. Hejazi, N. Mohtamedifar and M. Jahantab, *Spectrochimica Acta Part A*, 2014, **118**, 228-238.

91. F. S. Rodembusch, F. P. Leusin, L. B. Bordignon, M. R. Gallas and V. Stefani, *J. Photochem. Photobiol. A*, 2005, **173**, 81-92.

92. K. Das, N. Sarkar, A. K. Ghosh, D. Majumdar, D. N. Nath and K. Bhattacharyya, *J. Phys. Chem.*, 1994, **98**, 9126-9132.

93. A. Ohshima, M. Ikegami, Y. Shinohara, A. Momotake and T. Arai, *Bull. Chem. Soc. Jpn*., 2007, **80**, 561-566.

94. J. Seo, S. Kim, S. Park and S. Y. Park, *Bull. Korean Chem. Soc.*, 2005, **26**, 1707-1711.

95. N. Alarcos, M. Gutiérrez, M. Liras, F. Sánchez and A. Douhal, *Photochem. Photobiol. Sci.*, 2015, **14**, 1306-1318.

96. S. Luber, K. Adamczyk, E.T. J. Nibbering and V. S. Batista, *J. Phys. Chem. A*, 2013, **117**, 5269-5279.

97. L. Wilbraham, M. Savarese, N. Rega, C. Adamo and I. Ciofini, *J. Phys. Chem. B*, 2015, **119**, 2459-2466.

98. P. Yang, J. Zhao, W. Wu, X. Yu and Y. Liu, *J. Org. Chem.*, 2012, **77**, 6166-6178.

99. P. Majumdar and J. Zhao, *J. Phys. Chem. B*, 2015, **119**, 2384-2394.

100. H. - W. Tseng, J. - Q. Liu, Y. - A .Chen, C. - M. Chao, K. M. Liu, C. - L. Chen, T. - C. Lin, C. - H. Hung, Y. - L. Chou, T. C. Lin, T. - L. Wang and P. T. Chou, *J. Phys. Chem. Lett*, 2015, **6**, 1477-1486.

101. O. - H. Kwon and D. - J. Jang, *J. Phys. Chem. B*, 2005, **109**, 20479-20484.

102. C. A. Taylor, M. A. El - Bayoumi and M. Kasha, *Proc. Natl. Acad. Sci. USA*, 1969, **63**, 253-260.

103. M. Itoh, T. Adachi and K. Tokumura, *J. Am. Chem. Soc.* 1983, **105**, 4828-4829.

104. D. Gormin and M. Kasha, *Chem. Phys. Lett.*, 1988, **153**, 574-576.

105. D. Gormin and M. Kasha, *Chem. Phys.*, 1989, **136**, 321-334.

106. D. Gormin, J. Heldt and M. Kasha, *J. Phys. Chem.*, 1990, **94**, 1185-1189.

107. Y. Kim, M. Yoon and D. Kim, *J. Photochem. Photobiol. A.*, 2001, **138**, 167-175.

108. Y. Kim and M. Yoon, *Bull. Korean Chem. Soc.*, 1998, **19**, 980-985.

109. R. Ghosh and D. K. Palit, *Photochem. Photobiol. Sci.*, 2013, **12**, 987-995.

110. M. Ziólek, K. Filipczak and A. Maciejewski, *Chem. Phys. Lett.*, 2008, **464**, 181-186.

111. S. Jana, S. Dalapati and N. Guchhait, *J. Phys. Chem. A*, 2012, **116**, 10948-10958

112. T. -C. Fang, H. -Y. Tsai, M.-H. Luo, C. -W. Chang and K. -Y. Chen, *Chin. Chem. Lett.*, 2013, **24**, 145-148.

113. S. RíosVázquez, M. C. R. Rodríguez, M. Mosquera and F. Rodríguez-Prieto, *J. Phys. Chem. A*, 2008, **112**, 376-387.

114. C. - C. Hsieh, Y. -M. Cheng, C. - J. Hsu, K. - Y. Chen and P. - T. Chou, *J. Phys. Chem. A*, 2008, **112**, 8323-8332.

115. P. T. Chou, M. L. Martinez and J. H. J. Clements, *J. Phys. Chem.*, 1993, **97**, 2618-2622.

116. P. T. Chou, M. L. Martinez and J. H. Clements, *Chem. Phys. Lett.*, 1993, **204**, 395-399.

117. F. Parsapour and D. F. Kelley, *J. Phys. Chem.*, 1996, **100**, 2791-2798.

118. P. - T. Chou, C. Huang, S. - C. Pu, Y. - M. Cheng, Y. - H. Liu, Y. Wang and C. - T. Chen, *J. Phys. Chem. A.*, 2004, **108**, 6452-6454.

119. Y. - M Cheng, S. - C. Pu, Y. - C. Yu, P. - T. Chou, C. - H. Huang, C. - T. Chen, T. - H. Li and W. - P. Hu, *J. Phys. Chem. A.*, 2005, **109**, 11696-11706.

120. A. Mishra, S. Sahu, N. Dash, S. K. Behera and G. Krishnamoorthy, *J. Phys. Chem. B,* 2013, **117**, 9469-9477.

121. N. Dash, F. A. S. Chipem and G. Krishnamoorthy, *Photochem. Photobiol. Sci.,* 2009, **8**, 1708-1715.

122. G. Krishnamoorthy and S. K. Dogra, *J. Phys. Chem. A,* 2000, **104**, 2542-2551.

123. N. Barooah, J. Mohanty, H. Pal and A. C. Bhasikuttan, *Org. Biomol. Chem.,* 2012, **10**, 5055-5062.

124. A. Samanta, N. Guchhait and S. C. Bhattacharya, *J. Phys. Chem. B,* 2014, **118**, 13279-13289.

125. K. I. Assaf and W. M. Nau, *Chem. Soc. Rev.,* 2015, **44**, 394-418.

126. J. W. Lee, H. H. L. Lee, Y. H. Ko, K. Kim and H. I. Kim, *J. Phys. Chem. B*, 2015, **119**, 4628-4636.

127. K. Gavvala, R. K. Koninti, A. Sengupta and P. Hazra, *Phys. Chem. Chem. Phys.,* 2014, **16**, 2823-2826.

128. Y. J. Jeon, Y. H. Ko and K. Kim, *Bull. Korean Chem. Soc.* 2008, **29**, 2043-2046.

129. V. S. Patil, V. S. Padalkar, K. R. Phatangare, V. D. Gupta, P. G. Umape and N. Sekar, *J. Phys. Chem. A,* 2012, **116**, 536-545.

130. M. - K. Nah, S. - G. Rho, H. K. Kim and J. - G. Kang, *J. Phys. Chem. A*, 2007, **111**, 11437-11443.

131. Y. Xu and Yi Pang, *Chem. Commun.*, 2010, **46**, 4070-4072.

132. Y. Qian, S. Li, Q. Wang, X. Sheng, S. Wu, S. Wang, J. Lia and G. Yang, *Soft Matter*, 2012, **8**, 757-764.

133. T. Mutai, H. Sawatani, T. Shida, H. Shono and K. Araki, *J. Org. Chem.*, 2013, **78**, 2482-2489.

134. J. Luo, Z. Xie, J. W. Y. Lam, L. Cheng, H. Chen, C. Qiu, H. S. Kwok, X. Zhan, Y. Liu, D. Zhu and B. Z. Tang, *Chem. Commun.*, 2001, 1740-1741.

135. Z. Xie, B. Yang, F. Li, G. Cheng, L. Liu, G. Yang, H. Xu, L. Ye, M. Hanif, S. Liu and D. M. Y. Ma, *J. Am. Chem. Soc.*, 2005, **127**, 14152-14153.

136. S. J. Ananthakrishnan, E. Varathan, E. Ravindran, N. Somanathan, V. Subramanian, A. B. Mandal, J. D. Sudha and R. Ramakrishnan, *Chem. Commun.*, 2013, **49**, 10742-10744.

137. Z. Zhao, B. He, H. Nie, B. Chen, P. Lu, A. Qina and B. Z. Tang, *Chem. Commun.*, 2014, **50**, 1131-1133.

138. S. Choi, J. Bouffard and Y. Kim, *Chem. Sci.*, 2014, **5**, 751-755.

139. J. N. Wilson, M. D. Smith, V. Enkelmann and U. H. F. Bunz, *Chem. Commun.*, 2004, 1700.

140. J. Liu, Q. Meng, X. Zhang, X. Lu, P. He, L. Jiang, H. Dong and W.Hu, *Chem. Commun*, 2013, **49**, 1199-1201.

141. S. Mukherjee and P. Thilagar, *Chem. Commun.*, 2013, **49**, 7292-7294.

142. C. Niu, L .Zhao, T. Fang, X. Deng, H. Ma, J. Zhang, N. Na, J. Han, and J. Ouyang, *Langmuir*, 2014, **30**, 2351-2359.

143. S. Kamino, Y. Horio, S. Komeda, K. Minoura, H. Ichikawa, J. Horigome, A. Tatsumi, S. Kaji, T. Yamaguchi, Y. Usami, S. Hirota, S. Enomoto and Y. Fujita, *Chem. Commun.*, 2010, **46**, 9013-9015.

144. Y. Qian, M. - M. Cai, L. - H. Xie, G. - Q. Yang, S. - K. Wu and W. Huang, *Chem. Phys. Chem.*, 2011, **12**, 397-404.

145. P. - T. Chou, W. - S. Yu, Y. - M. Cheng, S. -C. Pu, Y. - C. Yu, Y. - C. Lin, Chen and C. -T. Huang, *J. Phys. Chem. A*, 2004, **108**, 6487-6498.

146. M. Z. Zgierski, T. Fujiwara and E. C. Lim, *J. Phys. Chem. A*, 2011, **115**, 10009-10017.

147. A. Brenlla, F. Rodríguez-Prieto, M. Mosquera, M. A. Ríos and M. C. R. Rodríguez, *J. Phys. Chem. A*, 2008, **113**, 56-67.

148. C. C. Hsieh, C. M. Jiang and P. T. Chou, *Acc. Chem. Res.*, 2010, **43**, 1364-1374.

149. S. Hammes-Schiffer and A. A. Stuchebrukhov, *Chem. Rev.*, 2010, **110**, 6939-6960.

150. D. R. Weinberg, C. J. Gagliardi, J. F. Hull, C. F. Murphy, C. A. Kent, B. C. Westlake, A. Paul, D. H. Ess, D. G. McCafferty and T. J. Meyer, *Chem. Rev.*, 2012, **112**, 4016-4093.

151. G. Krishnamoorthy and S.K. Dogra, *J. Lumin.*, 2001, **92**, 103-114.

152. V. Bavetsias, C. Sun, N. Bouloc, J. Reynisson, P. Workman, S. Linardopoulos and M. Edward, *Bioorg. Med. Chem. Lett.*, 2007, **17**, 6567-6571.

153. H. Yu, H. Kawanishi and H. Koshima, *J. Photochem. Photobiol. A*, 2006, **178**, 62-69.

154. F. Wu, C. M. Chamchoumis and R. P Thummel, *Inorg. Chem.*, 2000, **39**, 584-590.

155. Y. - P. Tong, S. - L. Zheng and X. - M. Chen, *J. Mol. Struct.*, 2007, **826**, 104-112.

156. C. M. Orlando, J. G. Wirth and D. R. Health, *J. Org. Chem.*, 1970, **35**, 3147-3149.

157. W. J. Coates, B. Connolly, D. Dhanak, S. T. Flynn and A. Worby, *J. Med. Chem.*, 1993, **36**, 1387-1392.

158. R. W. Middleton and D. G. Wibberly, *J. Heterocyclic Chem.* 1980, **17**, 1757-1760.

159. Master of Science in Chemistry Project Report by Sadhuragiri and M. Sathiyendiran, Department of Chemistry, University of Delhi.

160. G. A. Crosby and J. N. Demas, *J. Phys. Chem.*, 1971, **75**, 991-1024.

161. M. J. Frisch, G. W. Trucks, H. B. Schlegel, G. E. Scuseria, M. A. Robb, J. R. Cheeseman, G. Scalmani, V. Barone, B. Mennucci, G. A . Petersson, H. Nakatsuji, M. Caricato, X. Li, H. P. Hratchian, A. F. Izmaylov, J. Bloino, G. Zheng, J. L. Sonnenberg, M. Hada, M. Ehara, K. Toyota, R. Fukuda, J. Hasegawa, M. Ishida, T. Nakajima, Honda, Y. O. Kitao, H. Nakai, T. Vreven, J. A. Montgomery, Jr., J. E. Peralta, F. Ogliaro, M. Bearpark, J. J. Heyd, E. Brothers, K. N. Kudin, V. N. Staroverov, T. Keith, R. Kobayashi, J. Normand, K. Raghavachari, A. Rendell, J. C. Burant, S. S. Iyengar, J. Tomasi, M. Cossi, N. Rega, J. M. Millam, M. Klene, J. E. Knox, J. B. Cross, V. Bakken, C. Adamo, J. Jaramillo, R. Gomperts, R. E. Stratmann, O. Yazyev, A. J. Austin, R. Cammi, C. Pomelli, J. W. Ochterski, R. L. Martin, K. Morokuma, V. G. Zakrzewski, G. A. Voth, P. Salvador, J. J. Dannenberg, S. Dapprich, A. D. Daniels, O. Farkas, J. B. Foresman, J. V. Ortiz, J. Cioslowski, D. J. Fox, *Gaussian 09*, Revision D.01, Gaussian, Inc., Wallingford CT, **2013**.

162. S. Miertuš, E. Scrocco and J. Tomasi, *Chem. Phys.*, 1981, **55**, 117-129.

163. E. Cancès, B. Mennucci and J. Tomasi, *J. Chem. Phys.*, 1997, **107**, 3032-3041.

164. J. B. Foresman, M. Head-Gordon, J. A. Pople and M. J. Frisch, *J. Phys. Chem.***,** 1992, **96**, 135-149.

165. M. E. Casida, *Time-dependent density-functional response theory for molecules, in Recent advances in density functional methods, Part I*; World Scientific: Singapore, **1995**. p 155.

166. E. Gross, J. Dobson and M. Petersilka, *Top. Curr. Chem.*, 1996, **181**, 81-172.

167. F. A. S. Chipem and G. Krishnamoorthy, *J. Phys. Chem. A*, 2009, **113**, 12063-12070.

168. A. D. Becke, *J. Chem. Phys.*, 1993, **98**, 5648-5652.

169. C. Lee, W. Yang and R. G. Parr, *Phys. Rev. B*, 1988, **37**, 785-789.

170. T. Yanai, D. P. Tew and N. C. Handy. *Chem. Phys. Lett.*, 2004, **393**, 51-57.

171. S. Grimme, J. Antony, S. Ehrlich and H. Krieg, *J. Chem. Phys.*, 2010, **132**, 154104-154118.

172. E. Lippert, *Z. Elektrochem.* 1957, **61**, 962-975.

173. J. Wu, W. Liu, J. Ge, H. Zhang and P. Wang, *Chem. Soc. Rev.*, 2011, **40**, 3483-3495.

174. A. El Nahhas, T. Pascher, L. Leone, L. Panzella, A. Napolitano and V. Sundstrom, *J. Phys. Chem. Lett.*, 2014, **5**, 2094-2100.

175. N. Alarcos, J. Angel Organero, F. Sanchez and A. Douhal, *J. Phys. Chem. C*, 2014, **118**, 8217-8226.

176. Xi. - F. Yang, Q. Huang, Y. Zhong, Z. Li, H. Li, M. Lowry, J. O. Escobedo and R. M. Strongin, *Chem. Sci.*, 2014, **5**, 2177-2183.

177. G. Krishnamoorthy and S. K. Dogra, *Chem. Phys. Lett.*, 2000, **323**, 234-242.

178. V. Vetokhina, J. Nowacki, M. Pietrzak, M. F. Rode, A. L. Sobolewski, J. Waluk and J. Herbich, *J. Phys. Chem. A*, 2013, **117**, 9147-9155.

179. G. Krishnamoorthy and S. K. Dogra, *J. Org. Chem.*, 1999, **64**, 6566-6574.

180. R. Pomès, *Proton Relay in Membrane Proteins in 'Molecular Bioenergetics, Simulations of Electron, Proton, and Energy Transfer'*; American Chemical Society: **2004**. pp 159-173.

181. R. Schipfer, O. S. Wolfbeis and A. Knierzinger, *J. Chem. Soc. Perkin Trans.*, 1981, **2**, 1443-1448.

182. H. A. Benesi and J. H. Hildebrand, *J. Am. Chem. Soc.*, 1949, **71**, 2703-2707.

183. K. Kim and J. - I. Hoe, *Bull. Korean Chem. Soc.*, 2009, **30**, 837-845.

184. G. Krishnamoorhy, *Hydrogen Bonding and Transfer in the Excited State*; John Wiley & Sons Ltd: 2011. Vol. 1, pp 313-327.

185. V. Ramamurthy, *Acc. Chem. Res.*, 2015, **48**, 2904-2917.

186. R. N. Dsouza, U. Pischel and W. M. Nau, *Chem. Rev.*, 2011, **111**, 7941-7980.

187. B. D. Wagner, *Phys. Chem. Chem. Phys.*, 2012, **14**, 8825-8835.

188. J. Szejtli, *Chem. Rev.*, 1998, **98**, 1743-1754.

189. R. Choudhury, S. Gupta, J. P. Da Silva and V. Ramamurthy, *J. Org. Chem.*, 2013, **78**, 1824-1832.

190. J. Lagona, P. Mukhopadhyay, S. Chakrabarti and L. Isaacs, *Angew. Chem., Int. Ed.*, 2005, **44**, 4844-4870.

191. F. Sansone, L. Baldini, A. Casnati and R. Ungaro, *New J. Chem.*,2010, **34**, 2715-2728.

192. K. Kim, N. Selvapalam, Y. H. Ko, K. M. Park, D. Kim and J. Kim, *Chem. Soc. Rev.*, 2007, **36**, 267-279.

193. X. - L. Ni, X. Xiao, H. Cong, Q. - J. Zhu, S. F. Xue and Z. Tao, *Acc. Chem. Res.*, 2014, **47**, 1386-1395.

194. A. E. Kaifer, *Acc. Chem. Res.*, 2014, **47**, 2160-2167.

195. F. Biedermann, V. D. Uzunova, O. A. Scherman, W. M. Nau and A. De Simone, *J. Am. Chem. Soc.*, 2012, **134**, 15318-15323.

196. M. Gangopadhyay, A. K. Mandal, A. Maity, S. Ravindranathan, P. R. Rajamohanan and A. Das, *J. Org. Chem.*, 2016, **81**, 512-521.

197. D. H. Macartney, *Isr. J. Chem.*, 2011, **51**, 600-615.

198. B. D. Wagner, P. G. Boland, J. Lagona and L. Isaacs, *J. Phys. Chem. B*, 2005, **109**, 7686-7691.

199. S. D. Choudhury, J. Mohanty, H. Pal and A. C. Bhasikuttan, *J. Am. Chem. Soc.*, 2010, **132**, 1395-1401.

200. M. Megyesi, L. Biczók and I. Jablonkai, *J. Phys. Chem. C*, 2008, **112**, 3410-3416.

201. W. Ong and A. E. Kaifer, *Angew. Chem., Int. Ed.*, 2003, **42**, 2164-2167.

202. X. - L. Ni, J. - M. Yi, S. Song, Y. - Q. Zhang, S. - F. Xue, Q. - J. Zhu and Z. Tao, *Tetrahedron*, 2013, 69, 6219-6222.

203. M. Gupta, D. K. Maity, M. K. Singh, S. K. Nayak and A. K. Ray, *J. Phys. Chem. B*, 2012, **116**, 5551-5558.

204. D. Banik, J. Kuchlyan, A. Roy, N. Kundu and N. Sarkar, *J. Phys. Chem. B*, 2015, **119**, 2310-2322.

205. N. Basílio, C. A. T. Laia and F. Pina, *J. Phys. Chem. B*, 2015, **119**, 2749-2757.

206. C. P. Carvalho, V. D. Uzunova, J. P. Da Silva, W.M. Nau and U. Pischel, *Chem. Commun.*, 2011, **47**, 8793-8795.

207. M. Shaikh, S. D. Choudhury, J. Mohanty, A. C. Bhasikuttan, W. M. Nau and H. Pal, *Chem. Eur. J.*,2009, **15**, 12362-12370.

208. G. Krishnamoorthy and S. K. Dogra, *Spectrochim. Acta Part A*, 2001, **57**, 2617-2628.

209. Wang, L. Yuan, H. Ihmels and D. H. Macartney, *Chem. Eur. J.*, 2007, **13**, 6468-6473.

210. M. Sayed, M. Sundararajan, J. Mohanty, A. C. Bhasikuttan and H. Pal, *J. Phys. Chem. B*, 2015, **119**, 3046-3057.

211. K. Gavvala, A. Sengupta, R. K. Koninti and P. Hazra, *J. Phys. Chem. B*, 2013, **117**, 14099-14107.

212. F. A. S. Chipem, S. K. Behera and G. Krishnamoorthy, *J. Phys. Chem. A.*, 2013, **117**, 4084-4095.

213. S. He, C. Zhou, H. Zhang and X. Zhou, *J. Incl. Phenom. Macrocycl. Chem.*, 2013, **76**, 333-344.

214. Y. H. Kim, D. W. Cho, M. Yoon and D. Kim, *J. Phys. Chem.*, 1996, **100**, 15670-15676.

215. N. Dash and G. Krishnamoorthy, *J. Fluoresc.*, 2010, **20**, 135-142.

216. G. Krishnamoorthy and S. K. Dogra, *Phys. Chem. Chem. Phys.*, 2000, **2**, 2521-2528.

217. H. Konoshima, S. Nagao, I. Kiyota, K. Amimoto, N. Yamamoto, M. Sekine, M. Nakata, K. Furukawaa and H. Sekiya, *Phys. Chem. Chem. Phys.*, 2012, **14**, 16448-16457.

218. V. S. Padalkar, A. Tathe, V. D. Gupta, V. S. Patil, K. Phatangare and N. Sekar, *J. Fluoresc.*, 2012, **22**, 311-322.

219. A. Mordzinski and K. H. Grellmann, *J. Phys. Chem.*, 1986, **90**, 5503-5506.

220. S. M. Aly, A. Usman, M. AlZayer, G. A. Hamdi, E. Alarousu and O. F. Mohammed, *J. Phys. Chem. B*, 2015, **119**, 2596-2603.

221. K. -I. Sakai, T. Tsuzuki, Y. Itoh, M. Ichikawa and Y. Taniguchi, *Appl. Phys. Lett.*, 2005, **86**, 081103.

222. S. Hillebrand, M. Segala, T. Buckup, R. R. B.Correia, F. Horowitz and V. Stefani, *Chem. Phys.*, 2001, **273**, 1-10.

223. S. Kim, J. Seo, H. K. Jung, J-J. Kim and S. Y . Park. *Adv. Mater*, 2005, **17**, 2077-2082.

224. F. A. S. Chipem, S. K. Behera and G. Krishnamoorthy, *Sensors and Actuators B: Chem.*, 2014, **91**, 727-733.

225. V. Luxmi and S. Kumar, *New J. Chem.*, 2008, **32**, 2074-2079.

226. K. Tang, M. Chang, T. Lin, H. Pan, T. Fang, K. Chen, W. Hung, Y. Hsu and P. Chou, *J. Am. Chem. Soc.*, 2011, **133**, 17738-17745.

227. M. Forés, M. Duran, and M. Sola, M.Orozco and F. J. Luque, *J. Phys. Chem. A*, 1999, **103**, 4525-4532.

228. A. Mordzinski and A. Grabowska, *Chem. Phys. Lett.*, 1983, **101**, 291-296.

229. J. Zhao, J. Chen, J. Liu and M. R. Hoffmann, *Phys. Chem. Chem. Phys.*, 2015, **17**, 11990-11999.

230. N. Dash and G. Krishnamoorthy, *Photochem. Photobiol. A*, 2012, **95**, 540-546.

231. C. A. Potter, R. G. Brown, F. Vollmer and W. Rettig, *J. Chem. Soc., Faraday Trans.*,1994, **90**, 59-67.

232. L. Gourriérec, V. Kharlanov, R. G. Brown and W. Rettig, *J. Photochem. Photobiol. A*, 2000, **130**, 101-111.

233. F. A. S. Chipem and G. Krishnamoorthy, *J. Phys. Chem. B*, 2013, **117**, 14079-14088.

234. S. K. Behera, A. Karak and G. Krishnamoorthy, *Phys. Chem. B*, 2015, **119**, 2330-2344.

235. S. Jana, S. Dalapati and N. Guchhait, *J. Phys. Chem. A*, 2013, **117**, 4367-4376.

236. A. Brenlla, M. Veiga, J. Luis Pérez Lustres, M. C. R. Rodríguez, F. Rodríguez-Prieto and M. Mosquera, *J. Phys. Chem. B*, 2013, **117**, 884-896.

237. S. R.Vázquez, J. Luis Pérez Lustres, F. Rodríguez-Prieto, M. Mosquera and M. C. R. Rodríguez, *J. Phys. Chem. B*, 2015, **119**, 2475-2489.

238. F. J. M. Hoeben, P. Jonkheijm, E. W. Meijer and A. P. H. J. Schenning, *Chem. Rev.*, 2005, **105**, 1491-1546.

239. G. M. Whitesides and B. Grzybowski, *Science*, 2002, **295,** 2418-2421.

240. C. W. T. Leung, Y. Hong, S. Chen, E. Zhao, J. W. Y. Lam and B. Z. Tang, *J. Am. Chem. Soc.*, 2013, **135**, 62-65.

241. S. S. Babu, V. K. Praveen and A. Ajayaghosh, *Chem. Rev.*, 2014, **114**, 1973-2129.

242. J. H. Huang, J. H. Su, X. Li, M. K. Lan, K. M. Fung, H. H. Fan, K. W. Cheah, C. H. Chen and H. Tian, *J. Mater. Chem.*, 2011, **21**, 2957-2964.

243. H. B. Wu, L. Ying, W. Yang and Y. Cao, *Chem. Soc. Rev.*, 2009, **38**, 3391-3400.

244. S. Tao, L. Li, J. S. Yu, Y. D. Jiang, Y. C. Zhou, C. S. Li, S.T. Lee, X. H. Zhang and O. Kwon, *Chem. Mater.*, 2009, **21**, 1284-1287.

245. M. A. Baldo, M. E. Thompson and S. R. Forrest, *Nature*, 2000, **403**, 750-753.

246. Y. - L. Lei, Y. Jin, D. - Y. Zhou, W. Gu, X. - B. Shi, L. - S. Liao and S. - T. Lee, *Adv. Mater.*, 2012, **24**, 5345-5351.

247. L. Wang, Y. Shen, M. Yang, X. Zhang, W. Xu, Q. Zhu, J. Wu, Y. Tiana and H. Zhou, *Chem. Commun.*, 2014, **50**, 8723-8726.

248. J. Qian, Z. Zhu, A. Qin, W. Qin, L. Chu, F. Cai, H. Zhang, Q. Wu, R. Hu, B. Z. Tang and S. He, *Adv. Mater.*, 2015, **27**, 2332-2339.

249. Y. Shigemitsu, T. Mutai, H. Houjou and K. Araki, *Phys. Chem. Chem. Phys.*, 2014, **16**, 14388-14395.

250. J. Mei, N. L. C. Leung, R. T. K. Kwok, J. W. Y. Lam and B. Z. Tang, *Chem. Rev.*, 2015, **115**, 11718-11940.

251. J. Mei , Y. Hong , J. W. Y. Lam , A. Qin , Y. Tang and B. Z. Tang, *Adv. Mater.*, 2014, **26**, 5429-5479.

252. T. Zhang, H. Ma, Y. Niu, W. Li, D. Wang, Q. Peng, Z. Shuai and W. Liang, *J. Phys. Chem. C*, 2015, **119**, 5040-5047.

253. H. Tong, Y. Hong, Y. Dong, M. Haussler, Z. Li, J. W. Y. Lam, Y. Dong, H. H. Y. Sung, I. D. Williams and B. Z. Tang, *J. Phys. Chem. B*, 2007, **111**, 11817-11823.

254. M. Wang, D. Zhang, G. Zhang, Y. Tang, S. Wang and D. Zhu, *Anal. Chem.*, 2008, **80**, 6443-6448.

255. Y. Liu, C. Deng, L. Tang, A. Qin, R. Hu, J. Z. Sun and B. Z. Tang, *J. Am. Chem. Soc.*, 2011, **133**, 660-633.

256. P. Mazumdar, D. Das, G. P. Sahoo, G. Salgado-Morán and A. Misra, *Phys. Chem. Chem. Phys.*, 2015, **17**, 3343-3354.

257. S. Sharma, C. P. Pradeep and A. Dhir, *Mater. Sci. Eng.* C, 2014, **43**, 418-423.

258. C. Han, T. Huang, Q. Liu, H. Xu, Y. Zhuang, J. Li, J. Hu, A. Wang and K. Xu, *J. Mater. Chem. C*, 2014, **2**, 9077-9082.

259. V. Bhalla, A. Gupta and M. Kumar, *Dalton Trans.*, 2013, **42**, 4464-4469.

260. D. Ding, K. Li, B. Liu and B. Z. Tang, *Acc. Chem. Res.*, 2013, **46**, 2441-2453.

261. L. Kong, Y. - P. Tian, Q. -Y. Chen, Q. Zhang, H. Wang, D. -Q. Tan, Z. -M. Xue, J. - Y. Wu, H. P. Zhou and J. - X. Yang, *J. Mater. Chem. C*, 2015, **3**, 570-581.

262. Hu, C. F. A. Gomez-Duran, J. W. Y. Lam, J. L. Belmonte-Vazquez, C. Deng, S. Chen, R. Ye, E. Pena-Cabrera, Y. Zhong, K. S. Wong and B. Z. Tang, *Chem. Commun.*, 2012, **48**, 10099-10101.

263. J. Huang, A. Peng, H. Fu, Y. Ma, T. Zhai and J. Yao, *J. Phys. Chem. A*, 2006, **110**, 9079-9083.

264. Y. Qian, S. Li, G. Zhang, Q. Wang, S. Wang, H. Xu, C. Li, Y. Li and G. Yang, *J. Phys. Chem. B*, 2007**, 111**, 5861-5868.

265. R. Hu, S. Li, Y. Zeng, J. hen, S. Wang, Y. Li and G. Yang, *Phys. Chem. Chem. Phys.*, 2011, **13**, 2044-2051.

266. R. Wei, P. Song and A. Tong, *J. Phys. Chem. C*, 2013, **117**, 3467-3474.

267. A. Maity, F. Ali, H. Agarwalla, B. Anothumakkool and A. Das, *Chem. Commun.*, 2015, **51**, 2130-2133.

268. D. - E. Wu, Q. - C. Yao and M. Xia, *Phys. Chem. Chem. Phys.*, 2015, **17**, 3287-3294.

269. V. S. Padalkar, D. Sakamaki, N. Tohnai, T. Akutagawa, K. - I. Sakai and S. Seki, *RSC Adv.*, 2015, **5**, 80283-80296.

270. Y. H. Kim, S. - G. Roh, S. - D. Jung, M. - A. Chung, H. K. Kim and D. W. Cho, *Photochem. Photobiol. Sci.*, 2010, **9**, 722-729.

271. F. E. Critchfield, J. A. GibsonJr. and J. L. Hall, *J. Am. Chem. Soc.*, 1953, **75**, 6044-6045.

272. Y. Zhao, Y. Qian, N. Shi, B. Mi, L. Xie and W. Huang, *Phys. Chem. Chem. Phys.*, 2012, **14**, 5289-5296.

273. J. W. Chung, B. - K. An and S. Y. Park, *Chem. Mater.*, 2008, **20**, 6750-6755.

274. Y. Hong, J. W. Y. Lama and B. Z. Tang, *Chem. Commun.*, 2009, 4332-4353.

275. F. Wurthner, T. E. Kaiser and C. R. Saha - Moller, *Angew. Chem. Int. Ed.*, 2011, **50,** 3376-3410

276. E. W. Knapp, *Chem. Phys.*, 1984, **85**, 73-82.

277. M. Yang, D. Xu, W. Xi, L. Wang, J. Zheng, J. Huang, J. Zhang, H. Zhou, J. Wu and Y. Tian, *J. Org. Chem.*, 2013, **78**, 10344-10359.

278. Q. Zeng, Z. Li, Y. Dong, C. Di, A. Qin, Y. Hong, L. Ji, Z. Zhu, C. K. W. Jim, G. Yu, Q. Li, Z. Li, Y. Liu, J. Qin and B. Z. Tang, *Chem. Commun.*, 2007, 70-72.

279. B. Shankar, S. Sahu, N. Deibel, D. Schweinfurth, B. Sarkar, P. Elumalai, D. Gupta, F. Hussain, G. Krishnamoorthy and M. Sathiyendiran, *Inorg. Chem.*, 2014, **53**, 922-930.

280. H. Li, Y. Guo, G. Li, H. Xiao, Y. Lei, X. Huang, J. Chen, H. Wu, J. Ding and Y. Cheng, *J. Phys. Chem. C*, 2015, **119** , 6737-6748.

281. X. Feng, B. Tong, J. Shen, J. Shi, T. Han, L. Chen, J. Zhi, P. Lu, Y. Ma and Y. Dong, J. *Phys. Chem. B*, 2010, **114**, 16731-16736.

282. M. A. El-Kemary, *Chem. Phys.*, 2003, **295**, 1-10.

283. R. V. Pereira, A. P. G. Ferreira and M. H. Gehlen, *J. Phys. Chem. A.*, 2005, **109**, 5978-5983.

284. J. B. Birks, Photophysics of Aromatic Molecules, Wiley, New York, 1978.

285. J. Herbich and J. Waluk, *Chem. Phys.*, 1994, **188**, 247-265.

286. I. Szydłowska, A. Kyrychenko, J. Nowacki and J. Herbich, *Phys. Chem. Chem. Phys.*, 2003, **3**, 1032-1038.

287. I. F. Szydłowska, J. Nowacki and J. Herbich, *J. Photochem. Photobiol. A*, 2010, **209**, 135-146.

288. J. Herbich and A. Kapturkiewicz, *J. Am. Chem. Soc.*, 1998, **120**, 1014-1029.

289. M. M. Balamurali and S.K. Dogra, *J. Mol. Struct.*, 2004, **691**, 59-70.

290. Y. Kim, B. I. Lee and M. Yoon, *Chem. Phys. Lett*., 1998, **286**, 466–472.

291. M. J. Kamlet, J. - L. Abboud, M. H. Abraham and R. W.Taft, *J. Org. Chem.*,1983, **48**, 2877-2887.

List of Publications

1. F. A. S. Chipem, **S. K. Behera** and G. Krishnamoorthy, Enhancing Excited State Intramolecular Proton Transfer in 2‑(2′-Hydroxyphenyl)benzimidazole and Its Nitrogen-Substituted Analogues by β‑Cyclodextrin: The Effect of Nitrogen Substitution. *J. Phys. Chem. A,* 2013, **117**, 4084−4095.‡

2. A. Mishra, S. Sahu, N. Dash, **S. K. Behera** and G. Krishnamoorthy, Double Proton Transfer Induced Twisted Intramolecular Charge Transfer Emission in 2‑(4′‑N,N-Dimethylaminophenyl)imidazo[4,5-b]pyridine. *J. Phys. Chem. B*, 2013, **117**, 9469−9477. ‡

3. F. A. S. Chipem, **S. K. Behera** and G. Krishnamoorthy, Ratiometric Fluorescence Sensing Ability of 2-(2'-hydroxyphenyl)benzimidazole and Its Nitrogen Substituted Analogues Toward Metal Ions. *Sensors and Actuators B: Chemical* 2014,**191**,727-733.‡

4. F. A. S. Chipem, **S. K. Behera** and G. Krishnamoorthy, Excited State Proton Transfer of 2-(2′-hydroxyphenyl)benzimidazole and Its Nitrogen substituted Analogues in Bovine Serum Albumin. *Photochem. Photobiol. Sci.*, 2014, **13**, 1297-1304.‡

5. **S. K. Behera**, A. Karak and G. Krishnamoorthy, Photophysics of 2‑(4′-Amino-2′-hydroxyphenyl)‑*1H*‑imidazo-[4,5‑c]pyridine and Its Analogues: Intramolecular Proton Transfer Versus Intramolecular Charge Transfer. *J. Phys. Chem. B*, 2015, **119**, 2330–2344 (Special Issue Article).

6. **S. K. Behera** and G. Krishnamoorthy, Relay Proton Transfer Triggered Twisted Intramolecular Charge Transfer. *Photochem. Photobiol. Sci.*, 2015, **14**, 2225-2237.

7. **S. K. Behera,** G. Sadhuragiri, P. Elumalai, M. Sathiyendiran, and G. Krishnamoorthy, Exclusive Tautomer Emission from a 2-(2′-Hydroxyphenyl)benzimidazole Derivative. *RSC Adv.*, 2016, **6**, 59708-59717.

8. **S. K. Behera**, A. Mukherjee, G. Sadhuragiri, P. Elumalai, M. Sathiyendiran, M. Kumar, B. B. Mandal, and G. Krishnamoorthy, Aggregation Induced Enhanced and Exclusive Highly Stoke Shifted Emission from an Excited State Intramolecular Proton Transfer Exhibiting Molecule. *Faraday Discuss.*, 2016, DOI:10.1039/C6FD00171H.

9. **S. K. Behera** and G. Krishnamoorthy, Double Proton Transfer Induced Twisted Intramolecular Charge Transfer of 2‑(4′‑*N*,*N*-Dimethylaminophenyl)imidazo[4,5-b]pyridine in CB-7: Role of Internal Water Molecules, (Manuscript under preparation)

10. **S. K. Behera** and G. Krishnamoorthy, Realy Proton Transfer Induced Twisted Intramolecular Charge Transfer of 2‑(4′‑*N*,*N*-Dimethylaminophenyl)imidazo[4,5-c]pyridine in CB-7: Role of Internal Water Molecules, (Manuscript under preparation)

List of Conference Proceedings

1. **S. K. Behera** and G. Krishnamoorthy, Proton Transfer Induced Twisted Intramolecular Charge Transfer in 2-(4'-*N*,*N*-dimethylaminophenyl)imidazo[4,5-c]pyridine, 3rd National Symposium on Functional Applications of Colorants, Institute of Chemical Technology, Mumbai, October-2013. (Selected as Best Poster Presentation)

.

2. **S. K. Behera** and G. Krishnamoorthy, Spectral Properties of 2-(4'-*N*, *N*-dimethylaminophenyl)imidazo[4, 5-c]pyridine in Binary Solvent Mixture. Theme Meeting on Recent Trends in Spectroscopy, Indian Institute of Technology Madras, Tamil Nadu, India, June 20-21, 2014. (Selected as Best Oral Presentation)

3. **S. K. Behera**, A. Karak and G. Krishnamoorthy, Photophysics of 2-(4'-Amino-2'-hydroxyphenyl)-*1H*-imidazo-[4,5-c]pyridine and Its Analogues: Intramolecular Charge Transfer Suprresed by Intramolecular Proton Transfer**,** 8th Asian Photochemistry Conference (APC-2014), IISER- NIIST(CISR)Trivandrum, Kerala, Under the auspices of Photosciences Research Society of India ,November 9 - 13, 2014,Kovalam, Kerala, India

4. **S. K. Behera** and G. Krishnamoorthy, Intramolecular Charge Transfer Versus Intramolecular Proton Transfer, Research Conclave, organized by the PhD council of the Students Academic Board (SAB), IIT Guwahati, 23rd-26th March-2015.

5. **S. K. Behera** and G. Krishnamoorthy, Role of Protic Solvents in the Twisted Intramolecular Charge Transfer of 2-(4'-*N*, *N*-dimethylaminophenyl)imidazo[4,5-c]pyridine: A Relay Proton Transfer, Research Convene – 2015, Indian Institute of Guwahati, 8th April, 2015, India.

‡ **= not part of the present thesis**